

Charles University

Faculty of Science

Doctoral Study Programme

Molecular and Cellular Biology, Genetics and Virology



Mgr. Zuzana Matúšová

Gene expression profiling of glial cells in neurodegenerative diseases

Profilování genové exprese gliových buněk u neurodegenerativních onemocnění

Doctoral Thesis

Supervisor: **Ing. Lukáš Valihrach, Ph.D.**

Institute of Biotechnology of the Czech Academy of Sciences

Prague, 2024

Declaration

I hereby declare that I am the author of this dissertation, all the sources and literature are properly cited and the content of this thesis or its major part was not previously used for obtaining of the same or other academic degree.

Prohlášení

Prohlašuji, že jsem doktorskou práci zpracovala samostatně a že jsem uvedla všechny použité informační zdroje a literaturu. Tato práce ani její podstatná část nebyla předložena k získání jiného nebo stejného akademického titulu.

Table of contents

Acknowledgements	7
Abstract	8
Abstrakt	9
Abbreviations	10
1 Introduction	12
1.1 Neurodegenerative diseases	12
1.1.1 ALS	12
1.1.2 Alexander disease	14
1.2 Glia heterogeneity in health and disease	16
1.2.1 Astrocytes	17
1.2.2 Oligodendrocytes	19
1.2.3 Microglia	21
1.2.4 Radial glia	22
1.3 Models of neurodegenerative diseases	24
1.3.1 Animal models	25
1.3.2 <i>In vitro</i> models	26
1.4 High-throughput transcriptomic methods	28
1.4.1 Bulk RNA sequencing libraries	28
1.4.2 Single-cell RNA sequencing libraries	30
1.4.3 Sequencing considerations	33
1.4.4 Data analysis	33
2 Aims of the thesis	37
3 Experimental part	38
3.1 Results	38
3.2 Methods	78
3.3 Other publications and manuscripts	78
4 Discussion	80
4.1 Minimal changes in cortical glia in SOD1(G93A) mouse model of ALS	80
4.2 Abnormal neurodevelopment in iPSC-derived models of AxD	83
Conclusion	88
References	89

Acknowledgements

First of all, I would like to express my deepest gratitude to my supervisor Ing. Lukáš Valihrač, Ph.D., for his invaluable guidance and support throughout my Ph.D. journey. My sincere thanks go also to Ing. Pavel Abaffy, Ph.D., for his patience and willingness to share his knowledge about RNA sequencing and data analysis with me.

I am also very thankful to all members of the Laboratory of Gene Expression for our numerous scientific and non-scientific discussions and for the friendly and enthusiastic working environment that they have created within our team. It was a great pleasure to work with all of them.

I wish to extend my thanks to our collaborators from the Department of Cellular Neurophysiology at the Institute of Experimental Medicine of the Czech Academy of Sciences and to all international members of the ALEXANDER Consortium. I am also grateful to "Nadání Josefa, Marie a Zdeňky Hlávkových" Foundation for their financial support of my travels and to all the funding agencies without whom our projects would not exist.

Lastly, I would like to acknowledge my family and friends, who supported and motivated me during my academic journey.

Abstract

Neurodegenerative diseases are a wide group of disorders affecting the central (CNS) and peripheral nervous system. Despite enormous efforts of the scientific and medical communities, in many cases, the etiologies of neurodegenerative diseases remain unknown with no effective treatment available.

Recently, glial cells have entered the spotlight as important players in disease onset and progression, proving themselves as potentially interesting therapeutic targets. In healthy conditions, they maintain homeostasis in the CNS. However, upon its disturbance, they acquire reactive states, which affect the pathological processes in a positive or a negative manner. The reactive states are disease-specific, yet there are similarities linking reactive states of glia across pathologies, pointing to common mechanisms of coping with the disturbance of homeostasis in the CNS.

Single-cell RNA sequencing (scRNA-seq) belongs to modern high-throughput methods that enable studying transcriptional profiles of thousands of individual cells. Therefore, it can provide information on the representation of cell types across a variety of samples and reveal even small populations with unique, biologically interesting transcriptional signatures.

In this work, we applied scRNA-seq to investigate cell populations and transcriptional profiles in two neurodegenerative disorders with quite distinct etiologies – amyotrophic lateral sclerosis (ALS) and Alexander disease (AxD). ALS represents a neurodegenerative disease with a multifactorial cause. In this case, we used a well-established mouse model carrying a SOD1(G93A) mutation that causes only a minority of ALS cases. Addressing a controversial question of the extent to which the cortex is affected in the SOD1(G93A) mouse model, we found only limited signs of pathology in the SOD1 cortices. Thus, our in-depth transcriptomic analysis showed that this well-studied animal model does not recapitulate all aspects of human pathology, and another model should be used for the investigation of the cortex in ALS.

In contrast to ALS, Alexander disease belongs to rare diseases with well-defined and specific cause – mutations in the intermediate filament protein GFAP, which is primarily expressed by astrocytes and radial glia in the developing CNS. In this project, we focused on human induced pluripotent stem cell-derived (hiPSC) models in 2D co-culture as well as in brain organoids. We described these models using transcriptional profiling and found an interesting, early differentiation phenotype resulting in a reduction of mature astrocyte populations and overrepresentation of cells from other than neuroectodermal lineages. Thus, we revealed previously unknown effects of a GFAP mutation on cell type differentiation, offering new insights into AxD pathogenesis that should be considered in future research on this and related disorders.

Overall, the presented research projects demonstrate the usage of state-of-the-art transcriptomic methods to describe neurodegenerative diseases in high resolution, revealing information potentially important for future research on neurodegeneration with implications for the design of novel treatment strategies.

Abstrakt

Neurodegenerativní onemocnění jsou rozsáhlou skupinou poruch centrální (CNS) a periferní nervové soustavy. Navzdory úsilí vědecké a lékařské komunity jsou však v mnoha případech příčiny vzniku těchto onemocnění neznámé a neexistuje pro ně efektivní léčba.

V poslední době je velká pozornost věnována gliovým buňkám jakožto důležitým hráčům při vzniku a průběhu neurodegenerativních onemocnění. Za normálních okolností gliové buňky udržují homeostázi CNS. Při jejím narušení však přecházejí do reaktivních stavů, které pozitivním či negativním způsobem ovlivňují patologické procesy. Reaktivní stavy jsou specifické pro dané onemocnění, přesto existují podobnosti spojující reaktivní stavy glií napříč patologiemi, což naznačuje existenci společných mechanismů pro zvládnutí narušení homeostázy v CNS.

Sekvenování RNA jednotlivých buněk (scRNA-seq) patří mezi moderní vysokokapacitní metody, které umožňují studium transkripčních profilů tisíců jednotlivých buněk. Tato technika tedy poskytuje informaci o zastoupení buněčných typů napříč různými vzorky a odhalí i malé buněčné populace s jedinečnými biologicky zajímavými transkripčními profily.

V této práci jsme využili scRNA-seq k prozkoumání buněčných populací a transkripčních profilů ve dvou neurodegenerativních poruchách s poměrně odlišnou etiologií – amyotrofické laterální skleróze (ALS) a Alexandrově chorobě (AxD). ALS představuje neurodegenerativní onemocnění s multifaktoriální příčinou. V tomto případě jsme použili zavedený myší model nesoucí mutaci SOD1(G93A), která způsobuje pouze zlomek případů ALS. Zabývali jsme se kontroverzní otázkou, a sice, do jaké míry je v tomto modelu ovlivněna mozková kůra. Zjistili jsme pouze omezené známky patologie v mozkové kůře u myši s mutací SOD1. Naše hloubková transkriptomická analýza tak ukázala, že tento dobře popsáný zvířecí model nemusí napodobovat všechny aspekty lidské patologie a pro zkoumání mozkové kůry v ALS by měl být použit jiný model.

Alexandrova choroba patří mezi vzácná onemocnění s dobře definovanou a specifickou příčinou – mutacemi v proteinu intermediálních filament GFAP, který je primárně exprimován astrocyty a radiálními gliemi ve vyvíjející se CNS. V tomto projektu jsme se zaměřili na modely odvozené z lidských indukovaných pluripotentních kmenových buněk (hiPSC) ve 2D kultuře a také v mozkových organoidech. S využitím transkripčního profilování jsme popsali zajímavý raný diferenciativní fenotyp, který vede k redukci populace astrocytů a ke zvýšenému zastoupení buněk z jiných než neuroektodermálních vývojových linií. Odhalili jsme tak dosud neznámé účinky mutace GFAP na diferenciaci buněk, což nabízí nový náhled na patogenezi AxD, který by měl být zohledněn v budoucím výzkumu AxD a podobných onemocnění.

Tato práce ukazuje využití nejmodernějších metod transkriptomiky k podrobnému popisu neurodegenerativních onemocnění. Tyto metody pomáhají odhalit informace, které jsou potenciálně důležité pro výzkum neurodegenerace a mohou být využitelné při návrhu nových léčebných postupů.

Abbreviations

(f)AD	(familial) Alzheimer's disease
(s/f)ALS	(sporadic/familial) amyotrophic lateral sclerosis
APC	astrocyte progenitor cells
ARM	activated response microglia
ATM	axon tract-associated microglia
AxD	Alexander disease
CNS	central nervous system
COP	committed oligodendrocyte precursors
CPM	cycling and proliferating microglia
DAA	disease-associated astrocytes
DAM	disease-associated microglia
DEA	differential expression analysis
DEGs	differentially expressed genes
DOL	disease-associated oligodendrocytes
EAE	experimental autoimmune encephalomyelitis
ECM	extracellular matrix
ESC	embryonic stem cells
EST	expressed sequence tags
FACS	fluorescence-activated cell sorting
GFAP	glial fibrillary acidic protein
GSEA	Gene set enrichment analysis
HD	Huntington's disease
(hi)PSC	(human induced) pluripotent stem cells
IF	impact factor
IRM	interferon response microglia
LRT	likelihood-ratio test
MBP	myelin basic protein
MFOL	myelin-forming oligodendrocytes
MOL	mature oligodendrocytes
MS	multiple sclerosis
NSC	neural stem cell

NFOL	newly formed oligodendrocytes
NGS	next-generation sequencing
PAM	proliferative region-associated microglia
PCA	principal component analysis
PIPseq	particle-templated instant partition sequencing
PLP	proteolipid protein
OGD	oxygen-glucose deprivation
OPC	oligodendrocyte progenitor cell
ORA	over-representation analysis
oRG	outer radial glia
PCA	principal component analysis
(RT-q)PCR	(reverse transcription quantitative) polymerase chain reaction
PD	Parkinson's disease
RFs	Rosenthal fibers
RIN	RNA integrity number
(sc/sn)RNA-seq	(single-cell/single-nucleus) RNA sequencing
sci-RNA-seq	single-cell combinatorial indexing RNA sequencing
SAGE	serial analysis of gene expression
SPLiT-seq	split pool ligation-based transcriptome sequencing
SVZ	subventricular zone
tRG	truncated radial glia
t-SNE	t-distributed stochastic neighbourhood embedding
UMAP	uniform manifold approximation and projection
UMI	unique molecular identifier
vRG	ventricular zone radial glia
VZ	ventricular zone
WAM	white matter-associated microglia
WGCNA	weighted gene co-expression network analysis

1 Introduction

In the following chapters, the theoretical background underlying the ALS and AxD projects is summarized. Starting with the fundamental basis of the aforementioned neurodegenerative diseases, the current state of knowledge of glia heterogeneity and their role in such diseases is discussed. In the next methodological part of this overview, models used for studying neurodegeneration and transcriptomic methods applied in research are introduced. As data analysis comprises a large part of transcriptomic studies, this process is also clarified in this chapter.

1.1 Neurodegenerative diseases

Neurodegenerative diseases include a variety of disorders of the CNS that are usually accompanied by progressive neuron death, and consequently lead to neurological symptoms, such as motor disability, cognitive impairment, or seizures. Such diseases vary in the age of onset, severity of symptoms and pace of their progression, selective vulnerability of CNS regions, and heritability patterns. This variability exists even among different variants of one disease. The causative factors and disease mechanisms are also heterogeneous and often not fully understood.

On the other hand, there are characteristics shared among neurodegenerative diseases. At the molecular level, accumulation of proteins, influencing the balance between proteosynthesis and protein degradation, is one of the hallmarks used for post-mortem diagnosis. Chronic inflammation accompanying the dying neurons is also a common pattern identified across different neuropathologies. Recently, the role of glia in neuroinflammation and neurodegeneration has been emphasized, as they play an important role in homeostasis maintenance and evidently share common response patterns across pathologies (reviewed in Gleichman and Carmichael, 2020).

Nevertheless, due to the complexity of the CNS, many aspects of its pathology are unresolved. The majority of neurodegenerative diseases thus remain untreatable, although promising compounds and treatment strategies regularly enter clinical trials. However, their beneficial effects are often not sufficient. Therefore, identification of biomarkers and druggable targets allowing for early diagnosis and treatment is crucial and of a great interest in the current research.

1.1.1 ALS

ALS is a neurodegenerative disease predominantly affecting upper and lower motor neurons, resulting in their loss and progressive motor disability that eventually leads to respiratory failure and death within months or a few years. ALS is clinically presented by advancing limb weakness, bulbar symptoms, and respiratory problems. Based on the location of the first symptoms, multiple variants of ALS can be distinguished, including bulbar-, cervical-, lumbar-, and respiratory-onset ALS (reviewed in Gupta et al., 2023; Mezzini et al., 2019).

Multiple, somewhat opposing hypotheses about the directionality of ALS origin and progression exist and are supported by evidence (reviewed in Vucic et al., 2013). The “dying forward” hypothesis is generally more favored and considers the motor cortex to be the origin of the first pathological changes, which progress anterogradely to the spinal cord (Eisen et al., 1992). The “dying back” hypothesis suggests that the first changes appear in lower motor neurons at the neuromuscular junction and progress in a retrograde manner towards the spinal cord and the motor cortex (Chou and Norris, 1993). Lastly, upper and lower motor neuron degeneration may arise independently, as proposed by the poorly supported “independent degeneration” hypothesis (Vucic et al., 2013).

The etiology of ALS is complex, likely with a combined effect of genetics, environment, and aging. Most cases arise sporadically (sALS), while less than 10% of cases have a family history of the disease (fALS; Barberio et al., 2023). The majority of the sALS cases are of an unknown cause. Familial ALS, on the other hand, can often be attributed to mutations in specific genes (Mejzini et al., 2019). The most common ALS-linked genes are *C9ORF72* with an unclear function, superoxide dismutase *SOD1*, and RNA-binding proteins *TARDBP* and *FUS*, accounting for 33.7%, 14.8%, 4.2%, and 2.8%, respectively, of fALS cases in the European population (Zou et al., 2017). Nevertheless, in a genome-wide study, Zhang et al., 2022 identified as many as 690 ALS risk genes, showing that the genetic aspect of ALS is complex and most likely not linked to single mutations.

It is obvious that ALS is a very heterogeneous pathology. Actually, no universal disease mechanism has been isolated to date. On the contrary, multiple mechanisms are probably involved in the onset and progression of ALS, many of which are directly related to the function of the ALS-linked genes (Mejzini et al., 2019; Zhou and Xu, 2023). A few examples of the possible mechanisms are the impairment of protein turnover caused by aggregation, as described in *SOD1*-mutant cell cultures (Farrarwell and Yerbury, 2021), alterations in RNA metabolism (Humphrey et al., 2020), dysfunction of mitochondria, and increased oxidative stress (Zuo et al., 2021). Another common pattern noticeable across different variants of ALS is the disruption of neuronal morphogenesis, membrane transport, and signal transmission at synapses (Saez-Atienzar et al., 2021). Ultimately, the neuronal degeneration might be universally triggered by upregulation of *TGF β* signalling (Namboori et al., 2021).

ALS is also presented by neuroinflammation and reactive gliosis. Microglia and astrocytes participate in the ALS pathogenesis, co-regulating specialized gene expression programmes during the progression of the disease (Maniatis et al., 2019). Moreover, in the spinal cord, microglial dysfunction occurs before the onset of symptoms and progresses along the course of the disease (Maniatis et al., 2019). Microglia show the reactive phenotype (Keren-Shaul et al., 2017) and through secretion of cytokines induce reactive astrogliosis (Guttenplan et al., 2020; Liddelow et al., 2017; Ziff et al., 2022). Interestingly, the absence of reactive astrocytes slows the progress of the pathology, but does not stop its onset (Guttenplan et al., 2020), suggesting that reactive astrocytes strengthen the pro-inflammatory environment in ALS. In addition, reduction of glutamate uptake in ALS astrocytes contributes to excitotoxicity causing further

damage to neurons (Barton et al., 2020; Wallis et al., 2018). Oligodendrocytes should also not remain unnoticed. In fact, impaired oligodendrocyte maturation and demyelination have been reported even before symptom onset, implicating oligodendrocytes to be important contributors to motor neuron degeneration (Kang et al., 2013; Saez-Atienzar et al., 2021). Interestingly, other cell types, such as perivascular fibroblasts, show ALS-related changes preceding neuroinflammation and neuronal loss, suggesting that some disease mechanisms involving other systems besides the CNS-resident cell types remain unexplored (Månberg et al., 2021).

Although this overview is not exhaustive, it should illustrate the incredible complexity of ALS. Clearly, the disease is a result of a pathological interplay of many cell types, involving numerous cellular processes. ALS has been mainly studied in patient samples and mouse models, with the most widely studied model being SOD1(G93A) mouse (Gurney et al., 1994). In SOD1(G93A) mouse, the majority of studies detecting pathological changes in glia focus on the spinal cord (e.g., Guttenplan et al., 2020; Kang et al., 2013; MacLean et al., 2022; Maniatis et al., 2019; Miller et al., 2017), with some data also available for the brainstem (Liu et al., 2020). However, divergent and incomplete conclusions have been reached with respect to the extent of cortical pathology (Gomes et al., 2019; Migliarini et al., 2021; Miller et al., 2018; Niessen et al., 2006). Considering that cortical pathology is evident in symptomatic patients and represents the main presumption supporting the “dying forward” hypothesis (Vucic et al., 2013), it is necessary to unravel the actual usability of the mouse models in this context, in order to advance in the search for the ALS origin and the triggering mechanisms.

1.1.2 Alexander disease

Alexander disease belongs to rare leukodystrophies – neurodegenerative diseases affecting the white matter. Since its characterization in 1949, only around 550 cases of AxD have been reported worldwide, and the prevalence of AxD in the Japanese population was estimated to be 1 case per 2.7 million individuals (Yoshida et al., 2011). AxD is clinically manifested by variable symptoms including seizures, motor impairment, intellectual disability, overall developmental delay, and increased brain size (Messing et al., 2012; Prust et al., 2011). Based on the localization of lesions and the age of onset, at least three types of AxD can be distinguished (Messing et al., 2012; Prust et al., 2011; Yoshida et al., 2011), with the early-onset AxD – infantile and juvenile – being associated with higher incidence and mortality. On the other hand, late-onset AxD patients may sometimes be misdiagnosed due to the similarity of symptoms with other age-related neurodegenerative disorders.

AxD is caused by mutations in the GFAP protein that is expressed by astrocytes and radial glia in the CNS (Middeldorp et al., 2010). The mutations can arise sporadically or are inherited in an autosomal dominant manner (Messing et al., 2012). Several mutation hotspots within the GFAP-coding sequence have been identified and linked with the more severe early-onset AxD variants (Prust et al., 2011; Yoshida et al., 2011).

The AxD-causing mutations usually lead to overexpression of GFAP and its accumulation into Rosenthal fibers (RFs) that can be found in astrocytes and are considered to be the main

molecular hallmark of AxD (Hagemann, 2022; Messing et al., 2012). Besides GFAP, RFs contain a variety of proteins including highly abundant vimentin, ubiquitin, heat shock proteins, and α B-crystallin (Heaven et al., 2016). The composition of RFs implies the involvement of the ubiquitin-proteasome system, and indeed, overexpression and aberrant degradation have been proposed to create a positive feedback loop that eventually leads to protein accumulation into visible aggregates (Messing et al., 2012) and inhibition of proteasome function (Tang et al., 2010). The RFs have been shown to originate as small bundles along intermediate filaments, increasing in size over time and altering the structure of the filament network (Sosunov et al., 2017; Tanaka et al., 2007; Viedma-Poyatos et al., 2022; Yang et al., 2022). As a result, they interfere with astrocyte mitosis (Sosunov et al., 2017) and disrupt mitochondrial function (Viedma-Poyatos et al., 2022) and transfer (Gao et al., 2019). Actin cytoskeleton and mechanotransduction are also affected, and that results in increased stiffness of the CNS tissue (Wang et al., 2018). In addition, posttranslational modifications have been implicated in GFAP's susceptibility to damage, stress, and aggregation (Battaglia et al., 2019; Viedma-Poyatos et al., 2022).

GFAP-mutant astrocytes display signs of reactive gliosis and increased stress response (Hagemann et al., 2005; Heaven et al., 2022), and naturally, perturbations in astrocyte function are reflected in their interplay with other cell types. Oligodendrocyte progenitor (OPC) proliferation and oligodendrocyte maturation have been shown to be affected by GFAP-mutant astrocytes (Gomez-Pinedo et al., 2017; Li et al., 2018). Reactive microglia can also be found in AxD samples alongside reactive astrocytes, enhancing the inflammatory environment in the tissue (Hagemann et al., 2005; Heaven et al., 2022). On the other hand, a recent study reported a protective phenotype of microglia in AxD that could represent a disease-specific microglia response (Saito et al., 2024). Of course, astrocyte-neuron interaction and neuronal functions are affected by the GFAP mutation as well (Hagemann et al., 2005; Meisingset et al., 2010). Apparently, a combination of lack of support and toxicity of GFAP-mutant astrocytes are both the mechanisms at play in AxD.

Several animal models have been developed, mimicking AxD to some extent, including mouse (Hagemann et al., 2005), *Drosophila* (Wang et al., 2011), or zebrafish (Candiani et al., 2020). A novel rat model was introduced recently, along with an antisense oligonucleotide treatment strategy that proved to efficiently reduce GFAP accumulation and AxD symptoms in the tested rats (Hagemann et al., 2021) and proceeded to clinical trials. However, most of the animal models do not recapitulate all aspects of the human disease, and patient samples are lacking due to the rarity of AxD. Therefore, further progress of AxD research relies on alternative hiPSC-derived models, which have already been efficiently employed in several studies (Battaglia et al., 2019; Jones et al., 2018; Kondo et al., 2016; Li et al., 2018).

Cell cultures derived from iPSCs offer an opportunity to either model diseases in mature cell types or observe their differentiation throughout neurodevelopment in models such as brain organoids. The developmental aspect of AxD was only touched upon in a study by Hagemann et al., 2013, which showed deficits in adult neurogenesis and the presence of RFs in radial glia-

like cells in the hippocampus of the AxD mouse model. However, considering also the variety of cellular functions affected by a single GFAP mutation, the impact of GFAP mutations in radial glia and other cell types originating in radial glia during embryonic neurodevelopment could be another promising avenue for the research of AxD disease mechanisms (Valihrach and Benešová, 2022).

1.2 Glia heterogeneity in health and disease

Glia maintain homeostasis in the CNS, react to its disruption, support neuronal function, and participate in neurodevelopment. Historically, they have been considered 10-fold more numerous than neurons. However, recent estimations have decreased this ratio to approximately 1:1, although it can substantially vary across CNS regions, species, or developmental stage (**Fig. 1.1**; Allen and Lyons, 2018; Endo et al., 2022; von Bartheld et al., 2016). Glial cells include mainly astrocytes, oligodendrocytes, and microglia, but ependymal cells and radial glia are often counted among glia as well (Rasband, 2016). Additionally, specialized glia, such as Bergmann glia in the cerebellum, or Schwann cells, satellite glia, and enteric glia can be found also in the peripheral nervous system (Bellamy, 2006; Rasband, 2016).

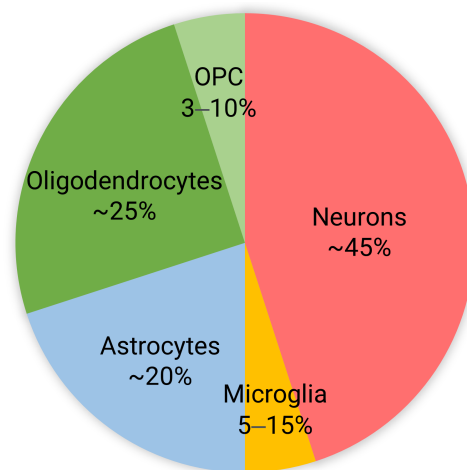


Figure 1.1: Pie chart with approximate estimated ratios of neurons, astrocytes, OPCs, oligodendrocytes, and microglia in the CNS, data according to Allen and Lyons, 2018.

It has been shown that glia form spatially and functionally heterogeneous populations even within individual cell types. **Tab. 1.1** summarizes selected marker genes identifying main populations of glia that are commonly distinguished in single-cell transcriptomic studies. This heterogeneity has been observed in healthy CNS, but also in disease (Floriddia et al., 2020; Habib et al., 2020; Mathys et al., 2017). Depending on the character and the stage of the pathology, disease-associated populations of glia have beneficial or negative effect on the disease progress, and supporting the beneficial effect while mitigating the detrimental effect in different diseases has been a major focus of glia research (Rahman et al., 2022).

Table 1.1: Table of selected markers defining main glia populations in pivotal mouse and human single-cell transcriptomic studies.

Cell type	Cell state	Markers	Characteristics	Reference
Astrocytes	Immature astrocytes	<i>HIST1H2AI, NUSAP1, TNC, HES6, MKI67, TOP2A</i>	Proliferating APC	Zhang et al., 2016
	Mature astrocytes	<i>CHI3LI, ALDH1LI, ALDOC, SLC1A2, CPE, GLUL</i>	Mature astrocytes compared to APC	Zhang et al., 2016
	Reactive astrocytes	<i>Gfap, Vim, Clu, Igfbp5, Id3, Cd9, Ctsb, Apoe, C4b, Serpina3n, Mt2</i>	DAA, located in the proximity of A β plaques in AD	Habib et al., 2020
Oligodendrocytes	OPC	<i>Ptprz1, Pdgfra, Serpine2, Cspg5, Vcan, Cspg4, Atp1a2, Fabp7</i>	Proliferative precursors, sharing several markers with radial glia	Marques et al., 2016
	Immature oligodendrocytes	<i>Neu4, Gpr17, Fyn, Tns3, Tcf7l2</i>	COP and NFOL, early states, migrating, starting to differentiate	Marques et al., 2016
	Mature oligodendrocytes	<i>Mal, Apod, Mog, Opalin, Mobp, Glul, Plp1</i>	MFOL and MOL	Marques et al., 2016
	Reactive oligodendrocytes	<i>Klk6, Serpina3n, C4b, H2-D1, H2-K1, B2m, Il33, Cd63, Cd9, Sgk1, Rnase4, Snca, Gstm1, Apoe</i>	DOL, enriched in the proximity of A β plaques in AD	Kenigsbuch et al., 2022
Microglia	Homeostatic microglia	<i>P2ry12, Tmem119, Sall1, Stab1, Crybb1, Cx3cr1</i>	The initial state from which ARM and IRM originate	Sala Frigerio et al., 2019
	Reactive microglia	<i>Apoe, Cst7, Spp1, Lpl, Cd74, Clec7a, H2-Ab1, Lyz2, H2-Aa, Ank</i>	ARM, enriched in the proximity of A β plaques in AD, but present also in healthy brain	Sala Frigerio et al., 2019
	IRM	<i>Apoe, Ifit2, Ifit3, Ccl12, Ifitm3, Rip4, Irf7, Lgals3bp, Oasl2, Ifi204</i>	Independent on A β plaques, present also in healthy brain	Sala Frigerio et al., 2019
Radial glia	Radial glia	<i>SOX2, PAX6, GLI3, HES1, VIM, ATP1A2, CLU</i>	Pan-radial glia signature, neural precursor cells	Pollen et al., 2015
	oRG	<i>HOPX, MOXD1, TNC, FABP7, FAM107A, PTPRZI, GFAP</i>	Found in SVZ, lost connection with VZ	Pollen et al., 2015
	vRG	<i>CRYAB, NR4A1, FBXO32, PDGFD, TAGLN2, PALLD</i>	Cell bodies lie in VZ, bipolar, reach from VZ to pia mater	Pollen et al., 2015

Abbreviations: AD – Alzheimer’s disease, APC – astrocyte progenitor cells, ARM – activated response microglia, COP – committed oligodendrocyte precursors, DAA – disease-associated astrocytes, DOL – disease-associated oligodendrocytes, IRM – interferon response microglia, MFOL – myelin-forming oligodendrocytes, MOL – mature oligodendrocytes, NFOL – newly formed oligodendrocytes, OPC – oligodendrocyte progenitor cells, oRG – outer radial glia, SVZ – subventricular zone, vRG – ventricular zone radial glia, VZ – ventricular zone.

1.2.1 Astrocytes

Astrocytes, named by their star-like highly-branched morphology, support normal function of the CNS. They participate in synaptogenesis, synaptic signalling and remodelling, neurotransmitter recycling, maintenance of ion homeostasis, and production of lactate as a source of energy for neurons. They also associate with the blood–brain barrier, maintain its integrity, regulate its permeability, and can respond to cytokines in the bloodstream coming from the periphery (reviewed in Lee et al., 2022b; Pekny and Pekna, 2014).

Based on their location and morphology several classes of astrocytes have been identified. Protoplasmic astrocytes are located in the grey matter and occupy large non-overlapping territories (Bushong et al., 2002; Oberheim et al., 2009), within which, in the human brain, they can contact up to 2 million synapses. While protoplasmic astrocytes reside in the middle cor-

tical layers, fibrous astrocytes can be found in the white matter and deep cortical layers, where they regulate myelination and signal transmission along myelinated axons (reviewed in Stogsdill et al., 2023; Traiffort et al., 2020). In addition, interlaminar astrocytes in upper cortical layers and varicose projection astrocytes in layers V-VI and the white matter, both of which occasionally show evenly distributed varicosities along their long processes, have been described in higher primates, reflecting the complexity of the CNS in these species (Falcone et al., 2022; Oberheim et al., 2009).

Single-cell transcriptomics has contributed to more detailed characterization of astrocyte populations. On one hand, it revealed many shared core features corresponding to astrocyte essential functions, but on the other, it uncovered a substantial diversity among brain regions (Batiuk et al., 2020; Endo et al., 2022), including for example a variable expression of genes associated with cholesterol and neurotransmitter homeostasis, synapse function, and phagocytosis. Moreover, cortical astrocytes have been found to organize into six layers, similar to but not overlapping with neuronal layering in the cortex (Bayraktar et al., 2020). This regional heterogeneity may arise from distinct progenitor populations, which are further shaped by their surrounding environment, and results consequently in their morphological and functional specialization (Batiuk et al., 2020; Endo et al., 2022). Adding another level to the variability, sex- and age-dependent expression profiles have been described in human astrocytes, potentially defining the susceptibility to various CNS diseases (Krawczyk et al., 2022).

Astrocyte progenitors are highly proliferating cells, often recognized also by outer radial glia (oRG) markers. As they mature, this progenitor signature decreases, astrocytes acquire their mature phenotype and increase their morphological complexity, which allows them to fulfill their proper functions. The mature expression profile includes genes involved in glutamate response, water transport, ion homeostasis, calcium signalling, signal transmission, cell-cell signalling, cell adhesion, lipid metabolism, and phagocytosis (Krawczyk et al., 2022; Sloan et al., 2017; Zhang et al., 2016). Aging is then accompanied by a reduction of synaptic interactions and energy metabolism and increase of cytokine signalling and senescence markers potentially partially responsible for age-related cognitive decline (Krawczyk et al., 2022), creating a pro-inflammatory environment prone to development of age-related disorders, such as Alzheimer's disease (AD; Andronie-Cioara et al., 2023).

In response to disruption of homeostasis, astrocytes enter a reactive state, which is often recognized by hypertrophy of cellular processes and an increase in GFAP immunoreactivity (Escartin et al., 2021; Pekny and Pekna, 2014). GFAP has been traditionally used as a marker of reactive astrocytes, however, a more detailed description of reactive astrogliosis is nowadays more preferable, assessing transcriptomic and proteomic profiles, morphology, function, but also underlying pathology, sex, or age (Escartin et al., 2021). At the molecular level, reactive astrogliosis is accompanied by upregulation of immune response genes, cell cycle, extracellular matrix (ECM) components, cytoskeletal proteins, and genes involved in adhesion (Zamanian et al., 2012). This transformation may be beneficial, but also harmful for the tissue. Upon a CNS injury, glial scar formed by astrocytes prevents the lesion from spreading but simultane-

ously inhibits regeneration of neuronal axons (Yang et al., 2020). Moreover, neuroinflammation accompanied by a long-lasting astrogliosis has been shown to have an overall negative effect on the progress of the pathology, not to mention the possible role of astrocytes in disease onset (Jiwaji and Hardingham, 2022; Liddelow and Barres, 2017; Liddelow et al., 2017; Van Harten et al., 2021).

Transcriptomic studies have identified numerous astrocyte populations in contexts of various CNS pathologies. A pivotal study by Zamanian et al., 2012 provided a classification into A1 pro-inflammatory and A2 anti-inflammatory reactive astrocytes emerging in mouse models of neuroinflammation and stroke, with A1 astrocytes being induced by microglial cytokines $IL-1\alpha$, $TNF\alpha$, and C1q (Liddelow et al., 2017). Since then, similar disease-associated populations have been identified across models, species, and pathologies, including AD (often referenced disease-associated astrocytes, DAA, described by Habib et al., 2020; Mathys et al., 2019; Morabito et al., 2021), Parkinson's disease (PD; Smajić et al., 2022), Huntington's disease (HD; Al-Dalahmah et al., 2020), multiple sclerosis (MS; Absinta et al., 2021; Leng et al., 2022; Wheeler et al., 2020), and in stroke (Ma et al., 2022; Shi et al., 2021) and CNS injuries (Li et al., 2022; Zamboni et al., 2020). Interestingly, while the overall astrocyte response is often pathology-specific, these populations share a common transcriptional signature, suggesting that a universal pattern of response to homeostasis disturbance exists and can be potentially targeted in treatment (Liddelow and Barres, 2017).

1.2.2 Oligodendrocytes

Oligodendrocytes are the most prevalent cell type in the white matter. Their basic function is to myelinate neuronal axons and thereby increase the speed of action potential conductance. The myelin sheath is an extension of the oligodendrocyte membrane, highly organized along neuronal axons and forming Ranvier nodes that allow fast saltatory conduction. Myelin is composed of 70-80% lipids and only a few highly specific proteins, such as myelin basic protein (MBP) or proteolipid protein (PLP). In addition, through specialized channels, oligodendrocytes provide metabolic support to neuronal axons, facilitating maintenance and proper function of the myelin sheath (reviewed in Seeker and Williams, 2022; Simons and Nave, 2015).

Oligodendrocytes are a heterogeneous population, and their heterogeneity can be assessed at multiple levels, including morphology, histological and anatomical regions, sex, age, but also developmental origin, stage of differentiation, and of course, transcriptome (Seeker and Williams, 2022). Oligodendrocytes differentiate in at least three waves (Kessaris et al., 2006), and populate the CNS at the stage of proliferative bipolar OPCs. Reaching their final destination, OPCs lose their migration capability and mature into highly branched myelinating oligodendrocytes that extend their processes to nearby axons (Chamling et al., 2021; Marton et al., 2019). These differentiation states in healthy CNS have been also defined in single-cell transcriptomic studies (Marques et al., 2016; Zeisel et al., 2015). The classification by Marques 2016 includes OPC, committed oligodendrocyte precursors (COP), newly formed oligodendrocytes (NFOL), and later myelinating stages, i.e., myelin-forming oligodendrocytes (MFOL)

and mature oligodendrocytes (MOL), and it has been adapted also in later studies (Falcão et al., 2018; Floriddia et al., 2020; Jäkel et al., 2019; Pandey et al., 2022). Moreover, different MOL populations have been found enriched in specific CNS regions, which showed different speed of oligodendrocyte differentiation and distinct stage-dependent response after traumatic injury, implicating their region-, age-, and context-specific functions, and the existence of specialized populations in disease (Floriddia et al., 2020; Marques et al., 2016).

OPCs, sometimes referred to as NG2 glia, are present in developing as well as adult CNS. Typically, they are defined by markers *Pdgfra*, *Cspg4*, and cell cycle genes (Marques et al., 2016). However, heterogeneous subpopulations within OPCs revealed their ability to respond to cytokines and their potential to generate also neurons and astrocytes (Chamling et al., 2021). As such, OPCs/NG2 glia have been shown to act in regeneration following an injury and participate in glial scar formation (Kirdajova et al., 2021; Valny et al., 2018). OPCs also possess phagocytic activity, suggesting their role in debris cleanup in disease (Falcão et al., 2018).

Oligodendrocytes are capable of renewing lost myelin through remyelination, which is orchestrated in cooperation with astrocytes and microglia (Molina-Gonzalez et al., 2023; Shen et al., 2021). While new OPCs are recruited to the lesion site in mice, remyelination in humans is also facilitated by mature oligodendrocytes (Jäkel et al., 2019). Of note, chronic dysfunction of the remyelination pathways often accompanies neurodegenerative diseases.

Perhaps the most studied disease with regards to oligodendrocyte dysfunction is MS, an autoimmune disease characterized by neuroinflammation, demyelination, and axon degeneration (Dobson and Giovannoni, 2019). Populations of oligodendrocytes with increased expression of immune response genes were identified in both MS patient samples (Jäkel et al., 2019) and in the experimental autoimmune encephalomyelitis (EAE) mouse model of MS (Falcão et al., 2018). Since then, oligodendrocyte disease-associated populations have been defined in targeted studies of models of MS, AD and other dementias, neuroinflammation model, and aging white matter (Kaya et al., 2022; Kenigsbuch et al., 2022; Lee et al., 2021; Pandey et al., 2022; Zhou et al., 2020). Surprisingly recurrent gene expression profile of these disease-associated oligodendrocytes (DOLs; Kenigsbuch et al., 2022) includes, among others, the genes *Serpina3n* and *C4b*, and genes of the interferon response and antigen presentation. As proposed by Kaya et al., 2022, the interferon response might be triggered by infiltrating CD8⁺ T-cells, while *Serpina3n* expression may provide protection to specific oligodendrocyte populations against direct damage by immune cells (Falcão et al., 2018). Interestingly, a similar signature has also been identified in astrocytes (Kenigsbuch et al., 2022), suggesting common response patterns across multiple glia cell types.

Most importantly, these studies have drawn attention to the potential active participation of oligodendrocytes in neurodegeneration, questioning previously valid assumptions about their mostly passive role in pathologies. Given that alterations in the oligodendrocyte lineage have been reported in a wide range of diseases, including various AD models (Grubman et al., 2019; Lau et al., 2020; Leng et al., 2021; Mathys et al., 2019; Sadick et al., 2022), PD (Agarwal et al., 2020), ALS (Ferraiuolo et al., 2016; Kang et al., 2013), major depressive disorder (Nagy et al.,

2020), and traumatic injury (Floriddia et al., 2020), more studies targeting oligodendrocytes can be expected in the near future. Nevertheless, considering also the differences in oligodendrocyte function and response to pathology between mouse and human (Jäkel et al., 2019; Pandey et al., 2022; Zhou et al., 2020), more extensive research is needed to uncover the mechanisms by which oligodendrocytes participate in different pathologies and models, their interactions with other cell types, and the therapeutic value of these findings.

1.2.3 Microglia

Microglia are the resident immune cells of the CNS. Their characteristic ramified morphology allows them to constantly actively scan their surroundings for any signals of homeostasis disturbance, sensing through a wide range of receptors for cytokines, hormones, neurotransmitters, or growth factors. Microglia participate in homeostasis maintenance by phagocytosing debris, remnants of apoptotic cells, or misfolded proteins. Additionally, they play a crucial role in developmental and adult synapse formation and plasticity, phagocytosing excessive cells and secreting neurotrophic factors, growth factors, and cytokines (reviewed in Butovsky and Weiner, 2018; Dadwal and Heneka, 2024; Gao et al., 2023).

Microglia belong to glial cells, but developmentally originate in the yolk sac and are members of the erythromyeloid lineage, closely related to macrophages (Ginhoux et al., 2010). They are generated in the first wave of embryonic haematopoiesis, in rodents around embryonic day 7 (Ginhoux et al., 2010) and in human around 28 days of development (Li et al., 2022). As primitive blood circulation forms, they migrate into the developing brain and are further shaped by the CNS environment. In the adult CNS, the microglial population is maintained by local self-renewal (Ajami et al., 2007).

Diverse microglial populations have been described with respect to their localization, expression of specific surface molecules, or appearance under a microscope (Baalman et al., 2015; Bisht et al., 2016; Dadwal and Heneka, 2024; Shigemoto-Mogami et al., 2014). However, recent single-cell transcriptomic studies have provided more detailed insights into microglial heterogeneity. Early microglia are highly proliferative, metabolically active, migratory, and variable, transitioning through intermediate states in their differentiation trajectory (Hammond et al., 2019; Li et al., 2019). At early postnatal days in mouse, axon tract-associated amoeboid microglia (ATM; Hammond et al., 2019) or proliferative region-associated microglia (PAM; Li et al., 2019) with a reactive-like signature were identified in pre-myelinated white matter, representing a transient, regionally restricted population with a specific function, i.e., phagocytosing early oligodendrocytes. Surprisingly, adult homeostatic microglia were shown to be less diverse across CNS regions, all sharing typical microglial markers including *P2ry12*, *Cx3cr1*, or *Tmem119* (Hammond et al., 2019; Li et al., 2019). During aging, inflammatory and interferon-responsive microglial states increase in number, although they do not prevail over normal microglia (Hammond et al., 2019).

Interestingly, reactive microglia in disease seem to recapitulate developmental expression programmes (Hammond et al., 2019), although with additional pathology-specific signatures.

Microgliosis is usually characterized by clonal proliferation, change of morphology to amoeboid, migration, and production of immune response-related molecules (Hammond et al., 2019; Krasemann et al., 2017; Tay et al., 2017). This functional change is accompanied by downregulation of homeostatic markers. While reactive microglia were originally classified into “M1” pro-inflammatory and “M2” anti-inflammatory types, it now appears that these states are much more diverse and dynamic (Gao et al., 2023).

In AD-like pathology, microglia were found to dynamically transition from a homeostatic state to a reactive state and were termed disease-associated (DAM; Keren-Shaul et al., 2017) or activated response microglia (ARM; Sala Frigerio et al., 2019). Upregulation of cell cycle genes was also reported to parallel this transition process. The reactive populations are localized near $A\beta$ plaques and express higher levels of cytokines, MHC molecules, and other immune response genes, many of which belong to AD risk genes (e.g., *ApoE*, *Trem2*, *Lpl*), suggesting an essential role of microglia dysfunction in AD (Keren-Shaul et al., 2017; Sala Frigerio et al., 2019). As proposed by Sala Frigerio et al., 2019 and Ellwanger et al., 2021, homeostatic microglia may also transition into other states characterized by increased interferon response (IRM), cell cycle genes (cycling and proliferating microglia, CPM), or MHC-II expression. Furthermore, a population of white matter-associated microglia (WAM; Safaiyan et al., 2021) dedicated to clearing up myelin debris was identified in aging and AD-affected brains, and rare but highly inflammatory *Ccl4*⁺ microglia were described in aging and demyelinating injury, where they were located within lesions (Hammond et al., 2019). Similar reactive populations have been found in ALS (Keren-Shaul et al., 2017), PD (Smajić et al., 2022), normal aging (Sala Frigerio et al., 2019), spinal cord injury (Matson et al., 2022), and MS model (Krasemann et al., 2017; Masuda et al., 2019). In addition, Masuda et al., 2019 reported temporally and regionally distinct microglial populations reflecting their local specification and unique profiles in neurodegeneration and demyelination models.

Thus, these studies show that within diseased CNS, distinct reactive microglial populations arise from the homeostatic pool. While they are protective at first, chronically activated and dysfunctional microglia contribute to the disease progress. Inhibition of the microglial pro-inflammatory phenotypes is one of the strategies that could be applied in therapy (Butovsky and Weiner, 2018). However, the positive effect of such an approach needs to be assessed with respect to the specific pathology, its stage, and potential effects on other cell types. Of interest for future studies will also be the interactions of microglia with other CNS-resident cell types, as well as peripheral immune cells and the microbiome, and the possible beneficial modulation of this crosstalk (Calafatti et al., 2023; Erny et al., 2015).

1.2.4 Radial glia

Radial glia, sometimes called neural stem cells (NSCs), are progenitor cells that give rise to the majority of cell types in the CNS. They differentiate from neuroepithelial stem cells and are located in the germinal zones around the neural tube. The elongated shape and the apical-basal polarity of radial glia allow them to contact the ventricular zone as well as the pia mater, and

provide a scaffold for newly generated neurons migrating towards the cortical surface and gradually forming six cortical neuronal layers (reviewed in Miranda-Negrón and García-Arrarás, 2022; Zhou et al., 2024; illustrated in **Fig. 1.2**).

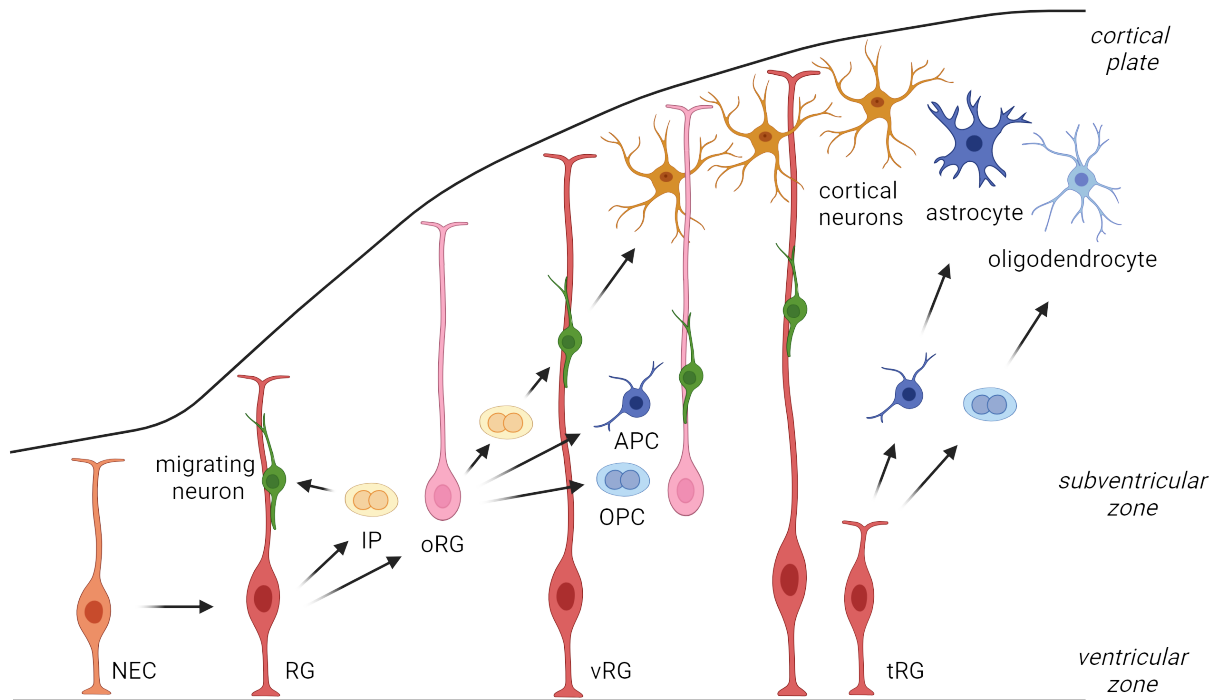


Figure 1.2: A simplified scheme of radial glia differentiation in the human cortex inspired by Zhou et al., 2024. **Abbreviations:** APC – astrocyte progenitor cells, IP – intermediate progenitors, NEC – neuroepithelial cells, OPC – oligodendrocyte progenitor cells, oRG – outer radial glia, RG – radial glia, tRG – truncated radial glia, vRG – ventricular zone radial glia. The image was created with BioRender.com.

In humans, the progressive shift from neuroepithelial identity towards radial glia identity occurs during the first trimester of gravidity. In the early stages, radial glia directly generate the first neurons. More extensive neurogenesis begins later, indirectly through intermediate progenitors (Eze et al., 2021). Since the second trimester, radial glia start to utilize their gliogenic potential, generating $EGFR^+$ glial progenitors that give rise to astrocytes and OPCs (Ramos et al., 2022). Although restricted to specific areas, such as the dentate gyrus of the hippocampus, radial glia-like cells with the potential to proliferate and generate new neurons and glia persist in the primate brain until adulthood (Hao et al., 2022). However, the regenerative capacity of adult mammalian CNS is highly limited and remains debatable (Miranda-Negrón and García-Arrarás, 2022).

The basic transcriptional program of radial glia seems to be conserved across brain regions (Eze et al., 2021; Hendriks et al., 2024), with regional specificity increasing along differentiation trajectory. However, in a study by Lee et al., 2022a, finer resolution and targeted analysis of radial glia revealed their early regional specification in segments of the ganglionic eminence, where distinct types of GABAergic interneurons originate.

The early radial glia differentiation is a continuous process, and the gene expression signatures of the individual progenitor states often overlap. Nevertheless, transcriptomic studies

have helped to distinguish several types of radial glia that can now be routinely identified in sufficiently detailed single-cell studies. *PAX6*, *SOX2*, *GLI3*, or *HES1* can be used as universal markers of radial glia (Camp et al., 2015; Pollen et al., 2015). Radial glia that detach from the ventricular zone and occupy the subventricular zone are called oRG. They are characterized by expression of *MOXD1* and *HOPX* and possess a great neurogenic potential, generating the majority of upper-layer cortical neurons, astrocyte progenitors, and OPCs. Interestingly, oRG are rare in rodents, and they are perhaps one of the prerequisites for the increased complexity of the primate brain compared to other mammals (Pollen et al., 2015). Ventricular zone radial glia (vRG) with cell bodies located in the ventricular zone and processes extending from the apical to the basal surface can be identified by expression of a specific gene set including *TAGLN2* and *FBXO32* (Pollen et al., 2015). During the second trimester of gravidity, vRG detach from the pia mater and terminate in the outer subventricular zone. These truncated radial glia (tRG) adopt a specific gene expression signature represented by *CRYAB* and *NR4A1* (Nowakowski et al., 2016). Besides providing a scaffold for neurons in late neurogenesis, tRG were shown to generate exclusively glial progenitors (Ramos et al., 2022). In addition, glycolytic radial glia are sometimes identified as a separate population (Hendriks et al., 2024). However, this likely reflects a general metabolic preference of progenitors rather than an isolated radial glia subtype (Uzquiano et al., 2022).

Although no neurodegenerative disease-associated populations of radial glia have been identified to date, it is known that dysfunction of neuronal progenitors may severely affect neurodevelopment and CNS structure (Guarnieri et al., 2018; Zhou and Xu, 2023). For example, reduced brain volume and gyrfication resulting from early brain developmental impairment have been described in lissencephaly caused by mutations, e.g., in *reelin* (Igreja et al., 2023) and *doublecortin* (Zare et al., 2019), or in the context of Down syndrome (Baburamani et al., 2020). Additionally, in the adult brain, radial glia-like cancer stem cells have been found within glioblastoma, contributing to its invasiveness and severity (Bhaduri et al., 2020).

Importantly, radial glia express a number of genes, whose levels decrease when entering the neuronal fate but remain detectable in glial progenitors and glia. Therefore, mutations in such proteins may affect not only the mature cell types but also the very early progenitors. GFAP can be an example: its expression in radial glia has been the premise of focusing on the developmental aspect of Alexander disease in our project.

1.3 Models of neurodegenerative diseases

Models of neurodegenerative diseases are designed to mimic human pathology as closely as possible, in all aspects – from genetic causes and molecular mechanisms to the progression of symptoms. Currently, the most widely used models of neurodegenerative diseases are still animal models, especially rodents. However, disease modelling with the use of *in vitro* culture systems and pluripotent stem cells (PSC) is becoming increasingly popular and is well comple-

menting research on animal models. Due to their relevance to this thesis, these model systems will be discussed below, along with their specifics, advantages, and shortcomings.

1.3.1 Animal models

The main advantage of animal models lies in the possibility to model diseases in living organisms genetically close to human, with all their complexities, including mature and functional CNS (MacDougall et al., 2021; Pasko et al., 2022). It is also possible to model diseases in relation to natural processes like aging or interaction with the environment, which is especially important as many neurodegenerative diseases are linked with these effects. The disease-like phenotype and progression of symptoms in animal models can also be tested with various behavioural tests. Moreover, methods of genetic engineering enable genetic labelling of cell populations and creating animals with defined genetic mutations and with transgenes introducing human mutations to animal genome.

However, genetic and phenotypic differences between model animals and humans will always present a challenge in the creation of truly accurate models of human disease. For instance, neurodevelopmental differences between rodents and humans, such as cortical structure, greater heterogeneity of precursors, or a different neurodevelopmental timeline, impede the modelling of neurodevelopmental disorders in rodents (reviewed in Zhang et al., 2023a). Conversely, the limited lifespan of laboratory rodents does not allow aging-related diseases to fully develop, raising the need to artificially accelerate the progression in the designed models (Dawson et al., 2018; MacDougall et al., 2021). Furthermore, as many neurodegenerative diseases have a complex etiology, the animal models need to take advantage of familial forms of the disease, focusing only on selected disease variants with known causative mutations and simplifying the human pathology (Chen and Zhang, 2022; Dawson et al., 2018; MacDougall et al., 2021).

To provide specific examples, AD rodent models are often based on mutations in *APOE*, *PSEN1*, and *PSEN2*, which are linked to a less common, familial form of AD (fAD; reviewed in Chen and Zhang, 2022). A widely used 5xFAD mouse carrying multiple fAD-linked mutations (Oakley et al., 2006) recapitulates several AD hallmarks including amyloidosis, neuronal loss, impaired motor function, altered gene expression, and involvement of the immune system, but lacks the tau pathology and does not fully mimic the cognitive aspect of AD (Oblak et al., 2021).

Similarly, SOD1-mutant models belong to a valuable source of information on ALS pathology, modelling SOD1 accumulation, progressive motor impairment, motor neuron loss, and gliosis, which are well documented in the spinal cord (Dawson et al., 2018; Gurney et al., 1994; Maniatis et al., 2019). However, disputable data exist on the cortical pathology in this model, ranging from no effect (D'Arrigo et al., 2010; Niessen et al., 2006) to early motor neuron loss with astrogliosis and microgliosis (Gomes et al., 2019; Migliarini et al., 2021; Özdinler et al., 2011). Moreover, SOD1 models lack the TDP-43 pathology presented by its aggregation and altered metabolism, which normally occur in ALS patients (Dawson et al., 2018; Ling et al., 2013). Therefore, separate models of ALS with genetically defined TDP-43 pathology (Huang et al., 2020), or mutations in other ALS-linked genes such as *FUS* or *C9ORF72* (O'Rourke

et al., 2015; Qiu et al., 2014) need to be used to mimic other ALS variants. Alternatively, the *wobbler* mouse, which resulted from a spontaneous mutation in the *Vps54* gene, can be used to model motor neuron degeneration. However, this mutation has not been associated with ALS in humans (Moser et al., 2013). Given that each mutation represents only a minority of familial ALS cases (Zou et al., 2017) if they occur at all, there is a need for a more complex ALS model encompassing multiple aspects of the human disease, which does not exist to date.

In diseases determined by a single mutation, such as AxD, the design of adequate models appears simpler, but also has its shortcomings. Pivotal studies using transgenic mouse models and knock-ins revealed the basis of GFAP mutations in AxD. It was shown that an increased expression of GFAP is sufficient to induce the formation of RFs and profound gene expression changes (Hagemann et al., 2005), and this AxD-like pathology was worsened by a GFAP mutation (Hagemann et al., 2006). On the contrary, the mutation without overexpression did not lead to an AxD-like phenotype (Tanaka et al., 2007). Nevertheless, all of these early models share an important limitation – the absence of white matter pathology and motor dysfunction (Hagemann et al., 2005, 2006; Tanaka et al., 2007). This was overcome in a rat model carrying a GFAP mutation orthologous to human (Hagemann et al., 2021), developing a severe phenotype accompanied by white matter pathology and showing that distinct rodent species may have a different disease modelling potential.

Overall, even partially accurate animal models have historically revealed much about disease mechanisms in neurodegeneration, and have guided the design and testing of treatment strategies. Therefore, despite the emergence of alternative modelling approaches, they still remain irreplaceable in neuroscience.

1.3.2 *In vitro* models

Cell culture models provide the possibility to study neurodevelopmental and neurodegenerative diseases in human cells, either in primary cultures or cultures derived from PSCs. With the use of defined differentiation factors, PSCs, either embryonic (ESC) or iPSCs, can be directed towards different CNS cell fates, including neurons (Lin et al., 2021) and their subtypes like GABAergic neurons (Grigor'eva et al., 2020) and motor neurons (Fujimori et al., 2018), or astrocytes (Canals et al., 2018), oligodendrocytes (Ehrlich et al., 2017), and microglia (Lanfer et al., 2022). These cells show morphological and functional features resembling the respective cell types *in vivo*, including branching, signal transmission, and responsiveness (Canals et al., 2018; Ehrlich et al., 2017; Grigor'eva et al., 2020; Lanfer et al., 2022). Moreover, through controlled cultivation conditions, the cells can be exposed to various external factors, simulating the disease environment. With respect to neurodegeneration, the relevant factors include oxygen-glucose deprivation simulating stroke (Tasca et al., 2015), bacterial lipopolysaccharide inducing neuroinflammation (Lanfer et al., 2022; Leng et al., 2022), conditioned media (Polazzi and Contestabile, 2003), or other cell types in a co-culture system (Luchena et al., 2022).

In order to better approximate the *in vivo* environment, iPSCs can be cultivated in a 3D culture supplemented with tissue patterning factors and ECM-like scaffold to generate organoids

(Lancaster and Knoblich, 2014), including so-called “mini-brains”. Cerebral or whole-brain organoids take advantage of the natural self-organizing capability of iPSCs, which results in formation of embryoid bodies, neuroectoderm, and finally, structured brain-like tissue with organized progenitor zones, separated brain regions, and distinct neuronal populations assembling to functional neuronal networks (Lancaster et al., 2013; Quadrato et al., 2017). At later timepoints, glia emerge within organoids as well (Marton et al., 2019; Quadrato et al., 2017; Verkerke et al., 2024).

Multiple studies have confirmed the accuracy of the brain organoid model and its resemblance to the fetal CNS (Camp et al., 2015; Quadrato et al., 2017; Velasco et al., 2019). Therefore, within a relatively short time period, organoids recapitulate major developmental milestones, which enables modelling of neurodevelopmental disorders such as microcephaly (Lancaster et al., 2013) and autism spectrum disorders (Li et al., 2023). Although the modelling of adult-onset neurodegeneration is limited by the lack of natural aging in organoids, they offer the possibility to model early, pre-symptomatic changes, which have so far been understudied in pathologies such as AD (Fiock et al., 2020), ALS (Szebenyi et al., 2021), frontotemporal dementia (Bowles et al., 2021), and HD (Mehta et al., 2018).

Diseases with selectively vulnerable CNS regions or neuronal populations can be modelled using organoids more stringently directed toward the cortex (Yoon et al., 2019), hypothalamus (Huang et al., 2021), midbrain (Smits et al., 2019), or highly specialized structures like the neuromuscular junction (Pereira et al., 2021). In addition, different types of brain organoids can be co-cultured together as assembloids, modelling interaction between brain regions. For instance, assembloids of dorsal and ventral cortical organoids can be used for studying neurodevelopmental diseases caused by impaired neuronal migration patterns (Birey et al., 2017).

Fine-tuned approaches facilitating even better representation of the *in vivo* tissue are constantly being developed. Modelling of diseases with a strong influence of environment or aging like MS can be improved by cell reprogramming with retained epigenetic information (Park et al., 2024). To complement the brain organoids with the immune system component, microglia can be introduced by co-cultivation with PSC-derived microglia (Xu et al., 2021). Alternatively, only with a little protocol modification, microglia can naturally differentiate from mesodermal progenitors within freely differentiating whole-brain organoids (Ormel et al., 2018). Furthermore, due to the absence of vasculature, organoids develop a necrotic core and grow only to a limited size (Lancaster et al., 2013). This can be resolved by co-cultivation with endothelial or vascular organoids (Song et al., 2019; Sun et al., 2022) and integration with microfluidic chips (Salmon et al., 2022). Organoids can also be transplanted into mouse brains, which directly provide the *in vivo* environment and vasculature, increasing heterogeneity and maturation level of the organoids (Wang et al., 2024).

Despite the abovementioned enhancements, cell cultures are still highly isolated systems, reliant on the culture conditions. Even minor deviations in protocols can have large impacts on organoid patterning, potentially introducing unwanted batch effects and variability (Jensen and Little, 2023; Quadrato et al., 2017; Sanchís-Calleja et al., 2024). While whole-brain organoids

are more variable and can develop cells from other than neuroectodermal origin, the directed organoids show greater specificity and reproducibility (Quadrato et al., 2017; Velasco et al., 2019). An additional level of variability is introduced by cell lines themselves, as they may show a cell line-specific differentiation efficiency (Jerber et al., 2021) and can develop variable cell population proportions within organoids (Kanton et al., 2019). Therefore, an optimal experimental design should consider the sources of variability and, accordingly, determine the appropriate number of replicates, batches, and cell lines.

Overall, while cell cultures do not fully substitute for *in vivo* animal models, they may facilitate the reduction of their total numbers used in research (Grimm et al., 2023) and provide a solution for modelling diseases where good animal models are lacking. The usage of established cell lines can also help to overcome legal struggles of working with fetal or patient material or the lack of samples from biopsies. Furthermore, the continually expanding range of methods enables disease modelling in complex systems of patient-derived cells, which also represents the foundation of personalized medicine.

1.4 High-throughput transcriptomic methods

Transcriptomic methods have been used to map active gene expression at the level of mRNA. Historically, multiple strategies were developed to capture and quantify RNA, including Northern blotting, expressed sequence tags (EST), or serial analysis of gene expression (SAGE) (Lowe et al., 2017). However, all became obsolete with the introduction of reverse transcription quantitative polymerase chain reaction (RT-qPCR) and microarrays, which, until recently, were the dominant techniques used for gene expression profiling. Despite the limited sample size and number of profiled genes, RT-qPCR remains popular for its sensitivity, simplicity, and low cost, especially in diagnostics and for validation of other experimental data. Microarrays, while capable of profiling thousands of genes at once, are limited to bulk samples, though some single-cell applications have been reported (Esumi et al., 2008). With the reduction of costs and increased throughput of next-generation sequencing (NGS) methods, microarrays have been overshadowed by RNA sequencing, allowing for truly large-scale, high-resolution gene expression profiling. The RNA sequencing process from library construction to data analysis is illustrated in **Fig. 1.3** and is discussed in this chapter.

1.4.1 Bulk RNA sequencing libraries

Bulk RNA sequencing does not require any specialized sample preparation, except for the isolation of RNA in sufficient amount and quality. Usually, total RNA is isolated from samples by standard procedures like phenol-chloroform extraction (TRIzol) or extraction with silicate columns (Scholes and Lewis, 2020). Sequencing libraries are then prepared with commercially available kits that ensure compatibility with sequencing technologies.

To illustrate the library preparation process, QuantSeq 3' mRNA-Seq Library Prep Kit (Lexogen; Moll et al., 2014) can serve as an example. Optimally, QuantSeq requires 1–500 ng of

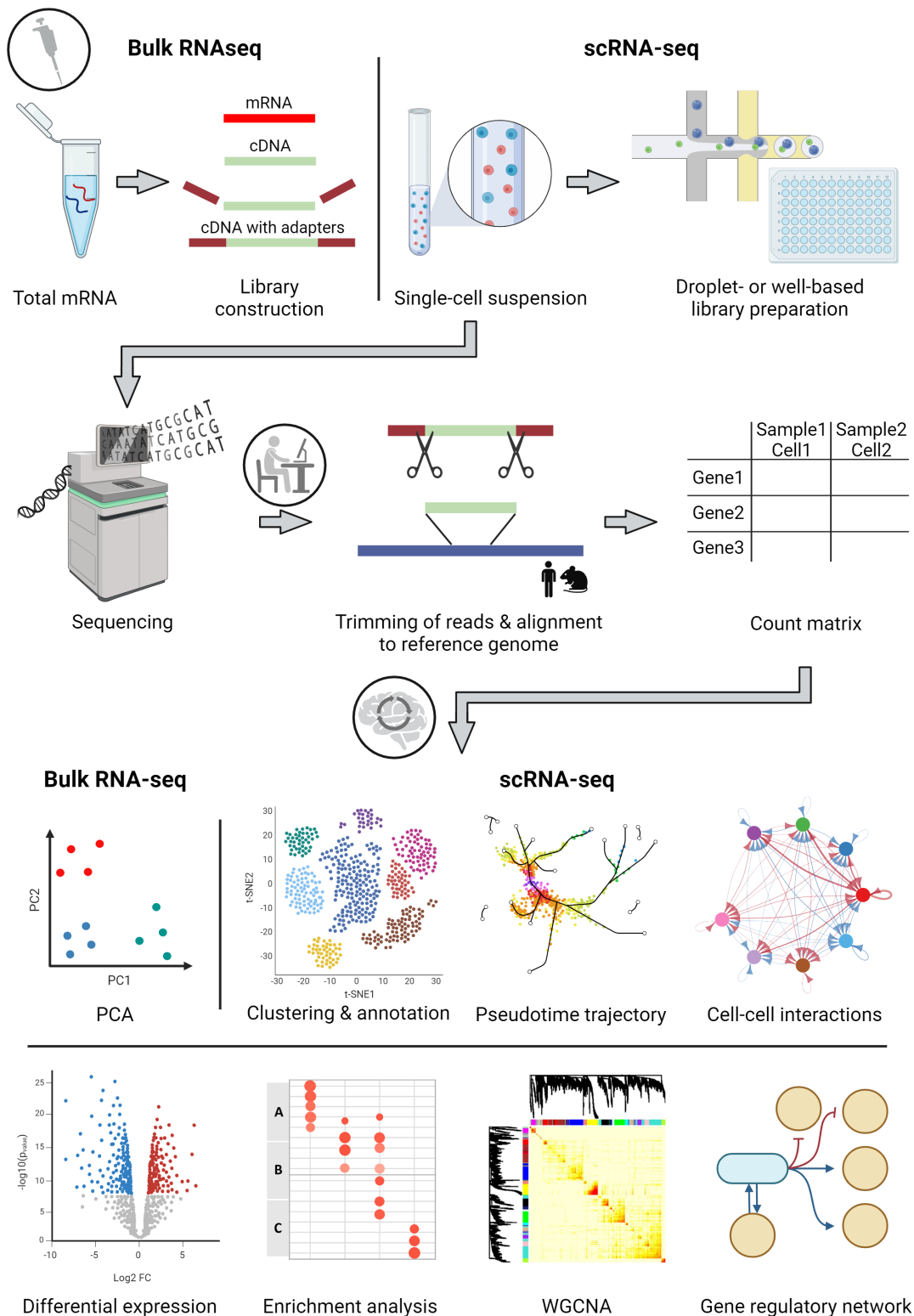


Figure 1.3: Schematic overview of RNA sequencing experiments, from library preparation to data pre-processing and analysis. The image was created with BioRender.com, WGCNA plot from Langfelder and Horvath, 2008. **Abbreviations:** PCA – principal component analysis, WGCNA – weighted gene co-expression network analysis.

total RNA as input, but an even smaller amount can be processed with modifications of the protocol. The quality of input RNA can be assessed using the 260/280 and 260/230 ratios and the RNA integrity number (RIN; Schroeder et al., 2006). Using poly(T) primers, only pro-

tein coding sequences are converted to cDNA, minimizing contamination with highly abundant rRNA or mtRNA transcripts without the poly(A) tail. In several steps, adapters and sample-identifying indices compatible with Illumina sequencing are attached, the library is amplified in polymerase chain reaction (PCR), and purified using magnetic beads, targeting the average library size of 200–300 bp. Control of quality, concentration, and library size is performed with microcapillary electrophoresis.

The process described above is applicable for gene expression profiling experiments, where the ultimate goal is to identify and quantify transcripts for the purposes of differential gene expression analysis. For that, 3'-end-targeting protocols generating short fragments are sufficient (Ma et al., 2019). However, for the detection of novel transcripts or splice variants, full-length sequencing is recommended. Furthermore, specialized protocols are available for small RNA profiling (Benesova et al., 2021), where an enrichment for short RNAs without the poly(A) tail is desired.

In general, profiling of thousands of genes from total RNA in tens of samples in one experiment represents the main advantage of bulk RNA-seq. Such “screening” experiments may provide important clues and insights into processes ongoing in the samples of interest, i.e., pathology, treatment, or time scales. Nonetheless, without prior sorting of cell types, the contribution of individual cell populations cannot be distinguished by bulk RNA-seq, and alternative approaches have been developed to overcome this shortcoming.

1.4.2 Single-cell RNA sequencing libraries

Single-cell RNA-seq overcomes an important limitation of bulk RNA-seq, and that is the single-cell resolution allowing for assessment of cell type heterogeneity. The sample and library preparation process requires additional steps, in which a single-cell suspension is generated and cellular identity is preserved by barcoding of transcripts with unique cell-specific oligonucleotide sequences. The library preparation protocols often introduce also unique molecular identifiers (UMI), which are specific for each transcript and facilitate more precise transcript counting (Islam et al., 2014).

Mechanical and enzymatic dissociation (e.g., with papain, accutase, or trypsin) followed by straining are commonly applied to achieve high-quality suspension without cell clumps (Lafzi et al., 2018). Ideal dissociation conditions usually need to be optimized with respect to the specific sample type. For example, cell cultures like brain organoids, which do not contain a strong ECM scaffold or myelin, require only enzymatic and very gentle mechanical dissociation with wide-bore pipettes (Kanton et al., 2019), while harsher mechanical dissociation with pre-mincing and Douncer homogenization might be necessary in primary brain tissue samples (Hammond et al., 2019).

Cell suspensions prepared from live cells need to be immediately processed to avoid any technical artifacts. Sample preparation has been shown to induce activation of immediate early genes, especially in highly sensitive cell types such as microglia (Marsh et al., 2022). Therefore, adjustments in the cell preparation protocols like the use of transcriptional and transla-

tional inhibitors (Marsh et al., 2022) or operating in cold conditions (Hammond et al., 2019; Sala Frigerio et al., 2019) are necessary to increase the biological accuracy of single-cell experiments. As fragile cell types are often underrepresented in single-cell data, enrichment of cell populations with sorting based on specific surface markers can also be used to achieve better resolution (Sadick et al., 2022).

In experiments with brain tissue containing many highly branched and sensitive cell types, isolation of nuclei instead of whole cells is often the preferable option (as in, e.g., Habib et al., 2020; Mathys et al., 2019; Sadick et al., 2022). Single-nucleus RNA-seq (snRNA-seq) has been shown to preserve the cellular identity of neurons and glia and yield results comparable to scRNA-seq (Bakken et al., 2018; Gerrits et al., 2020). Fixation of the suspension using methanol-based protocols with long-term storing at -80°C can also be applied without a substantial loss of information (Alles et al., 2017). Both alternatives are especially convenient when a delay between sample collection and processing is expected, for example in patient-derived samples or in studies involving several timepoints. Importantly, fixed samples are nowadays supported by the most popular single-cell library preparation protocols.

Single-cell or single-nucleus suspension is further processed using one of the strategies for cell separation and barcoding resulting in final sequencing library. The appropriate method needs to be selected based on prior hypotheses, expected resolution, and cost and labour efficiency. A comparison of throughput, demands, and costs of some of the popular commercially available methods can be found in **Tab. 1.2**. Based on the strategy of separation and labelling of single cells, these methods can be grouped into well-based and droplet-based technologies.

Table 1.2: Table comparing main characteristics of selected scRNA-seq technologies. Data from De Simone et al., 2024; Haque et al., 2017, and the respective manufacturers.

Technology	Throughput	Requirements	Coverage	Cell ID	Costs	Reference
Chromium (10X Genomics)	< 10,000 cells/sample, 8 samples/chip	Chromium controller	3'-end, 5'-end, or probes	droplets with barcodes	\$\$\$	Zheng et al., 2017
Smart-seq2	1 cell per well in 96/384 plates	no instrument	full-length	i5 and i7 Illumina indices	\$\$	Picelli et al., 2013
Smart-seq3xpress	1 cell per well in 384 plates	no instrument	full-length	i5 and i7 Illumina indices	\$	Hagemann-Jensen et al., 2022
PIPseq TM (Fluent BioSciences)	< 20,000 cells/sample, < 8 samples	vortex	3'-end	droplets with barcodes	\$	Clark et al., 2023
Evercode TM WT (Parse Biosciences)	scalable: hundreds to thousands of cells, < 96 samples	no instrument	full-length with 3'-end bias	split-pool barcoding in wells	\$	Rosenberg et al., 2018
Single Cell RNA Kit (Scale Biosciences)	scalable: < 500,000 cells, tens to hundreds of samples	no instrument	3'-end	split-pool barcoding in wells	\$	Cao et al., 2017

Well-based technologies, such as Smart-seq (Hagemann-Jensen et al., 2022; Picelli et al., 2013, 2014), use 96 or 384-well plates, each containing a single cell that has been sorted by one of the cell sorting methods. Individual reactions are, therefore, completely separated, until the final pooling of the sequencing library, which follows the introduction of cell-specific combinations of Illumina i5 and i7 indices.

In droplet-based technologies, the single cells are mixed with gel beads in emulsion, resulting in the encapsulation of cells in droplets (Zheng et al., 2017). Each droplet represents a stand-alone reaction chamber containing cell-specific barcodes, oligo(dT) primers, UMIs, and sequencing adaptors. A widely used protocol provided by 10X Genomics requires the use of an 8-sample microfluidic chip along with a microfluidic device (the Chromium controller), which substantially increases the price of such scRNA-seq experiment.

In a comparative study by Wang et al., 2021b, Smart-seq2 proved to capture more genes per cell than the 10X Genomics method and enabled the detection of alternative splicing thanks to full-length sequencing. On the other hand, despite increased noise in 10X Genomics data, high numbers of captured cells facilitated higher resolution of this method and identification of rare cell populations. In general, well-based methods are usually cost- and labour-efficient in small-scale experiments counting hundreds of cells, with sample size limited only by the number of simultaneously processed plates. The 10X technology is applicable for large-scale experiments, where thousands of cells per sample are profiled at once. The default lower sample size can be increased using multiplexing methods, although this comes at additional costs.

Recently introduced alternative technologies offer a solution largely scalable to high cell and sample numbers. For example, particle-templated instant partition sequencing (PIPseq) by Fluent BioSciences captures cells in droplets only by emulsification with vortexing (Clark et al., 2023). Another approach that takes advantage of combinatorial barcoding, uniquely labelling cells in several rounds of suspension splitting, barcoding, and pooling, which can be done in microwells, was developed as split pool ligation-based transcriptome sequencing (SPLiT-seq; Rosenberg et al., 2018) and as single-cell combinatorial indexing RNA sequencing (sci-RNA-seq; Cao et al., 2017). Both technologies are now commercially offered by two rival companies – Parse Biosciences and Scale Biosciences, respectively. In addition, these protocols do not require any specialized instruments, which makes them very attractive alternatives to the other existing technologies.

Regardless of technology, single-cell library preparation is a rather straightforward process requiring following the manufacturer's instructions. However, a number of aspects need to be considered beforehand, as a precise experimental design is crucial for such experiments. Firstly, the single-cell preparation process should be optimized for every sample type so that high-quality suspensions are generated. Secondly, the choice of the appropriate library generation and sequencing strategies should be aligned with the number of samples and conditions entering the analysis, targeted cell numbers, the total amount of information expected to be recovered, and the available resources. Finally, prior knowledge and well-defined hypotheses are essential and can markedly aid in data analysis.

1.4.3 Sequencing considerations

The selection of optimal sequencing strategy belongs to the important aspects of bulk and scRNA-seq experimental design, as sequencing accounts for a large portion of the total experimental costs. The options to be considered include sequencing technology, depth, and coverage, all with respect to the experimental questions and the total number of samples and cells.

Currently, the most widely used and supported sequencing technology suitable for gene expression profiling is provided by Illumina. A general recommendation from Illumina is that bulk gene expression profiling requires 50–75 bp single-end reads totalling 5–25 million reads per sample. For comparison, transcriptome-mapping experiments benefit from paired-end sequencing with 75- or 100-bp reads, counting up to 200 million reads per sample (Illumina.com, 2024). In the case of single-cell gene expression profiling, the read counts depend on the library preparation strategy and the number of sequencing cycles. For example, full-length protocols typically require 1 million reads per cell, while in 3'-end-targeting protocols, 10–100 thousand reads per cell are sufficient (Haque et al., 2017; Illumina, Inc., 2024).

Other sequencing technologies, such as NanoPore, offering long-read sequencing of whole DNA or RNA molecules, promise to provide full-length information unbiased by library fragmentation and amplification. Single-cell application has been implemented as well, in combination with modified 10X library preparation protocol (Shiau et al., 2023) and coupled with short-read Illumina sequencing (Wang et al., 2021a). However, as the Nanopore technology is still associated with a high error rate, its real benefits for gene expression profiling are yet to be determined.

1.4.4 Data analysis

Pre-processing

Sequencing data analysis involves several pre-processing steps, including quality control of the sequencing output, demultiplexing, recognition and removal of artificially introduced sequences such as barcodes or sequencing indices, and alignment to the appropriate reference genome (Lafzi et al., 2018). In scRNA-seq data, it is also necessary to distinguish wells or droplets that are empty or contain highly damaged cells. Companies providing the scRNA-seq library preparation kits, such as 10X Genomics and Parse Biosciences, offer their own software allowing for standardized automatized pre-processing and downstream analysis (e.g., Cell Ranger software by 10X Genomics, Zheng et al., 2017, and Parse pipeline by Parse Biosciences). In addition, a wide range of tools in various programming languages is available for each pre-processing step (see database at <http://www.scrna-tools.org/>; Zappia et al., 2018). They facilitate better control over parameter settings and customization of individual steps. Ultimately, the pre-processing generates a count matrix with thousands of genes and individual samples in bulk RNA-seq or individual barcoded cells in scRNA-seq data.

Normalization and clustering

Various pipelines for further processing and analysis of the data have been developed and implement a number of statistical methods to efficiently handle large datasets with great biological and technical variability and noise. R programming language (R Core Team, 2022) with the DESeq2 package (Love et al., 2014) and the Seurat package (Hao et al., 2021) belong to the widely used pipelines for analysis of bulk and single-cell RNA-seq data, respectively, and will henceforth be mostly referred to.

Data normalization enabling inter-sample comparisons is one of the first steps in an analysis. Normalization of bulk data with DESeq2 includes the estimation of sample-specific size factors, accounting for varying sequencing depths across samples (Anders and Huber, 2010). In scRNA-seq data, which need to control for variability between individual cells, this is achieved with specialized methods within the Seurat package (Hafemeister and Satija, 2019).

Considering the high dimensionality of RNA-seq data, dimensionality reduction needs to be applied to identify the sources of variability. Principal component analysis (PCA) is a convenient way to do so in bulk RNA-seq data, with data points representing individual samples (Koch et al., 2018). Therefore, PCA can reveal outliers or inter-sample comparisons that may be worth investigating in differential expression analysis (DEA).

In scRNA-seq datasets, linear “pre-reduction” PCA is usually followed by another, non-linear dimensionality reduction method, most often the uniform manifold approximation and projection (UMAP) or the t-distributed stochastic neighbourhood embedding (t-SNE) (Xiang et al., 2021). These plots visualize cells as data points in a 2D space, preserving their local relationships. The cells are then clustered based on similarities in their expression profile and mapped onto the UMAP or t-SNE plots, revealing separate cell populations. The optimal clustering resolution needs to be defined so that it corresponds to the biological composition of the samples as well as possible. This can be achieved either manually or using an objective analysis (Liu et al., 2021).

Marker genes of clusters can be calculated with one of the available tools (Pullin and McCarthy, 2024) comparing gene expression in one cluster with all others. Based on the marker genes, the biological cell populations can be annotated either using automated annotators or manually (Pasquini et al., 2021). While automated annotation is often reliable for identification of distinct cell types, such as neurons or glia, a detailed characterization of cell types and their subpopulations might require manual annotation coordinated with known marker genes and literature.

Quality control

Quality control of scRNA-seq data can be performed at multiple stages during analysis. Number of genes, number of transcripts, percentage of mitochondrial RNA, and percentage of ribosomal RNA per cell, cluster, or sample are examples of metrics that should be used to assess data quality (Ilicic et al., 2016). Cells or whole clusters with too few genes and transcripts and/or too high a percentage of mitochondrial and ribosomal genes may be of low quality, potentially

introducing bias if they are kept in the dataset. High numbers of transcripts, on the other hand, may indicate the presence of multiplets in droplet-based experiments. These can be controlled by packages such as DoubletFinder (McGinnis et al., 2019). Importantly, the optimal thresholds for filtering based on these metrics may differ across datasets. Therefore, quality control criteria need to be determined specifically for each dataset, as they largely depend on library preparation and sequencing techniques, cell type composition, and sample origin.

Down-stream analyses

Analyses performed after the single-cell data cleanup usually involve a descriptive analysis of cell populations, such as assessment of the differential abundance of clusters between conditions and identification of clusters with condition-specific gene expression supported by statistics. This can be achieved through functions within the Seurat pipeline or with the use of specialized packages (Skinnider et al., 2021; Zhao et al., 2021).

Selected clusters or the whole single-cell, as well as bulk datasets, are usually subjected to DEA, identifying differentially expressed genes (DEGs) between conditions of interest using one of the available tools (Nguyen et al., 2023). Seurat's *FindMarkers()* function offers multiple options with respect to the statistical tests that can be applied, including Wilcoxon or *t*-test (Hao et al., 2021). In DESeq2, a statistical model used for testing must be defined to indicate relationships between variables (Love et al., 2014). The Wald test is then applied in simple experimental designs, while the likelihood-ratio test (LRT) can be selected typically in more complex time-scale experiments. The DEA results can be further filtered for adjusted *p*-value after *p*-value correction for multiple comparisons and often also \log_2 fold change to obtain the most biologically relevant DEGs.

When a large number of DEGs are detected, it is beneficial to include also an enrichment analysis that links the DEGs to biological processes, cell compartments, or disease profiles. Gene Ontology (Gene Ontology Consortium, 2021), KEGG (Kanehisa and Goto, 2000), or Wiki pathways (Agrawal et al., 2024) are examples of commonly used databases of biological terms that are manually curated and hierarchical. Over-representation analysis (ORA; Draghici et al., 2003), which uses a list of filtered DEGs as input, or Gene set enrichment analysis (GSEA; Subramanian et al., 2005) that works with a complete ranked gene list can be performed either in R with, for example, the clusterProfiler package (Wu et al., 2021), or using online tools such as WebGestalt (Liao et al., 2019).

DEGs can also be clustered into modules that follow similar expression patterns and might be co-regulated. Weighted gene co-expression network analysis (WGCNA; Langfelder and Horvath, 2008) or its alternatives can facilitate this task. Tools for identification of transcriptional regulators and regulons in single-cell datasets are available as well, with SCENIC being one of the popular examples (Aibar et al., 2017).

In studies where a variety of differentiation states is expected, pseudotime trajectory analysis implemented by the Monocle package (Trapnell et al., 2014) can be used to order cells along pseudotime based on dynamic changes in their expression profiles. Alternatively, RNA velocity

analysis can be used to estimate cellular differentiation states by recognizing spliced and unspliced variants of transcripts (La Manno et al., 2018). These analyses may aid in answering questions about developmental relationships between cell states and their diversification from common progenitors, and reveal genes regulated along differentiation trajectories.

Interactions between cell populations can be assessed using one of the available packages that detect ligand and receptor pairs in the analyzed dataset (Wang et al., 2022). Manually curated (CellChat; Jin et al., 2021) or more automated and extensive databases of cell-cell interactions (NicheNet; Browaeys et al., 2020) can be used for this purpose.

The wide spectrum of available tools offers countless ways how to approach the analysis, mine the data, and generate large amounts of results. Therefore, the choice of the optimal approach depends on the experimental design, the nature of the samples, the research questions, and the underlying biology, ideally resulting in logically ordered and meaningful analysis steps. Numerous benchmarking studies comparing different methods exist and may aid in selecting the most convenient approach in individual cases.

Data interpretation

Analysis of RNA-seq and scRNA-seq/snRNA-seq data is often an iterative process. Therefore, data processing and analyses should be well documented to ensure reproducibility of the results. Importantly, all of the abovementioned analyses and packages offer a variety of visualization options that facilitate better understanding and interpretation of the results and allow their visually appealing presentation.

The data interpretation is largely dependent on alignment with published reference datasets and other available resources. Data integration with Seurat can be used to overlay several datasets, minimizing technical variability and batch effect, albeit potentially losing modest biological heterogeneity (Hao et al., 2021). Existing datasets can also be explored in databases (Franzén et al., 2019) or as comprehensive tissue atlases (Eze et al., 2021; Yao et al., 2023), whose ultimate goal is to map tissue heterogeneity of human or animal models in health as well as in disease.

To ensure the biological relevance of the conclusions resulting from RNA-seq experiments, independent validation experiments always need to be performed following the RNA-seq analysis. While RT-qPCR, independent RNA-seq experiments, or *in situ* hybridization can be used to validate the conclusions at the level of mRNA, immunohistochemistry, Western blot, or mass spectrometry can provide information about the protein level. Correlation between mRNA and protein levels is also an interesting path to pursue when addressing biological problems with large-scale methods. Moreover, technologies derived from classic RNA-seq such as spatial transcriptomics (Ståhl et al., 2016) or ATAC-seq (Buenrostro et al., 2015) may provide additional information regarding the spatial location of cell populations and transcripts within histological sections of the tissue or map regions of accessible chromatin, respectively. Thus, multiomics and a combination of methods can give a more robust view considering multiple levels of gene expression and its regulation.

2 Aims of the thesis

This thesis aims to introduce the application of scRNA-seq in the characterization of different neurodegenerative diseases. Recent research has shown substantial involvement of glia in the onset and progression of neurodegeneration. With its capability to distinguish cell populations at high resolution, scRNA-seq can be used to characterize even small disease-related populations of neurons and glia either at later stages of the disease or at very early stages even before the onset of any symptoms. A variety of disease-related populations with characteristic transcriptional profiles have already been identified. Interestingly, these profiles are partially shared among different pathologies, while maintaining pathology-specific features.

Moreover, combined with iPSC-derived models such as brain organoids, scRNA-seq represents a powerful approach to reveal developmental changes linked with disease-causing mutations, that are almost impossible to be studied in patients. Recently, many studies utilizing organoids and large-scale transcriptomics have emerged offering detailed analyses of models of human organs in health, disease, and development.

ScRNA-seq, especially in combination with other multiomic methods can provide new insights into the pathogenesis of neurodegeneration, clarify the beneficial or negative role of disease-related cell populations, and reveal druggable targets in the form of gene expression regulators, structural and secreted proteins, or entire signalling pathways that are disturbed in disease.

In our projects, we addressed the role of glia in a frequently used mouse model of ALS, and we introduced a novel model of AxD with a remarkable differentiation phenotype, potentially directing future research toward previously unexplored areas. The aims of this thesis can be summarized into the following goals:

1. Characterize transcriptomic changes in the cortical glia of the SOD1(G93A) mouse model of ALS at the single-cell resolution and address the controversial question of the involvement of the cortex in the ALS-like pathology in this model. **(Publication I)**
2. Using scRNA-seq, assess transcriptional profiles of novel hiPSC-derived models of AxD and identify GFAP mutation-related changes causing the abnormal phenotype observed in these models. **(Publication II)**

3 Experimental part

During my Ph.D. studies, I have participated in the preparation of five publications that have been published in impacted scientific journals. Two of them are my first author primary research publications (in shared first authorship) and are listed below in the Results section for their relevance to this doctoral thesis. A brief summary of their contents can be found underneath each citation along with specification of my contribution, followed by copies of the respective papers. In the Methods section, the methods used in these studies are listed and divided based on the contribution of the authors.

The list of other publications and manuscripts consists of all other co-authored work either published or in preparation, including two mini-reviews on the topic of astrocyte and oligodendrocyte populations identified in single-cell transcriptomic studies, and three research papers, where I was involved in the transcriptomic data analysis part of the work.

3.1 Results

• Publication I

Filipi, T.*, Matusova, Z.*, Abaffy, P., Vanatko, O., Tureckova, J., Benesova, S., Kubiskova, M., Kirdajova, D., Zahumensky, D., Valihrach, L., Anderova, M. **Cortical glia in SOD1-(G93A) mice are subtly affected by ALS-like pathology.** *Scientific Reports*, 13(1):6538, 2023. doi: 10.1038/s41598-023-33608-y.

* shared first authors

Journal: *Scientific Reports*, IF 3.8 (2023)

Summary: In this project, we applied single-cell transcriptomics on the cortex of the SOD1-(G93A) mouse model of ALS. In the context of the pathology in mouse models of ALS, the cortex is an understudied region and the available studies offer contradicting conclusions regarding its involvement in the pathology. Enriching for glial cells within our samples, we aimed to characterize different populations of astrocytes, oligodendrocytes, and microglia in the cortex of the SOD1(G93A) model and identify differences in gene expression between SOD1 model and controls at the single-cell level. Our results showed only mild signs of activation of microglia and oligodendrocytes. Despite its popularity, this model does not recapitulate the human disease to its full extent and should not be used for modelling the cortical pathology in ALS.

Contribution: I contributed to this project with the analysis and interpretation of the scRNA-seq data. I was involved in the manuscript text preparation and its final proofreading and editing, with a special focus on the transcriptomic part and the respective figures.



OPEN

Cortical glia in SOD1(G93A) mice are subtly affected by ALS-like pathology

Tereza Filipi^{1,2,7}, Zuzana Matusova^{3,4,7}, Pavel Abaffy³, Ondrej Vanatko^{1,2}, Jana Tureckova¹, Sarka Benesova^{3,5}, Monika Kubiskova¹, Denisa Kirdajova¹, Jakub Zahumensky⁶, Lukas Valihrach³✉ & Miroslava Anderova¹✉

The role of glia in amyotrophic lateral sclerosis (ALS) is undeniable. Their disease-related activity has been extensively studied in the spinal cord, but only partly in the brain. We present herein a comprehensive study of glia in the cortex of SOD1(G93A) mice—a widely used model of ALS. Using single-cell RNA sequencing (scRNA-seq) and immunohistochemistry, we inspected astrocytes, microglia, and oligodendrocytes, in four stages of the disease, respecting the factor of sex. We report minimal changes of glia throughout the disease progression and regardless of sex. Pseudobulk and single-cell analyses revealed subtle disease-related transcriptional alterations at the end-stage in microglia and oligodendrocytes, which were supported by immunohistochemistry. Therefore, our data support the hypothesis that the SOD1(G93A) mouse cortex does not recapitulate the disease in patients, and we recommend the use of a different model for future studies of the cortical ALS pathology.

The characteristic degeneration of motor neurons (MNs) in ALS initially causes progressive muscle atrophy leading to difficulties with movement, speaking and swallowing, and respiratory failure in the final stage. Generally, ALS is considered as a multifactorial disease with poorly understood pathological mechanisms, and with a median survival of three to five years. There is currently no cure or prevention available, only symptomatic treatment.

Although MNs are recognized as the primary cell type affected by the pathology, multiple studies have confirmed that also non-neuronal cells including glia undergo changes and participate in ALS progression^{1,2}. Glial cells respond to neurodegeneration or injury by various mechanisms. Microglia and astrocytes acquire a so-called reactive state marked by changes of gene expression and morphology. By the activation of inflammatory and anti-inflammatory pathways, they protect the tissue from further damage. However, in the chronic stage of diseases they have a harmful effect and contribute to the progression of neurodegeneration. Traditionally, reactive astrocytes and microglia were divided into A1 and A2 or M1 and M2 subtypes, respectively. However, this terminology is currently considered outdated, as many various subpopulations of glia with specific gene signatures have recently been described in different disease models^{3–5}. Disease-associated astrocytes (DAA), disease-associated microglia (DAM), activated response microglia (ARM), and interferon response microglia (IRM), are just a few examples of these. Oligodendrocytes, on the other hand, are more susceptible to pathological changes. In reaction to disease, they tend to degenerate, rather than transform into a reactive state. However, their passive role in the progression of disease has recently been questioned by studies describing their contribution to immunoprotection, interferon signaling and antigen processing and presentation^{6,7}.

The role of astrocytes, microglia and oligodendrocytes, and their respective pathology-related changes, have been reported in ALS patients multiple times^{8–10}. The majority of available data come from the spinal cord, but a few studies also reported glial pathology in the cortex¹¹. The known pathological changes were mostly identified

¹Department of Cellular Neurophysiology, Institute of Experimental Medicine, Czech Academy of Sciences, Videnska 1083, 14220 Prague, Czech Republic. ²Second Faculty of Medicine, Charles University, V Uvalu 84, 15006 Prague, Czech Republic. ³Laboratory of Gene Expression, Institute of Biotechnology CAS, BIOCEV, Prumyslova 595, 25250 Vestec, Czech Republic. ⁴Faculty of Science, Charles University, Albertov 6, 12800 Prague, Czech Republic. ⁵Department of Informatics and Chemistry, Faculty of Chemical Technology, University of Chemistry and Technology, Technicka 5, 16628 Prague, Czech Republic. ⁶Department of Functional Organization of Biomembranes, Institute of Experimental Medicine, Czech Academy of Sciences, Videnska 1083, 14220 Prague, Czech Republic. ⁷These authors contributed equally: Tereza Filipi and Zuzana Benesova. ✉email: lukas.valihrach@ibt.cas.cz; Miroslava.Anderova@iem.cas.cz

in *post mortem* tissue, which does not allow for study of the disease mechanisms, increasing the need for a reliable animal model. Currently, the SOD1(G93A) mouse represents the most widely used model resembling familial ALS¹². Phenotypically the model matches the disease course, and studies in the spinal cord and brainstem reported ALS-related cellular changes previously found in patients^{2,8,13–16}. The cortex, however, seems to be a subject of controversy. The number of studies is limited, and the results suggest contradictory outcomes. While some show that cortical glial cells and MNs are affected by the ALS-like phenotype^{17–20}, others report no effect in the cortical area in the SOD1(G93A) model²¹.

In this study, we aimed to provide a comprehensive insight into the SOD1 glial pathology in the cortex of the SOD1(G93A) mouse. Combining robust and high-throughput methods such as scRNA-seq and immunohistochemistry, we analyzed astrocytes, microglia, and oligodendrocytes, during the complete course of the disease, which was characterized by behavioral tests. The scRNA-seq was used to monitor transcriptional changes in individual glial cells in time, and to investigate the composition of distinct glial populations with a particular focus on disease-associated subpopulations. To complete the characterization of the cortical pathology, we evaluated the morphological and quantitative changes of glial cells using immunohistochemistry, measuring canonical protein markers.

Methods

Animals. For all experiments, we used transgenic mice expressing high levels of human SOD1(G93A) (JAX Strain: 004435 C57BL/6 J-Tg (SOD1*G93A)1Gur/J) and their non-carrier littermates¹². This strain contains ~25 copies of the transgene, and its 50% survival ranges 157 ± 9.3 days (<https://www.jax.org/strain/004435>). All experimental protocols were approved by the Czech Republic Animal Care Committee (approval number 40/2019). All methods using animals were carried out in accordance with the European Communities Council Directive (86/609/EEC). All animals used for experiments were sacrificed using pentobarbital followed by decapitation. Due to an advanced stage of the disease, mutant mice were euthanized using carbon dioxide shortly after reaching five months of age. All efforts were made to minimize both the suffering and the number of animals used. The study is reported in accordance with the ARRIVE guidelines.

Behavioral testing. We conducted the wire grid hang test and the rota-rod test (Mouse RotaRod NG 47650, Ugo Basile, Italy) to assess muscle strength, function, and coordination throughout the disease. Weight was also measured as an additional parameter of the symptom progression. Testing consisted of a single three-attempt session every week, beginning at P30, and lasted for 14 weeks. Before the experiment, all animals performed training. Data are presented as mean or mean ± standard error of the mean (SEM) for *n* animals. Repeated measures two-way ANOVA with Holm-Sidak's multiple comparison correction was used to analyze the differences between groups.

Wire grid hang test. The mouse was placed on a custom-made wire lid, approximately 60 cm above a wood chip covered bottom, and turned upside down. The latency to fall was measured. At the beginning of a testing period, we trained each mouse three consecutive times for at least 180 s. In the experimental session, the mouse had three attempts to hold on to the lid. We noted the best score out of the three with a maximum of 180 s.

Rota-rod test. The mouse was placed on a stationary rod facing against the direction of rotation. The rod started rotating at a constant speed of 15 rpm, and the latency to fall was measured. Each mouse was trained three consecutive times of at least 180 s at 5, 10 and 15 rpm speed. In the experimental session, the mouse had three attempts to remain on the rod. We noted the best score out of the three with a maximum of 180 s.

Immunohistochemistry. For immunohistochemical analyses, the animals were deeply anesthetized with PTB (100 mg/kg, i.p.), perfused transcardially with 20 ml of saline solution followed by 20 ml of cooled 4% paraformaldehyde (PFA) in 0.1 M phosphate buffer and decapitated. The brains and spinal cords were dissected out, postfixed overnight with PFA and treated with a sucrose gradient (ranging from 10 to 30%) for cryoprotection. Coronal 30-µm-thick slices were prepared using a cryostat (Leica CM1850, Leica Microsystems, Wetzlar, Germany).

For immunohistochemical staining, the slices were washed in a phosphate buffer saline followed by blocking of the nonspecific binding sites with 5% Chemiblocker (Millipore, Billerica, MA), and 0.2% Triton in phosphate buffer saline. The blocking solution was also used as the diluent for the antisera. The slices were incubated with the primary antibodies overnight, and the secondary antibodies were applied for 2 h at 4–8 °C.

The following primary antibodies were used: rabbit anti-aldehyde dehydrogenase 1 family, member L1 (ALDH1L1 1:500; Abcam, Cambridge, UK), rat anti-myelin basic protein (MBP, 1:500, Biorad, Hercules, CA, US), rabbit anti-choline acetyltransferase (ChAT, 1:200, Merck, Darmstadt, Germany), rabbit anti-ionized calcium-binding adapter molecule 1 (Iba-1, 1:500, Abcam, Cambridge, UK), rabbit cleaved caspase-3 (CC3, 1:50, CellSignaling, Massachusetts, USA) and adenomatous polyposis coli (APC, 1:200, Merck, Darmstadt, Germany). The secondary antibodies were goat anti-rabbit IgG or goat anti-mouse IgG conjugated with Alexa Fluor 488, and chicken anti-rat IgG conjugated with Alexa Fluor 488 (1:500, Invitrogen, Waltham, MA, US). Cell nuclei were visualized by DAPI staining (Merck, Darmstadt, Germany). A Zeiss LSM 880 Airyscan confocal microscope equipped with Ar/HeNe lasers and × 40 water or × 63 oil objectives were used for the immunohistochemical analysis.

Image analysis and quantification. All analysis were done using FIJI image processing software (ImageJ 2.9.0/1.53t)²². Confocal images (212 × 212 × 30 μm) were taken from brain coronal slices (1 mm and 2 mm from bregma), covering area of primary and secondary motor and primary somatosensory cortex (five to six zones per hemisphere).

To quantify the ALDH1L1 fluorescence intensity, we used six animals for each group and two slices from each animal. The thresholding method (Yen method) was used to filter out the background. We calculated the mean integrated density limited to the threshold for each animal.

To quantify changes in morphology of microglia, we conducted Sholl analysis on IBA1 positive cells using Sholl analysis plugin²³. We used six animals for group and two brain slices from each animal. For each brain slice, a minimum of eight cells was analyzed. For the Sholl analysis, the consecutive z-stack images were converted to maximum intensity projection and the projection was thresholded for creating a binary mask. We counted the number of intersections starting from 5 μm from the center of soma, with radius step size of 5 μm.

To quantify the APC and CC3-positive cells, three animals from each group and one slice (1 mm from bregma) from each animal was used for the analysis. The number of APC or CC3-positive cells was determined from superimposed images and expressed as the percentage of marker expressing cells from the total number of DAPI + cells. The percentage of apoptotic cells was then expressed as a ratio of CC3 + to the previously counted APC + cells.

An Olympus FV10i confocal microscope equipped with × 60 oil objective was used for the analysis of MBP staining. We used six animals for each group and two slices for each animal and scanned 12 zones per each hemisphere. MBP expression density was determined using custom-written FIJI (ImageJ) macro (available at: https://github.com/jakubzahumensky/JT_paper). In brief, to keep the dimensionality of analyzed images equal, the macro extracted a substack of the 20 brightest frames from each z-stack. This was followed by creating a binary mask of the fibers in each frame and measurement of the frame fraction covered by the mask. Within each substack, the mean of this value was calculated, resulting in the volume fraction taken up by the fibers. The statistical analysis of the differences among groups was performed using unpaired t-test. All error bars in plots represent standard error of mean (SEM).

The preparation of single-cell suspension. The mice were deeply anaesthetized with pentobarbital (PTB) (100 mg/kg, i.p.), and perfused transcardially with a cold (4–8 °C) isolation buffer containing (in mM): NaCl 136.0, KCl 5.4, HEPES 10.0, glucose 5.5, osmolality 290 ± 3 mOsmol/kg. We isolated motor and primary somatosensory cortex and followed the Adult Brain dissociation protocol for mice and rats (Miltenyi-Biotec, Germany) but omitted the red blood cell removal step. To prevent the activation of immediate early genes (IEGs), we used transcriptional inhibitor actinomycin D (Sigma–Aldrich, St. Louis, MO), 30 μM during enzymatic dissociation and 3 μM in the following steps²⁴. After the debris removal, the cells were layered on top of 5 ml of ovomucoid inhibitor solution (Worthington, NJ) and harvested by centrifugation (300 × g for 6 min). Potential cell aggregates were removed by 70 μm cell strainers (Becton Dickinson, NJ). We labeled the final suspension with ACSA-2, Cd11b and O4 antibodies conjugated with allophycocyanin and phycoerythrin respectively (4 °C, 10 min; Miltenyi-Biotec, Germany) to allow for the enrichment of astrocytes²⁵, microglia and oligodendrocytes. The cells were enriched using flow cytometry (FACS; BD Influx), calibrated to sort ACSA-2+, Cd11b+ and O4+ cells. Hoechst 33258 (ThermoFisher Scientific, Waltham, MA) was used to check viability. The cells were collected into 200 μl of Advanced Dulbecco's Modified Eagle Medium, supplemented with 10% fetal bovine serum (ThermoFisher Scientific Waltham, MA). Four animals per condition were pooled for the preparation of cell suspension. After FACS, the cell suspension was spun down, concentrated, and used for library preparation.

scRNA-seq. Chromium Next GEM Single Cell 3' Reagent Kits v3.1 (10 × Genomics, Pleasanton, CA) was used to prepare the sequencing libraries, and the protocol was performed according to the manufacturer's instructions. Briefly, 10 × Chromium platform was used to encapsulate individual cells into droplets along with beads covered in cell-specific 10 × Barcodes, unique molecular identifiers (UMIs) and poly(dT) sequences. After reverse transcription, the cDNA libraries were amplified (13–14 cycles), fragmented and ligated to sequencing adaptors. SPRISelect magnetic beads were used for purification of the cDNA suspension and size selection of the fragments. Concentration and quality of the libraries was measured using Qubit dsDNA HS Assay Kit (Invitrogen) and Fragment Analyzer HS NGS Fragment Kit (#DNF-474, Agilent). The libraries were pooled and sequenced in paired-end mode using Illumina NovaSeq 6000 SP Reagent Kit, Read 1 containing a barcode and a UMI, and Read 2 covering the sequence of interest. Sequencing data comprised of approx. 100–200 million reads per sample (Supp. Tab. 4).

Data analysis. The sequencing data were aligned to the reference mouse genome GRCm38 and annotated (GENCODE version M8 annotation) by STARsolo (STAR version 2.7.3a)²⁶. EmptyDrops function (DropletUtils R package)²⁷ with a threshold of 100 UMIs and FDR < = 0.001 was applied to preserve only cell-containing droplets. Cells were counted based on the barcodes specific for each droplet/cell. The final number of detected cells differed among samples and was in the range approx. from 2500 to 6800 cells (Supp. Tab. 4).

The data were further processed using Seurat R package (version 4.1.1)²⁸. First, data from all samples were SCTransformed and integrated (excluding mitochondrial and ribosomal genes, prefixed by mt- or Rps/Rpl, respectively). Uniform Manifold Approximation and Projection (UMAP) was used to visualize 17 principal components (PC), which were subsequently clustered (FindNeighbors and FindClusters functions, UMAP resolution 0.5). Clusters were annotated based on the expression of known marker genes of the expected cell populations, and their correspondence to the markers found by the FindAllMarkers function (at least 80 % cells in the cluster expressing the markers). DoubletFinder²⁹ R package was used for the identification of droplets potentially

containing more than one cell. Doublet formation rate was set to 3.9 % as estimated by 10× Genomics, and the data were processed according to the authors' recommendations. Clusters expressing ambiguous markers and containing a higher number of doublets were filtered out of the data set.

Sex (male, female) was assigned to individual cells based on the expression of genes encoded by X (*Xist*) and Y chromosome, and those not matching our criteria (male: counts of *Xist* < 1, nFeature_Y > 0; female: counts of *Xist* > 0, nFeature_Y < 2, nCount_Y < 2; nFeature_Y being a number of Y-encoded genes and nCount_Y being a number of transcripts mapping to Y chromosome) were excluded from the dataset (Supp. Fig. 1a). These cells classified as 'Undefined' comprised almost 1/3 of the total number of cells and represented low quality cells (Supp. Fig. 1b).

A specific gene expression profile was also used to determine a phase of the cell cycle of each cell (CellCycle-Scoring Seurat function) to ensure that the cells in all phases are equally distributed among clusters. Individual cell types were filtered based on the number of genes detected (nFeature_RNA), number of counts (nCount_RNA) and amount of mitochondrial RNA (percent.mt). The cut-offs specific for each cell type of interest were the following: astrocytes—nFeature_RNA > 1000, 2000 < nCount_RNA < 10,000, percent.mt < 8; microglia—nFeature_RNA > 700, 1000 < nCount_RNA < 10,000, percent.mt < 5; oligodendrocytes—nFeature_RNA > 1300, 2500 < nCount_RNA < 50,000, percent.mt < 5 (Supp. Fig. 1d). Tissue dissociation may induce the expression of IEGs, the first rapid cellular response to stimuli^{24,30}. A set of the IEGs (e. g. *Fos* and *Jun* transcription factors) was projected onto the UMAP using AddModuleScore function to investigate the level of induction of these genes by sample preparation (Supp. Fig. 1c). The SoupX R package (version 1.5.2)³¹ was applied to remove the contaminating RNA background. The unfiltered and annotated data were supplied as the input. The contamination fraction was estimated by the automated method and was in the range from 1 to 2 % for individual samples. The count values were subsequently corrected for the contamination.

To view the overall differences between samples by pseudobulk principal component analysis (PCA), the normalized and scaled data set was used to create a pseudobulk data by summing up the gene counts of cells belonging to the same condition, age, and sex.

Differential expression analysis and Gene Set Enrichment Analysis. Differentially expressed genes (DEGs) in the single-cell data set were identified by t-test in Seurat's FindMarkers function. Normalized and scaled data in the RNA assay were used in this analysis. *P*-adjusted value (p_{adj}) threshold was set to 0.05, and genes with \log_2 fold change (\log_2FC) > 1 or < -1 were considered differentially expressed. Males and females were compared at each time point for each cell type and condition. Control (CTRL) and SOD1 pairs were also tested at each time point and for each cell type (end-stage DEGs in Supp. Tab. 1). The Gene Set Enrichment Analysis (GSEA)³² was performed using clusterProfiler R package (version 4.0.5)^{33,34}. Reference gene set size was limited to 10–800 genes and the significance threshold was set to $p_{adj}=0.05$. Only results where more than one gene contributed to the enrichment (core enrichment) were considered relevant.

The analysis of cellular subtypes. Individual cell types of interest (astrocytes, microglia, oligodendrocytes) were analyzed separately. Mitochondrial and ribosomal genes were not included in the subsequent analyses. The filtered, normalized, scaled and SCTransformed data were then subjected to PCA. Within the scope of quality control, several genes were excluded, as they introduced additional undesirable variability in the clustering (*Sod1*, *Gm8566*, *Cmss1*, *Cdk8* and lncRNAs *Xist*, *Gm42418*, *Gm424181*, *Malat1*). 16 PC for microglia and astrocytes, and 17 PC for oligodendrocytes were visualized using UMAP, and clustered at a resolution of 0.2 (FindNeighbors and FindClusters functions). A cluster of male control cells at the 3 M time point was excluded from the astrocyte and oligodendrocyte subsets, as it expressed potentially stress related marker genes (e.g., *Cdkn1a*, *Fkbp5*), which might have been induced during sample preparation (Supp. Fig. 2).

Markers of the subclusters were identified using the default Wilcoxon test in the FindAllMarkers function (at least 10 % cells in a cluster expressing the given marker, $\log_2FC > 0.25$, Supp. Tab. 3). The identity of the subclusters was determined by comparison with available gene signatures of various previously described cellular subtypes using the AddModuleScore function and by manual annotation based on the calculated marker genes. Reference gene expression signatures were taken from Habib et al.⁵ (Gfap-Low and Gfap-High astrocytes), Sala Frigerio et al.⁴ (ARM, IRM) and Marques et al.³⁵ (MFOL1/2, MOL2, MOL5/6). The intermediate state of astrocytes was visualized using a gene set containing calculated markers of cluster 2 and markers of transition state published by Habib et al.⁵. The signature of homeostatic microglia resulted from the combination of homeostatic markers mentioned in Keren-Shaul et al.³, Mathys et al.³⁶ and Butovsky and Weiner³⁷. The top 30 genes were used for the projection in astrocytes, and 20 genes were used in the microglia and oligodendrocytes. Numbers of cells entering differential expression analysis (DEA) and subpopulation analysis are provided in Supp. Tab. 4.

Results

Behavioral tests confirmed ALS-like phenotype. Firstly, we investigated the expected disease-related phenotypic changes characteristic for the animal model used in this study. Our goal was to assess the main turning points of the disease and characterize its progression.

To study the phenotype, we used two types of behavioral testing—the wire grid hang test and the rotarod performance test. We tested comparable groups of animals harboring SOD1(G93A) mutation (SOD1), and control animals (CTRL) with even numbers of males and females within each group. At the beginning of the testing period (1 month), all the animals performed for the maximum time (180 s) in both tests (see "Methods" section). The differences between CTRL and SOD1 animals were first noticeable in the wire grid hang test, where primarily the muscle strength is tested (Fig. 1a). The differences became significant at two months of age, so we considered this point an onset. The performance then slowly declined until a sudden drop at three months,

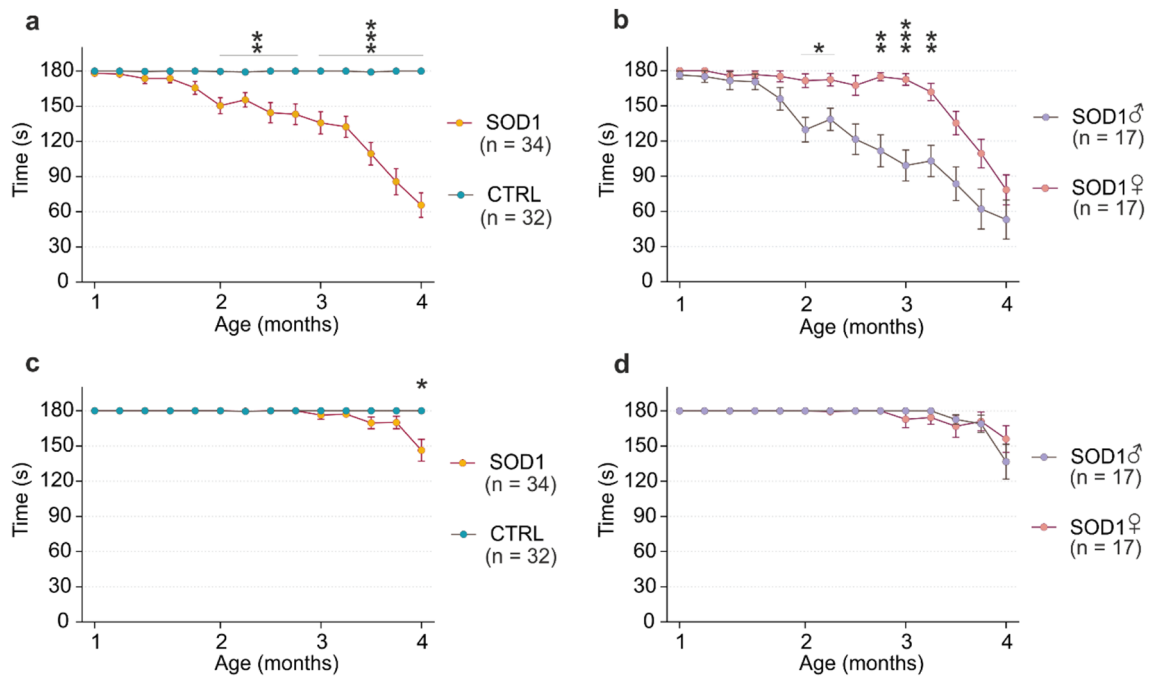


Figure 1. The cortical pathology evaluation by behavioral testing and immunohistochemistry. (a) The hanging wire test confirmed the motor skills decline in SOD1 animals during progression compared to the CTRLs. (b) Results from the hanging wire test comparing SOD1 animals divided based on sex revealed phenotypical differences in onset. (c), (d) The rotarod results comparing the CTRL and SOD1 animals did not reveal significant changes in progression. Statistical significance was determined using two-way ANOVA with Holm-Sidak's post-hoc test, error bars representing SEM. * $p_{\text{adj}} \leq 0.05$, ** $p_{\text{adj}} \leq 0.01$, *** $p_{\text{adj}} \leq 0.001$. n states the number of performing animals.

signaling the beginning of the symptomatic stage. This stage, accompanied by an even further performance decline, lasted approximately a month, after which the animals reached the end-stage marked by seriously impaired motor functions. The decrease in motor coordination of the animals measured by the rotarod (Fig. 1c) was only significant at the end-stage.

Investigating the SOD1 male versus female performance, the wire grid hang test revealed differences in the symptom onset and the progression in general (Fig. 1b). The onset in males appeared earlier, and overall they performed worse than the females, which is in agreement with human pathology³⁸. However, despite the later onset, the female performance in the symptomatic stage declined faster than the male, resulting in similar results for both sexes at the end-stage. The rotarod measurements did not reveal any significant sex-related differences in motor coordination during the progression.

Thus, behavioral tests confirmed the characteristic features of the model, identified sex-related differences, and determined the four main time points of the disease, which we considered in the following experiments.

Identical cell populations were identified in the control and SOD1 mouse cortex using scRNA-seq. The scRNA-seq experiment was designed as follows (Fig. 2a): CTRL and SOD1 mice were sacrificed at four time points, representing the main stages of the disease, with two males and two females used per condition at each time point. All cell suspensions were prepared from the motor and somatosensory cortical tissue and were enriched for three glial cell types—astrocytes, microglia, and oligodendrocytes—using FACS.

The scRNA-seq data followed an initial quality control, filtering, and clustering, and the resulting set of single cells was annotated using the expression of canonical marker genes of individual glial cell populations (Fig. 2b,d). As expected, the most numerous clusters in the data set were identified as astrocytes (*Aqp4*, *Aldh1l1*, *Gjb6*), microglia (*Cx3cr1*, *Aif1*), and oligodendrocytes (*Mobp*, *Apod*). Oligodendrocyte precursor cells (OPC) and committed oligodendrocyte precursor cells (COP) clustered separately from the mature oligodendrocytes that prevailed in the data set. The marker genes of these populations partially overlapped, indicating a gradual maturation of OPCs into oligodendrocytes (*Emid1*, *Pdgfra*, *Sox6*, *Vcan*, *Plp1*, *Cldn11* and others). In addition, perivascular macrophages, pericytes, and endothelial cells were present in the minority.

Each cell was assigned a sex identity based on the expression of X and Y chromosome-associated genes. Cells that did not fulfil the criteria for sex determination (see *Methods*, Supp. Fig. 1a, b) were excluded from further analyses. No cell cluster was overrepresented specifically in CTRL or SOD1, or in the male or female samples, confirming the robustness of cell preparation (Fig. 2c). Furthermore, the low proportion of mitochondrial reads and minimal activation of immediate early genes further validated the data quality (Supp. Fig. 1c, d). Overall, we successfully identified the targeted cell populations in the dataset and observed their equal proportions in both conditions and sexes.

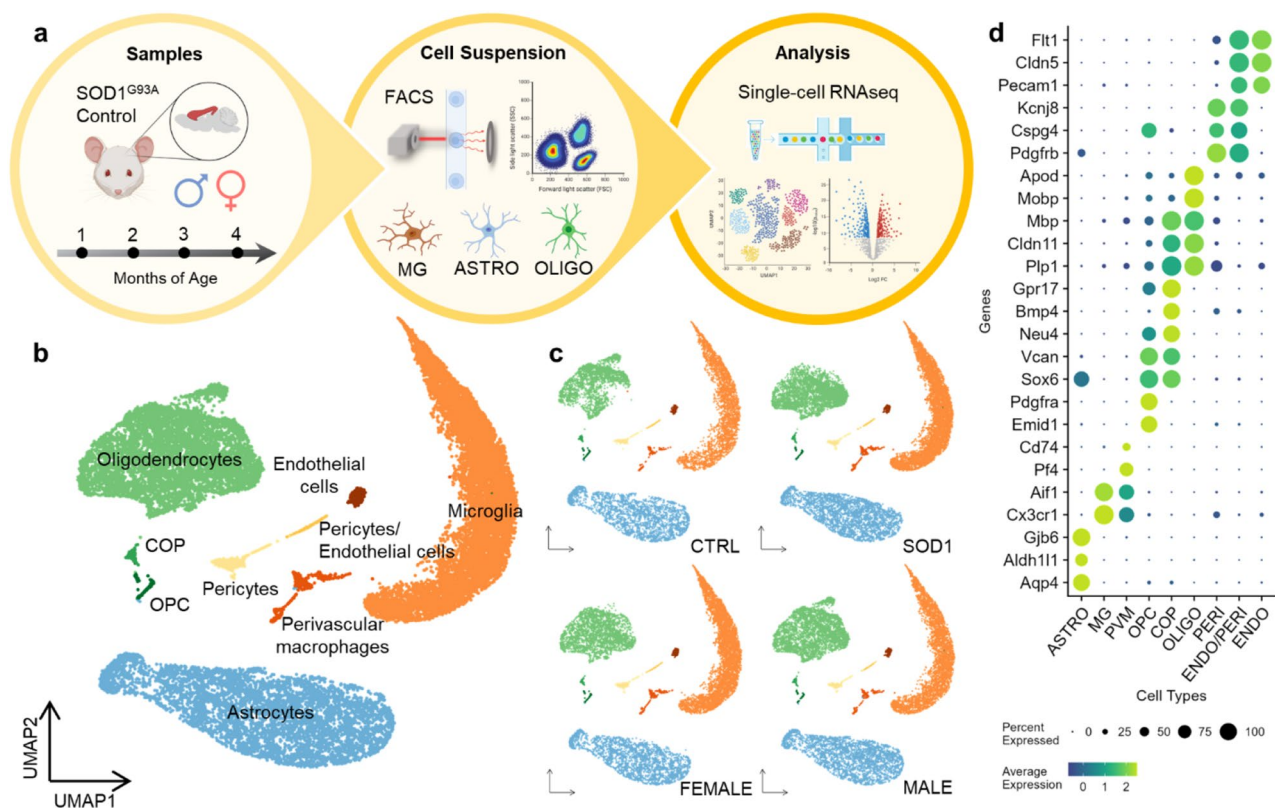


Figure 2. Single-cell RNA sequencing experiment overview. **(a)** A scheme summarizing the process of the sequencing experiment. (Created with BioRender.com) **(b)** A UMAP plot visualization of the identified cell clusters, containing cells from all samples. ASTRO $n = 5536$, MG $n = 8429$, OLIGO $n = 6180$, PVM $n = 434$, OPC $n = 165$, COP $n = 98$, PERI $n = 395$, ENDO $n = 235$, ENDO/PERI $n = 108$, total $n = 21,580$. **(c)** A visualization of cluster representation and the prevalence of targeted glia in both conditions and sexes. CTRL $n = 7646$, SOD1 $n = 12,499$, female $n = 10,246$, male $n = 9899$. **(d)** A list of canonical marker genes used for identification of cell clusters. ASTRO—astrocytes, MG—microglia, PVM—perivascular macrophages, OPC—oligodendrocyte precursor cells, COP—committed oligodendrocyte precursors, OLIGO—oligodendrocytes, PERI—pericytes, ENDO—endothelial cells.

The cortical glia of SOD1 mice showed minor changes in gene expression at the late stage of the ALS-like pathology.

To provide a general view on the gene expression changes in SOD1 mice, each of the main cell types was subjected to PCA as a pseudobulk (Fig. 3a). The analysis revealed a minor alteration between the CTRL and SOD1 samples in both sexes during disease progression. The first apparent shift between the samples appeared at four months of age in microglia and oligodendrocytes, suggesting their reaction to ALS-like pathology. The SOD1 astrocytes, frequently reported to be activated in SOD1(G93A) and other models of ALS^{14,18,19,39}, remained unchanged and clustered with the CTRL samples. Notably, the clustering showed a displacement of three-month-old (3 M) male data points. This was most prominent in astrocytes, where it represented the highest source of variability (reflected by separation in PCA1). Exploring the source of the variability, we identified a minor cluster of cells within astrocytes and oligodendrocytes, which was only present in 3 M CTRL males (Supp. Fig. 2). The cluster was characterized by the expression of stress-related genes *Cdkn1a* and *Fkbp5*, which had the most extreme values of loadings in respective principal components (PCs) in the pseudobulk analysis, confirming the effect of the cluster on the displacement of 3 M CTRL male data points. As the presence of the cluster had a negligible effect on further analysis, we considered it as a technical artifact of sample processing and removed it from the dataset. This finding, however, showed the power of the single-cell analysis to characterize even minor changes in cell subpopulations, which might otherwise be hard to interpret in traditional bulk analysis.

Based on the sex-related differences in behavioral tests (Fig. 1a–d), we examined the potential ALS-associated gene expression variations between the sexes by DEA, and compared the male and female cells for CTRL and SOD1 separately. The analysis yielded only a few DEGs based on the set thresholds of $|\log_2FC| > 1$ and $p_{adj} < 0.05$. The X chromosome gene *Xist* was significantly upregulated in the females in all three cell types, regardless of genotype. The *Xist* gene plays a major role in the gene dosage compensation in females by silencing one of the X chromosomes, and is therefore expressed only in female cells⁴⁰. Two genes encoded by chromosome Y (*Eif2s3y*, *Uty*) were upregulated in males, but the difference in their expression only exceeded the \log_2FC threshold in astrocytes (Fig. 3b). Apart from these, no other dysregulated genes related to the pathology progression and sex were found in our data.

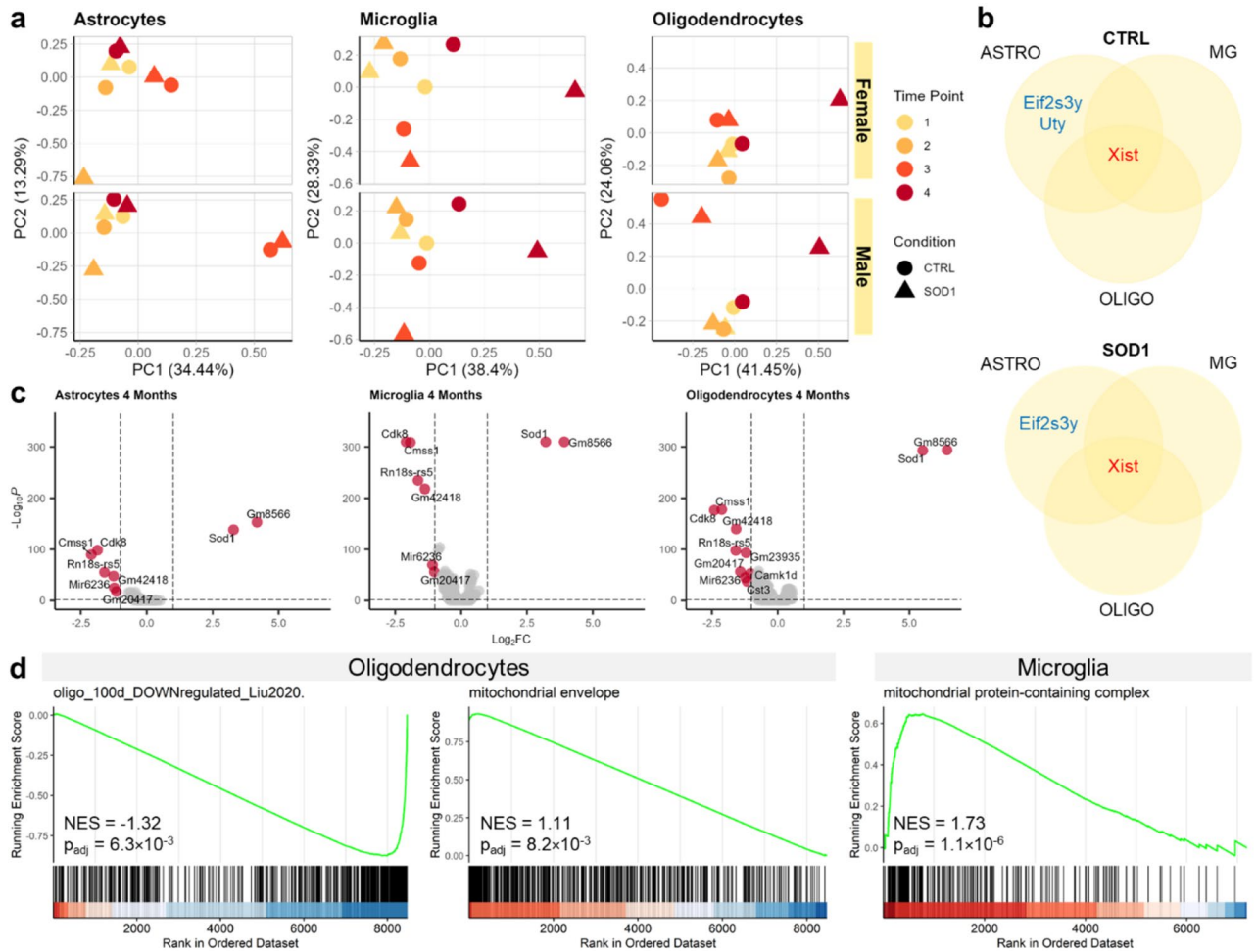


Figure 3. Pseudobulk and differential expression analysis reveals only minor changes in gene expression. **(a)** Pseudobulk PCA clustering comparison of male and female samples showing a shared reaction to the ongoing pathology in microglia and oligodendrocytes at 4 M. **(b)** A visualization of the few differentially expressed genes found dysregulated in males and females in all cell types at 4 M time point. *Xist* clearly distinguishes female cells, whereas *Eif2s3y* and *Uty* are both expressed by male chromosome Y. **(c)** Results of the DEA comparing CTRL and SOD1 4 M samples show a limited number of up- and downregulated genes at the final stage. **(d)** Enrichment curves visualising the results of the GSEA at 4 M. One reference gene set was enriched among genes downregulated in oligodendrocytes. Analysis of GO terms showed mitochondrial components to be enriched among genes upregulated in oligodendrocytes and microglia.

To investigate disease-related transcriptional changes, we performed the DEA on the comparisons of CTRL and SOD1 samples at each time point and for each cell type, considering males and females together. The *Sod1* gene was the only one significantly upregulated DEG in all the measured stages of the disease, including the end-stage as shown in Fig. 3c and Supp. Tab. 1 ($|\log_2FC| > 1$, $p_{adj} < 0.05$), confirming the validity of the SOD1(G93A) model. Other dysregulated genes were mostly noncoding or ribosomal transcripts that evaded quality control. Additionally, the 4 M CTRL samples were marked by an increased expression of genes *Cdk8* and *Cmss1* across all cell types. These two genes were identified in the subsequent analysis as confounders negatively effecting sub-clustering results (Supp. Fig. 2a, b). Therefore, they were considered as biasing factors without connection to the ALS-like pathology. Together, these results show minimal variation in gene expression related to the pathology progression in the cortex of the SOD1(G93A) mouse, regardless of sex, with the indication of subtle changes in microglia and oligodendrocytes in the late phase of the disease.

The GSEA indicated an altered mitochondrial function in cortical microglia and oligodendrocytes of SOD1 mice. To investigate the potential biological significance of the minimal changes in gene expression detected by DEA, we utilized the GSEA³² focused on the most affected 4 M time point. As GSEA considers the expression of all genes, regardless of cut-offs in \log_2FC or p-value, it allows for the finding of any dysregulated processes even if the change of the individual genes is minor.

First, we employed a meta-analysis approach, and collected the gene signatures of glial cells affected by SOD1 mutation from 15 transcriptomic studies published in the last 20 years (Supp. Tab. 2). This set includes data mostly derived from the spinal cord of the SOD1(G93A) model. Using GSEA, we detected the enrichment of only

a single gene set that was recently reported by Liu, et al.¹⁵ as downregulated in brainstem oligodendrocytes in 100-day-old mice. In concordance, our results showed a negative enrichment in oligodendrocytes (NES = -1.32, $p_{\text{adj}} = 6.3 \times 10^{-3}$; NES—normalized enrichment score; Fig. 3d), indicating small, but significant changes in the cortical 4 M SOD1 oligodendrocytes. No gene set was found enriched for microglia or astrocytes.

In addition to the meta-analysis, we also looked for Gene Ontology (GO) terms^{41,42} enriched in our data. Two activated terms related to mitochondria turned out to be upregulated in our data set: *mitochondrial envelope* in oligodendrocytes (NES = 1.11, $p_{\text{adj}} = 8.2 \times 10^{-3}$) and *mitochondrial protein-containing complex* in microglia (NES = 1.73, $p_{\text{adj}} = 1.1 \times 10^{-6}$) (Fig. 3d). In support of our data, mitochondrial dysfunction has been extensively discussed as one of the factors contributing to ALS pathology, not only in relation to the mutant *Sod1* gene, but also to other ALS-linked genetic perturbations (reviewed in Jankovic et al.⁴³).

Taken together, despite the low number of DEGs, we identified subtle changes in the mitochondria function in cortical oligodendrocytes and microglia. However, considering the number of enriched terms and their significance, the severity of the dysfunction is rather low.

The subpopulation analysis confirmed subtle changes in oligodendrocytes and microglia. As the pseudobulk analyses revealed only subtle variations in the gene expression of the SOD1(G93A) cortical glia, we speculated that the pathological changes could be represented by a small fraction of cells, hidden at the population level. Therefore, we conducted an in-depth sub-clustering analysis with the goal to identify subpopulations potentially playing a role in the disease progression.

Starting with astrocytes, we identified three clusters that were present in both the CTRL and SOD1 samples in a similar proportion (Fig. 4a). To annotate these clusters, we calculated their marker genes (Supp. Tab. 3) and visualized the gene signatures of astrocytic subtypes described by Habib et al.⁵ in a mouse model of Alzheimer's disease (AD). The study identified two similar subpopulations of astrocytes expressing markers of reactivity – Gfap-High and DAAs. While Gfap-high were present in controls and in AD samples, DAAs were unique to the AD model, and the authors suggested their potential role in the disease progression. Marker genes of cluster 3 in our data partially overlapped with the markers of the Gfap-High cluster (e. g. genes *Mt1*, *Mt2*, *Id3*, *Cd9*, *Vim*), but we did not detect the DAAs specifically in SOD1 samples. Of note, *Gfap* and *Vim* expression levels were low, suggesting a limited pathological reaction of astrocytes in the cortex of the mutant SOD1(G93A) mice. This finding complies with the results of the pseudobulk analysis, showing no changes in astrocytes. Cluster 1 shared common genes with Gfap-low astrocytes (e. g. *Luzp2*, *Trpm3*), and the remaining cluster 2 expressed markers of both Gfap-High and Gfap-Low clusters, therefore representing an intermediate state cluster.

Microglia were grouped into four clusters as shown in the UMAP plot in Fig. 4b. Cluster 1 was characterized by the expression of homeostatic markers^{3,36,37}. The gene signatures of microglia in clusters 2 and 3 resembled the expression profile of ARM, that were described in a model of AD, but also in a smaller proportion in a healthy brain^{3,4}. These activated microglia characteristically downregulate homeostatic genes such as *Cx3cr1*, *P2ry12*, and *Sall1*, which is also noticeable in our data (Fig. 4b). Additionally, cluster 3 was marked by a higher expression of *Apoe*, which is a major regulator of microglial neurodegenerative phenotype⁴⁴. Cluster 4 represented IRM⁴, and was clearly distinguishable by the expression of *Ifit2*, *Ifit3*, and *Ifitm3*, the genes involved in the interferon response pathway. However, the proportion of IRM was very low in both conditions. Nevertheless, we detected a small increase in the subpopulation of activated microglia in SOD1 samples (cluster 2), suggesting a starting activation of microglia in response to pathological stimuli.

Oligodendrocytes formed four clusters (Fig. 4c). Cluster 1 shared a similar gene expression signature with myelin forming oligodendrocytes (MFO) described by Marques, et al.³⁵, including the expression of *Mal*, *Plp1*, *Mog*, and *Opalin* genes. These cells were predominantly present at the one month (1 M) time point (Fig. 4d), which coincides with the extensive myelination in rodents during the early weeks after birth⁴⁵. Cluster 2 represents mature oligodendrocytes (MOL2) expressing *Klk6*, but also mature oligodendrocyte marker *Apod* and genes typical for myelinating cells *Pmp22*, *S100b*, and *Apc*^{7,35,46}. Floriddia et al.⁷ reported the MOL2 population to be more abundant in the white matter of the spinal cord, but also to a lesser extent in the cortex³⁵. The proportions in both conditions were similar for clusters 1 and 2. As for clusters 3 and 4, they showed an increased expression of several genes found in mature oligodendrocyte populations MOL5/6^{7,35}. Interestingly, cluster 4 was present almost exclusively in the SOD1 samples (Fig. 4d), and it was characterized by a higher expression of *Apoe* and *Il33*. *Il33* is upregulated in oligodendrocytes and astrocytes in lesions and can be released by stressed or damaged cells. It has an anti-inflammatory effect and promotes the activation of microglia (reviewed in Sun et al.⁴⁷). Upregulation of *Il33* has been previously reported in disease-associated oligodendrocytes in a mouse model of AD^{48,49}. *Apoe* was identified as a marker gene of immune oligodendroglia (ImOLG)⁵⁰, which were enriched in multiple sclerosis lesions, suggesting their role in chronic demyelination and continuous attempts to remyelinate⁵¹. Thus, we hypothesize that cluster 4 represents a damaged or reactive state of oligodendrocytes, responding to the pathological stimuli in the 4 M SOD1 cortex. It is tempting to speculate whether the small increase in numbers of activated microglia and possibly the shift to the intermediate state in astrocytes that we observed in the SOD1 (Fig. 4a,b, respectively) might be a response to the damaged/activated oligodendrocytes. This kind of interaction between disease-associated states of glial cells was recently described in AD⁵², and also in ALS².

Overall, we were able to identify multiple subpopulations of astrocytes, microglia, and oligodendrocytes, and we recognized the gene expression patterns of specific, previously described, cellular subtypes. However, in contrast with our expectations, we did not detect any disease-associated subpopulations in the SOD1 samples, apart from the damaged/activated oligodendrocytes.

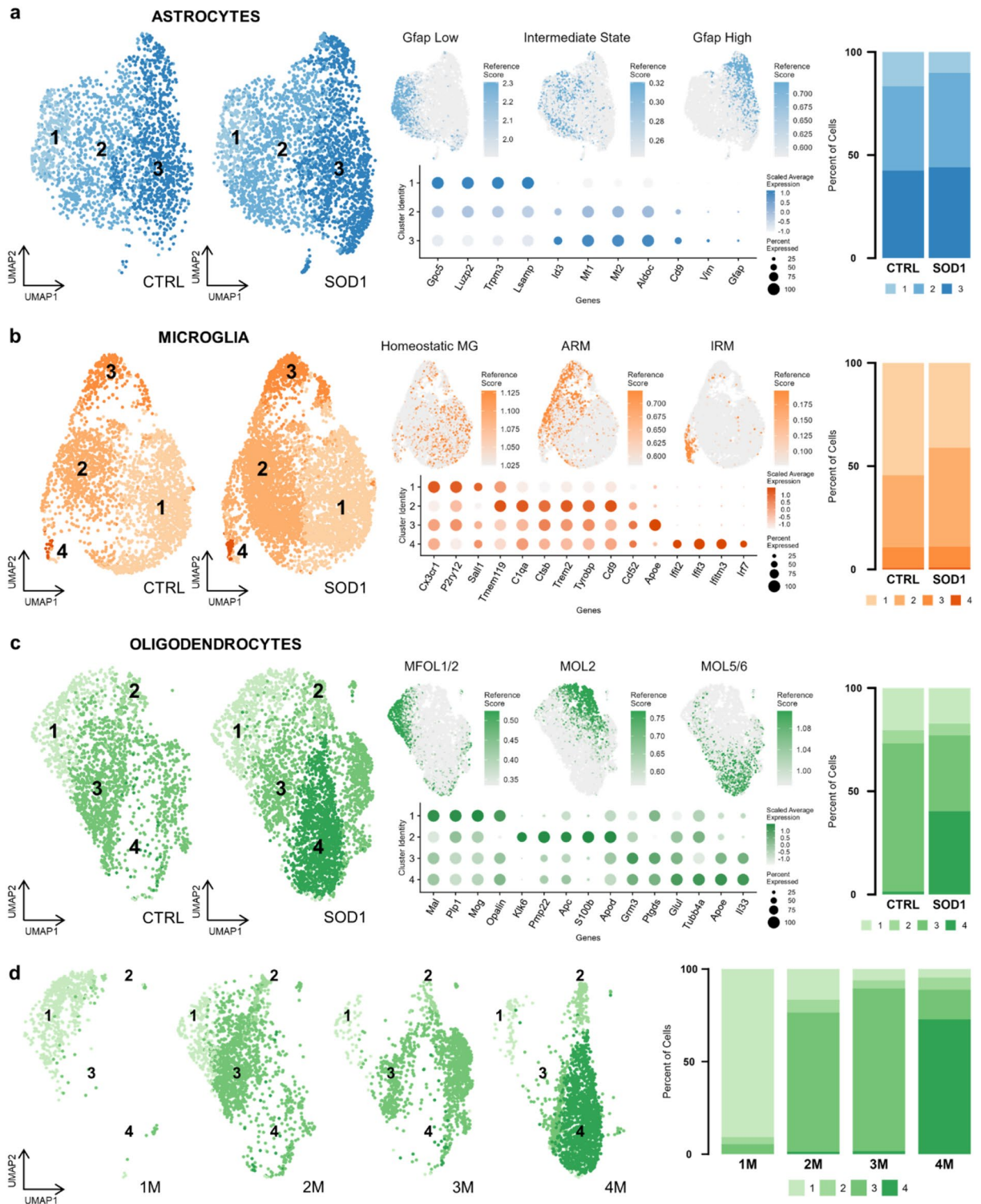


Figure 4. The subpopulation analysis revealed a unique subpopulation of oligodendrocytes in SOD1 samples. UMAP visualization of subpopulations of astrocytes ($n = 5292$) (a), microglia ($n = 8414$) (b), and oligodendrocytes ($n = 5876$) (c) split to CTRL and SOD1 condition (left), including cells from all four time points. Gene expression signatures of previously described subpopulations are shown projected onto UMAP (middle-top). A list of representative cluster markers used for their annotation (middle-bottom). Proportions of subpopulations in CTRL and SOD1, including cells from all four time points. (d) UMAP visualization of CTRL and SOD1 oligodendrocytes split according to age (1 M: $n = 682$, 2 M: $n = 1697$, 3 M: $n = 1430$, 4 M: $n = 2067$). Bar plot shows proportions of subpopulations at each time point.

The immunohistochemical identification of changes in the cortical and spinal glia of SOD1 mice. The results of the scRNA-seq analysis suggested minor changes in the cortical glia of the SOD1(G93A) mouse model. To further explore and validate this conclusion, we conducted an immunohistochemical analysis of glia in the motor and primary somatosensory cortex (the identical region used for the sequencing) at the 4 M time point, when the phenotypic changes are the most pronounced. The imaged zones within areas of interest are represented in Fig. 5a. As the morphological changes are well described in the spinal cord, we also stained the lumbar region of the spinal cord at the end-stage (4 M), and used those pictures as a reference for advanced gliosis in our animals.

Astrocytes were stained using ALDH1L1 marker, which allowed the inspection of the whole cell morphology, including the processes. Astroglial gliosis, a morphological change marked by enlargement of the cellular body and shortened, thickened processes, is a characteristic response of astrocytes in pathological states, and it was well described in the ALS spinal cord^{13,14}. In the cortex we conducted fluorescence analysis in order to find any morphological differences (Fig. 5b), but the analysis showed very similar fluorescence values of both SOD1 and CTRL astrocytes, suggesting there is no cell enlargement associated with activation. The similar morphology can be seen in Fig. 5c in comparison with astrocytes in the ventral horns of the spinal lumbar region, which showed an enlarged body with distinctively shortened processes. The results from fluorescence analysis align with little or no change detected in astrocytes at the level of gene expression.

Microglia, like astrocytes, change their morphology in response to pathological stimuli. They retract processes and adopt a specific amoebic shape, typical for their activated state. To visualize microglia, we used IBA1 antibody and stained both the cortex and lumbar spinal cord for comparison. The Sholl analysis we used to evaluate the changes in morphology (Fig. 5d) is frequently conducted to quantify the complexity of cell's arborization. The analysis confirmed that the SOD1 cortical microglia morphology does not significantly differ from CTRL animals. We did not detect shorter processes or reduced branching, which would suggest activated phenotype. However, during the analysis we noticed some tips of the processes looking bulbous and enlarged (Fig. 5e). These structures, called *bulbous termini*, appear as the microglia's first reaction after injury⁵³, and may represent an initial phase of microglia activation observed in the transcriptomic data. The SOD1 microglia in the ventral horns of the spinal cord on the other hand display the typical amoebic shape with very short and thickened processes associated with activation.

The previous analysis identified a SOD1-specific oligodendrocyte cluster (cluster 4) suggesting a certain portion of cells as being apoptotic, we thus focused on the protein expression changes related to chronic demyelination, necrosis, or apoptosis. Accordingly, we stained for myelin basic protein (MBP)—a marker of myelination, adenomatous polyposis coli (APC)—a marker of adult oligodendrocytes, and cleaved caspase 3 (CC3)—an apoptotic marker. The quantification of MBP signal intensity as well as the number of APC + oligodendrocytes in the cortex of the SOD1 animals excluded the demyelination processes as there was no significant decrease of MBP or APC + cells compared to the CTRLs (Fig. 5f). Similarly, the co-staining of CC3 with APC did not reveal a different abundance of CC3 + oligodendrocytes in either the SOD1 or CTRLs, suggesting a similar rate of apoptosis (Fig. 5f). MBP staining and representative image of a cell positive for APC and CC3 can be found in Fig. 5g. Collectively, the data showed no significant demyelination or degeneration of oligodendrocytes, therefore it is likely that the SOD1-specific cluster 4 identified in scRNA-seq in 4 M animals does not represent dying or damaged cells.

Taken together, we did not detect any profound morphological changes in the cortical glia of the SOD1 mice. Oligodendrocytes did not show an increased cell death or loss of MBP protein, suggesting its maintained function in the cortex of the ALS mice.

Discussion

ALS is a devastating neurodegenerative disease with fast progression and no effective treatment strategies. Although it is primarily recognized as a motor-neuron disease, the other cell types, including glial cells, contribute to the disease progression and thus represent a potential target for future therapies. In the past, multiple experimental models have been developed to understand the mechanisms of the disease, as well as to facilitate the search for therapeutic targets. Among them, the SOD1(G93A) mouse model has the prime position as the best-characterized mouse strain used in current ALS research. Despite its long-term application, the effect of the pathological changes across different CNS regions is still not fully understood.

The pathological effect on cortex is of special interest due to its role in the planning, control, and execution of voluntary movements, which are severely affected by ALS. Pathological changes in the cortex of ALS patients have been reported since the first description of the disease in 1869, and the monitoring of cortical structural abnormalities became a standard ALS diagnostic procedure⁵⁴. Along with cortical MN death, changes in glia have also been observed, including microgliosis^{11,55–57}, accompanied by the DAM-like gene expression signature⁵⁶, demyelination⁸, and change of oligodendrocyte function from myelinating to neuro-supportive⁵⁷.

While the changes are well documented in humans, less is known about the effect of the ALS-like pathology on the cortex of the SOD1 models. In the SOD1(G93A) model, the cortical MN degeneration was observed early by Özdinler et al.¹⁷ and others, together with the changes in glia^{18–20}. Reactive astrocytes in the SOD1(G93A) cortex were shown to differ from their spinal counterparts, while still maintaining a toxic effect on neurons^{18,19,58}. However, Gomes et al.¹⁹ also reported no significant gene expression changes in microglia or oligodendrocytes. Moreover, others suggested the pathology in the SOD1 model as being restricted to only spinal and bulbar motor neurons, not affecting the motor cortex²¹. Thus, such opposing data raise questions as to what extent the cortex is affected in the SOD1 mouse model, and how well this model recapitulates the cortical pathology in humans.

To fill this knowledge gap, we applied single-cell RNA sequencing supported by immunohistochemistry to detect gene expression changes, the presence of disease-associated cell populations, and morphological or

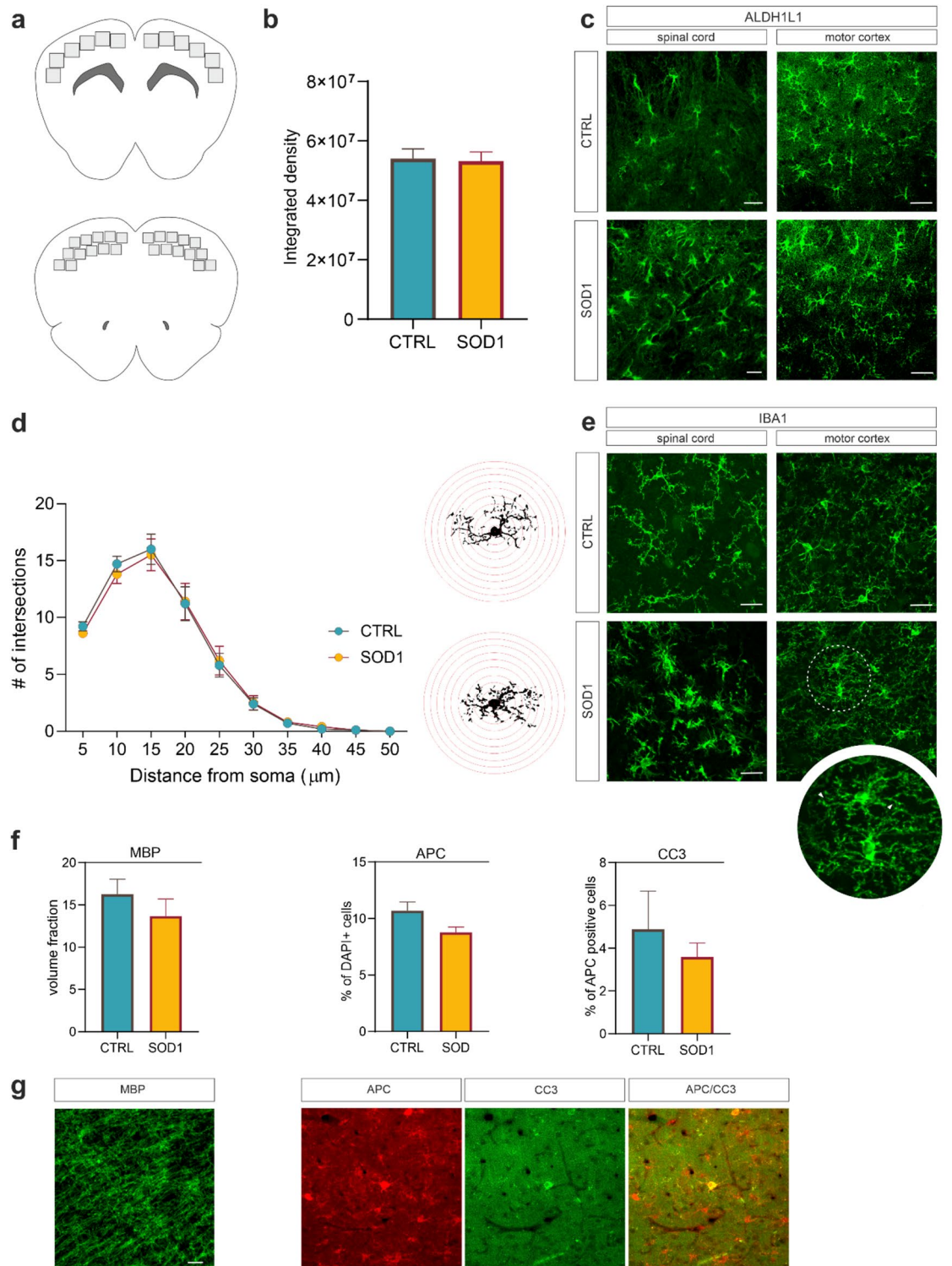


Figure 5. The immunohistochemistry (a) An upper cartoon depicts 12 areas scanned for the investigation of morphological changes and quantification of APC and CC3. Lower cartoon shows 24 areas scanned for the MBP analysis. (b) Fluorescence analysis did not reveal any significant differences in morphology between cortical astrocytes in SOD1 (n=6) and CTRL (n=6) animals. (c) Representative pictures of ALDH1L1 staining in cortex and spinal cord comparing astrocytes show morphological difference between SOD1 and CTRL in the spinal cord but no noticeable difference in the cortex. (d) The results of Sholl analysis indicated very similar microglia complexity in both CTRL (n=6) and SOD1 (n=6) samples. Sholl masks with red concentric radii depict single thresholded microglia as they were used for the analysis. (e) Representative images of cortical and spinal slices stained with IBA1 show evident amoebic morphology of spinal microglia but only subtle morphological changes represented by *bulbous termini* (see close up) in the cortex. (f) The quantification of MBP in the cortex revealed insignificant difference between SOD1 (n=6) and CTRLs (n=6). The number of APC+ cells was consistent between SOD1 (n=3) and CTRLs (n=3) and the number of APC+ cells co-stained with CC3 used as a marker of apoptosis in oligodendrocytes also remained similar, suggesting no apparent oligodendrocyte degenerations. (g) Representative images of MBP, APC, and CC3 staining. Scale bars, 20 μm. The statistical significance was determined using unpaired t-test. Error bars represent SEM. n states the number of used animals.

other pathological modifications in cortical glia accompanying the ALS-like pathology in the SOD1(G93A) mouse model. The ALS-like phenotype was confirmed by behavioral testing, including sex-dependent differences in disease progression as reported by McCombe and Henderson³⁸. The results of scRNA-seq focused on glia revealed minor changes in microglia and oligodendrocytes, and showed no significant ALS-related shift in astrocytes, which contradicts several studies reporting the reactive phenotype of astrocytes^{18,19,58}. Although the only significantly dysregulated gene in the SOD1(G93A) model was *Sod1*, GSEA indicated the mitochondrial dysfunction in microglia and oligodendrocytes. Similar changes have recently been observed by Liu et al.¹⁵ in the oligodendrocytes isolated from the brainstem of 100-day-old SOD1 mice, suggesting the possible dysregulation of energetic pathways.

As our data were generated within the motor and primary somatosensory cortex, representing an end-point region of corticospinal tract affected by ALS, they allow basic questions to be addressed regarding the site of origin and the direction of ALS progression. Currently, there are two hypotheses, both supported by lines of evidence (reviewed in van den Bos et al.⁵⁹). The 'dying forward' hypothesis suggests ALS originates in the cortex and spreads towards the spinal MNs. On the other hand, the 'dying back' hypothesis proposes ALS begins within muscles or neuromuscular junctions. Considering the advanced ALS-like phenotype of the end-stage SOD1 mice and the more pronounced changes in the brainstem and the spinal cord observed elsewhere, the milder changes in the cortex indicated by our data are more in favor of the 'dying back' hypothesis in SOD1(G93A) mice. Interestingly, this contrasts with a report from Burg et al.⁶⁰, which indicates the cortex as the initiating point of ALS in SOD1(G86R) mice. The contradictory data might suggest a differential effect of specific point mutations on the character of the disease, requiring further investigation.

Many of the previous reports exploring the effect of the SOD1 mutation on motor cortex relied on measuring the limited number of genes and proteins^{19,20,55}, or analysis of the bulk population of cells^{18,61}. This consequently decreased the sensitivity of the analysis and limited the interpretability of the data. In this study, we used high-throughput scRNA-seq, allowing for an in-depth analysis of small cell populations that cannot be distinguished by bulk approaches. Using scRNA-seq, recent seminal studies revealed various disease-associated populations of glia, playing a major role in the disease progression^{3–6}. Interestingly, many of these populations are present in multiple diseases, suggesting common mechanisms employed by glial cells in response to pathological stimuli. For example, a DAM-like population was identified not only in Alzheimer's disease, but also in the spinal cord of the SOD1(G93A) mouse³, and in a spinal cord injury model⁶². In our work, we searched for these populations without any success, which confirmed the minimal changes observed at bulk transcriptional level, as well as by immunohistochemistry. We mostly found similar cellular composition between the control and SOD1(G93A) animals, except for microglia and oligodendrocytes. In the case of microglia, we observed a little increase in the proportion of the activated microglia, suggesting a starting phase of their activation. The data were completed by immunohistochemistry revealing *bulbous termini* on microglial processes. More apparent changes were observed in oligodendrocytes, where sub-clustering analysis identified the existence of a unique population of oligodendrocytes, characterized by an increased expression of *Apoe* and *Il33*, and enriched specifically in 4 M SOD1 samples. Considering no profound loss of oligodendrocytes or a higher apoptotic rate in immunohistochemistry, we could speculate about the active role of this population of oligodendrocytes in disease progression. This is also in line with recent evidence suggesting the active role of oligodendrocytes in the progression of multiple sclerosis⁶ and in aging white matter⁶³, which contrasts with their widely accepted passive role. Notably, we did not observe any expression patterns similar to previously reported disease-associated oligodendrocytes^{6,48–50}, except *Apoe* or *Il33* mentioned above. However, this might be related to the overall mild changes in gene expression observed throughout our data.

In conclusion, our study demonstrates that cortical glia are only subtly affected in the SOD1(G93A) model, even at the very end-stage of disease. Furthermore, owing to the power of scRNA-seq, we showed that oligodendrocytes potentially actively participate in the pathology, emphasizing the importance of addressing their role in further research. Finally, on reflection of our results, we suggest that the SOD1(G93A) mouse model does not fully recapitulate the human disease and we recommend using a different model system for studying the cortical ALS pathology.

Conclusions

Collectively, our results suggest the ALS-like pathological changes present in the sensorimotor cortex of SOD1(G93A) mice are minimal. There is an ongoing discussion in the field whether the model mimics the disease completely including the pathology occurring in the cortex and the published results are disputable. Our collective findings inspecting glial cells on multiple levels did not reveal any significant changes of SOD1 astrocytes and only subtle changes of microglia and oligodendrocytes at the final stage. The changes of microglia and oligodendrocytes suggest starting activation linked to the pathology, but the extent of change does not correspond to the pathology described in human tissue. The SOD1 specific oligodendrocytes identified at the final stage, however, contribute to the recently published evidence reporting their active role in neurodegeneration, largely rejecting long-lasting dogma presenting oligodendrocytes as solely passive in the CNS diseases. However, despite the signs of activation, the effect of ALS-like pathology on the glial cells in the cortex of SOD1(G93A) mice is minor and our data provide supporting evidence against the use of this model for studying cortical pathology of ALS.

Data availability

The scRNA-seq data generated during this current study are available in NCBI's Gene Expression Omnibus⁶⁴ and are accessible through GEO Series accession number GSE206330 (<https://www.ncbi.nlm.nih.gov/geo/query/acc.cgi?acc=GSE206330>).

Received: 25 October 2022; Accepted: 15 April 2023
Published online: 21 April 2023

References

- Baufeld, C., O’Loughlin, E., Calcagno, N., Madore, C. & Butovsky, O. Differential contribution of microglia and monocytes in neurodegenerative diseases. *J. Neural Transm. (Vienna)* **125**, 809–826. <https://doi.org/10.1007/s00702-017-1795-7> (2018).
- Maniatis, S. *et al.* Spatiotemporal dynamics of molecular pathology in amyotrophic lateral sclerosis. *Science* **364**, 89–93. <https://doi.org/10.1126/science.aav9776> (2019).
- Keren-Shaul, H. *et al.* A Unique microglia type associated with restricting development of Alzheimer’s disease. *Cell* **169**, 1276–1290 e1217. <https://doi.org/10.1016/j.cell.2017.05.018> (2017).
- Sala Frigerio, C. *et al.* The major risk factors for Alzheimer’s disease: Age, sex, and genes modulate the microglia response to Aβ plaques. *Cell Rep.* **27**, 1293–1306 e1296. <https://doi.org/10.1016/j.celrep.2019.03.099> (2019).
- Habib, N. *et al.* Disease-associated astrocytes in Alzheimer’s disease and aging. *Nat. Neurosci.* **23**, 701–706. <https://doi.org/10.1038/s41593-020-0624-8> (2020).
- Falcao, A. M. *et al.* Disease-specific oligodendrocyte lineage cells arise in multiple sclerosis. *Nat. Med.* **24**, 1837–1844. <https://doi.org/10.1038/s41591-018-0236-y> (2018).
- Floriddia, E. M. *et al.* Distinct oligodendrocyte populations have spatial preference and different responses to spinal cord injury. *Nat. Commun.* **11**, 5860. <https://doi.org/10.1038/s41467-020-19453-x> (2020).
- Kang, S. H. *et al.* Degeneration and impaired regeneration of gray matter oligodendrocytes in amyotrophic lateral sclerosis. *Nat. Neurosci.* **16**, 571–579. <https://doi.org/10.1038/nn.3357> (2013).
- Phillips, T. *et al.* Oligodendrocyte dysfunction in the pathogenesis of amyotrophic lateral sclerosis. *Brain* **136**, 471–482. <https://doi.org/10.1093/brain/aws339> (2013).
- Zürcher, N. R. *et al.* Increased in vivo glial activation in patients with amyotrophic lateral sclerosis: Assessed with [(11)C]-PBR28. *Neuroimage Clin.* **7**, 409–414. <https://doi.org/10.1016/j.nicl.2015.01.009> (2015).
- Nolan, M. *et al.* Quantitative patterns of motor cortex proteinopathy across ALS genotypes. *Acta Neuropathol. Commun.* **8**, 98. <https://doi.org/10.1186/s40478-020-00961-2> (2020).
- Gurney, M. E. *et al.* Motor neuron degeneration in mice that express a human Cu, Zn superoxide dismutase mutation. *Science* **264**, 1772–1775. <https://doi.org/10.1126/science.8209258> (1994).
- Miller, S. J., Zhang, P. W., Glatzer, J. & Rothstein, J. D. Astroglial transcriptome dysregulation in early disease of an ALS mutant SOD1 mouse model. *J. Neurogenet.* **31**, 37–48. <https://doi.org/10.1080/01677063.2016.1260128> (2017).
- Guttenplan, K. A. *et al.* Knockout of reactive astrocyte activating factors slows disease progression in an ALS mouse model. *Nat. Commun.* **11**, 3753. <https://doi.org/10.1038/s41467-020-17514-9> (2020).
- Liu, W. *et al.* Single-cell RNA-seq analysis of the brainstem of mutant SOD1 mice reveals perturbed cell types and pathways of amyotrophic lateral sclerosis. *Neurobiol. Dis.* **141**, 104877. <https://doi.org/10.1016/j.nbd.2020.104877> (2020).
- MacLean, M., Lopez-Diez, R., Vasquez, C., Gugger, P. F. & Schmidt, A. M. Neuronal-glia communication perturbations in murine SOD1(G93A) spinal cord. *Commun. Biol.* **5**, 177. <https://doi.org/10.1038/s42003-022-03128-y> (2022).
- Özdinler, P. H. *et al.* Corticospinal motor neurons and related subcerebral projection neurons undergo early and specific neurodegeneration in hSOD1G(9)(3)A transgenic ALS mice. *J. Neurosci.* **31**, 4166–4177. <https://doi.org/10.1523/JNEUROSCI.4184-10.2011> (2011).
- Miller, S. J., Glatzer, J. C., Hsieh, Y. C. & Rothstein, J. D. Cortical astroglia undergo transcriptomic dysregulation in the G93A SOD1 ALS mouse model. *J. Neurogenet.* **32**, 322–335. <https://doi.org/10.1080/01677063.2018.1513508> (2018).
- Gomes, C. *et al.* Cortical neurotoxic astrocytes with early ALS pathology and miR-146a deficit replicate gliosis markers of symptomatic SOD1G93A mouse model. *Mol. Neurobiol.* **56**, 2137–2158. <https://doi.org/10.1007/s12035-018-1220-8> (2019).
- Migliarini, S. *et al.* Microglia morphological changes in the motor cortex of hSOD1(G93A) transgenic ALS mice. *Brain Sci.* <https://doi.org/10.3390/brainsci11060807> (2021).
- Niessen, H. G. *et al.* In vivo quantification of spinal and bulbar motor neuron degeneration in the G93A-SOD1 transgenic mouse model of ALS by T2 relaxation time and apparent diffusion coefficient. *Exp. Neurol.* **201**, 293–300. <https://doi.org/10.1016/j.expneurol.2006.04.007> (2006).
- Schindelin, J. *et al.* Fiji: An open-source platform for biological-image analysis. *Nat. Methods* **9**, 676–682. <https://doi.org/10.1038/nmeth.2019> (2012).
- Ferreira, T. A. *et al.* Neuronal morphometry directly from bitmap images. *Nat. Methods* **11**, 982–984. <https://doi.org/10.1038/nmeth.3125> (2014).
- Wu, Y. E., Pan, L., Zuo, Y., Li, X. & Hong, W. Detecting activated cell populations using single-cell RNA-seq. *Neuron* **96**, 313–329 e316. <https://doi.org/10.1016/j.neuron.2017.09.026> (2017).
- Kantzer, C. G. *et al.* Anti-ACSA-2 defines a novel monoclonal antibody for prospective isolation of living neonatal and adult astrocytes. *Glia* **65**, 990–1004. <https://doi.org/10.1002/glia.23140> (2017).
- Dobin, A. *et al.* STAR: Ultrafast universal RNA-seq aligner. *Bioinformatics* **29**, 15–21. <https://doi.org/10.1093/bioinformatics/bts635> (2013).
- Lun, A. T. L. *et al.* EmptyDrops: Distinguishing cells from empty droplets in droplet-based single-cell RNA sequencing data. *Genome Biol.* **20**, 63. <https://doi.org/10.1186/s13059-019-1662-y> (2019).
- Hao, Y. *et al.* Integrated analysis of multimodal single-cell data. *Cell* **184**, 3573–3587 e3529. <https://doi.org/10.1016/j.cell.2021.04.048> (2021).
- McGinnis, C. S., Murrow, L. M. & Gartner, Z. J. DoubletFinder: Doublet detection in single-cell RNA sequencing data using artificial nearest neighbors. *Cell Syst* **8**, 329–337 e324. <https://doi.org/10.1016/j.cels.2019.03.003> (2019).
- Marsh, S. E. *et al.* Single cell sequencing reveals glial specific responses to tissue processing & enzymatic dissociation in mice and humans. Preprint at: <https://www.biorxiv.org/content/https://doi.org/10.1101/2020.11.12.1103.408542v408541> (2020).
- Young, M. D. & Behjati, S. SoupX removes ambient RNA contamination from droplet-based single-cell RNA sequencing data. *Gigascience* <https://doi.org/10.1093/gigascience/giaa151> (2020).
- Subramanian, A. *et al.* Gene set enrichment analysis: A knowledge-based approach for interpreting genome-wide expression profiles. *Proc. Natl. Acad. Sci. U. S. A.* **102**, 15545–15550. <https://doi.org/10.1073/pnas.0506580102> (2005).
- Yu, G., Wang, L. G., Yan, G. R. & He, Q. Y. DOSE: An R/Bioconductor package for disease ontology semantic and enrichment analysis. *Bioinformatics* **31**, 608–609. <https://doi.org/10.1093/bioinformatics/btu684> (2015).
- Wu, T. *et al.* clusterProfiler 4.0: A universal enrichment tool for interpreting omics data. *Innovation (N Y)* **2**, 100141. <https://doi.org/10.1016/j.xinn.2021.100141> (2021).
- Marques, S. *et al.* Oligodendrocyte heterogeneity in the mouse juvenile and adult central nervous system. *Science* **352**, 1326–1329. <https://doi.org/10.1126/science.aaf6463> (2016).
- Mathys, H. *et al.* Temporal tracking of microglia activation in neurodegeneration at single-cell resolution. *Cell Rep.* **21**, 366–380. <https://doi.org/10.1016/j.celrep.2017.09.039> (2017).
- Butovsky, O. & Weiner, H. L. Microglial signatures and their role in health and disease. *Nat. Rev. Neurosci.* **19**, 622–635. <https://doi.org/10.1038/s41583-018-0057-5> (2018).

38. McCombe, P. A. & Henderson, R. D. Effects of gender in amyotrophic lateral sclerosis. *Gend. Med.* **7**, 557–570. <https://doi.org/10.1016/j.genm.2010.11.010> (2010).
39. Ziff, O. J. *et al.* Meta-analysis of human and mouse ALS astrocytes reveals multi-omic signatures of inflammatory reactive states. *Genome Res.* **32**, 71–84. <https://doi.org/10.1101/gr.275939.121> (2022).
40. Loda, A. & Heard, E. Xist RNA in action: Past, present, and future. *PLoS Genet.* **15**, e1008333. <https://doi.org/10.1371/journal.pgen.1008333> (2019).
41. Ashburner, M. *et al.* Gene ontology: Tool for the unification of biology. The Gene Ontology Consortium. *Nat. Genet.* **25**, 25–29. <https://doi.org/10.1038/75556> (2000).
42. Gene Ontology Consortium. The gene ontology resource: Enriching a GOLD mine. *Nucleic Acids Res.* **49**, D325–D334. <https://doi.org/10.1093/nar/gkaa1113> (2021).
43. Jankovic, M. *et al.* Current concepts on genetic aspects of mitochondrial dysfunction in amyotrophic lateral sclerosis. *Int. J. Mol. Sci.* <https://doi.org/10.3390/ijms22189832> (2021).
44. Krasemann, S. *et al.* The TREM2-APOE pathway drives the transcriptional phenotype of dysfunctional microglia in neurodegenerative diseases. *Immunity* **47**, 566–581 e569. <https://doi.org/10.1016/j.immuni.2017.08.008> (2017).
45. Doretto, S. *et al.* Oligodendrocytes as regulators of neuronal networks during early postnatal development. *PLoS One* **6**, e19849. <https://doi.org/10.1371/journal.pone.0019849> (2011).
46. Su, X., Vasilkovska, T., Fröhlich, N. & Garaschuk, O. Characterization of cell type-specific S100B expression in the mouse olfactory bulb. *Cell Calcium* **94**, 102334. <https://doi.org/10.1016/j.ceca.2020.102334> (2021).
47. Sun, Y. *et al.* Therapeutic opportunities of interleukin-33 in the central nervous system. *Front Immunol.* **12**, 654626. <https://doi.org/10.3389/fimmu.2021.654626> (2021).
48. Kenigsbuch, M. *et al.* A shared disease-associated oligodendrocyte signature among multiple CNS pathologies. *Nat. Neurosci.* **25**, 876–886. <https://doi.org/10.1038/s41593-022-01104-7> (2022).
49. Lee, S. H. *et al.* TREM2-independent oligodendrocyte, astrocyte, and T cell responses to tau and amyloid pathology in mouse models of Alzheimer disease. *Cell Rep.* **37**, 110158. <https://doi.org/10.1016/j.celrep.2021.110158> (2021).
50. Jäkel, S. *et al.* Altered human oligodendrocyte heterogeneity in multiple sclerosis. *Nature* **566**, 543–547. <https://doi.org/10.1038/s41586-019-0903-2> (2019).
51. Berghoff, S. A. *et al.* Neuronal cholesterol synthesis is essential for repair of chronically demyelinated lesions in mice. *Cell Rep.* **37**, 109889. <https://doi.org/10.1016/j.celrep.2021.109889> (2021).
52. Cain, A. *et al.* Multi-cellular communities are perturbed in the aging human brain and with Alzheimer's disease. Preprint at: <https://www.biorxiv.org/content/https://doi.org/10.1101/2020.1112.1122.424084v424081> (2020).
53. Davalos, D. *et al.* ATP mediates rapid microglial response to local brain injury in vivo. *Nat. Neurosci.* **8**, 752–758. <https://doi.org/10.1038/nn1472> (2005).
54. Vucic, S., Pavey, N., Haidar, M., Turner, B. J. & Kiernan, M. C. Cortical hyperexcitability: Diagnostic and pathogenic biomarker of ALS. *Neurosci. Lett.* **759**, 136039. <https://doi.org/10.1016/j.neulet.2021.136039> (2021).
55. Jara, J. H. *et al.* Evidence for an early innate immune response in the motor cortex of ALS. *J. Neuroinflamm.* **14**, 129. <https://doi.org/10.1186/s12974-017-0896-4> (2017).
56. Dols-Icardo, O. *et al.* Motor cortex transcriptome reveals microglial key events in amyotrophic lateral sclerosis. *Neurol. Neuroimmunol. Neuroinflamm.* <https://doi.org/10.1212/NXI.0000000000000829> (2020).
57. Limone, F. *et al.* Single-nucleus sequencing reveals enriched expression of genetic risk factors sensitises motor neurons to degeneration in ALS. Preprint at: <https://www.biorxiv.org/content/https://doi.org/10.1101/2021.1107.1112.452054v452051> (2021).
58. Gomes, C. *et al.* Astrocyte regional diversity in ALS includes distinct aberrant phenotypes with common and causal pathological processes. *Exp. Cell Res.* **395**, 112209. <https://doi.org/10.1016/j.yexcr.2020.112209> (2020).
59. van den Bos, M. A. J., Geevasinga, N., Higashihara, M., Menon, P. & Vucic, S. Pathophysiology and diagnosis of ALS: Insights from advances in neurophysiological techniques. *Int. J. Mol. Sci.* <https://doi.org/10.3390/ijms20112818> (2019).
60. Burg, T. *et al.* Absence of subcerebral projection neurons is beneficial in a mouse model of amyotrophic lateral sclerosis. *Ann. Neurol.* **88**, 688–702. <https://doi.org/10.1002/ana.25833> (2020).
61. Phatnani, H. P. *et al.* Intricate interplay between astrocytes and motor neurons in ALS. *Proc. Natl. Acad. Sci. U. S. A.* **110**, E756–765. <https://doi.org/10.1073/pnas.1222361110> (2013).
62. Matson, K. J. E. *et al.* A single cell atlas of spared tissue below a spinal cord injury reveals cellular mechanisms of repair. Preprint at: <https://www.biorxiv.org/content/https://doi.org/10.1101/2021.1104.1128.441862v441861> (2021).
63. Kaya, T. *et al.* T cells induce interferon-responsive oligodendrocytes during white matter aging. Preprint at: <https://www.biorxiv.org/content/https://doi.org/10.1101/2022.1103.1126.485917v485911.full> (2022).
64. Edgar, R., Domrachev, M. & Lash, A. E. Gene expression omnibus: NCBI gene expression and hybridization array data repository. *Nucleic Acids Res.* **30**, 207–210. <https://doi.org/10.1093/nar/30.1.207> (2002).
65. Ferraiuolo, L. *et al.* Dysregulation of astrocyte-motoneuron cross-talk in mutant superoxide dismutase 1-related amyotrophic lateral sclerosis. *Brain* **134**, 2627–2641. <https://doi.org/10.1093/brain/awr193> (2011).
66. Sun, S. *et al.* Translational profiling identifies a cascade of damage initiated in motor neurons and spreading to glia in mutant SOD1-mediated ALS. *Proc. Natl. Acad. Sci. U. S. A.* **112**, E6993–7002. <https://doi.org/10.1073/pnas.1520639112> (2015).
67. Butovsky, O. *et al.* Modulating inflammatory monocytes with a unique microRNA gene signature ameliorates murine ALS. *J. Clin. Invest.* **122**, 3063–3087. <https://doi.org/10.1172/JCI62636> (2012).
68. Butovsky, O. *et al.* Targeting miR-155 restores abnormal microglia and attenuates disease in SOD1 mice. *Ann. Neurol.* **77**, 75–99. <https://doi.org/10.1002/ana.24304> (2015).
69. Fukada, Y. *et al.* Gene expression analysis of the murine model of amyotrophic lateral sclerosis: Studies of the Leu126delTT mutation in SOD1. *Brain Res.* **1160**, 1–10. <https://doi.org/10.1016/j.brainres.2007.05.044> (2007).
70. Yoshihara, T. *et al.* Differential expression of inflammation- and apoptosis-related genes in spinal cords of a mutant SOD1 transgenic mouse model of familial amyotrophic lateral sclerosis. *J. Neurochem.* **80**, 158–167. <https://doi.org/10.1046/j.0022-3042.2001.00683.x> (2002).
71. Kudo, L. C. *et al.* Integrative gene-tissue microarray-based approach for identification of human disease biomarkers: Application to amyotrophic lateral sclerosis. *Hum. Mol. Genet.* **19**, 3233–3253. <https://doi.org/10.1093/hmg/ddq232> (2010).
72. Chen, H. *et al.* Differential expression and alternative splicing of genes in lumbar spinal cord of an amyotrophic lateral sclerosis mouse model. *Brain Res.* **1340**, 52–69. <https://doi.org/10.1016/j.brainres.2010.03.075> (2010).
73. Wang, R., Yang, B. & Zhang, D. Activation of interferon signaling pathways in spinal cord astrocytes from an ALS mouse model. *Glia* **59**, 946–958. <https://doi.org/10.1002/glia.21167> (2011).
74. D'Arrigo, A. *et al.* Transcriptional profiling in the lumbar spinal cord of a mouse model of amyotrophic lateral sclerosis: A role for wild-type superoxide dismutase 1 in sporadic disease?. *J. Mol. Neurosci.* **41**, 404–415. <https://doi.org/10.1007/s12031-010-9332-2> (2010).
75. Baker, D. J. *et al.* Lysosomal and phagocytic activity is increased in astrocytes during disease progression in the SOD1 (G93A) mouse model of amyotrophic lateral sclerosis. *Front. Cell Neurosci.* **9**, 410. <https://doi.org/10.3389/fncel.2015.00410> (2015).

Acknowledgements

The authors would like to thank Helena Pavlikova and Marketa Hemerova for their excellent technical assistance and Frances Zatrepaalkova for proofreading the manuscript. This study was supported by grants 23-05327S and 19-02046S from the Czech Science Foundation, by the Charles University Grant Agency (Grant Number 158320), by the Institutional support RVO 86652036, by MEYS CR (CZ.1.05/1.1.00/02.0109), by the Czech Academy of Sciences (Strategy AV21, grant number VP29), by European Union's Horizon 2020 research and innovation programme under the EJP RD COFUND- EJP N° 825575 and by EU – Next generation EU, LX22NPO5107 (MEYS). Microscopy was done at the Microscopy Service Centre of the Institute of Experimental Medicine CAS supported by the MEYS CR (LM2023050 Czech-Bioimaging).

Author contributions

T.F. and Z.M. interpreted the data, wrote the manuscript and prepared all figures. T.F., Z.M., P.A., O.V., J.T., M.K. and D.K. performed experiments. T.F., Z.M., P.A., L.V., J.T., O.V. and S.B. analyzed data. J.Z. wrote a macro for immunohistochemical analysis. M.A. and L.V. conceived and supervised the study. All authors reviewed and edited the manuscript.

Competing interests

The authors declare no competing interests.

Additional information

Supplementary Information The online version contains supplementary material available at <https://doi.org/10.1038/s41598-023-33608-y>.

Correspondence and requests for materials should be addressed to L.V. or M.A.

Reprints and permissions information is available at www.nature.com/reprints.

Publisher's note Springer Nature remains neutral with regard to jurisdictional claims in published maps and institutional affiliations.



Open Access This article is licensed under a Creative Commons Attribution 4.0 International License, which permits use, sharing, adaptation, distribution and reproduction in any medium or format, as long as you give appropriate credit to the original author(s) and the source, provide a link to the Creative Commons licence, and indicate if changes were made. The images or other third party material in this article are included in the article's Creative Commons licence, unless indicated otherwise in a credit line to the material. If material is not included in the article's Creative Commons licence and your intended use is not permitted by statutory regulation or exceeds the permitted use, you will need to obtain permission directly from the copyright holder. To view a copy of this licence, visit <http://creativecommons.org/licenses/by/4.0/>.

© The Author(s) 2023

- **Publication II**

Matusova, Z.*, Dykstra, W.*, de Pablo, Y., Zetterdahl, O. G., Canals, I., van Gelder, C. A. G. H., Vos H. R., Pérez-Sala, D., Kubista, M., Abaffy, P., Ahlenius, H., Valihrach, L., Hol, E. M., Pekny, M. **Aberrant neurodevelopment in human iPSC cell-derived models of Alexander disease.** *Glia*, 2024. doi: 10.1002/glia.24618.

* shared first authors














Journal: *Glia*, IF 5.4 (2023)

Summary: Human iPSC-derived models offer an opportunity to model diseases on human genetic background. In this project, joint efforts of members of the ALEXANDER Consortium yielded two new models of AxD, which is caused by mutations in GFAP. We focused on hiPSC-derived cell cultures, namely astrocyte-neuron and brain organoids, and we analyzed them with scRNA-seq. Interestingly, we revealed an increased abundance of less mature cells in samples that contained cells with the GFAP mutation and the absence of mature astrocytes in brain organoids. Furthermore, the overrepresentation of cell types from other lineages than neuroectoderm suggested impaired lineage commitment in the AxD samples. Our results bring previously unexplored insights into the AxD pathology and imply that the GFAP mutation might have a negative effect on human neurodevelopment.

Contribution: ScRNA-seq represents the backbone of this publication. I participated in the discussions on the experimental design, prepared organoid sequencing libraries, and analyzed and interpreted the transcriptomic data. I prepared the manuscript text and the majority of the figures, supervised the incorporation of non-transcriptomic elements, and was involved in the editing process of the whole manuscript.

RESEARCH ARTICLE

Aberrant neurodevelopment in human iPS cell-derived models of Alexander disease

Zuzana Matusova^{1,2}  | Werner Dykstra³  | Yolanda de Pablo⁴  |
 Oskar G. Zetterdahl^{5,6}  | Isaac Canals^{6,7,8}  | Charlotte A. G. H. van Gelder⁹  |
 Harmjan R. Vos⁹  | Dolores Pérez-Sala¹⁰  | Mikael Kubista^{1,11}  |
 Pavel Abaffy¹  | Henrik Ahlenius⁵  | Lukas Valihrach^{1,12}  | Elly M. Hol³  |
 Milos Pekny^{4,13,14} 

¹Laboratory of Gene Expression, Institute of Biotechnology of the Czech Academy of Sciences, Vestec, Czechia

²Faculty of Science, Charles University, Prague, Czechia

³Department of Translational Neuroscience, University Medical Centre Utrecht Brain Centre, Utrecht University, Utrecht, The Netherlands

⁴Laboratory of Astrocyte Biology and CNS Regeneration, Center for Brain Repair, Department of Clinical Neuroscience, Institute of Neuroscience and Physiology, Sahlgrenska Academy at the University of Gothenburg, Gothenburg, Sweden

⁵Stem Cells, Aging and Neurodegeneration Lab, Department of Experimental Medical Science, Faculty of Medicine, Lund Stem Cell Center, Lund University, Lund, Sweden

⁶Glial and Neuronal Biology Lab, Department of Experimental Medical Science, Faculty of Medicine, Lund Stem Cell Center, Lund University, Lund, Sweden

⁷Division of Metabolism, University Children's Hospital Zurich, University of Zurich, Zurich, Switzerland

⁸ITINERARE–Innovative therapies in rare diseases, University Research Priority Program, University of Zurich, Zurich, Switzerland

⁹Oncode Institute and Molecular Cancer Research, Center for Molecular Medicine, University Medical Center Utrecht, Utrecht University, Utrecht, The Netherlands

¹⁰Centro de Investigaciones Biológicas Margarita Salas, Madrid, Spain

¹¹Institute of Biomedicine, University of Gothenburg, Gothenburg, Sweden

¹²Department of Cellular Neurophysiology, Institute of Experimental Medicine of the Czech Academy of Sciences, Prague, Czechia

¹³Florey Institute of Neuroscience and Mental Health, Parkville, Victoria, Australia

¹⁴University of Newcastle, Newcastle, New South Wales, Australia

Correspondence

Lukas Valihrach, Laboratory of Gene Expression, Institute of Biotechnology of the Czech Academy of Sciences, Vestec, Czechia.
 Email: lukas.valihrach@ibt.cas.cz

Elly M. Hol, Department of Translational Neuroscience, University Medical Centre Utrecht Brain Centre, Utrecht University, Utrecht, The Netherlands.
 Email: e.m.hol-2@umcutrecht.nl

Milos Pekny, Laboratory of Astrocyte Biology and CNS Regeneration, Center for Brain Repair, Department of Clinical Neuroscience, Institute of Neuroscience and Physiology, Sahlgrenska Academy at the University of

Abstract

Alexander disease (AxD) is a rare and severe neurodegenerative disorder caused by mutations in glial fibrillary acidic protein (GFAP). While the exact disease mechanism remains unknown, previous studies suggest that mutant GFAP influences many cellular processes, including cytoskeleton stability, mechanosensing, metabolism, and proteasome function. While most studies have primarily focused on GFAP-expressing astrocytes, GFAP is also expressed by radial glia and neural progenitor cells, prompting questions about the impact of GFAP mutations on central nervous system (CNS) development. In this study, we observed impaired differentiation of astrocytes and neurons in co-cultures of astrocytes and neurons, as well as in neural organoids, both

Zuzana Matusova and Werner Dykstra are first authors. Elly M. Hol and Milos Pekny are shared senior authors.

This is an open access article under the terms of the [Creative Commons Attribution](https://creativecommons.org/licenses/by/4.0/) License, which permits use, distribution and reproduction in any medium, provided the original work is properly cited.

© 2024 The Author(s). GLIA published by Wiley Periodicals LLC.



Gothenburg, Gothenburg, Sweden.
Email: milos.pekny@neuro.gu.se

Funding information

EJP RD – European Joint Programme on Rare Diseases, Grant/Award Number: 825575; Swedish Research Council, Grant/Award Numbers: 2017-02255, 2019-00284, 2020-01148; 'la Caixa' Foundation, Grant/Award Number: LCF/PR/HR21/52410002; Avtal om Läkarutbildning och Forskning (ALF) Gothenburg, Grant/Award Numbers: 146051, 965939; Amlöv's Foundation; E. Jacobson's Donation Fund, Grant/Award Number: PID2021-126827OB-I00; Institutional support (Czech Republic), Grant/Award Number: RVO 86652036; Czech Science Foundation, Grant/Award Numbers: 24-11364S, 24-12028S; Petrus och Augusta Hedlunds stiftelse; Hjärnfonden, Grant/Award Number: FO02021-0082; MCIN/AEI/10.13039/501100011033/ERDF, Grant/Award Number: PID2021-126827OB-I00; Swedish Foundation for Strategic Research, Grant/Award Number: SM23-0033; X-Omics initiative, Grant/Award Number: 184.034.019; ZonMw, Grant/Award Number: 463002004; Swedish Society for Medical Research; Söderberg's Foundations; Hagströmer's Foundation Millennium

generated from AxD patient-derived induced pluripotent stem (iPS) cells with a GFAP^{R239C} mutation. Leveraging single-cell RNA sequencing (scRNA-seq), we identified distinct cell populations and transcriptomic differences between the mutant GFAP cultures and a corrected isogenic control. These findings were supported by results obtained with immunocytochemistry and proteomics. In co-cultures, the GFAP^{R239C} mutation resulted in an increased abundance of immature cells, while in unguided neural organoids and cortical organoids, we observed altered lineage commitment and reduced abundance of astrocytes. Gene expression analysis revealed increased stress susceptibility, cytoskeletal abnormalities, and altered extracellular matrix and cell–cell communication patterns in the AxD cultures, which also exhibited higher cell death after stress. Overall, our results point to altered cell differentiation in AxD patient-derived iPS-cell models, opening new avenues for AxD research.

KEYWORDS

Alexander disease, GFAP, iPS cells, neural organoids

1 | INTRODUCTION

Alexander disease (AxD) is a rare and severe neurodegenerative disorder affecting primarily the white matter. It is caused by mutations in glial fibrillary acidic protein (GFAP), which in the central nervous system (CNS) is expressed by astrocytes and neural stem cells. Mutant GFAP together with several associated proteins form aggregates in astrocytes known as Rosenthal fibers (RFs), which are the main neuropathological hallmark of AxD (reviewed in Hagemann (2022), Pajares et al. (2023), Pekny et al. (2016)). To date, a number of pivotal studies using rodent (Hagemann et al., 2005; Hagemann et al., 2006; Heaven et al., 2022; Meisingset et al., 2010; Tanaka et al., 2007), *Drosophila* (Wang et al., 2011), zebrafish (Lee et al., 2017), human cell culture models (Jones et al., 2018; Kondo et al., 2016), or patient post-mortem brain samples (Olabarria et al., 2015; Tang et al., 2010; Walker et al., 2014) brought important insights into AxD pathogenesis, revealing that overexpression and aggregation of mutant GFAP in astrocytes is accompanied by a stress response, neuroinflammation, and reactive gliosis as well as disruption of vesicular trafficking, proteasome function, and glutamate and calcium homeostasis. AxD astrocytes exhibit altered posttranslational modifications of GFAP (Battaglia et al., 2019; Viedma-Poyatos et al., 2022), impaired intermediate filament organization (Yang et al., 2022) and their increased sensitivity to oxidative stress further enhances GFAP aggregation (Viedma-Poyatos et al., 2022). Sosunov et al. observed AxD astrocytes with reactive-like features, some of them containing multiple nuclei as a consequence of mitosis arrest

(Sosunov et al., 2013; Sosunov et al., 2017). Abnormal organelle morphology and distribution (Jones et al., 2018), including mitochondria (Viedma-Poyatos et al., 2022), were detected in AxD astrocytes. Impaired mitochondria transfer between astrocytes and neurons may contribute to the disease pathogenesis (Gao et al., 2019). Linking GFAP mutation to white matter degeneration, AxD astrocytes were shown to inhibit proliferation of oligodendrocyte progenitor cells (OPCs) and reduce their myelination potential (Li, Tian, et al., 2018).

GFAP is also expressed in multipotent neural stem cells (Imura et al., 2003) and in radial glia (RG) of the developing brain (Dimou & Gotz, 2014), but the effect of GFAP mutations on brain development is largely unexplored. Hagemann et al. (2013) reported aberrant adult neurogenesis in the hippocampus of the Gfap^{+/R236H} AxD mouse model, observing RG-like cells with RFs and hypertrophic morphology, absence of immature neurons, and diminished proliferation of neural progenitors, possibly a consequence of disturbed ubiquitin-proteasome system, which normally regulates essential developmental pathways such as Notch, WNT, Hedgehog, and TGF β (Baloghova et al., 2019; Dutta et al., 2022; Gao et al., 2014; Hsia et al., 2015; Imamura et al., 2013).

Here, we used an AxD patient-derived induced pluripotent stem (iPS) cell line carrying a GFAP^{R239C} mutation and a CRISPR/Cas9-corrected isogenic control cell line to generate astrocyte-neuron co-cultures, as well as unguided neural organoids and cortical organoids. Leveraging single-cell RNA sequencing (scRNA-seq), we describe a differentiation impairment and increased sensitivity to oxygen–glucose deprivation (OGD) challenge in AxD co-cultures. In

AxD unguided neural organoids and cortical organoids, we observed almost complete absence of astrocytes, reduced neurogenesis and enrichment of mesoderm- and endoderm-derived cell populations, suggesting a neural lineage commitment defect.

2 | METHODS

2.1 | iPS cells

AxD iPS cells, derived from a 6-year-old AxD patient carrying the heterozygous point mutation in *GFAP* (c.715C > T, p.R239C), and isogenic CRISPR/Cas9-corrected control iPS cells were received from Natasha Snider (Department of Cell Biology and Physiology, University of North Carolina at Chapel Hill, USA) and were described previously (Battaglia et al., 2019).

2.2 | Lentiviral production

Lentiviral vectors used were M2-rtTA (rtTA, reverse tetracycline-controlled transactivator, Addgene #20342), tet-O-Ngn2-puro (Addgene #52047, Zhang et al. (2013)), tetO-Sox9-Puro (Addgene #117269), and tetO-Nfib-Hygro (Addgene #117271). Nfib, Ngn2, Sox9, and rtTA lentiviruses were produced in HEK 293 T cells, as described in Canals et al. (2018). Briefly, the HEK 293 T cells were cotransfected with the packaging plasmids pMDLg/pRRE (Addgene #12251), pMD2.G (Addgene #12259), and pRSV-Rev (Addgene #12253) in addition to the lentivectors, approximately 44 h following transfection the viruses were pelleted by centrifugation (20,000 rpm at 4°C for 2 h), and the supernatant was subsequently aspirated. A total of 100 µL of Dulbecco's modified Eagle's medium (DMEM) was added to the pellet without resuspending. One day later, the viruses were resuspended, aliquoted and frozen at -80°C for long-term storage.

2.3 | iPS cell culturing for neuronal and astrocyte co-cultures

Cell lines were maintained in mTeSR1/mTeSR+ media on ES-qualified Matrigel-coated 6 W plates at 37°C in humidified air with 5% CO₂ with daily medium change. Cells were passaged with accutase (StemPro Accutase Cell Dissociation Reagent) upon attaining confluency of ~80%. Upon dissociation, the cells were centrifuged at 300 × g and replated onto fresh Matrigel-coated 6-well plates at a density of 2–2.5 × 10⁵ cells/well using medium supplemented with 10 µM of ROCK Inhibitor (RI) in the initial 24 h after replating to enhance the rate of cell survival.

2.4 | Differentiation of induced astrocytes

Human iPS cells at ~80% confluency were dissociated with accutase on Day -2, and 4 × 10⁵ cells were plated on Matrigel-coated

6-well plates with mTeSR supplemented with 10 µM RI. The following day (Day -1), the medium was replaced with fresh mTeSR medium, and 1 µL of rtTA Sox9 and Nfib lentivirus was added to each well. On Day 0, the medium was replaced with fresh mTeSR medium containing Doxycycline (Dox; 2.5 µg/mL), which was added to the medium throughout the experiments. Sox9 and Nfib lentiviral overexpression was used for astrocyte induction (Canals et al., 2018). On Days 1 and 2 the iAs were cultured in expansion medium (DMEM/F12, 10% FBS, 1% N2, and 1% GlutaMax). Between Day 3 and 5, expansion medium was gradually changed to FGF medium (Neurobasal, 2% B27, 1% NEEA, 1% GlutaMax, 1% FBS, 8 ng/mL FGF, 5 ng/mL CNTF, and 10 ng/mL BMP4). Overall, 72 h of puromycin (2.5 µg/mL) selection and 5 days of hygromycin (200 µg/mL) selection was performed.

2.5 | Differentiation of glutamatergic induced neurons

Human iPS cells at ~80% confluency were dissociated with accutase on Day -2, and 3 × 10⁵ cells were plated on Matrigel-coated 6-well plates with mTeSR-1 supplemented with 10 µM RI. The following day (Day -1), the medium was replaced with fresh mTeSR-1 medium, and 1 µL of rtTA and Ngn2 lentivirus was added to each well. On Day 0, the medium was replaced with fresh mTeSR-1 medium containing Doxycycline (Dox; 2.5 µg/mL), which was added to the medium throughout the experiments. Ngn2 lentiviral overexpression was used for neuronal induction (Zhang et al., 2013). From Day 1, supplemented BrainPhys medium (BrainPhys, 0.5% N2 supplement, 1% B27 supplement) was used and 72 h of puromycin (2.5 µg/mL) selection was performed. From Day 5, the medium was supplemented with NT3 (10 ng/mL) and BDNF (10 ng/mL).

2.6 | Co-cultures of iAs and iNs

On Day 7, iAs and iNs were dissociated with accutase supplemented with DNase I for 10 min. The iAs were then pelleted for 5 min at 300 × g. The iNs were dissociated in accutase for 10 min, followed by manual resuspension in the accutase for 5 more minutes before being pelleted for 5 min at 300 × g. The iNs were then strained through a 40 µm mesh to avoid neuronal aggregates. 3.9 × 10⁴ iAs were plated together with 1.11 × 10⁵ iNs on PEI + rhLam521-coated Ibidi 24 well µ-Plates. For the scRNAseq, 2.6 × 10⁵ iAs and 7.4 × 10⁵ iNs were plated on Matrigel-coated six well plates. The medium henceforth consisted of 50% iNs medium and 50% iAs medium. On Day 8, the medium was replaced with 1:1 BrainPhys and FGF medium. From Day 9 on, the FGF medium was changed to Maturation medium (1:1 DMEM/F12 and Neurobasal, 1% N2, 1% Na Pyruvate, 10 µg/mL NAC, 10 ng/mL hbEGF, 10 ng/mL CNTF, 10 ng/mL BMP4, 500 µg/mL dbcAMP) and half of the medium would be changed every 2 days. Between Days 9 and 21, 5-Fluoro-2'-deoxyuridine (FUDR; 20 µM/mL) was added to the medium to inhibit cell division. Co-cultures were maintained for 42 days before being used for experiments.



2.7 | Oxygen–glucose deprivation challenge

After 5 weeks in co-culture, medium was changed to deoxygenated ischemic medium (DMEM w/o glucose, 2.5 $\mu\text{g}/\text{mL}$ Dox, 5 ng/mL NT3, 5 ng/mL BDNF, 10 $\mu\text{g}/\text{mL}$ NAC, 10 ng/mL hbEGF, 5 ng/mL CNTF, 5 ng/mL BMP4, 250 $\mu\text{g}/\text{mL}$ dbcAMP) for cells to be subjected to the OGD, and co-culture medium for the control (1:1 BrainPhys and Maturation media, with factors). The OGD cells were incubated at 37°C in humidified air with 1% O_2 and 5% CO_2 , and control cells at normal culturing conditions (37°C in humidified air with 5% CO_2), for 4 h. Subsequently, a medium change to fresh co-culture media for all cells was performed, followed by 2 h of recovery under normal culturing conditions for the LDH assay and 16 h of recovery for the single-cell RNA sequencing.

2.8 | LDH assay

Media samples were taken following the 2 h reperfusion period after OGD challenge, from both OGD-exposed and control cells. One well of each condition was lysed by adding Triton-X 100 to final concentration of 1%, to obtain the Max LDH release. Cytotoxicity was assessed using Takara Bio LDH Cytotoxicity Detection Kit. Absorbance was measured at 490 nm (600 nm as a reference wavelength) and cytotoxicity was calculated using the formula: $\text{Cytotoxicity (\%)} = \frac{\text{Absorbance}_{(490-600)} \text{ LDH Sample}}{\text{Absorbance}_{(490-600)} \text{ Max LDH Release}} \times 100$.

2.9 | Single-cell suspension for scRNA-seq

Medium was aspirated and cells were washed with cold phosphate-buffered saline (PBS) ^{Ca²⁺/Mg²⁺}. Cells were dissociated with accutase supplemented with 30 μM ActD and incubated until most cells were detached. The accutase was then inhibited with DMEM supplemented with 3 μM ActD and 2% B27 and cells were collected in LoBind 15 mL tubes and kept on ice for the rest of the protocol. Using a wide-bore pipette, cells were gently resuspended. Cells were strained before being centrifuged at 250 $\times g$ at 4°C for 5 min. Supernatant was removed and cells were gently resuspended in cold DMEM (with 3 μM ActD and 2% B27) using a wide-bore pipette tip. Cells were centrifuged at 150 $\times g$ at 4°C for 5 min. Supernatant was once again removed. The volume of cell suspension was adjusted using cold DMEM with 3 μM ActD and 2% B27. Samples were then strained, and an additional cell count was performed. If necessary, the volumes of samples were adjusted to obtain a target cell concentration of 700–1200 cells/ μL and a target cell count of 10,000 cells per sample.

2.10 | Immunofluorescence of co-cultures

For immunofluorescence imaging, cells were plated on PEI + rhLam521-coated Ibidi 24-well μ -Plates. Cells were washed with room temperature PBS ^{Ca²⁺/Mg²⁺} and then fixed in 4% paraformaldehyde

(PFA) in PBS at room temperature for 15 min. Cells were washed three times with potassium-phosphate-buffered saline (KPBS) before being blocked with KPBS containing 0.025% Triton X-100 (TKPBS) and either 5% normal donkey serum or 2.5% normal donkey serum and 2.5% normal goat serum for 60 min. Primary antibodies were incubated in blocking solution overnight at 4°C. Cells were washed twice with 0.025% TKPBS and once with blocking solution for 5 min. Secondary antibody together with nuclear staining incubation was performed at room temperature for 2 h in blocking solution. Cells were washed once with 0.025% TKPBS for 5 min and twice for 5 min with KPBS, PVA:DABCO was used to mount coverslips on top of stained cells.

Images of the co-cultures were acquired using an epifluorescence Leica microscope and were analyzed using Fiji (Schindelin et al., 2012). Images for the assessment of the morphology of GFAP-positive cells were acquired using a 40 \times objective. The GFAP outline was traced manually, circularity, and perimeter were measured using Fiji shape descriptors. Each datapoint represents a cell. Images for cell counts were taken using a 10 \times objective, MAP2⁺, Vimentin⁺, or GFAP⁺ cells were counted manually. Undifferentiated cells were identified manually based on their spherical morphology on phase contrast images. Each datapoint represents a separate culture. Normal distribution of the data was tested with the Shapiro–Wilk normality test. The Wilcoxon rank sum test with continuity correction was used to compare nonnormally distributed data, Student's *t*-test was used to compare normally distributed data.

2.11 | iPS cell culture for neural organoid generation

iPS cells were maintained in Stemflex medium (Life technologies, A3349401) on Geltrex-coated (Life technologies, A1413202) dishes in feeder-free conditions at 37°C with 5% CO_2 . The medium was changed daily, and cells were split in Stemflex medium containing 5 μM Y27632 (Axon Biochemicals, AXON 1683) as soon as they reached 80% confluency by incubating them with 0.5 mM EDTA for 3 min at 37°C. After 24 h, the medium was changed to regular Stemflex medium. The number of passages was kept below 40 and routine testing for mycoplasma (Lonza, LT07-318, Lonza Bioscience Solutions, Basel, Switzerland) was performed.

2.12 | Generation of unguided neural organoids

Unguided neural organoids were generated according to a combined protocol of Ormel et al. (2018), Lancaster et al. (2013), and Verkerke et al. (2024). Briefly, at Day 0, iPS cells that reached 80% confluency were dissociated into single cells following a 2-min incubation period with 0.5 mM EDTA in PBS and a 4-min incubation period with accutase at 37°C. After counting, ~ 9000 iPS cells were allowed to form an embryoid body at 37°C with 5% CO_2 in a well of an ultra-low attachment round-bottom shaped 96-well plate (Corning 3474) containing a

total of 150 μ L HES medium consisting of DMEM/F-12 (ThermoFisher Scientific, 31330038), 20% KOSR (Life Technologies, 10828028), 3% FBS (ThermoFisher Scientific, 10082147), 1% l-glutamine (Life Technologies, 25030024), 1% NEAAs (ThermoFisher Scientific, 11140035), 0.1 mM 2-Mercaptoethanol (Merck, 8057400005) supplemented with 4 ng/mL bFGF (Pepro-Tech 100-18B), and 50 μ M Y27632 (Axon Biochemicals, AXON 1683) (HES4+ medium). At Day 2, 100 μ L of medium was replaced by 150 μ L of HES4+ medium. At Day 4, 150 μ L of medium was removed and replaced by 150 μ L HES medium. At Day 6, 150 μ L of medium was replaced with 150 μ L neural induction medium (NIM) consisting of DMEM/F-12 (ThermoFisher Scientific, 31330038), 1% N2 (Life Technologies, 17502048), 1% L-glutamine (Life Technologies, 25030024), 1% NEAA (ThermoFisher Scientific, 11140035), and 0.5 μ g/mL heparin (Sigma-Aldrich, H3149). At Day 8, 10, and 12, 150 μ L of the medium was replaced with fresh NIM. At Day 13, unguided neural organoids were embedded in 30 μ L droplets of Matrigel (Corning, 356234), incubated for 25 min at 37°C, and transferred to a 6 cm ultra-low attachment culture dish (Corning, 3261) containing 6 mL of differentiation medium without vitamin A (B27-medium) consisting of DMEM/F-12 (ThermoFisher Scientific, 31330038) in a 1:1 ratio with neurobasal medium (ThermoFisher Scientific, 21103049) supplemented with 1% B27-vitamin A (ThermoFisher Scientific, 12587001), 1% penicillin-streptomycin (Life Technologies, 15140122), 1% L-glutamine (Life Technologies, 25030024), 0.5% NEAA (ThermoFisher Scientific, 11140035), 0.5% N2 (Life Technologies, 17502048), 125 μ L Insulin (Sigma-Aldrich, I9278), 174 μ L 2-Mercaptoethanol (Merck, 8057400005) diluted 1:100 in DMEM/F-12. After 4 days of stationary culture, at Day 17, unguided neural organoids were transferred to an orbital shaker and cultured in 6 mL of differentiation medium containing vitamin A (B27+ medium) consisting of DMEM/F-12 (ThermoFisher Scientific, 31330038), neurobasal medium (ThermoFisher Scientific, 21103049) (1:1) supplemented with 1% B27 + vitamin A (ThermoFisher Scientific, 17504001), 1% penicillin-streptomycin (Life Technologies, 15140122), 1% L-glutamine (Life Technologies, 25030024), 0.5% NEAA (ThermoFisher Scientific, 11140035), 0.5% N2 (Life Technologies, 17502048), 125 μ L Insulin (Sigma-Aldrich, I9278), and 174 μ L 2-Mercaptoethanol (Merck, 8057400005) diluted 1:100 in DMEM/F-12. Until harvested, the medium was replaced every 3 to 4 days.

2.13 | Generation of cortical organoids

Cortical organoids were generated according to an adapted version of Yoon et al. (2019). Briefly, iPS cells that reached 80% confluency were dissociated into single cells following a 7-min incubation period with accutase at 37°C. After counting, 3.5×10^6 iPS cells were seeded in a well of an Aggrewell™800 plate (STEMCELL technologies, 34811) in 2 mL human embryonic stem (HES) medium consisting of DMEM/F-12 (ThermoFisher Scientific, 31330038), 20% KOSR (Life Technologies, 10828028), 3% FBS (ThermoFisher Scientific, 10082147), 1% Glutamax (ThermoFisher Scientific, 35050061), 1% NEAAs (ThermoFisher Scientific, 11140035), 3.5 μ L

2-Mercaptoethanol (Merck, 8057400005) supplemented with 4 ng/mL bFGF, and 50 μ M Y27632 (Axon Biochemicals, AXON 1683) (HES4+). Embryoid bodies were allowed to form at 37°C with 5% CO₂. After 24 h, 1.5 mL of medium was replaced with fresh HES4+ medium. At Day 2, properly formed embryoid bodies were transferred to an ultra-low attachment round-bottom shaped 96-well plate (Corning, 3474) containing a total of 150 μ L of HES medium supplemented with two SMAD pathway inhibitors—Dorsomorphin (2.5 μ M; Tocris 3093) and +SB431542 (10 μ M; Axon biochemicals 1661) to start neural induction. At Day 4, 100 μ L of medium was replaced with 150 μ L of fresh medium. At Day 6, 150 μ L of medium was replaced by 150 μ L of neural medium consisting of neurobasal medium (ThermoFisher Scientific, 21103049), 2% B27-vitamin A (ThermoFisher Scientific, 12587001), 1% penicillin-streptomycin (Life Technologies, 15140122), and 1% L-glutamine (Life Technologies, 25030024) supplemented with 20 ng/mL EGF (R&D systems 236-EG) and 20 ng/mL bFGF (Pepro-Tech 100-18B). After the medium was refreshed every 2 days, at Day 24, EGF and bFGF were replaced by 20 ng/mL BDNF (STEMCELL Technologies 78005.1) and 20 ng/mL NT-3 (Tebu-bio 450-03-B). After a period of bi-daily medium changes, at Day 42, cortical organoids were transferred to a 6 cm ultra-low attachment culture dish (Corning, 3261), and the medium was replaced by neural medium without the addition of growth factors. Subsequently, cortical organoids were cultured on an orbital shaker until harvest with medium changes every 3 to 4 days.

2.14 | Immunofluorescence of organoids

Neural organoids were fixed in 4% PFA in PBS overnight at 4°C and washed three times for 10 min in PBS before being incubated overnight at 4°C in 30% sucrose in PBS. Subsequently, neural organoids were embedded in Tissue-Tek(R) O.C.T. Compound (Sakura Finetek, 4583), snap-frozen in a dry ice/ethanol slurry and stored at -80°C until further use. Sections of 20 μ m thickness were obtained with a Leica CM1950 cryostat (Leica Biosystems, Illinois, USA), collected on SuperFrost(R) PLUS (VWR, 631-0108) slides and stored at -80°C until further processing. Sections were blocked in blocking buffer consisting of 10% normal donkey serum (Jackson ImmunoResearch, 017-000-121), 3% BSA (Sigma-Aldrich, A4503-100) and 0.1% Triton-X (Sigma-Aldrich, T8787-100) in PBS at room temperature for 1 h. Next, samples were incubated with primary antibodies in blocking buffer at 4°C overnight. Slides were then washed three times for 10 min in PBS containing 0.05% Tween 20 (Merck, 817,072) (PBS-T) before being incubated with secondary antibodies and Hoechst (Sigma-Aldrich, 94403) in blocking buffer at room temperature for 1 h. Then, slides were washed three times for 10 min in PBS-T. The antibodies that were used in the current study can be found in Table S2. Finally, samples were mounted on glass coverslips using Fluorosave (CalBioChem, 345789) and imaged using a Zeiss Axioscope A1 (Zeiss, Oberkochen, Germany) and a Zeiss LSM 880 confocal microscope (Zeiss, Oberkochen, Germany). Negative controls are shown in Figure S9.



2.15 | Quantification of immunofluorescent images of organoids

20 \times epifluorescent microscopy images were used. To quantify Hoechst⁺, SOX9⁺, and FOXG1⁺ cells, images were processed using ImageJ software as follows. First, background was subtracted using the subtract background function. Next, a threshold was set to generate binary images. To decrease noise, the despeckle function was used. Hereafter, the watershed function was applied to reduce nuclei clumping. Following this, cells were counted using the analyze particles function, whereby the minimum size of the particles was set at 10 μ m. Three pictures from the outer edge of three organoids were analyzed, thereby generating nine datapoints. DCX integrated density was measured from four organoids per genotype and presented as integrated density per μ m². No difference in the Hoechst signal was observed. Shapiro–Wilk test was used to determine normal distribution of the data and Wilcoxon test (SOX9, FOXG1) and t-test (DCX) were used for statistical comparison between CTRL and AxD samples.

2.16 | RNA isolation and cDNA synthesis

For RNA isolation, five or more neural organoids were pooled and homogenized in 1 mL of Qiazol (QIAGEN, 79306) with an ULTRA-TURRAX(R) (IKA, 0003737000), followed by the addition of chloroform in a 1:5 ratio to Qiazol and centrifuged at 12000 \times g at 4°C for 20 min. The aqueous top phase was collected and mixed with 500 μ L isopropanol and stored overnight at –20°C to allow the RNA to precipitate. Subsequently, samples were centrifuged at 12000 \times g at 4°C for 30 min and the supernatant was aspirated. Pellets were washed three times with 75% ethanol, air-dried, and dissolved in TE-buffer (Invitrogen, 12090-015). RNA concentration was measured using a Varioskan Flash (Thermo Scientific, N06354) or NanoDrop (ThermoFisher Scientific, ND-2000) and cDNA was synthesized using a Quantitect Reverse Transcription kit (QIAGEN, 205311) as follows. After removal of potential genomic DNA contamination using gDNA wipe-out buffer from the kit, 500 ng of RNA was reverse transcribed at 42°C for 30 min followed by incubation at 95°C for 3 min to deactivate the RT enzyme. Samples were diluted 1:20 in RNase-free water and stored at –20°C.

2.17 | RT-qPCR

Real-time quantitative PCR (RT-qPCR) was performed on QuantStudio 6 Flex Real-Time PCR System (ThermoFisher Scientific Inc.) using a 384-well plate under the following conditions: denaturing at 95°C for 10 min, 40 cycles with 95°C for 15 s and annealing at 60°C for 1 min, followed by a dissociation stage where the temperature was increased from 60 to 95°C. Per reaction, 5 μ L FastStart Universal SYBR Green Master (Roche, 04913914001), 3 μ L MQ (Millipore, SYNS00000), 1 μ L cDNA (RNA input

concentration 2.5 ng/ μ L), and 1 μ L of 0.5 μ mol/mL forward and reverse primer mix. Primers are listed in Table S1. Reactions were run in triplicates. Melting curve analysis was performed as a quality check. Gene expression was normalized to reference genes *SDHA*, *TBP*, and *RPII* in unguided neural organoids and to *GAPDH*, β -*Actin*, *TBP*, *SDHA*, and *RPII* in cortical organoids, and the data were visualized in a log₂FC scale of 2^{– $\Delta\Delta$ Ct} relative to the average of Δ Ct of controls. Normal distribution of the data was assessed with Shapiro–Wilk test. Statistical comparison was made with Student's t-test or the Wilcoxon test.

2.18 | Preparation of neural organoids for single-cell RNA sequencing

Eight to 10 neural organoids were washed in an abundance of warm PBS and subsequently chopped into small pieces using a sterile blade. The minced organoids were dissociated in 5 mL of DMEM/F-12 (ThermoFisher Scientific, 31330038) with freshly dissolved DNase (1/23 units/mL, Worthington LS006361) and papain (22 units/mL, Worthington LS003118) by gently passing them through a 1 mL pipet tip about 20 times, followed by incubation on an orbital shaker at 37°C with 5% CO₂ for 10 min. Trituration and centrifugation were repeated three times in total with the last incubation lasting 5 min. After the final dissociation, the enzymes were inactivated by addition of 2% FBS in DMEM/F-12. Cells were passed through a 40 μ m mesh and spun down for 5 min at 300 \times g. After removal of the supernatant and resuspension in 1 mL of DMEM/F-12 + 2% FBS, cells were counted using an automated cell counter (Countess II). 1 \times 10⁶ cells were fixed for 20 h at 4°C using 10x Fixation of Cells & Nuclei for Chromium Fixed RNA Profiling, (10x Genomics) according to the manufacturer's instructions.

2.19 | Preparation of scRNA-seq libraries

Single-cell suspensions from co-cultures were processed using Chromium Next GEM Single Cell 3' Reagent Kit v3.1 (10x Genomics, Pleasanton, CA) according to the manufacturer's instructions by the Center for Translational Genomics, Lund University. Suspension from 165D-old organoids was fixed and processed using Chromium Fixed RNA Kit (10x Genomics, Pleasanton, CA) according to the manufacturer's instructions. In this case, a pre-defined set of probes is used to capture protein-coding genes, mitigating the risk of contamination by ribosomal and mitochondrial genes and other highly abundant transcripts. The concentration and quality of the libraries were measured using Qubit dsDNA HS Assay Kit (Invitrogen) and Fragment Analyzer HS NGS Fragment Kit (#DNF-474, Agilent).

The libraries were sequenced in paired-end dual indexing mode with NovaSeq 6000 SP Reagent Kit v1.5 (100 cycles). Cell-specific 10x GEM Barcodes (16 bp) and molecule-specific UMIs (12 bp) were contained within Read 1 (28 bp), and target sequence was contained within Read 2 (90 bp). Details can be found in Table S3.

2.20 | Data processing and analyses

Initial quality control of sequencing data was performed using FastQ Screen (0.11.1, Wingett and Andrews (2018)). Sequences were trimmed with TrimmomaticSE (0.36, Bolger et al. (2014)). STARsolo (STAR 2.7.9a, Dobin et al. (2013)) was applied to align sequences to human genome *Homo sapiens* GRCh38 (annotated with GENCODE version 21). EmptyDrops (DropletUtils R package 1.16.0, Lun et al. (2019)) with FDR ≤ 0.01 was used to filter out empty droplets.

The data were further processed using R programming language (4.1.1 and 4.2.2, R Core Team (2022)) and the Seurat package (4.1.0 and 4.3.0, Hao et al. (2021)). The data were SCTransformed and integrated excluding mitochondrial and ribosomal genes prefixed by *MT-* and *RPS-/RPL-*, if applicable (Chromium Fixed RNA Kit does not contain probes for rRNA). Further, the data went through an iterative process of quality control and filtering, including identification of doublets with DoubletFinder (2.0.3, McGinnis et al. (2019)) and removal of cells containing high levels of mitochondrial or contaminating transcripts. In the co-culture dataset, the expression values were corrected according to the contamination estimated by SoupX package (1.5.2, Young and Behjati (2020)). Quality control process for both datasets is summarized in Figures S1B–D and S6A,B.

NormalizeData(), *ScaleData()*, and *SCTransform()* Seurat functions were used for normalization, scaling, and transformation. The data were visualized with UMAP and *FindNeighbors()* and *FindClusters()* functions were used to identify clusters. Cell cycle score was assigned to cells by *CellCycleScoring()* function. *FindAllMarkers()* was used to identify cluster markers using the default Wilcoxon test (Tables S4A, S7A, S8A). The three cell groups identified in co-culture data (the AxD cell cluster, astrocytes, neurons) were clustered and analyzed separately, excluding mitochondrial and ribosomal genes. For the purposes of visualization in Figure 1, the three cell groups were merged, while maintaining clustering labels from individual analyses. Also, the merged dataset entered the analysis of cell–cell communication potential performed using CellChat (1.6.1, Jin et al. (2021)) package. Unguided and cortical organoid data were treated as separate datasets. Because of large difference between cortical control and AxD obtained with standard processing, an additional integration step was applied to overlay similar cell populations. To identify stressed cells originating in the organoid core, we applied the recently introduced Gruffi package (0.7.4, Vértessy et al. (2022)) with *neurogenesis* GO:0022008 set for negative filtering. Additionally, using Seurat *AddModuleScore()* function, we visualized expression of stress-related gene sets from the Gene Ontology database (Gene Ontology Consortium, 2021) suggested by the authors of Gruffi—*glycolysis* GO:0006096 and *endoplasmic reticulum stress* GO:0034976 (Figure S6E–H).

The differential expression analysis (DEA) was performed on the clusters of interest using *t*-test in *FindMarkers(logfc.threshold = 0, min.pct = 0.1, test.use = "t")* function. The significance threshold for differentially expressed genes (DEGs) was $|\log_2FC| > 0.65$ and $p_{adj} < 0.05$ with Bonferroni correction. The enrichment of Gene Ontology terms (Gene Ontology Consortium, 2021) (biological process, molecular function, and cellular component) was analyzed with clusterProfiler (4.2.2 and 4.4.4, Wu

et al. (2021)) package. The Gene Set Enrichment Analysis (GSEA) and Overrepresentation Analysis (ORA) were implemented with functions *gseGO(ont = "ALL", keyType = "ALIAS", minGSSize = 3, maxGSSize = 800, pvalueCutoff = 0.1, pAdjustMethod = "BH")* and *enrichGO(keyType = "ALIAS", OrgDb = org.Hs.eg.db, ont = "ALL", pAdjustMethod = "fdr", pvalueCutoff = 0.1, minGSSize = 3)*. ORA of custom gene sets from Zeng et al. (2023) was performed with *enricher()* function.

Top 10 markers of each co-culture cluster (the AxD cell cluster and iAs: $\log_2FC > 1$, $p_{adj} < 0.05$; iNs: $\log_2FC > 0.65$, $p_{adj} < 0.05$) were projected on organoid UMAPs using *Seurat::AddModuleScore()* function. Overlap of the co-culture and organoid data was calculated using *clusterProfiler::enricher()* function. Organoid cluster markers (broad markers were considered: $\log_2FC > 0.25$, $p_{adj} < 0.05$) were supplied in the TERM2GENE argument, and the enrichment was calculated separately for each co-culture cluster. The results were summarized in a matrix and a heatmap, where each row and its p_{adj} values correspond to one enrichment analysis. NA p_{adj} values were replaced by 1, and for this case the number of shared genes among cluster markers was set to 0.

2.21 | Proteomics

Single 150-day-old cortical organoids were lysed in 100 mM triethylammonium bicarbonate buffer pH 8.5 and 0.2% *n*-Dodecyl β -D-maltoside and resuspended thoroughly. Proteins were digested with 20 μ g trypsin (Worthington) supplemented with 5 mM $CaCl_2$ for 2 h at 50°C. Peptides were fractionated in 8 pH fractions using strong anion exchange (flow through, pH 11, 8, 6, 5, 4, 3, and 2) and dried in vacuo. Peptides were cleaned using in-house manufactured C18 stagetip columns and eluates were dried in vacuo.

Samples were separated on a 20-cm pico-tip column (50 μ m ID, New Objective) packed in-house with C18 material (1.9 μ m aquapur gold, dr. Maisch) using a two-step 140-min gradient that was adjusted slightly for each SAX fraction: (F1 and F2: 5%–24% ACN/0.2% FA in 80 min, and to 50% in 40 min; F3: 5%–27% ACN/0.2% FA in 80 min, and to 50% in 40 min; F4: 6%–29% ACN/0.2% FA in 80 min, and to 52% in 40 min; F5: 7%–30% ACN/0.2% FA in 80 min, and to 55% in 40 min; F6: 8%–33% ACN/0.2% FA in 80 min, and to 58% in 40 min; F7: 10%–34% ACN/0.2% FA in 80 min, and to 58% in 40 min) using an easy-nLC 1200 system (Thermo Fisher Scientific). Peptides were electro-sprayed directly into an Orbitrap Exploris 480 Mass Spectrometer (Thermo Fisher Scientific). The column temperature was maintained at 45°C using a column oven (Sonation). Spray voltage was set to 2.1 kV, funnel RF level at 60, and the transfer capillary temperature at 275°C. The FAIMS device was set at standard resolution and a carrier gas flow of 3.8 and alternated between CV-45 and CV-65. The MS was operated in DDA mode, and full scans were acquired with a resolution of 120,000 and a scan range from 450 to 1200 m/z, with an AGC target of 300% and a maximum injection time of 50 ms. Most intense precursor ions were selected for fragmentation for 2 s at a normalized collision energy (NCE) of 32%, after reaching the AGC target of 200% or maximum injection time of 200 ms. MS/MS was acquired at a resolution of 30,000, with an exclusion duration of 120 s.



RAW data files were split into two based on their FAIMS compensation voltages using FreeStyle 1.8 SP2 QF1 (Thermo Fisher Scientific) and then processed with MaxQuant (1.6.3.4, Cox and Mann (2008)), and MS2 spectra were searched with the Andromeda search engine against the SwissProt protein database of *H. sapiens* spiked with common contaminants. Methionine oxidation and protein N-term acetylation were set as variable modifications. Trypsin was specified as enzyme and a maximum of two missed cleavages was allowed. Filtering was done at 1% false discovery rate (FDR) at the protein and peptide level. Label-free quantification (LFQ) was performed, and “match between runs” was enabled. The data were further processed using Perseus (1.6.0.7, Tyanova et al. (2016)). Only proteins that were identified in 3 out of 4 replicates in at least one condition were considered for further analysis. Empty values were imputed from a normal distribution (width 0.3, down shift 1.8).

Differentially expressed proteins (DEPs) were identified with *t*-test (FDR < 0.05; Table S9A). For correlation calculation, DEGs in scRNA-seq dataset were determined in a pseudo bulk manner comparing control and AxD samples across all clusters simultaneously (Table S9B). Correlation of DEGs with DEPs was calculated using Pearson's correlation coefficient. Only genes present in the DEG as well as the DEP set, with $p_{adj} < 0.05$, were used (2521 genes).

Enrichment of biological processes from the Gene Ontology database among the upregulated and downregulated DEPs was calculated using clusterProfiler (4.4.4) R package with the function *enrichGO(keyType = “ALIAS”, OrgDb = org.Hs.eg.db, ont = “BP”, pAdjustMethod = “fdr”, pvalueCutoff = 0.1, minGSSize = 5, maxGSSize = 800)*.

3 | RESULTS

3.1 | scRNA-seq reveals a population of less differentiated cells in astrocyte-neuron co-cultures containing AxD astrocytes

We differentiated AxD patient-derived iPS cells and their isogenic controls (Battaglia et al., 2019) into induced astrocytes (iAs) and induced neurons (iNs) using lentiviral transduction of Sox9 and Nfih or Ngn2, respectively (Canals et al., 2018; Zhang et al., 2013) (Figure S1A). To assess the effect of the GFAP^{R239C} mutation on the transcriptome at the single-cell level, we applied scRNA-seq on a co-culture system of iAs and iNs. In individual co-cultures, we combined iAs and iNs carrying either the corrected or the mutant GFAP gene, resulting in fully corrected co-cultures (astroC/neuroC), fully mutant co-cultures (astroAxD/neuroAxD), and a combination of mutant iAs and corrected iNs (astroAxD/neuroC) (see experimental setup in Figure 1a).

Using marker genes, the scRNA-seq data revealed two groups of cells annotated as iNs and iAs. A third, AxD-specific cell population (AxD cluster) appeared almost exclusively in astroAxD/neuroC and astroAxD/neuroAxD co-cultures and was characterized by the increased expression of epithelial markers (Figure 1b–d), including CLDN7, CDH1, and EPCAM (Dong et al., 2018). Furthermore, Gene

Ontology (GO) enrichment analysis (Figure 1g and Table S4B,C) of the AxD cluster markers showed differences in *cell-substrate junction*, *structural constituent of cytoskeleton*, and *cytoskeleton-dependent intracellular transport*. Levels of SOX9 and NFIB expression suggested that the AxD cluster originated from iPS cells that had been induced into astrocytes, rather than neurons (Figure S2E). To clarify the identity of the AxD cluster, we performed an enrichment analysis using a reference study by Zeng et al. (2023), which had mapped early stages of human gastrulation by scRNA-seq and therefore, constitutes a suitable resource of gene signatures defining cell populations during early development. This analysis revealed a substantial overlap between the AxD cluster markers and the markers of epithelial cells derived from surface ectoderm, as defined by Zeng et al. (2023) (Figure S1E). The enriched populations included diverse nonneural cell populations. The simultaneous expression of epithelial, neuronal, and astrocyte genes within the AxD cluster points to mixed identity of these cells (Figure S2C). Together, these results imply a differentiation impairment in co-cultures containing AxD astrocytes.

Within the iAs and iNs populations, multiple clusters with varying abundance across samples were identified (Figure 1e, Figure S2, Table S4A). Four astrocyte clusters (ASTRO 1–4) included mature astrocytes (ASTRO 2) characterized by the expression of canonical astrocyte markers GFAP and S100B (Figure S2A and Figure 1f). Cells in the ASTRO 3 cluster expressed high levels of collagens, the increase of which was reported in astrocytes in vitro (Heck et al., 2003). ASTRO 1 and ASTRO 4 (Figure S2A) shared multiple markers that suggested a lower degree of maturation (CRLF1, CD9, and ITGA7) (Chaboub et al., 2016; Haas et al., 2017; Podergajs et al., 2016). The ASTRO 4 cluster additionally expressed cell proliferation genes (e. g., NUSAP1 and MKI67). Clusters NEURO 1–3 represented different maturation states of neurons (DCX, MAP2, NEFM, NEFL; Figure 1c, Figure S2B). NEURO 1 markers included genes that are increased in neuronal precursors (IGFBP2, FTL, SERF2, and VIM) (Freed et al., 2008; Kirkcaldie & Dwyer, 2017; Shen et al., 2019). NEURO 3 shared some of these markers and expressed also genes involved in hormone secretion (PTH2, UCN, and TRH). Interestingly, while NEURO 1 was more abundant in astroAxD/neuroAxD co-cultures (Figure 1e), NEURO 3 was enriched in astroAxD/neuroC co-cultures, suggesting unique gene expression signatures of corrected and AxD neurons in co-cultures with AxD astrocytes. The NEURO 2 cluster, enriched in astroC/neuroC co-cultures (Figure 1e, Figure S2B), was characterized by expression of NNAT, encoding for neuronatin, a proteolipid membrane protein expressed in the developing brain (Pitale et al., 2017), as well as SCG2, PCSK1, and SYT4 genes involved in neuropeptide processing and secretion (Fischer-Colbrie et al., 1995; Wang et al., 2017; Zhang et al., 2009), indicating their more differentiated state compared to NEURO 1 and NEURO 3. The NEURO 4 cluster was annotated as peripheral neurons (PHOX2B and ISL1) (Lin et al., 2021) and was represented similarly across conditions. Overall, the analysis of cell populations in the scRNA-seq co-culture data showed the presence of a specific AxD cluster and an increased proportion of less mature astrocytes and neurons in co-cultures that contained AxD astrocytes.

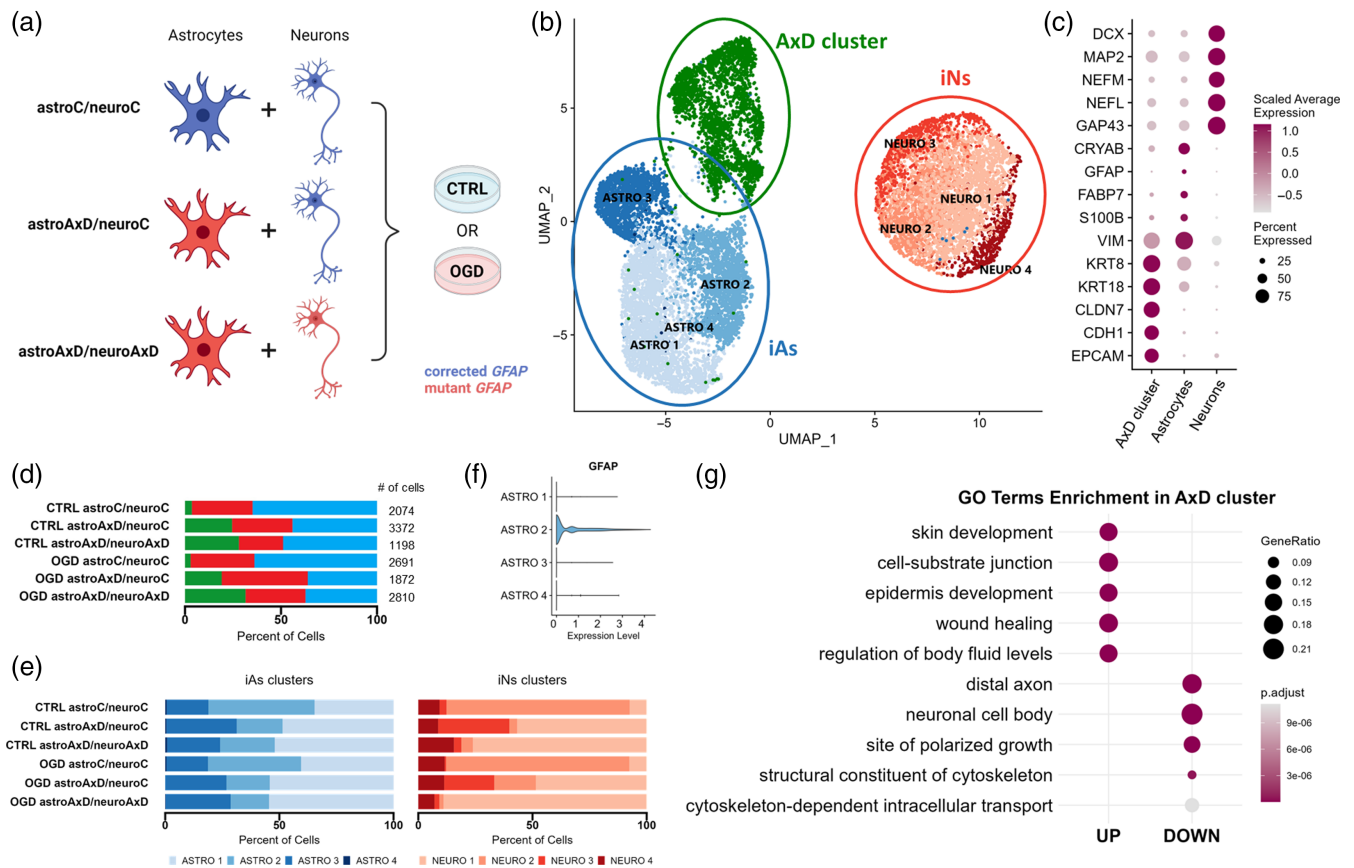


FIGURE 1 Overview of the scRNA-seq dataset derived from astrocyte-neuron co-cultures. (a) Experimental design explaining co-culture compositions and conditions entering the scRNA-seq analysis. (b) UMAP plot showing three main cellular populations and their clusters across all six samples. AxD cluster: $n = 2558$, iAs: $n = 6855$, iNs: $n = 4604$ (c) Dotplot with selected marker genes of the cluster of the AxD cluster, iAs, and iNs. Wilcoxon test with Bonferroni correction was used to determine marker genes. (d, e) Proportional barplots showing higher abundance of the population of the AxD cluster and less mature cells in astroAxD/neuroC and astroAxD/neuroAxD samples. Oxygen-glucose deprivation (OGD) challenge did not significantly reflect in population proportions. (f) Violin plot showing that GFAP was expressed predominantly in the ASTRO 2 cluster. (g) Overrepresentation analysis results showing top five upregulated and downregulated GO terms distinguishing the AxD cluster from iAs and iNs ($p_{adj} < 0.1$, false discovery rate (FDR) was used to correct for multiple comparisons). astroC/neuroC, corrected co-cultures; astroAxD/neuroC, co-cultures with AxD astrocytes and corrected neurons; astroAxD/neuroAxD, co-culture with AxD astrocytes and neurons; AxD, Alexander disease; CTRL, control without OGD challenge; GO, gene ontology; iAs, induced astrocytes; iNs, induced neurons; OGD, oxygen-glucose deprivation.

3.2 | Impaired astrocyte differentiation in co-cultures containing AxD astrocytes

Since the single-cell transcriptomics data showed the presence of less mature astrocytes and neurons in astroAxD/neuroC co-cultures, we further characterized the cell populations by immunocytochemistry using antibodies against MAP2 to visualize neurons, and antibodies against vimentin to visualize astrocytes (Figure 2a). The astroC/neuroC and astroAxD/neuroC co-cultures contained comparable numbers of vimentin-positive astrocytes and MAP2-positive neurons (Figure 2b). The density of undifferentiated cells (identified by their spherical morphology, the lack of cellular processes and distinctly larger size than neurons) was higher in co-cultures containing AxD astrocytes (Figure 2a,b). The proportion of cells identified across both genotypes using immunofluorescence was 9/7/0.5 (neurons/astrocytes/undifferentiated cells), while the

neuron/astrocyte/AxD cluster ratio was identified as 3/5/1 by scRNA-seq (Figure 1b,d). This implies an increased loss of neurons during the preparation of single-cell suspensions, as expected due to their more fragile nature (Cuevas-Díaz Duran et al., 2022; Lafzi et al., 2018), resulting in an overrepresentation of undifferentiated cells. GFAP immunolabeling and cell quantification showed no statistically significant difference in the number of GFAP-positive cells between astroC/neuroC and astroAxD/neuroC (Figure 2c,d). As GFAP is expressed also in RG, we next quantitatively assessed selected morphological features of the GFAP-positive cells. We found that GFAP-positive cells in co-cultures containing AxD astrocytes exhibited lower circularity and a larger perimeter (Figure 2e), indicative of a more RG-like morphology, that is, a less differentiated astrocyte phenotype (Liour & Yu, 2003). Jointly, the immunocytochemical analysis of the co-cultures indicated a lower degree of differentiation of co-cultures containing AxD astrocytes.

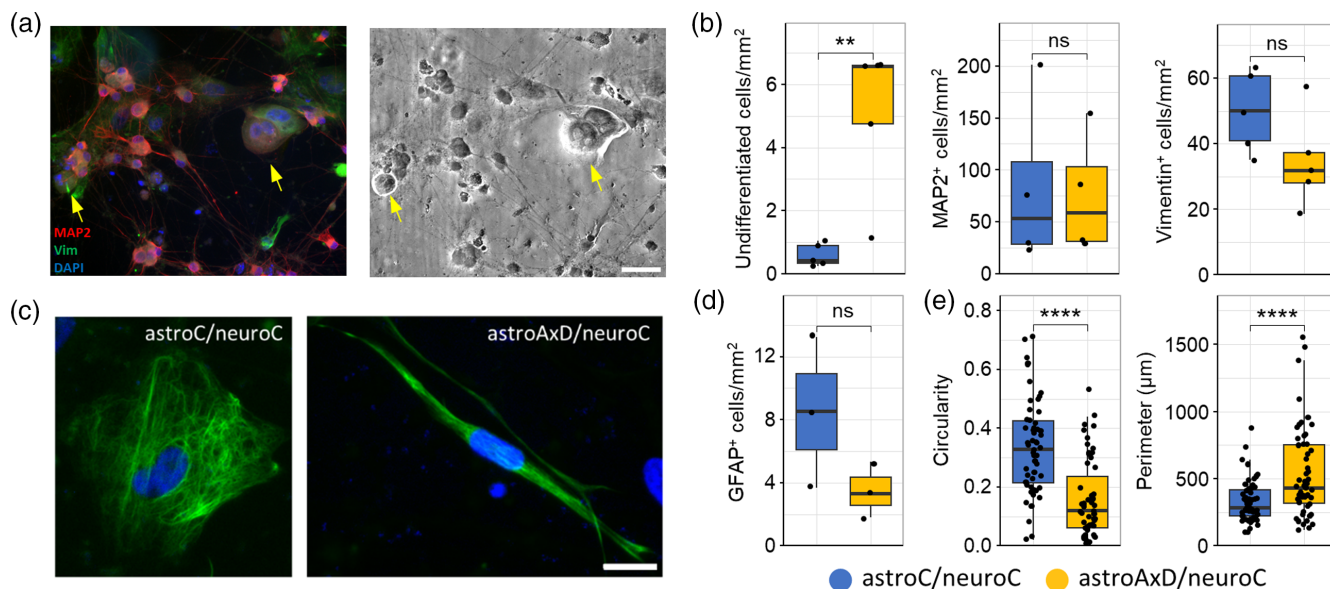


FIGURE 2 Immunocytochemistry identified less mature cells in astroAxD/neuroC co-cultures. (a) Co-cultures of iAs and iNs were labeled with antibodies against MAP2 (red), vimentin (green), and nuclei were visualized with DAPI (blue). Arrows point to undifferentiated cells; scale bar, 50 μm . (b) Number of undifferentiated cells, MAP2⁺, and vimentin⁺ cells. $n = 5, 4,$ and 5 independent sets of astroC/neuroC and astroAxD/neuroC cultures. Wilcoxon test (undifferentiated cells) and t -test (MAP2, vimentin) were used for statistical comparison. (c) Representative image of GFAP⁺ astrocytes (GFAP, green; DAPI, blue); scale bar, 20 μm . (d) Number of GFAP⁺ astrocytes, $n = 3$ independent sets of astroC/neuroC and astroAxD/neuroC cultures. T -test was used for statistical comparison. (e) Circularity and perimeter of GFAP⁺ signal for individual astrocytes (astroC/neuroC: $n = 55$, astroAxD/neuroC: $n = 55$). Wilcoxon test was used for statistical comparison. ns: not significant, ** $p \leq 0.01$; **** $p \leq 0.0001$. In b, d, and e Shapiro–Wilk test was used for normality assessment. astroC/neuroC, corrected co-cultures; astroAxD/neuroC, co-cultures with AxD astrocytes and corrected neurons; iAs, induced astrocytes; iNs, induced neurons.

3.3 | The AxD mutation affects the development and interactions of iAs and iNs

To identify the effect of the $\text{GFAP}^{\text{R239C}}$ mutation on gene expression in individual cell types in the co-culture systems, we performed DEA. First, we took advantage of the astroAxD/neuroC co-cultures, where only astrocytes carry the GFAP mutation. The mutant GFAP astrocytes downregulated genes such as GFAP , S100B , ACAN , and PTPRZ1 , indicating impaired astrocyte differentiation. The upregulation of metallothioneins MT2A and MT1X suggested an increased stress response (Juárez-Rebollar et al., 2017; Ruttkay-Nedecký et al., 2013) in astroAxD/neuroC co-cultures (Figure 3a,b). These genes were differentially expressed in AxD astrocytes regardless of the genotype of the co-cultured neurons (Figure 3b, Table S5A). In total, we identified 21 upregulated and 26 downregulated genes shared between the two comparisons (i.e., astroAxD/neuroC vs. astroC/neuroC and astroAxD/neuroAxD vs. astroC/neuroC, Figure S4A). Importantly, assessing the gene expression changes in neurons, we found that regardless of the neuronal genotype, the AxD astrocytes affected expression of neuronal genes (Figure 3a,b, Figure S4A, Table S5C). The downregulated genes included NNAT involved in development and calcium signaling (Pitale et al., 2017) and glutathione S-transferase GSTP1 . The genes upregulated in AxD astrocyte-containing co-cultures included genes participating in oxidative stress response (STC1 , Bonfante et al. (2020)), ion channel function (S100A10 , Seo and Svenningsson (2020)), protein aggregation (SERF2 , Stroo et al. (2023)), ubiquitination

(UBA52 , Kobayashi et al. (2016)), and mitochondrial function (ATP5I , UQCR11).

To assess whether the genotype of neurons affected the mutant GFAP astrocytes, we analyzed differential gene expression between astrocytes from astroAxD/neuroC and astroAxD/neuroAxD co-cultures (Figure S4B, Table S5A). This comparison revealed several genes downregulated in astroAxD/neuroAxD co-cultures, including VGF nerve growth factor inducible (VGF) and synaptotagmin 4 (SYT4). These differences were reflected in GO enrichment analysis as synapse and cell–cell signaling (Figure S4C, Table S5B). Addressing the difference between AxD and corrected isogenic control neurons co-cultured with AxD astrocytes, we found upregulation of neurodevelopmental genes (SOX4 and PCDH17) (Braccioli et al., 2018; Peek et al., 2017) and the mature neuronal marker gene (NEFM) in astroAxD/neuroAxD. AxD neurons showed also downregulation of genes coding for neuropeptides (CRH , TAC1 , PTH2 , and UCN), synaptic proteins (SYT4), and genes involved in hormone secretion (TRH , SCG5) (Figure S4B, Table S5C). Thus, both comparisons suggested altered cell–cell communication between astrocytes and neurons in astroAxD/neuroAxD co-cultures, possibly due to immaturity of AxD neurons.

Given the indications of cell–cell interaction changes in AxD co-cultures, we further focused on the astroAxD/neuroC co-cultures and investigated the cell–cell interaction potential of the AxD cluster, iAs, and iNs using the CellChat analysis (Jin et al., 2021). We identified increased number and strength of interactions in astroAxD/neuroC co-culture compared to astroC/neuroC (Figure 3c), involving

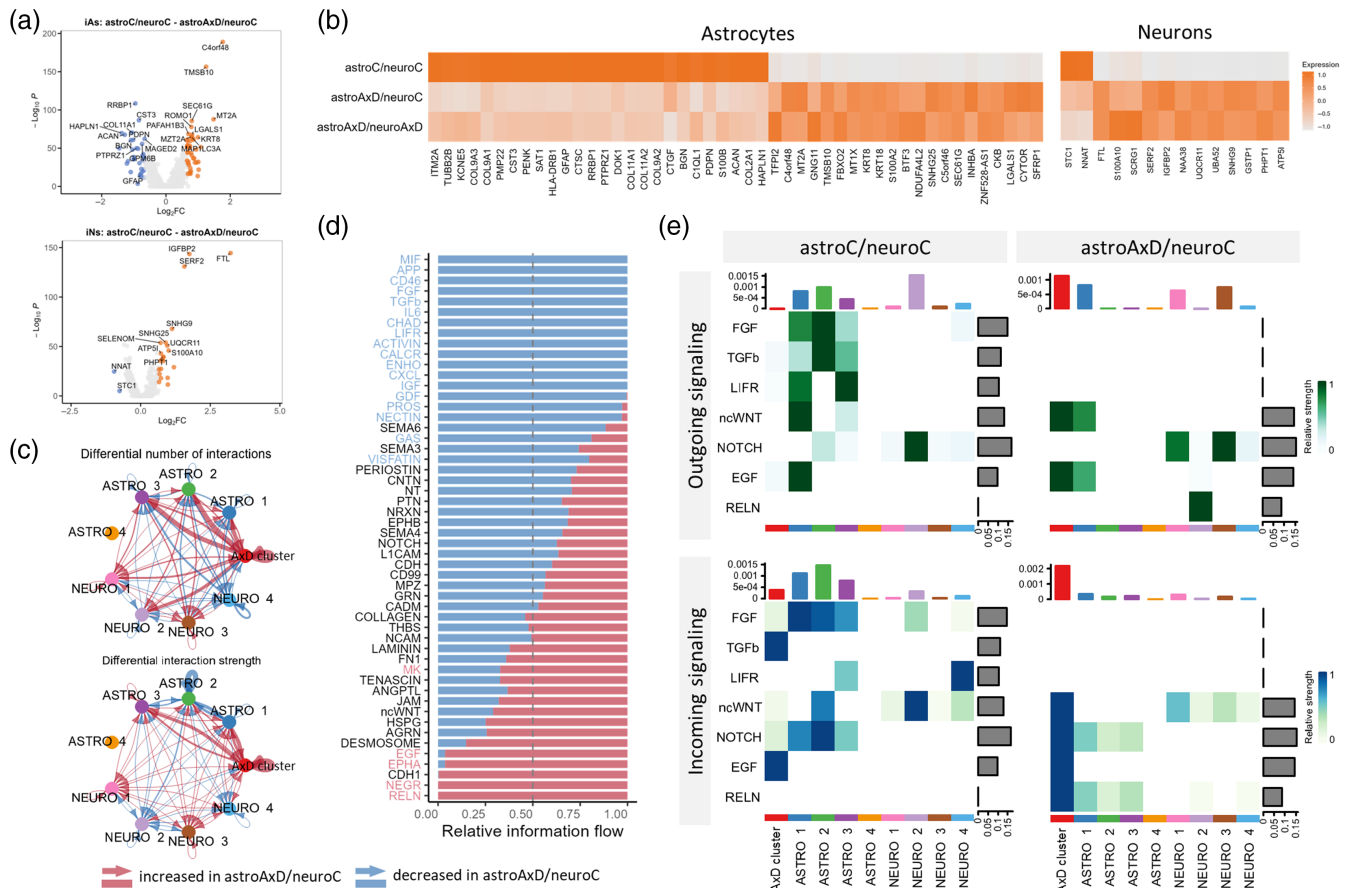


FIGURE 3 Results of differential expression analysis of iAs and iNs and cell-cell interaction analysis. (a) Volcano plot showing DEGs between astroC/neuroC and astroAxD/neuroC astrocytes and neurons ($|\log_2FC| > 0.65$ and $p_{adj} < 0.05$, t-test was used to calculate DEGs, Bonferroni correction was used to correct for multiple comparisons). (b) Heatmap shows expression of DEGs shared between comparisons of astroC/neuroC with astroAxD/neuroC and with astroAxD/neuroAxD. (c) Differential number of interactions (top) and differential interaction strength (bottom) between astroC/neuroC and astroAxD/neuroC defined by CellChat analysis (red—increase in astroAxD/neuroC, blue—decrease in astroAxD/neuroC). (d) Information flow chart from the CellChat analysis of cell-cell interactions presents the pathways identified in both conditions. Significantly dysregulated pathways (paired Wilcoxon test, p -value < 0.05) are highlighted in colors (red—increase in astroAxD/neuroC, blue—decrease in astroAxD/neuroC). (e) Heatmap divided to outgoing (ligands) and incoming (receptors) signaling patterns shows selected neurodevelopmental and astrogenesis-related pathways that were changed in astroAxD/neuroC compared to astroC/neuroC co-cultures. astroC/neuroC, corrected co-cultures; astroAxD/neuroC, co-cultures with AxD astrocytes and corrected neurons; astroAxD/neuroAxD, co-culture with AxD astrocytes and neurons; AxD, Alexander disease; DEGs, differentially expressed genes; iAs, induced astrocytes; iNs, induced neurons.

specifically the AxD cluster. As the CellChat analysis controlled for different size of cell clusters, this suggested an increased signaling activity of the AxD cluster. The ASTRO 2 cluster representing mature astrocytes was less involved in cell communication in astroAxD/neuroC. The ASTRO 4 cluster contained very few cells for any ligands and receptors to be reliably detected. Multiple pathways were dysregulated in astroAxD/neuroC compared to astroC/neuroC (Figure 3d). For instance, astroAxD/neuroC upregulated RELN and EGF pathways. RELN expression was activated in the NEURO 2 cluster, and astrocytes and the AxD cluster expressed RELN receptors *ITGA3* and *ITGB1* (Figure 3e, Figure S3B). The interactions between reelin and integrins participate in neuronal migration along RG during corticogenesis (Belvindrah et al., 2007; Dulabon et al., 2000). Thus, these results indicate that the isogenic control neurons signal to AxD astrocytes,

targeting mainly their less differentiated, more RG-like states, while such interactions with less differentiated astrocytes were absent in the astroC/neuroC and astroAxD/neuroAxD co-cultures (Figure 3e, Figure S3C,D). EGF signaling (HBEGF/AREG-(EGFR+ERBB2)), which has a prominent role in gliogenesis (Zhang et al., 2023), was enhanced in the astroAxD/neuroC AxD cluster (Figure 3e, Figure S3A,B). EGFR⁺ progenitor cells are present in the developing cortex around the period of the gliogenic switch (Fu et al., 2021), and therefore, the increased EGF signaling potential in the astroAxD/neuroC AxD cluster would be compatible with delayed or halted differentiation of the AxD cluster. Other pathways associated with astrogenesis (Voss et al., 2023; Zarei-Kheirabadi et al., 2020) and mediating communication between astrocytes and neurons in astroC/neuroC were absent in astroAxD/neuroC (Figure 3e). These included FGF (pair FGF2-FGFR1),



TGF β (ligands TGFB1 and TGFB2), and LIFR (LIF-(LIFR+IL6ST), CLCF1-(CNTFR+LIFR)) (Figure 3e, Figure S3A). Additionally, in astroC/neuroC, we detected the ASTRO 1 immature astrocytes, more mature ASTRO 2 astrocytes, and NEURO 2 as the main senders and receivers of the non-canonical WNT (ncWNT) signaling (mainly WNT5B-FZD3/FZD6). In astroAxD/neuroC this pathway was enhanced in the AxD cluster. Similarly, the cells of the AxD cluster were also the main recipients of NOTCH signaling coming from neuronal clusters (mainly DLL3-NOTCH2) (Figure 3e, Figure S3A,B). Both the ncWNT and Notch signaling play an important role in neurodevelopment, with WNT5B participating in cytoskeleton rearrangement, mechanosensing, and neural tissue patterning (Suthon et al., 2021) and Notch maintaining the pool of progenitors and being dependent of astrocyte intermediate filaments (Lampada & Taylor, 2023; Suthon et al., 2021; Wilhelmsson et al., 2012).

Together, these results support the concept of impaired astrocyte differentiation and point to an increased stress level in mutant GFAP co-cultures. Moreover, neuronal development was found to be affected by iAs with the AxD mutation, and the cell–cell interaction analysis showed the absence of or impaired signaling potential related to astrogenesis and neurodevelopment in astroAxD/neuroC astrocyte–neuron co-cultures.

3.4 | OGD challenge enhances the effect of the AxD mutation

To investigate the susceptibility and adaptation of the co-cultures to stress, we subjected them to a mild OGD challenge for 4 h followed by a 16 h long recovery period (Figure 4a). Cell death measured 2 h after the challenge as a release of lactate dehydrogenase (LDH) indicated no OGD-induced cell death in astroC/neuroC co-cultures, while in astroAxD/neuroC co-cultures an increase in OGD-induced cell death was found (Figure 4b).

We collected and analyzed samples after the recovery period and performed scRNA-seq. The OGD challenge was not significantly reflected in population proportions (Figure 1d,e). To address the effect of OGD on individual cell types, we performed DEA comparing the control (unchallenged) and the respective OGD samples in astroC/neuroC and astroAxD/neuroC co-cultures. In corrected iAs and iNs, no genes were differentially expressed (Figure 4c), and only a single differentially expressed gene was detected in the corrected cells within the AxD cluster. In contrast, several genes were downregulated in OGD in all three cell populations in the astroAxD/neuroC co-cultures (Figure 4c, Figure S4D, Table S6A). The most affected cell type appeared to be the cells of the AxD cluster. In these cells 14 genes were downregulated after the OGD challenge. Using gene set enrichment analysis (GSEA) we identified an upregulation of the GO terms *cell adhesion molecule binding*, *anchoring junction*, and *plasma membrane region* (Figure S4E, Table S6B), and a downregulation of GO terms related to mitochondrial function and respiration (e.g., *mitochondrial protein-containing complex*, *cellular respiration*), which might reflect the increased sensitivity of cells of the AxD cluster to the OGD challenge.

The analysis of cell–cell interactions with CellChat showed that 18 signaling pathways were exclusively upregulated in astroAxD/neuroC co-cultures after OGD and recovery, compared to the astroAxD/neuroC co-cultures without OGD (Figure 4d,e), many with cells of the AxD cluster and immature astrocytes as signal sending or signal receiving cells. These included TGF β -related pathways (ACTIVIN, TGF β , and BMP), along with neuregulin (NRG) signaling previously linked to the differentiation of RG into astrocytes (Schmid et al., 2003) (Figure 4f). In astroC/neuroC co-cultures, only three pathways were exclusively detected after OGD and recovery, including PDGF signaling, specifically PDGF-C astrocyte–astrocyte signaling via PDGFR α (Figure 4g,h). Interestingly, the PDGF-C signaling to PDGFR α , which was previously associated with the astrocyte response to stress (Miyata et al., 2014), was absent in astroAxD/neuroC co-cultures, indicating reduced adaptation of AxD astrocytes to OGD-induced stress.

3.5 | scRNA-seq reveals altered differentiation in AxD unguided neural organoids

The differentiation defect observed in GFAP-mutant astrocyte–neuron co-cultures prompted us to investigate the effect of the GFAP^{R239C} mutation in an organoid model, which better mimics the in vivo development. To do so, we generated unguided neural organoids (Lancaster et al., 2013; Ormel et al., 2018) from the same AxD iPSCs and their isogenic corrected controls as were used for the astrocyte–neuron co-cultures. We cultured the organoids until Day 165, by which time several cell populations, including astrocytes and neurons, had emerged, and subjected them to scRNA-seq (Figure S5A). Using marker genes, we annotated 20 cell populations (Figure 5a,b, Figure S6C, Table S7A), including cell types of the neural lineage, such as RG (PAX6, SOX2), pre-oligodendrocyte progenitor cells (pre-OPCs; OLIG1, EGFR, DLL3) (Van Bruggen et al., 2022), intermediate progenitors (EOMES) (Kanton et al., 2019), and CNS excitatory neurons (NEUROD2, NEUROD6, and GRIA2) (Kanton et al., 2019). We also identified a peripheral neuron-like population (PHOX2B, PRPH, and ISL1) (Lin et al., 2021), a population of choroid plexus cells (TTR, TRPM3, and CA2) (Pellegrini et al., 2020), and a population of astrocytes expressing GFAP, S100B, and FOXJ1 (Jacquet et al., 2009; Li, Floriddia, et al., 2018). We detected cells of mesodermal origin, that is, mesenchymal-like cells/fibroblasts (DCN and COL1A1) (Pfau et al., 2024), satellite cells (MYF5 and PAX7) (Motohashi & Asakura, 2014), muscle cells (MYOG and TNNT2) (Liu et al., 2012), and mesothelial cells (LRRN4 and UPK3B) (Kanamori-Katayama et al., 2011). Additionally, there were populations of epithelial cells (EPCAM and ELF3) (Dong et al., 2018), pancreatic-like acinar cells (CLPS, CTBR1, CTBR2 and CPA2) (Ma et al., 2023), and a cluster of cells characterized by increased glycolysis and endoplasmic reticulum stress (VEGFA, DDIT4; Figure S6E,F), known to originate in the organoid center where there is a limited supply of nutrients and oxygen (Vértesy et al., 2022). RT-qPCR of control and AxD unguided neural organoids revealed reduced expression of markers of choroid plexus cells (TRPM3), and neurons (PHOX2B), and increased expression of markers of muscle cells (MYF5), and pancreatic acinar cells (CLPS) in the AxD

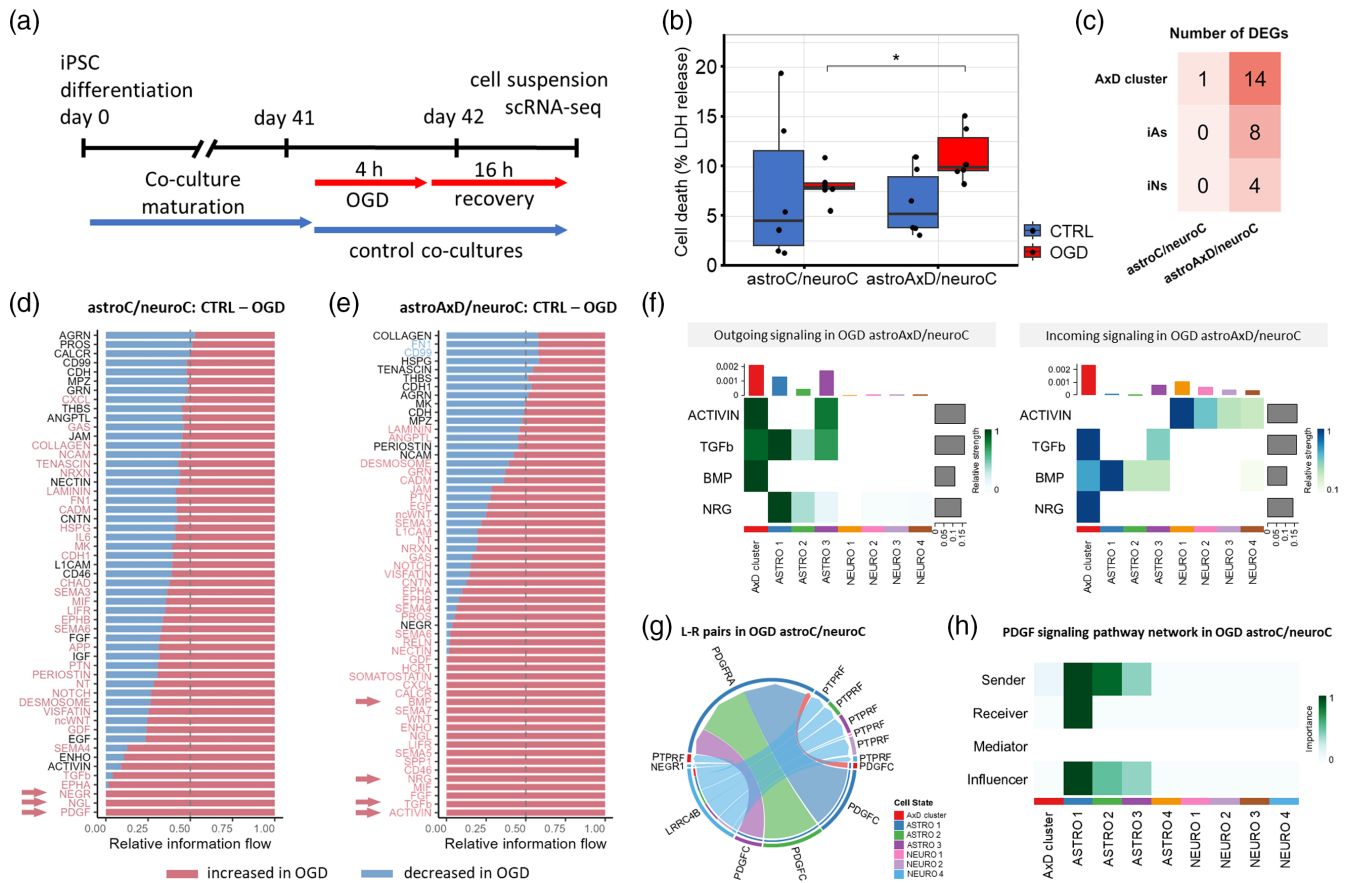


FIGURE 4 The OGD challenge enhanced the effect of the GFAP mutation in the AxD cluster. (a) A scheme of the timeline of the OGD challenge. (b) LDH assay measuring cell death showed increased LDH release in OGD astroAxD/neuroC co-culture compared to OGD astroC/neuroC and astroAxD/neuroC without stress, $n = 6$ sets of cultures of CTRL and OGD, astroC/neuroC and astroAxD/neuroC. T -test was used for statistical comparison, Shapiro–Wilk test was used for normality assessment, * $p < 0.05$. (c) Heatmap summarizing numbers of DEGs showing that the AxD cluster was the most affected by the OGD challenge ($|\log_2FC| > 0.65$ and $p_{adj} < 0.05$; t -test with Bonferroni correction). (d, e) Information flow chart showing pathways affected by the OGD challenge in astroC/neuroC (d) and astroAxD/neuroC (e) co-cultures. Significant change is marked by colors: red—increased in OGD, blue—decreased in OGD; paired Wilcoxon test, p -value < 0.05 . Arrows highlight pathways included in panels f–h. (f) Heatmap of selected pathways that are enriched in astroAxD/neuroC co-cultures after OGD challenge. (g) Ligand-receptor pairs of three pathways uniquely enriched in astroC/neuroC co-cultures after OGD. Clusters of senders and receivers are distinguished by colors. (h) Detailed heatmap of PDGF signaling pathway shows roles of individual clusters in this signaling based on statistical and network analysis by CellChat. astroC/neuroC, corrected co-cultures; astroAxD/neuroC, co-cultures with AxD astrocytes and corrected neurons; AxD, Alexander disease; CTRL, control co-culture without stress; DEGs, differentially expressed genes; iAs, induced astrocytes; iNs, induced neurons; LDH, lactate dehydrogenase; L-R pairs, ligand-receptor pairs; OGD, oxygen–glucose deprivation.

organoids, reflecting changes in the abundance of the cell populations as detected by scRNA-seq (Figure S7A).

Importantly, the AxD unguided neural organoids showed only very small number of peripheral neurons, astrocytes, pre-OPCs, and choroid plexus cells, and they were enriched for the acinar cells and the mesenchymal-like populations (Figure 5a), suggesting an altered differentiation trajectory in AxD organoids. To explore the potential cause of the differentiation defect, we focused on the progenitors giving rise to neurons as well as astrocytes, and we performed DEA on the clusters of RG comparing AxD and control unguided organoids (Figure 5c, Table S7B). The DEGs downregulated in AxD RG included neuronal markers *GAP43* and *STMN2*, which were also reflected in GO enrichment analysis as *axonogenesis* and *regulation of neuron projection development* (Figure 5c, Table S7C,D). Interestingly, outer RG markers *MOXD1* and *HOPX* were upregulated in AxD RG, along with

pancreatic genes *CLPS* and *REG3G*. *Integrin binding*, *epithelial cell proliferation*, and *gliogenesis* belonged to the GO terms upregulated in AxD RG. In addition, DEA of the neuronal clusters showed dysregulation of several protocadherin genes (e.g., *PCKDHA2*, *PCDHGA8*, and *PCDHGB6*) that play a role in neurodevelopment (Peek et al., 2017), as well as pancreatic genes *CLPS* and *REG3G* (Figure 5c, Table S7E). The GO enrichment analysis of neuronal DEGs showed upregulation of homophilic cell adhesion via plasma membrane adhesion molecules and downregulation of regulation of neurogenesis in AxD unguided organoids (Table S7F,G).

Immunofluorescence analysis showed the presence of GFAP⁺ cells in both control and AxD unguided neural organoids (Figure 5d). To assess the abundance of astroglial cells between control and AxD organoids, we performed immunocytochemistry for both GFAP and S100B, another marker of astrocytes (Haan et al., 1982). The AxD

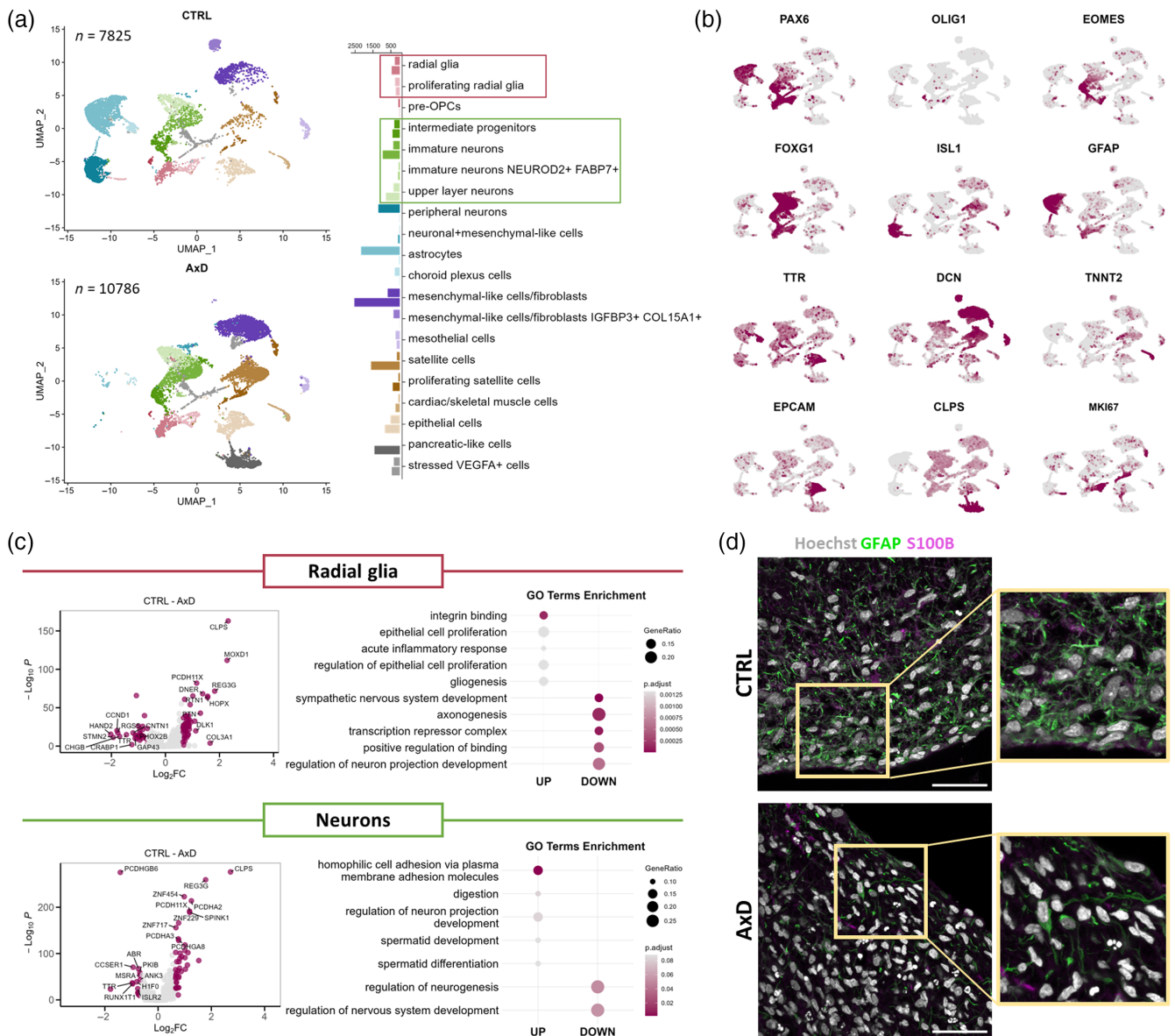


FIGURE 5 GFAP mutant unguided neural organoids partially diverged their differentiation into other than neuroectodermal lineage and did not develop astrocyte-like cells. (a) UMAP plot showing various cell types that were identified in 165 days old unguided organoids, split to conditions. Legend includes a barplot depicting abundance (absolute cell counts) of clusters in each condition (top bar = CTRL, bottom bar = AxD). (b) Selected markers highlighting clusters of neuroectodermal lineage, as well as off-target populations that were overrepresented in AxD organoids. (c) DEA was performed on clusters of radial glia (in a highlighted with a magenta rectangle) and neuronal clusters (in a highlighted with a green rectangle) comparing CTRL and AxD. Volcano plots show DEGs ($|\log_2FC| > 0.65$ and $p_{adj} < 0.05$; t -test with Bonferroni correction). GO overrepresentation analysis was performed on the DEGs, with FDR used to correct for multiple comparisons and $p_{adj} < 0.1$ used as significance threshold for the results. (d) Immunofluorescent microscopy images showing a Hoechst (nuclei), GFAP, and S100B staining of Day 165 CTRL and AxD unguided organoids. Scale bar, 50 μ m. AxD, Alexander disease; CTRL, control; DEA, differential expression analysis; DEGs, differentially expressed genes; FDR, false discovery rate; GO, gene ontology; \log_2FC , \log_2 fold change; p_{adj} , adjusted p -value; pre-OPCs, pre-oligodendrocyte progenitor cells.

organoids showed a reduction in the GFAP immunoreactivity (Figure 5d), a finding supporting the transcriptomics data that showed a reduced number of astrocytes in AxD organoids. Together, these results suggest that in the AxD unguided organoids, mesodermal and endodermal differentiation was favored, while the neuroectoderm-derived cells failed to achieve the same degree of differentiation as they did in control organoids.

3.6 | scRNA-seq and proteomics analyses reveal altered differentiation of AxD cortical organoids

Since unguided neural organoids are characterized by their relatively wide differentiation capabilities, we aimed to investigate whether the neural lineage commitment defect in AxD organoids could be rescued by dual SMAD inhibition (inhibition of BMP and TGF β pathways), a

method known to induce neuroectoderm and generate cortical organoids (Yoon et al., 2019). We generated AxD and isogenic control cortical organoids and performed scRNA-seq on 165 days old

organoids (Figure S5A). This revealed, as expected (Yoon et al., 2019), a lower diversity of cell populations compared to unguided neural organoids (Figure 6a,b, Figure S6D,G,H, Table S8A).

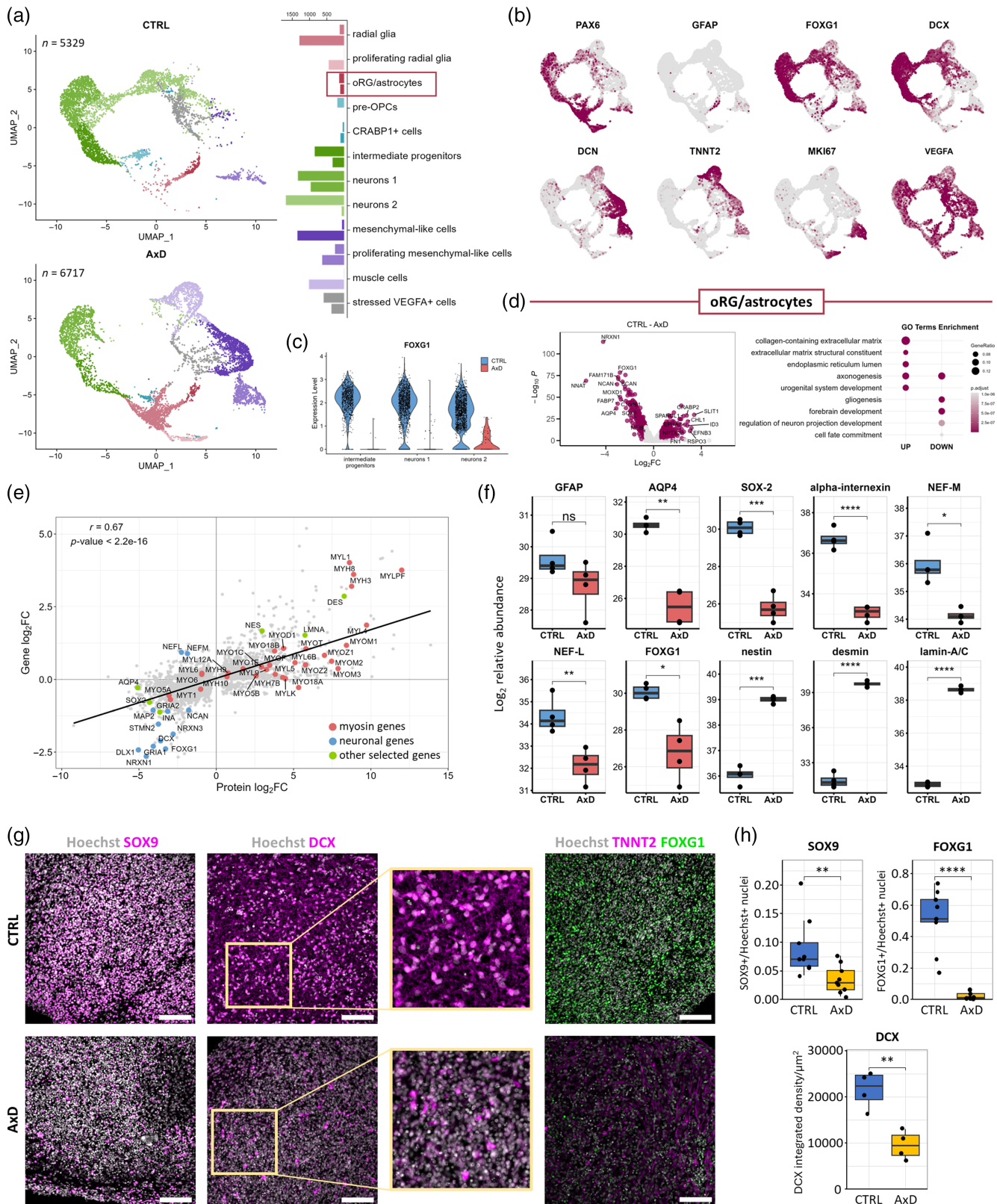


FIGURE 6 Legend on next page.



We identified cell populations representing outer radial glia (oRG)/astrocytes (*TNC*, *HOPX*, *FABP7*, *SOX9*, and *AQP4*), and neurons at different stages of maturation (*DCX*, *STMN2*, and *GRIA2*). AxD neuronal populations were strongly reduced and the neurons that did develop lacked expression of the forebrain marker *FOXP1* (Figure 6c). The AxD cortical organoids lacked pre-OPCs (*GSX2*, *ASCL1*, *EGFR*, *SMOC1*, and *HES6*) (Van Bruggen et al., 2022), were strongly enriched for RG (*SOX2* and *PAX6*), and, in contrast to control organoids, contained proliferating RG (*TOP2A* and *MKI67*). We observed nonneural differentiation in AxD cortical organoids. For example, compared to controls, the AxD cortical organoids contained much larger populations of mesenchymal-like (*DCN*) and muscle cells (*TNNT2*; Figure 6a), indicating a differentiation defect as observed in the AxD unguided neural organoids.

To address how the development of astrocytes was affected in AxD cortical organoids, we performed DEA on the AxD and control oRG/astrocyte populations (Figure 6d, Table S8B). The most prominently downregulated genes in AxD included synaptic protein *NRXN1*, neurogenesis marker *NNAT*, forebrain transcription factor *FOXP1*, and astrocyte markers *NCAN*, *BCAN*, *FABP7*, and *AQP4*. Importantly, gliogenic transcription factors *SOX9* and *NFIB* were also downregulated in AxD oRG/astrocyte population. Among the upregulated genes in AxD cortical organoids were *CHL1*, encoding a neural cell adhesion protein, extracellular matrix components *FN1* and *SPARCL1*, and retinol binding *CRABP2*. The upregulated genes in AxD cortical organoids were reflected in GO enrichment analysis as *collagen-containing extracellular matrix*, *endoplasmic reticulum lumen*, and *axonogenesis*, whereas the downregulated GO terms included *gliogenesis*, *forebrain development*, and *cell fate commitment* (Figure 6d, Table S8C,D). We validated these findings with RT-qPCR, detecting a decrease in the expression of neurodevelopmental genes (*NCAN* and *NNAT*) and gliogenesis-related genes (*AQP4* and *NFIA*), and an increase in the expression of muscle cell marker *TNNT2* (Wei & Jin, 2016) (Figure 6b). The CellChat analysis performed on cell populations of neural lineage in the cortical

organoids showed—similar to co-cultures of AxD astrocytes and isogenic corrected neurons after OGD challenge—dysregulation of TGF β signaling (represented by *ACTIVIN*, TGF β) in AxD organoids (Figure 6c,d). PDGF signaling (*PDGFD* and *PDGFA* via *PDGFRB*) was downregulated in AxD organoids and did not involve the oRG/astrocyte cluster as signal senders. Other dysregulated pathways included EGF, NOTCH (ligands *DLL1/3* and *JAG1* and receptors *NOTCH1-3*), FGF, *RELN*, *HH* (Hedgehog), and the *ncWNT* pathways, pointing to a developmental impairment in AxD organoids.

To determine differences in protein abundance between control and AxD cortical organoids, we performed mass spectrometry on 150-day-old cortical organoids. Comparison of transcriptomic and proteomic data showed a significant positive correlation between the DEGs and DEPs (Pearson's correlation coefficient = 0.67, p -value < 2.2×10^{-16} ; Figure 6e, Table S9A,B). Among the upregulated proteins in the AxD cortical organoids, we identified several myosins and other muscle-related proteins, such as desmin (Figure 6e,f, Figure S7E). Lamin A/C was also upregulated in AxD organoids. The upregulation of lamin A/C was reported in both rat and *Drosophila* models of AxD as well as in human AxD tissue (Hagemann et al., 2021; Wang et al., 2018), and it can also reflect higher abundance of muscle cells in AxD organoids (Röber et al., 1989). In line with the observation of impaired astrogenesis and neurogenesis, we identified GFAP, *AQP4*, *SOX2*, and the neuronal proteins α -internexin, neurofilament light chain (NF-L) and neurofilament medium chain (NF-M) as less abundant in AxD cortical organoids (Figure 6f). The DEPs reflected in GO enrichment analysis as *synapse* and *neuronal function*-related terms (e.g., *neuron development*, *synaptic signaling*) were downregulated in AxD cortical organoids, while muscle development-related terms were upregulated (Figure 6f). Overall, the proteomics data revealed a reduced abundance of neural proteins and an increase of muscle proteins, thereby confirming the transcriptomics data and supporting the concept of a reduced neural differentiation and off-target differentiation into muscle cells.

FIGURE 6 GFAP mutant cortical organoids showed delayed development and were enriched for mesoderm-derived cell populations. (a) UMAP plot showing various cell types that were identified in 165 days old cortical organoids, split to conditions. Legend includes barplot depicting abundance (absolute cell counts) of clusters in each condition (top bar = CTRL, bottom bar = AxD). (b) Selected markers highlighting clusters of neuroectodermal lineage, as well as off-target populations that were overrepresented in AxD organoids. (c) Expression plot of telencephalic marker *FOXP1* showing only limited expression in neuronal clusters in the AxD organoids. (d) DEA was performed on the cluster of oRG/astrocytes (in a highlighted with magenta rectangle) comparing CTRL and AxD. Volcano plot shows DEGs ($|\log_2FC| > 0.65$ and $p_{adj} < 0.05$; t -test with Bonferroni correction). GO overrepresentation analysis was performed on DEGs with FDR used to correct for multiple comparisons and $p_{adj} < 0.1$ used as significance threshold for the results. Top five upregulated and downregulated terms are shown in the dotplot. (e) DEGs ($p_{adj} < 0.05$) and DEPs (FDR < 0.05) were plotted against each other, with fitted line, Pearson's correlation coefficient (r) and statistical significance. Myosin genes are highlighted in red, selected neuronal genes are highlighted in blue, and other genes of interest are highlighted in green. (f) Normalized intensities of selected proteins were compared in CTRL and AxD organoids using t -test; ns: not significant, $*p \leq 0.05$; $**p \leq 0.01$; $***p \leq 0.001$; $****p \leq 0.0001$. (g) Immunofluorescent microscopy images showing *SOX9*, *DCX*, *FOXP1*, and *TNNT2* for Day 165 CTRL and AxD cortical organoids. Nuclei are stained by Hoechst; scale bar, 100 μ m. (h) Quantification of immunofluorescent signal of *SOX9* and *FOXP1* proteins in ratio to nuclei staining with Hoechst. Data points represent three images taken from three individual organoids. *DCX* integrated density was measured from four organoids per genotype and presented as integrated density per μ m². No difference in the Hoechst signal was observed. Shapiro–Wilk test was used to determine normal distribution of the data Wilcoxon test (*SOX9*, *FOXP1*) and t -test (*DCX*) were used to compare CTRL and AxD samples. AxD, Alexander disease; CTRL, control; DEA, differential expression analysis; DEGs, differentially expressed genes; DEPs, differentially expressed proteins; FDR, false discovery rate; GO, gene ontology; \log_2FC , \log_2 fold change; oRG, outer radial glia; p_{adj} , adjusted p -value; pre-OPCs, pre-oligodendrocyte progenitor cells.

To compare the number of astroglial cells between control and AxD cortical organoids, we performed immunocytochemistry using antibodies against SOX9, a marker of astrocytes and RG (Sun et al., 2017). The AxD cortical organoids showed a reduction in the SOX9⁺ immunoreactivity (Figure 6g,h), which is consistent with the transcriptomics results showing a prominent reduction in the number of astrocytes in AxD cortical organoids. Immunocytochemical analysis with antibodies against DCX, an early neuronal marker (Sarnat, 2015), showed decreased DCX immunoreactivity in AxD compared to control organoids (Figure 6g,h). This implicates that astrogenesis and neurogenesis are both decreased in AxD organoids. In comparison to control organoids, AxD organoids exhibited fewer cells positive for the forebrain marker FOXG1 (Hou et al., 2020) (Figure 6g,h), and a higher number of cells positive for the muscle marker TNNT2 (Figure 6g).

Taken together, scRNA-seq, proteomics and immunocytochemistry showed a decrease in neural differentiation and an altered lineage commitment trajectory in AxD cortical organoids, complementing the previous observations of abnormal neurodevelopment in AxD unguided neural organoids and in AxD co-cultures.

3.7 | Co-culture clusters resemble the cell populations in unguided neural organoids and cortical organoids

Given that the astroAxD/neuroC co-cultures, AxD unguided neural organoids, and AxD cortical organoids all showed impaired differentiation of astrocytes and neurons, we explored the similarity of the cell populations and the effect of the GFAP^{R239C} mutation across the models. We projected the top 10 co-culture cluster marker genes on the unguided neural and cortical organoid UMAPs (Figure S8A–C) and we also identified marker genes overlapping between co-culture clusters and all the organoid cell populations (Figure S8D,E).

In the unguided neural organoid dataset, co-culture clusters including mature ASTRO 2, NEURO 2, and peripheral NEURO 4 shared several marker genes with the organoid populations of astrocytes (*S100B*, *FABP7*, and *GFAP*), neurons (*NNAT* and *SCG2*), and peripheral neurons (*ISL1*, *PRPH*, and *PHOX2B*). Interestingly, immature ASTRO 1 showed similarities not only to the organoid astrocytes (*CD9*, *CRIP2*, and *CLU*), but also to the mesenchymal-like population (*ELN*, *HSPB6*, *MGP*, and *COL6A2*). We also found that the AxD cluster mapped to the populations of epithelial (*KRT81*, *EPCAM*, *JUP*, *SAT1*, and *ELF3*) and mesothelial cells (*KRT19*, *CDH3*, *SDC4*, and *DSG2*), sharing several genes with the pancreatic-like acinar cells (*KRT18*, *KRT8*, *DSP*, *FLNB*, and *LAMA5*), which are also of epithelial origin (Ma et al., 2023) (Figure S8B,D).

We also overlapped the astrocyte-neuron co-culture clusters and cell populations of cortical organoids and found that the AxD cluster and clusters of less mature ASTRO 1 in co-cultures mapped to RG (*SLC2A3*, *SLC2A1* and *NGFR*, *CLU*, respectively), oRG glia/astrocytes (*APOE*, *EGFR* in the AxD cluster and *CD9* in both) and to the cell populations that exhibited an aberrant differentiation and were enriched in

AxD cortical organoids (*FN1*, *PLEC* and *COL6A2*, *ITGA7*) (Figure S8C,E). Although the ASTRO 2 signature appeared more scattered, since the control cortical organoids largely lacked mature astrocytes, it was enriched in oRG/astrocyte (*COL11A1*, *CRYAB*, *DBI*, and *SIRT2*) and RG populations (*FABP7*, *PTPRZ1*, and *ID4*). Despite the lack of shared marker genes, the mature NEURO 2 signature was detected mostly in neuronal clusters of the control cortical organoids, and the signature of immature NEURO 1 was localized to AxD-enriched RG and mesenchymal-like and muscle cells in organoids.

Overall, these data indicate an aberrant differentiation of astrocytes and neurons in three different AxD models derived from AxD patient iPS cells carrying the GFAP^{R239C} mutation, potentially pointing to a new unexplored pathophysiological mechanism in AxD patients.

4 | DISCUSSION

AxD is a devastating disorder caused by mutations in *GFAP*, with no effective treatment available. Apart from the recently introduced rat model (Hagemann et al., 2021), other animal models do not fully recapitulate AxD pathology or require simultaneous presence of the AxD mutation and an overexpression of normal *GFAP* (Hagemann, 2022). Patient iPS cell-derived models allow to study AxD pathogenesis in a human model system. Previously, these models were shown to recapitulate some neuropathological hallmarks of AxD including RFs (Battaglia et al., 2019; Canals et al., 2018; Jones et al., 2018; Kondo et al., 2016; Li, Tian, et al., 2018), revealed abnormal organelle morphology and distribution (Jones et al., 2018), shed some light on the impact of AxD astrocytes on oligodendrocytes (Li, Tian, et al., 2018), and suggested a role of *GFAP* hyperphosphorylation in AxD pathology (Battaglia et al., 2019). In this study, we used an existing patient-derived iPS cell line carrying the GFAP^{R239C} mutation and its respective isogenic control cell line (Battaglia et al., 2019) to generate an astrocyte-neuron co-culture system that combines isogenically corrected neurons with AxD astrocytes. We also generated unguided neural organoids and cortical organoids from the same AxD and corrected control iPS cell line. In all three systems, we observed a distinct differentiation phenotype pointing to the effect of the GFAP^{R239C} mutation on neural development.

Astrocyte intermediate filaments positively contribute to the ability of astrocytes to handle various stresses (Pekny & Lane, 2007; Ridge et al., 2022), including mechanical, ischemic, and hypoxic stress (De Pablo et al., 2013; Ding et al., 1998; Li et al., 2008; Lundkvist et al., 2004; Nawashiro et al., 1998; Verardo et al., 2008; Wunderlich et al., 2015). Here, we report signs of an increased stress response of human iPS cell-derived AxD co-cultures as well as their increased sensitivity to OGD-induced stress. DEGs in astroAxD/neuroC co-cultures showed increased stress response as indicated by upregulation of metallothioneins (*MT2A* and *MT1X*). This supports previous observations of increased oxidative stress and activation of stress response pathways in AxD astrocytes (Hagemann et al., 2005; Heaven et al., 2022; Sosunov et al., 2018; Viedma-Poyatos et al., 2022; Wang et al., 2011), including the upregulation of metallothioneins (Hagemann et al., 2005). The



exposure of astrocyte-neuron co-cultures to a mild OGD challenge followed by a recovery period identified an increased susceptibility to stress in the astroAxD/neuroC co-cultures. This is in agreement with the previous reports showing that AxD astrocytes exhibit increased sensitivity to specific stresses (Cho & Messing, 2009; Viedma-Poyatos et al., 2022). One possible link is the lack of PDGF-C to PDGFR α signaling potential in astroAxD/neuroC, but not in astroC/neuroC, co-cultures after exposure to OGD, since PDGF-C was previously shown to be induced by the stress triggered by radiation injury (Miyata et al., 2014). OGD in astroAxD/neuroC co-cultures induced signaling potential through several pathways that were absent in corrected control co-cultures exposed to OGD, and this could reflect maladaptive effects: SPP1 and NRG were reported to have multiple detrimental roles in the CNS and other tissues, respectively (Basak et al., 2023; Cappellano et al., 2021; Schramm et al., 2022). Exposure to various stresses during in vitro differentiation or prenatal development is known to result in a differentiation/developmental delay, and consequently, it is possible that the increased sensitivity of the AxD cells to stress is a driving factor behind the impaired development seen in AxD co-cultures and AxD neural organoids.

Using scRNA-seq, we found a population of less differentiated cells in astrocyte-neuron co-cultures containing AxD astrocytes. These cells, which we termed the AxD cluster, were characterized by genes expressed by epithelia (Dong et al., 2018). Importantly, in co-cultures containing AxD astrocytes, less differentiated cells were also identified within the populations of astrocytes and neurons, and we observed downregulation of astrocyte-specific marker genes (e.g., *GFAP*, *S100B*). The assessment of morphological parameters of GFAP⁺ cells in co-cultures showed more RG-like morphology of AxD astrocytes compared to controls. Unguided neural organoids are well suited for investigating differentiation, as they allow a variety of cell types to develop and self-organize in a 3D environment, and in that sense mimic the in vivo development (Lancaster & Knoblich, 2014; Ormel et al., 2018; Verkerke et al., 2024). In 165 days old AxD unguided neural organoids, astrocytes were almost absent, and neurogenesis was reduced. Our data suggest a neural lineage commitment defect in AxD unguided neural organoids that resulted in an aberrant differentiation, generating epithelial, mesoderm-derived, or pancreatic acinar cells. Interestingly, Hagemann et al. (2005) reported in a mouse model of AxD, a downregulation of genes related to neuronal development and function, and this might reflect a neuronal loss or impaired neurodevelopment in AxD. Another, more advanced study, showed that AxD mice have reduced proliferation of hippocampal neural progenitor cells, decreased adult neurogenesis, RG with atypical morphology and an increased fraction of undifferentiated neural cells, possibly due to dysregulation of pathways regulating renewal of neural stem cells and neural differentiation (Notch, WNT, Hedgehog, and TGF β) (Hagemann et al., 2013).

Here we show a dysregulation of some of the same pathways in astroAxD/neuroC co-cultures and in AxD cortical organoids using CellChat analysis. Signaling pathways such as Notch, WNT, FGF, or EGF, are known to regulate both CNS and pancreatic development (Alkailani et al., 2022; Gonçalves et al., 2021; Lampada & Taylor, 2023; Li

et al., 2015; Napolitano et al., 2023; Tomé et al., 2023; Zhang et al., 2023). Therefore, an imbalance of these pathways in AxD organoids may have resulted in the increased presence of cell populations other than those of neuroectodermal origin. These pathways are regulated by the proteasome system (Baloghova et al., 2019; Dutta et al., 2022; Gao et al., 2014; Hsia et al., 2015; Imamura et al., 2013), which was previously shown to be defective in AxD due to the presence of GFAP aggregates (Tang et al., 2010).

Cortical organoids were generated using dual SMAD inhibition of the TGF β and BMP pathways. Interestingly, this did not rescue the differentiation phenotype seen in the AxD unguided neural organoids. The AxD cortical organoids showed impaired neural differentiation with mesoderm-derived cells dominating over neural cell types. The overrepresentation of RG and neurons lacking *FOXG1* expression, and severe depletion of astrocytes and oligodendrocyte precursors suggest a failure of differentiation into the cortical lineage and impaired gliogenesis. Mass spectrometry analysis of AxD and control cortical organoids revealed a positive correlation between DEGs and DEPs in AxD cortical organoids compared to controls. Proteomics data showed lower levels of the astrocyte marker GFAP, and neuronal proteins α -internexin, NF-L, and NF-M in AxD organoids, corroborating the transcriptomics and immunocytochemical data, and implying impaired neural differentiation in AxD organoids. We observed downregulation of the AQP4 water channel in AxD cortical organoids at the level of protein as well as mRNA, which supports the recently reported finding of a reduced expression of AQP4 in different regions of the CNS in the AxD rat model (Hagemann et al., 2021). The myogenic markers desmin and nestin were upregulated in AxD organoids, as were many of the proteins involved in muscle differentiation or markers of muscle cells (e.g., myosins), a finding that further confirms the aberrant differentiation in AxD organoids along the myogenic lineage.

In conclusion, by using a combination of approaches and experimental systems ranging from iPS cell-derived astrocytes and neurons to iPS cell-derived neural organoids, we show that the AxD GFAP^{R239C} mutation increases the sensitivity of AxD cells to stress and leads to impaired astrocyte and neuronal differentiation. This finding needs to be validated on iPS cell lines from other AxD patients, and if confirmed, it might indicate that a proportion of individuals carrying the AxD mutations might be lost prenatally as a consequence of impaired neuronal and astrocyte differentiation. It also remains to be seen to what extent this abnormal neural differentiation is reflected in AxD animal models and AxD patients.

AUTHOR CONTRIBUTIONS

EMH, MP, LV, and HA conceived the study and supervised the experiments, ZM, WD, YDP, OGZ, PA, MK, IC, and CAGHVG and HRV performed the experiments, analyzed and interpreted the data, ZM, WD, YDP, DPS, LV, EMH, and MP prepared the manuscript and figures, and all the authors edited and approved the manuscript.

ACKNOWLEDGMENTS

We thank Prof. Albee Messing, Prof. Marcela Pekna, and Dr. María A. Pajares for their comments on the manuscript, and Dr. Natasha

Snider for providing the iPS cells and commenting on the manuscript. This work was supported by grants from EJP RD COFUND-EJP N° 825575 Alexander to EMH, MP, MK, HA, and DPS and from la Caixa Foundation, Grant Agreement LCF/PR/HR21/52410002 to DPS, MP and EMH; grants from the Swedish Research Council (2017-02255, 2020-01148, and 2019-00284), ALF Gothenburg (146051), The Swedish Society for Medical Research, Hjärfonden (FO02021-0082), ALF (965939), Söderberg's Foundations, Hagström's Foundation Millennium, Amlöv's Foundation, and E. Jacobson's Donation Fund to MP, and a mobility grant from the Swedish Foundation for Strategic Research (SM23-0033) to MK; grants from the Czech Science Foundation (24-11364S, 24-12028S) to LV, and Institutional support (RVO 86652036) to MK; grant from ZonMw 463002004 to EMH; grants from The Swedish Research Council, Hjärfonden and Petrus och Augusta Hedlunds stiftelse to HA, grants from MCIN/AEI/10.13039/501100011033 and "ERDF A way of making Europe" (PID2021-126827OB-I00) to DPS, and grants from X-Omics initiative (184.034.019) the Onco Institute to CAGHVG and HRV; grants from the Swedish Society for Medical Research to IC. We thank the Center for Translational Genomics (CTG), Lund University, Sweden, for preparation of the co-culture sequencing libraries. Some images were created with BioRender.com.

CONFLICT OF INTEREST STATEMENT

The authors declare no conflicts of interest.

DATA AVAILABILITY STATEMENT

The transcriptomic data have been stored at NCBI's Gene Expression Omnibus (Edgar et al., 2002) under accession number GSE261158. Code used for preprocessing and analysis of the transcriptomic data is available at GitHub repository: https://github.com/LabGenExp/hiPSC-derived_AxD_models.

The proteomics data have been deposited at the ProteomeXchange Consortium via the PRIDE partner repository with the data set identifier: PXD048606.

ORCID

Zuzana Matusova  <https://orcid.org/0000-0002-5014-5801>

Werner Dykstra  <https://orcid.org/0000-0002-7663-4689>

Yolanda de Pablo  <https://orcid.org/0000-0001-5208-2114>

Oskar G. Zetterdahl  <https://orcid.org/0000-0003-1010-4287>

Isaac Canals  <https://orcid.org/0000-0002-2689-268X>

Charlotte A. G. H. van Gelder  <https://orcid.org/0000-0002-6110-0502>

Harmjan R. Vos  <https://orcid.org/0000-0002-4696-6068>

Dolores Pérez-Sala  <https://orcid.org/0000-0003-0600-665X>

Mikael Kubista  <https://orcid.org/0000-0002-2940-352X>

Pavel Abaffy  <https://orcid.org/0000-0002-7571-8880>

Henrik Ahlenius  <https://orcid.org/0000-0001-8958-6148>

Lukas Valihrach  <https://orcid.org/0000-0002-6704-4337>

Elly M. Hol  <https://orcid.org/0000-0001-5604-2603>

Milos Pekny  <https://orcid.org/0000-0003-1607-8075>

REFERENCES

- Alkailani, M. I., Aittaleb, M., & Tissir, F. (2022). WNT signaling at the intersection between neurogenesis and brain tumorigenesis. *Frontiers in Molecular Neuroscience*, 15, 1017568. <https://doi.org/10.3389/fnmol.2022.1017568>
- Baloghova, N., Lidak, T., & Cermak, L. (2019). Ubiquitin ligases involved in the regulation of Wnt, TGF-beta, and Notch signaling pathways and their roles in mouse development and homeostasis. *Genes (Basel)*, 10(10), 815. <https://doi.org/10.3390/genes10100815>
- Basak, M., Sengar, A. S., Das, K., Mahata, T., Kumar, M., Kumar, D., Biswas, S., Sarkar, S., Kumar, P., Das, P., Stewart, A., & Maity, B. (2023). A RGS7-CaMKII complex drives myocyte-intrinsic and myocyte-extrinsic mechanisms of chemotherapy-induced cardiotoxicity. *Proceedings of the National Academy of Sciences*, 120(1), e2213537120. <https://doi.org/10.1073/pnas.2213537120>
- Battaglia, R. A., Beltran, A. S., Delic, S., Dumitru, R., Robinson, J. A., Kabiraj, P., Herring, L. E., Madden, V. J., Ravinder, N., Willems, E., Newman, R. A., Quinlan, R. A., Goldman, J. E., Perng, M. D., Inagaki, M., & Snider, N. T. (2019). Site-specific phosphorylation and caspase cleavage of GFAP are new markers of Alexander disease severity. *eLife*, 8, e47789. <https://doi.org/10.7554/eLife.47789>
- Belvindrah, R., Graus-Porta, D., Goebbels, S., Nave, K. A., & Müller, U. (2007). Beta1 integrins in radial glia but not in migrating neurons are essential for the formation of cell layers in the cerebral cortex. *The Journal of Neuroscience*, 27(50), 13854–13865. <https://doi.org/10.1523/JNEUROSCI.4494-07.2007>
- Bolger, A. M., Lohse, M., & Usadel, B. (2014). Trimmomatic: A flexible trimmer for Illumina sequence data. *Bioinformatics*, 30(15), 2114–2120. <https://doi.org/10.1093/bioinformatics/btu170>
- Bonfante, S., Della Giustina, A., Danielski, L. G., Denicol, T., Joaquim, L., Biehl, E., Scopel, G., de Carli, R. J., Hubner, M., Cardoso, T., Tuon, T., Generoso, J., Barichello, T., Terra, S., & Petronilho, F. (2020). Stanniocalcin-1 ameliorates cerebral ischemia by decrease oxidative stress and blood brain barrier permeability. *Microvascular Research*, 128, 103956. <https://doi.org/10.1016/j.mvr.2019.103956>
- Braccioli, L., Vervoort, S. J., Puma, G., Nijboer, C. H., & Coffey, P. J. (2018). SOX4 inhibits oligodendrocyte differentiation of embryonic neural stem cells in vitro by inducing Hes5 expression. *Stem Cell Research*, 33, 110–119. <https://doi.org/10.1016/j.scr.2018.10.005>
- van Bruggen, D., Pohl, F., Langseth, C. M., Kukanja, P., Lee, H., Albiach, A. M., Kabbe, M., Meijer, M., Linnarsson, S., Hilscher, M. M., Nilsson, M., Sundström, E., & Castelo-Branco, G. (2022). Developmental landscape of human forebrain at a single-cell level identifies early waves of oligodendrogenesis. *Developmental Cell*, 57(11), 1421–1436. e5. <https://doi.org/10.1016/j.devcel.2022.04.016>
- Canals, I., Ginisty, A., Quist, E., Timmerman, R., Fritze, J., Miskinyte, G., Monni, E., Hansen, M. G., Hidalgo, I., Bryder, D., Bengzon, J., & Ahlenius, H. (2018). Rapid and efficient induction of functional astrocytes from human pluripotent stem cells. *Nature Methods*, 15(9), 693–696. <https://doi.org/10.1038/s41592-018-0103-2>
- Cappellano, G., Vecchio, D., Magistrelli, L., Clemente, N., Raineri, D., Barbero, M. C., Virgilio, E., Dianzani, U., Chiochetti, A., & Comi, C. (2021). The Yin-Yang of osteopontin in nervous system diseases: Damage versus repair. *Neural Regeneration Research*, 16(6), 1131–1137. <https://doi.org/10.4103/1673-5374.300328>
- Chaboub, L. S., Manalo, J. M., Lee, H. K., Glasgow, S. M., Chen, F., Kawasaki, Y., Akiyama, T., Kuo, C. T., Creighton, C. J., Mohila, C. A., & Deneen, B. (2016). Temporal profiling of astrocyte precursors reveals parallel roles for Asef during development and after injury. *The Journal of Neuroscience*, 36(47), 11904–11917. <https://doi.org/10.1523/JNEUROSCI.1658-16.2016>
- Cho, W., & Messing, A. (2009). Properties of astrocytes cultured from GFAP over-expressing and GFAP mutant mice. *Experimental Cell Research*, 315(7), 1260–1272. <https://doi.org/10.1016/j.yexcr.2008.12.012>

- Cox, J., & Mann, M. (2008). MaxQuant enables high peptide identification rates, individualized p.p.b.-range mass accuracies and proteome-wide protein quantification. *Nature Biotechnology*, 26(12), 1367–1372. <https://doi.org/10.1038/nbt.1511>
- Cuevas-Díaz Duran, R., González-Orozco, J. C., Velasco, I., & Wu, J. Q. (2022). Single-cell and single-nuclei RNA sequencing as powerful tools to decipher cellular heterogeneity and dysregulation in neurodegenerative diseases. *Frontiers in Cell and Development Biology*, 10, 884748. <https://doi.org/10.3389/fcell.2022.884748>
- Dimou, L., & Götz, M. (2014). Glial cells as progenitors and stem cells: New roles in the healthy and diseased brain. *Physiological Reviews*, 94(3), 709–737. <https://doi.org/10.1152/physrev.00036.2013>
- Ding, M., Eliasson, C., Betsholtz, C., Hamberger, A., & Pekny, M. (1998). Altered taurine release following hypotonic stress in astrocytes from mice deficient for GFAP and vimentin. *Molecular Brain Research*, 62(1), 77–81. [https://doi.org/10.1016/s0169-328x\(98\)00240-x](https://doi.org/10.1016/s0169-328x(98)00240-x)
- Dobin, A., Davis, C. A., Schlesinger, F., Drenkow, J., Zaleski, C., Jha, S., Batut, P., Chaisson, M., & Gingeras, T. R. (2013). STAR: ultrafast universal RNA-seq aligner. *Bioinformatics*, 29(1), 15–21. <https://doi.org/10.1093/bioinformatics/bts635>
- Dong, J., Hu, Y., Fan, X., Wu, X., Mao, Y., Hu, B., Guo, H., Wen, L., & Tang, F. (2018). Single-cell RNA-seq analysis unveils a prevalent epithelial/mesenchymal hybrid state during mouse organogenesis. *Genome Biology*, 19(1), 31. <https://doi.org/10.1186/s13059-018-1416-2>
- Dulabon, L., Olson, E. C., Taglienti, M. G., Eisenhuth, S., McGrath, B., Walsh, C. A., Kreidberg, J. A., & Anton, E. S. (2000). Reelin binds alpha3beta1 integrin and inhibits neuronal migration. *Neuron*, 27(1), 33–44. [https://doi.org/10.1016/s0896-6273\(00\)00007-6](https://doi.org/10.1016/s0896-6273(00)00007-6)
- Dutta, D., Sharma, V., Mutsuddi, M., & Mukherjee, A. (2022). Regulation of Notch signaling by E3 ubiquitin ligases. *The FEBS Journal*, 289(4), 937–954. <https://doi.org/10.1111/febs.15792>
- Edgar, R., Domrachev, M., & Lash, A. E. (2002). Gene expression omnibus: NCBI gene expression and hybridization array data repository. *Nucleic Acids Research*, 30(1), 207–210. <https://doi.org/10.1093/nar/30.1.207>
- Fischer-Colbrie, R., Laslop, A., & Kirchmair, R. (1995). Secretogranin II: Molecular properties, regulation of biosynthesis and processing to the neuropeptide secretoneurin. *Progress in Neurobiology*, 46(1), 49–70. [https://doi.org/10.1016/0301-0082\(94\)00060-u](https://doi.org/10.1016/0301-0082(94)00060-u)
- Freed, W. J., Chen, J., Backman, C. M., Schwartz, C. M., Vazin, T., Cai, J., Spivak, C. E., Lupica, C. R., Rao, M. S., & Zeng, X. (2008). Gene expression profile of neuronal progenitor cells derived from hESCs: Activation of chromosome 11p15.5 and comparison to human dopaminergic neurons. *PLoS One*, 3(1), e1422. <https://doi.org/10.1371/journal.pone.0001422>
- Fu, Y., Yang, M., Yu, H., Wang, Y., Wu, X., Yong, J., Mao, Y., Cui, Y., Fan, X., Wen, L., Qiao, J., & Tang, F. (2021). Heterogeneity of glial progenitor cells during the neurogenesis-to-gliogenesis switch in the developing human cerebral cortex. *Cell Reports*, 34(9), 108788. <https://doi.org/10.1016/j.celrep.2021.108788>
- Gao, C., Xiao, G., & Hu, J. (2014). Regulation of Wnt/beta-catenin signaling by posttranslational modifications. *Cell & Bioscience*, 4(1), 13. <https://doi.org/10.1186/2045-3701-4-13>
- Gao, L., Zhang, Z., Lu, J., & Pei, G. (2019). Mitochondria are dynamically transferring between human neural cells and Alexander disease-associated GFAP mutations impair the astrocytic transfer. *Frontiers in Cellular Neuroscience*, 13, 316. <https://doi.org/10.3389/fncel.2019.00316>
- Gene Ontology Consortium. (2021). The Gene Ontology resource: Enriching a GOld mine. *Nucleic Acids Research*, 49(D1), D325–D334. <https://doi.org/10.1093/nar/gkaa1113>
- Gonçalves, C. A., Larsen, M., Jung, S., Stratmann, J., Nakamura, A., Leuschner, M., Hersemann, L., Keshara, R., Perlman, S., Lundvall, L., Thuesen, L. L., Hare, K. J., Amit, I., Jørgensen, A., Kim, Y. H., del Sol, A., & Grapin-Botton, A. (2021). A 3D system to model human pancreas development and its reference single-cell transcriptome atlas identify signaling pathways required for progenitor expansion. *Nature Communications*, 12(1), 3144. <https://doi.org/10.1038/s41467-021-23295-6>
- Haan, E. A., Boss, B. D., & Cowan, W. M. (1982). Production and characterization of monoclonal antibodies against the "brain-specific" proteins 14-3-2 and S-100. *Proceedings of the National Academy of Sciences*, 79(23), 7585–7589. <https://doi.org/10.1073/pnas.79.23.7585>
- Haas, T. L., Sciuto, M. R., Brunetto, L., Valvo, C., Signore, M., Fiori, M. E., Martino, D. I., Giannetti, S., Morgante, L., Boe, A., Patrizii, M., Warnken, U., Schnölzer, M., Ciolfi, A., Di Stefano, C., Biffoni, M., Ricci-Vitiani, L., Pallini, R., & DE Maria, R. (2017). Integrin alpha7 is a functional marker and potential therapeutic target in glioblastoma. *Cell Stem Cell*, 21(1), 35–50.e9. <https://doi.org/10.1016/j.stem.2017.04.009>
- Hagemann, T. L. (2022). Alexander disease: Models, mechanisms, and medicine. *Current Opinion in Neurobiology*, 72, 140–147. <https://doi.org/10.1016/j.conb.2021.10.002>
- Hagemann, T. L., Connor, J. X., & Messing, A. (2006). Alexander disease-associated glial fibrillary acidic protein mutations in mice induce Rosenthal fiber formation and a white matter stress response. *The Journal of Neuroscience*, 26(43), 11162–11173. <https://doi.org/10.1523/JNEUROSCI.3260-06.2006>
- Hagemann, T. L., Gaeta, S. A., Smith, M. A., Johnson, D. A., Johnson, J. A., & Messing, A. (2005). Gene expression analysis in mice with elevated glial fibrillary acidic protein and Rosenthal fibers reveals a stress response followed by glial activation and neuronal dysfunction. *Human Molecular Genetics*, 14(16), 2443–2458. <https://doi.org/10.1093/hmg/ddi248>
- Hagemann, T. L., Paylor, R., & Messing, A. (2013). Deficits in adult neurogenesis, contextual fear conditioning, and spatial learning in a Gfap mutant mouse model of Alexander disease. *The Journal of Neuroscience*, 33(47), 18698–18706. <https://doi.org/10.1523/JNEUROSCI.3693-13.2013>
- Hagemann, T. L., Powers, B., Lin, N. H., Mohamed, A. F., Dague, K. L., Hannah, S. C., Bachmann, G., Mazur, C., Rigo, F., Olsen, A. L., Feany, M. B., Perng, M. D., Berman, R. F., & Messing, A. (2021). Antisense therapy in a rat model of Alexander disease reverses GFAP pathology, white matter deficits, and motor impairment. *Science Translational Medicine*, 13(620), eabg4711. <https://doi.org/10.1126/scitranslmed.abg4711>
- Hao, Y., Hao, S., Andersen-Nissen, E., Mauck, W. M., 3rd, Zheng, S., Butler, A., Lee, M. J., Wilk, A. J., Darby, C., Zager, M., Hoffman, P., Stoeckius, M., Papalexi, E., Mimitou, E. P., Jain, J., Srivastava, A., Stuart, T., Fleming, L. M., Yeung, B., Rogers, A. J., McElrath, J. M., Blish, C. A., Gottardo, R., Smibert, P., & Satija, R. (2021). Integrated analysis of multimodal single-cell data. *Cell*, 184(13), 3573–3587. <https://doi.org/10.1016/j.cell.2021.04.048>
- Heaven, M. R., Herren, A. W., Flint, D. L., Pacheco, N. L., Li, J., Tang, A., Khan, F., Goldman, J. E., Phinney, B. S., & Olsen, M. L. (2022). Metabolic enzyme alterations and astrocyte dysfunction in a murine model of Alexander disease with severe reactive gliosis. *Molecular & Cellular Proteomics*, 21(1), 100180. <https://doi.org/10.1016/j.mcpro.2021.100180>
- Heck, N., Garwood, J., Schütte, K., Fawcett, J., & Faissner, A. (2003). Astrocytes in culture express fibrillar collagen. *Glia*, 41(4), 382–392. <https://doi.org/10.1002/glia.10184>
- Hou, P. S., Ó hAilín, D., Vogel, T., & Hanashima, C. (2020). Transcription and beyond: Delineating FOXG1 function in cortical development and disorders. *Frontiers in Cellular Neuroscience*, 14, 35. <https://doi.org/10.3389/fncel.2020.00035>
- Hsia, E. Y., Gui, Y., & Zheng, X. (2015). Regulation of hedgehog signaling by ubiquitination. *Frontiers in Biology (Beijing)*, 10(3), 203–220. <https://doi.org/10.1007/s11515-015-1343-5>
- Imamura, T., Oshima, Y., & Hikita, A. (2013). Regulation of TGF-beta family signalling by ubiquitination and deubiquitination. *Journal of Biochemistry*, 154(6), 481–489. <https://doi.org/10.1093/jb/mvt097>
- Imura, T., Kornblum, H. I., & Sofroniew, M. V. (2003). The predominant neural stem cell isolated from postnatal and adult forebrain but not early

- embryonic forebrain expresses GFAP. *The Journal of Neuroscience*, 23(7), 2824–2832. <https://doi.org/10.1523/JNEUROSCI.23-07-02824.2003>
- Jacquet, B. V., Salinas-Mondragon, R., Liang, H., Therit, B., Buie, J. D., Dykstra, M., Campbell, K., Ostrowski, L. E., Brody, S. L., & Ghashghaei, H. T. (2009). FoxJ1-dependent gene expression is required for differentiation of radial glia into ependymal cells and a subset of astrocytes in the postnatal brain. *Development*, 136(23), 4021–4031. <https://doi.org/10.1242/dev.041129>
- Jin, S., Guerrero-Juarez, C. F., Zhang, L., Chang, I., Ramos, R., Kuan, C. H., Myung, P., Plikus, M. V., & Nie, Q. (2021). Inference and analysis of cell–cell communication using CellChat. *Nature Communications*, 12, 1088. <https://doi.org/10.1038/s41467-021-21246-9>
- Jones, J. R., Kong, L., Hanna, M. G. T., Hoffman, B., Krencik, R., Bradley, R., Hagemann, T., Choi, J., Doers, M., Dubovis, M., Sherafat, M. A., Bhattacharyya, A., Kendzierski, C., Audhya, A., Messing, A., & Zhang, S. C. (2018). Mutations in GFAP disrupt the distribution and function of organelles in human astrocytes. *Cell Reports*, 25(4), 947–958.e4. <https://doi.org/10.1016/j.celrep.2018.09.083>
- Juárez-Rebollar, D., Rios, C., Nava-Ruiz, C., & Méndez-Armenta, M. (2017). Metallothionein in brain disorders. *Oxidative Medicine and Cellular Longevity*, 2017, 5828056. <https://doi.org/10.1155/2017/5828056>
- Kanamori-Katayama, M., Kaiho, A., Ishizu, Y., Okamura-Oho, Y., Hino, O., Abe, M., Kishimoto, T., Sekihara, H., Nakamura, Y., Suzuki, H., Forrest, A. R., & Hayashizaki, Y. (2011). LRRN4 and UPK3B are markers of primary mesothelial cells. *PLoS One*, 6(10), e25391. <https://doi.org/10.1371/journal.pone.0025391>
- Kanton, S., Boyle, M. J., He, Z., Santel, M., Weigert, A., Sanchis-Calleja, F., Guíjarro, P., Sidow, L., Fleck, J. S., Han, D., Qian, Z., Heide, M., Huttner, W. B., Khaitovich, P., Pääbo, S., Treutlein, B., & Camp, J. G. (2019). Organoid single-cell genomic atlas uncovers human-specific features of brain development. *Nature*, 574(7778), 418–422. <https://doi.org/10.1038/s41586-019-1654-9>
- Kirkcaldie, M. T. K., & Dwyer, S. T. (2017). The third wave: Intermediate filaments in the maturing nervous system. *Molecular and Cellular Neurosciences*, 84, 68–76. <https://doi.org/10.1016/j.mcn.2017.05.010>
- Kobayashi, M., Oshima, S., Maeyashiki, C., Nibe, Y., Otsubo, K., Matsuzawa, Y., Nemoto, Y., Nagaishi, T., Okamoto, R., Tsuchiya, K., Nakamura, T., & Watanabe, M. (2016). The ubiquitin hybrid gene UBA52 regulates ubiquitination of ribosome and sustains embryonic development. *Scientific Reports*, 6, 36780. <https://doi.org/10.1038/srep36780>
- Kondo, T., Funayama, M., Miyake, M., Tsukita, K., Era, T., Osaka, H., Ayaki, T., Takahashi, R., & Inoue, H. (2016). Modeling Alexander disease with patient iPSCs reveals cellular and molecular pathology of astrocytes. *Acta Neuropathologica Communications*, 4(1), 69. <https://doi.org/10.1186/s40478-016-0337-0>
- Lafzi, A., Moutinho, C., Picelli, S., & Heyn, H. (2018). Tutorial: Guidelines for the experimental design of single-cell RNA sequencing studies. *Nature Protocols*, 13(12), 2742–2757. <https://doi.org/10.1038/s41596-018-0073-y>
- Lampada, A., & Taylor, V. (2023). Notch signaling as a master regulator of adult neurogenesis. *Frontiers in Neuroscience*, 17, 1179011. <https://doi.org/10.3389/fnins.2023.1179011>
- Lancaster, M. A., & Knoblich, J. A. (2014). Organogenesis in a dish: Modeling development and disease using organoid technologies. *Science*, 345(6194), 1247125. <https://doi.org/10.1126/science.1247125>
- Lancaster, M. A., Renner, M., Martin, C. A., Wenzel, D., Bicknell, L. S., Hurles, M. E., Homfray, T., Penninger, J. M., Jackson, A. P., & Knoblich, J. A. (2013). Cerebral organoids model human brain development and microcephaly. *Nature*, 501(7467), 373–379. <https://doi.org/10.1038/nature12517>
- Lee, S. H., Nam, T. S., Kim, K. H., Kim, J. H., Yoon, W., Heo, S. H., Kim, M. J., Shin, B. A., Perng, M. D., Choy, H. E., Jo, J., Kim, M. K., & Choi, S. Y. (2017). Aggregation-prone GFAP mutation in Alexander disease validated using a zebrafish model. *BMC Neurology*, 17(1), 175. <https://doi.org/10.1186/s12883-017-0938-7>
- Li, L., Lundkvist, A., Andersson, D., Wilhelmsson, U., Nagai, N., Pardo, A. C., Nodin, C., Ståhlberg, A., Aprico, K., Larsson, K., Yabe, T., Moons, L., Fotheringham, A., Davies, I., Carmeliet, P., Schwartz, J. P., Pekna, M., Kubista, M., Blomstrand, F., Maragakis, N., Nilsson, M., & Pekny, M. (2008). Protective role of reactive astrocytes in brain ischemia. *Journal of Cerebral Blood Flow and Metabolism*, 28(3), 468–481. <https://doi.org/10.1038/sj.jcbfm.9600546>
- Li, L., Tian, E., Chen, X., Chao, J., Klein, J., Qu, Q., Sun, G., Sun, G., Huang, Y., Warden, C. D., Ye, P., Feng, L., Li, X., Cui, Q., Sultan, A., Douvaras, P., Fossati, V., Sanjana, N. E., Riggs, A. D., & Shi, Y. (2018). GFAP mutations in astrocytes impair oligodendrocyte progenitor proliferation and myelination in an hiPSC model of Alexander disease. *Cell Stem Cell*, 23(2), 239–251. <https://doi.org/10.1016/j.stem.2018.07.009>
- Li, X., Floriddia, E. M., Toskas, K., Chalfouh, C., Honore, A., Aumont, A., Vallières, N., Lacroix, S., Fernandes, K. J. L., Guéroul, N., & Barnabé-Heider, F. (2018). FoxJ1 regulates spinal cord development and is required for the maintenance of spinal cord stem cell potential. *Experimental Cell Research*, 368(1), 84–100. <https://doi.org/10.1016/j.yexcr.2018.04.017>
- Li, X. Y., Zhai, W. J., & Teng, C. B. (2015). Notch signaling in pancreatic development. *International Journal of Molecular Sciences*, 17(1), 48. <https://doi.org/10.3390/ijms17010048>
- Lin, H. C., He, Z., Ebert, S., Schornig, M., Santel, M., Nikolova, M. T., Weigert, A., Hevers, W., Kasri, N. N., Taverna, E., Camp, J. G., & Treutlein, B. (2021). NGN2 induces diverse neuron types from human pluripotency. *Stem Cell Reports*, 16(9), 2118–2127. <https://doi.org/10.1016/j.stemcr.2021.07.006>
- Liour, S. S., & Yu, R. K. (2003). Differentiation of radial glia-like cells from embryonic stem cells. *Glia*, 42(2), 109–117. <https://doi.org/10.1002/glia.10202>
- Liu, Q. C., Zha, X. H., Faralli, H., Yin, H., Louis-Jeune, C., Perdiguero, E., Prankevicene, E., Muñoz-Cánoves, P., Rudnicki, M. A., Brand, M., Perez-Iratxeta, C., & Dilworth, F. J. (2012). Comparative expression profiling identifies differential roles for myogenin and p38alpha MAPK signaling in myogenesis. *Journal of Molecular Cell Biology*, 4(6), 386–397. <https://doi.org/10.1093/jmcb/mjs045>
- Lun, A. T. L., Riesenfeld, S., Andrews, T., Dao, T. P., Gomes, T., Participants in the 1ST Human Cell Atlas, & Marioni, J. C. (2019). EmptyDrops: Distinguishing cells from empty droplets in droplet-based single-cell RNA sequencing data. *Genome Biology*, 20(1), 63. <https://doi.org/10.1186/s13059-019-1662-y>
- Lundkvist, A., Reichenbach, A., Betsholtz, C., Carmeliet, P., Wolburg, H., & Pekny, M. (2004). Under stress, the absence of intermediate filaments from Muller cells in the retina has structural and functional consequences. *Journal of Cell Science*, 117(16), 3481–3488. <https://doi.org/10.1242/jcs.01221>
- Ma, Z., Zhang, X., Zhong, W., Yi, H., Chen, X., Zhao, Y., Ma, Y., Song, E., & Xu, T. (2023). Deciphering early human pancreas development at the single-cell level. *Nature Communications*, 14(1), 5354. <https://doi.org/10.1038/s41467-023-40893-8>
- McGinnis, C. S., Murrow, L. M., & Gartner, Z. J. (2019). DoubletFinder: Doublet detection in single-cell RNA sequencing data using artificial nearest neighbors. *Cell Systems*, 8(4), 329–337.e4. <https://doi.org/10.1016/j.cels.2019.03.003>
- Meisingset, T. W., Risa, O., Brenner, M., Messing, A., & Sonnewald, U. (2010). Alteration of glial-neuronal metabolic interactions in a mouse model of Alexander disease. *Glia*, 58(10), 1228–1234. <https://doi.org/10.1002/glia.21003>
- Miyata, T., Toho, T., Nonoguchi, N., Furuse, M., Kuwabara, H., Yoritsune, E., Kawabata, S., Kuroiwa, T., & Miyatake, S. (2014). The roles of platelet-derived growth factors and their receptors in brain radiation necrosis. *Radiation Oncology*, 9, 51. <https://doi.org/10.1186/1748-717X-9-51>
- Motohashi, N., & Asakura, A. (2014). Muscle satellite cell heterogeneity and self-renewal. *Frontiers in Cell and Development Biology*, 2, 1. <https://doi.org/10.3389/fcell.2014.00001>



- Napolitano, T., Silvano, S., Ayachi, C., Plaisant, M., SousaDa-Veiga, A., Fofo, H., Charles, B., & Collombat, P. (2023). Wnt pathway in pancreatic development and pathophysiology. *Cells*, 12(4), 565. <https://doi.org/10.3390/cells12040565>
- Nawashiro, H., Messing, A., Azzam, N., & Brenner, M. (1998). Mice lacking GFAP are hypersensitive to traumatic cerebrospinal injury. *Neuroreport*, 9(8), 1691–1696. <https://doi.org/10.1097/00001756-199806010-00004>
- Olabarria, M., Putilina, M., Riemer, E. C., & Goldman, J. E. (2015). Astrocyte pathology in Alexander disease causes a marked inflammatory environment. *Acta Neuropathologica*, 130(4), 469–486. <https://doi.org/10.1007/s00401-015-1469-1>
- Ormel, P. R., Vieira de Sá, R., van Bodegraven, E. J., Karst, H., Harschnitz, O., Sneebouwer, M. A. M., Johansen, L. E., van Dijk, R. E., Scheefhals, N., Berdenis van Berlekom, A., Ribes Martínez, E., Kling, S., MacGillivray, H. D., van den Berg, L. H., Kahn, R. S., Hol, E. M., de Witte, L. D., & Pasterkamp, R. J. (2018). Microglia innately develop within cerebral organoids. *Nature Communications*, 9, 4167. <https://doi.org/10.1038/s41467-018-06684-2>
- de Pablo, Y., Nilsson, M., Pekna, M., & Pekny, M. (2013). Intermediate filaments are important for astrocyte response to oxidative stress induced by oxygen-glucose deprivation and reperfusion. *Histochemistry and Cell Biology*, 140(1), 81–91. <https://doi.org/10.1007/s00418-013-1110-0>
- Pajares, M. A., Hernández-Gerez, E., Pekny, M., & Pérez-Sala, D. (2023). Alexander disease: The road ahead. *Neural Regeneration Research*, 18(10), 2156–2160. <https://doi.org/10.4103/1673-5374.369097>
- Peek, S. L., Mah, K. M., & Weiner, J. A. (2017). Regulation of neural circuit formation by protocadherins. *Cellular and Molecular Life Sciences*, 74(22), 4133–4157. <https://doi.org/10.1007/s00018-017-2572-3>
- Pekny, M., & Lane, E. B. (2007). Intermediate filaments and stress. *Experimental Cell Research*, 313(10), 2244–2254. <https://doi.org/10.1016/j.yexcr.2007.04.023>
- Pekny, M., Pekna, M., Messing, A., Steinhauser, C., Lee, J. M., Parpura, V., Hol, E. M., Sofroniew, M. V., & Verkhratsky, A. (2016). Astrocytes: a central element in neurological diseases. *Acta Neuropathologica*, 131(3), 323–345. <https://doi.org/10.1007/s00401-015-1513-1>
- Pellegrini, L., Bonfio, C., Chadwick, J., Begum, F., Skehel, M., & Lancaster, M. A. (2020). Human CNS barrier-forming organoids with cerebrospinal fluid production. *Science*, 369(6500), eaaz5626. <https://doi.org/10.1126/science.aaz5626>
- Pfau, S. J., Langen, U. H., Fisher, T. M., Prakash, I., Nagpurwala, F., Lozoya, R. A., Lee, W.-C. A., Wu, Z., & Gu, C. (2024). Characteristics of blood-brain barrier heterogeneity between brain regions revealed by profiling vascular and perivascular cells. *Nature Neuroscience*, Epub ahead of print. <https://doi.org/10.1038/s41593-024-01743-y>
- Pitale, P. M., Howse, W., & Gorbatyuk, M. (2017). Neuronatin protein in health and disease. *Journal of Cellular Physiology*, 232(3), 477–481. <https://doi.org/10.1002/jcp.25498>
- Podergajs, N., Motaln, H., Rajcovic, U., Verbovsek, U., Korsic, M., Obad, N., Espedal, H., Vittori, M., Herold-Mende, C., Miletic, H., Bjerkvig, R., & Turnsek, T. L. (2016). Transmembrane protein CD9 is glioblastoma biomarker, relevant for maintenance of glioblastoma stem cells. *Oncotarget*, 7(1), 593–609. <https://doi.org/10.18632/oncotarget.5477>
- R Core Team. (2022). *R: A language and environment for statistical computing*. R Foundation for Statistical Computing, Vienna. <https://www.R-project.org>
- Ridge, K. M., Eriksson, J. E., Pekny, M., & Goldman, R. D. (2022). Roles of vimentin in health and disease. *Genes & Development*, 36(7–8), 391–407. <https://doi.org/10.1101/gad.349358.122>
- Röber, R. A., Weber, K., & Osborn, M. (1989). Differential timing of nuclear lamin A/C expression in the various organs of the mouse embryo and the young animal: A developmental study. *Development*, 105(2), 365–378. <https://doi.org/10.1242/dev.105.2.365>
- Ruttkey-Nedecky, B., Nejdli, L., Gumulec, J., Zitka, O., Masarik, M., Eckschlager, T., Stiborova, M., Adam, V., & Kizek, R. (2013). The role of metallothionein in oxidative stress. *International Journal of Molecular Sciences*, 14(3), 6044–6066. <https://doi.org/10.3390/ijms14036044>
- Sarnat, H. B. (2015). Immunocytochemical markers of neuronal maturation in human diagnostic neuropathology. *Cell and Tissue Research*, 359(1), 279–294. <https://doi.org/10.1007/s00441-014-1988-4>
- Schindelin, J., Arganda-Carreras, I., Frise, E., Kaynig, V., Longair, M., Pietzsch, T., Preibisch, S., Rueden, C., Saalfeld, S., Schmid, B., Tinevez, J. Y., White, D. J., Hartenstein, V., Eliceiri, K., Tomancak, P., & Cardona, A. (2012). Fiji: An open-source platform for biological-image analysis. *Nature Methods*, 9(7), 676–682. <https://doi.org/10.1038/nmeth.2019>
- Schmid, R. S., McGrath, B., Berechid, B. E., Boyles, B., Marchionni, M., Sestan, N., & Anton, E. S. (2003). Neuregulin 1-erbB2 signaling is required for the establishment of radial glia and their transformation into astrocytes in cerebral cortex. *Proceedings of the National Academy of Sciences*, 100(7), 4251–4256. <https://doi.org/10.1073/pnas.0630496100>
- Schramm, F., Schaefer, L., & Wygrecka, M. (2022). EGFR signaling in lung fibrosis. *Cells*, 11(6), 986. <https://doi.org/10.3390/cells11060986>
- Seo, J. S., & Svenningsson, P. (2020). Modulation of ion channels and receptors by p11 (S100A10). *Trends in Pharmacological Sciences*, 41(7), 487–497. <https://doi.org/10.1016/j.tips.2020.04.004>
- Shen, F., Song, C., Liu, Y., Zhang, J., & Song, S. W. (2019). IGFBP2 promotes neural stem cell maintenance and proliferation differentially associated with glioblastoma subtypes. *Brain Research*, 1704, 174–186. <https://doi.org/10.1016/j.brainres.2018.10.018>
- Sosunov, A., Olabarria, M., & Goldman, J. E. (2018). Alexander disease: An astrocytopathy that produces a leukodystrophy. *Brain Pathology*, 28(3), 388–398. <https://doi.org/10.1111/bpa.12601>
- Sosunov, A. A., Guilfoyle, E., Wu, X., McKhann, G. M., & Goldman, J. E. (2013). Phenotypic conversions of "protoplasmic" to "reactive" astrocytes in Alexander disease. *The Journal of Neuroscience*, 33(17), 7439–7450. <https://doi.org/10.1523/JNEUROSCI.4506-12.2013>
- Sosunov, A. A., McKhann, G. M., & Goldman, J. E. (2017). The origin of Rosenthal fibers and their contributions to astrocyte pathology in Alexander disease. *Acta Neuropathologica Communications*, 5(1), 27. <https://doi.org/10.1186/s40478-017-0425-9>
- Stroob, E., Janssen, L., Sin, O., Hogewerf, W., Koster, M., Harkema, L., Youssef, S. A., Beschorner, N., Wolters, A. H., Bakker, B., Becker, L., Garrett, L., Marschall, S., Hoelter, S. M., Wurst, W., Fuchs, H., Gailus-Durner, V., Hrabe de Angelis, M., Thathiah, A., Foijer, F., van de Sluis, B., van Deursen, J., Jucker, M., de Bruin, A., & Nollen, E. A. (2023). Deletion of SERF2 in mice delays embryonic development and alters amyloid deposit structure in the brain. *Life Science Alliance*, 6(7), e202201730. <https://doi.org/10.26508/lsa.202201730>
- Sun, W., Cornwell, A., Li, J., Peng, S., Osorio, M. J., Aalling, N., Wang, S., Benraiss, A., Lou, N., Goldman, S. A., & Nedergaard, M. (2017). SOX9 is an astrocyte-specific nuclear marker in the adult brain outside the neurogenic regions. *The Journal of Neuroscience*, 37(17), 4493–4507. <https://doi.org/10.1523/JNEUROSCI.3199-16.2017>
- Suthon, S., Perkins, R. S., Bryja, V., Miranda-Carboni, G. A., & Krum, S. A. (2021). WNT5B in physiology and disease. *Frontiers in Cell and Developmental Biology*, 9, 667581. <https://doi.org/10.3389/fcell.2021.667581>
- Tanaka, K. F., Takebayashi, H., Yamazaki, Y., Ono, K., Naruse, M., Iwasato, T., Itoharu, S., Kato, H., & Ikenaka, K. (2007). Murine model of Alexander disease: Analysis of GFAP aggregate formation and its pathological significance. *Glia*, 55(6), 617–631. <https://doi.org/10.1002/glia.20486>
- Tang, G., Perng, M. D., Wilk, S., Quinlan, R., & Goldman, J. E. (2010). Oligomers of mutant glial fibrillary acidic protein (GFAP) inhibit the proteasome system in alexander disease astrocytes, and the small heat shock protein alphaB-crystallin reverses the inhibition. *The Journal of Biological Chemistry*, 285(14), 10527–10537. <https://doi.org/10.1074/jbc.M109.067975>

- Tomé, D., Dias, M. S., Correia, J., & Almeida, R. D. (2023). Fibroblast growth factor signaling in axons: From development to disease. *Cell Communication and Signaling: CCS*, 21(1), 290. <https://doi.org/10.1186/s12964-023-01284-0>
- Tyanova, S., Temu, T., Sinitcyn, P., Carlson, A., Hein, M. Y., Geiger, T., Mann, M., & Cox, J. (2016). The Perseus computational platform for comprehensive analysis of (prote)omics data. *Nature Methods*, 13(9), 731–740. <https://doi.org/10.1038/nmeth.3901>
- Verardo, M. R., Lewis, G. P., Takeda, M., Linberg, K. A., Byun, J., Luna, G., Wilhelmsson, U., Pekny, M., Chen, D. F., & Fisher, S. K. (2008). Abnormal reactivity of Müller cells after retinal detachment in mice deficient in GFAP and vimentin. *Investigative Ophthalmology & Visual Science*, 49(8), 3659–3665. <https://doi.org/10.1167/iovs.07-1474>
- Verkerke, M., Berdenis van Berlekom, A., Donega, V., Vonk, D., Sluijs, J. A., Butt, N. F., Kistemaker, L., de Witte, L. D., Pasterkamp, R. J., Middeldorp, J., & Hol, E. M. (2024). Transcriptomic and morphological maturation of human astrocytes in cerebral organoids. *Glia*, 72(2), 362–374. <https://doi.org/10.1002/glia.24479>
- Vértesy, A., Eichmüller, O. L., Naas, J., Novatchkova, M., Esk, C., Balmaña, M., Ladstaetter, S., Bock, C., von Haeseler, A., & Knoblich, J. A. (2022). Gruffi: An algorithm for computational removal of stressed cells from brain organoid transcriptomic datasets. *The EMBO Journal*, 41(17), e111118. <https://doi.org/10.15252/embj.2022111118>
- Viedma-Poyatos, A., González-Jiménez, P., Pajares, M. A., & Pérez-Sala, D. (2022). Alexander disease GFAP R239C mutant shows increased susceptibility to lipoxidation and elicits mitochondrial dysfunction and oxidative stress. *Redox Biology*, 55, 102415. <https://doi.org/10.1016/j.redox.2022.102415>
- Voss, A. J., Lanjewar, S. N., Sampson, M. M., King, A., Hill, E. J., Sing, A., Sojka, C., Bhatia, T. N., Spangle, J. M., & Sloan, S. A. (2023). Identification of ligand-receptor pairs that drive human astrocyte development. *Nature Neuroscience*, 26(8), 1339–1351. <https://doi.org/10.1038/s41593-023-01375-8>
- Walker, A. K., Daniels, C. M., Goldman, J. E., Trojanowski, J. Q., Lee, V. M., & Messing, A. (2014). Astrocytic TDP-43 pathology in Alexander disease. *The Journal of Neuroscience*, 34(19), 6448–6458. <https://doi.org/10.1523/JNEUROSCI.0248-14.2014>
- Wang, L., Colodner, K. J., & Feany, M. B. (2011). Protein misfolding and oxidative stress promote glial-mediated neurodegeneration in an Alexander disease model. *The Journal of Neuroscience*, 31(8), 2868–2877. <https://doi.org/10.1523/JNEUROSCI.3410-10.2011>
- Wang, L., Sui, L., Panigrahi, S. K., Meece, K., Xin, Y., Kim, J., Gromada, J., Doege, C. A., Wardlaw, S. L., Egli, D., & Leibel, R. L. (2017). PC1/3 deficiency impacts pro-opiomelanocortin processing in human embryonic stem cell-derived hypothalamic neurons. *Stem Cell Reports*, 8(2), 264–277. <https://doi.org/10.1016/j.stemcr.2016.12.021>
- Wang, L., Xia, J., Li, J., Hagemann, T. L., Jones, J. R., Fraenkel, E., Weitz, D. A., Zhang, S. C., Messing, A., & Feany, M. B. (2018). Tissue and cellular rigidity and mechanosensitive signaling activation in Alexander disease. *Nature Communications*, 9(1), 1899. <https://doi.org/10.1038/s41467-018-04269-7>
- Wei, B., & Jin, J. P. (2016). TNNT1, TNNT2, and TNNT3: Isoform genes, regulation, and structure-function relationships. *Gene*, 582(1), 1–13. <https://doi.org/10.1016/j.gene.2016.01.006>
- Wilhelmsson, U., Faiz, M., de Pablo, Y., Sjöqvist, M., Andersson, D., Widestrand, A., Potokar, M., Stenovec, M., Smith, P. L., Shinjyo, N., Pekny, T., Zorec, R., Ståhlberg, A., Pekna, M., Sahlgren, C., & Pekny, M. (2012). Astrocytes negatively regulate neurogenesis through the Jagged1-mediated Notch pathway. *Stem Cells*, 30(10), 2320–2329. <https://doi.org/10.1002/stem.1196>
- Wingett, S. W., & Andrews, S. (2018). FastQ screen: A tool for multi-genome mapping and quality control. *F1000Res*, 7, 1338. <https://doi.org/10.12688/f1000research.15931.2>
- Wu, T., Hu, E., Xu, S., Chen, M., Guo, P., Dai, Z., Feng, T., Zhou, L., Tang, W., Zhan, L., Fu, X., Liu, S., Bo, X., & Yu, G. (2021). clusterProfiler 4.0: A universal enrichment tool for interpreting omics data. *The Innovation (Cambridge)*, 2(3), 100141. <https://doi.org/10.1016/j.xinn.2021.100141>
- Wunderlich, K. A., Tanimoto, N., Grosche, A., Zrenner, E., Pekny, M., Reichenbach, A., Seeliger, M. W., Pannicke, T., & Perez, M. T. (2015). Retinal functional alterations in mice lacking intermediate filament proteins glial fibrillary acidic protein and vimentin. *The FASEB Journal*, 29(12), 4815–4828. <https://doi.org/10.1096/fj.15-272963>
- Yang, A. W., Lin, N. H., Yeh, T. H., Snider, N., & Perng, M. D. (2022). Effects of Alexander disease-associated mutations on the assembly and organization of GFAP intermediate filaments. *Molecular Biology of the Cell*, 33(8), ar69. <https://doi.org/10.1091/mbc.E22-01-0013>
- Yoon, S. J., Elahi, L. S., Pasca, A. M., Marton, R. M., Gordon, A., Revah, O., Miura, Y., Walczak, E. M., Holdgate, G. M., Fan, H. C., Huguenard, J. R., Geschwind, D. H., & Pasca, S. P. (2019). Reliability of human cortical organoid generation. *Nature Methods*, 16(1), 75–78. <https://doi.org/10.1038/s41592-018-0255-0>
- Young, M. D., & Behjati, S. (2020). SoupX removes ambient RNA contamination from droplet-based single-cell RNA sequencing data. *GigaScience*, 9(12), gaa151. <https://doi.org/10.1093/gigascience/gaa151>
- Zarei-Kheirabadi, M., Vaccaro, A. R., Rahimi-Movaghar, V., Kiani, S., & Baharvand, H. (2020). An overview of extrinsic and intrinsic mechanisms involved in astrocyte development in the central nervous system. *Stem Cells and Development*, 29(5), 266–280. <https://doi.org/10.1089/scd.2019.0189>
- Zeng, B., Liu, Z., Lu, Y., Zhong, S., Qin, S., Huang, L., Zeng, Y., Li, Z., Dong, H., Shi, Y., Yang, J., Dai, Y., Ma, Q., Sun, L., Bian, L., Han, D., Chen, Y., Qiu, X., Wang, W., Marín, O., Wu, Q., Wang, Y., & Wang, X. (2023). The single-cell and spatial transcriptional landscape of human gastrulation and early brain development. *Cell Stem Cell*, 30(6), 851–866.e7. <https://doi.org/10.1016/j.stem.2023.04.016>
- Zhang, X., Xiao, G., Johnson, C., Cai, Y., Horowitz, Z. K., Mennicke, C., Coffey, R., Haider, M., Threadgill, D., Eliscu, R., Oldham, M. C., Greenbaum, A., & Ghashghaei, H. T. (2023). Bulk and mosaic deletions of Egrf reveal regionally defined gliogenesis in the developing mouse fore-brain. *iScience*, 26(3), 106242. <https://doi.org/10.1016/j.isci.2023.106242>
- Zhang, Y., Pak, C., Han, Y., Ahlenius, H., Zhang, Z., Chanda, S., Marro, S., Patzke, C., Acuna, C., Covy, J., Xu, W., Yang, N., Danko, T., Chen, L., Wernig, M., & Südhof, T. C. (2013). Rapid single-step induction of functional neurons from human pluripotent stem cells. *Neuron*, 78(5), 785–798. <https://doi.org/10.1016/j.neuron.2013.05.029>
- Zhang, Z., Bhalla, A., Dean, C., Chapman, E. R., & Jackson, M. B. (2009). Synaptotagmin IV: A multifunctional regulator of peptidergic nerve terminals. *Nature Neuroscience*, 12(2), 163–171. <https://doi.org/10.1038/nn.2252>

SUPPORTING INFORMATION

Additional supporting information can be found online in the Supporting Information section at the end of this article.

How to cite this article: Matusova, Z., Dykstra, W., de Pablo, Y., Zetterdahl, O. G., Canals, I., van Gelder, C. A. G. H., Vos, H. R., Pérez-Sala, D., Kubista, M., Abaffy, P., Ahlenius, H., Valihrach, L., Hol, E. M., & Pekny, M. (2024). Aberrant neurodevelopment in human iPSC cell-derived models of Alexander disease. *Glia*, 1–23. <https://doi.org/10.1002/glia.24618>

3.2 Methods

The methods utilized in the abovementioned projects resulting in the two main first-author publications are listed below.

Performed by me:

- Preparation of sequencing libraries (**Publication I & II**)
- Processing of the scRNA-seq data, including quality control and filtering (**Publication I & II**)
- Cell population analysis with cell type annotation (**Publication I & II**)
- Differential gene expression analysis and Gene Ontology enrichment analysis between conditions (**Publication I & II**)
- Cell-cell interaction analysis (**Publication II**)
- Result interpretation with respect to other experimental data and relevant literature (**Publication I & II**)

Performed by co-authors:

- Behavioural testing of model animals (**Publication I**)
- Cell type enrichment with FACS (**Publication I**)
- Generation of co-cultures and organoids (**Publication II**)
- Preparation of single-cell suspensions and sequencing libraries (**Publication I & II**)
- Processing of the sequencing data, including quality control and filtering (**Publication I & II**)
- Immunohistochemistry (**Publication I & II**)
- RT-qPCR (**Publication II**)
- Mass spectrometry (**Publication II**)

3.3 Other publications and manuscripts

Other co-authored publications and manuscripts in preparation are listed below.

• **Publication III – review**

Valihrach, L., Matusova, Z., Zucha, D., Klassen, R., Benesova, S., Abaffy, P., Kubista, M., Anderova, M. **Recent advances in deciphering oligodendrocyte heterogeneity with single-cell transcriptomics.** *Frontiers in Cellular Neuroscience*, 16:1025012, 2022. doi: 10.3389/fncel.2022.1025012.

Journal: *Frontiers in Cellular Neuroscience*, IF 5.3 (2022)

Contribution: Literature search, proofreading, and editing.

- **Publication IV**

Fedorova, V.*, Pospisilova, V.*, Vanova, T.*, Cerna, K. A.*, Abaffy, P., Sedmik, J., Raska, J., Vochyanova, S., Matusova, Z., Houserova, J., Valihrach, L., Hodny, Z., Bohaciakova, D. **Glioblastoma and cerebral organoids: development and analysis of an in vitro model for glioblastoma migration.** *Molecular Oncology*, 17(4):647–663, 2023. doi: 10.1002/1878-0261.13389.

* shared first authors

Journal: *Molecular Oncology*, IF 5 (2023)

Contribution: Transcriptomic figure preparation, help with data analysis.

- **Publication V – review**

Matusova, Z., Hol, E. M., Pekny, M., Kubista, M., Valihrach, L. **Reactive astrogliosis in the era of single-cell transcriptomics.** *Frontiers in Cellular Neuroscience*, 17:1173200, 2023. doi: 10.3389/fncel.2023.1173200.

Journal: *Frontiers in Cellular Neuroscience*, IF 4.2 (2023)

Contribution: Literature search, manuscript and figure preparation.

- **Manuscript in preparation I**

Dykstra, W.*, Matusova, Z.*, Battaglia, R. A., Abaffy, P., Goya-Iglesias, N., Pérez-Sala, D., Ahlenius, H., Kubista, M., Pasterkamp, R. J., Li, L., Chao, J., Shi, Y., Valihrach, L., Pekny, M., Hol, E. M. **Mutant GFAP alters lineage commitment of neural organoids.**

* shared first authors

Contribution: Optimization of experimental design, preparation of the sequencing libraries, data analysis and interpretation, manuscript preparation with focus on the transcriptomic sections and figures.

- **Manuscript in preparation II**

Berankova, M.*, Holoubek, J.*, Hönig, V.*, Matusova, Z.*, Palus, M.*, Salat, J., Vojtiskova, J., Svoboda, P., Pranclova, V., Valihrach, L., Lipoldova, M., Ruzek, D. **Genotype-driven sensitivity in mice to tick-borne encephalitis virus correlates with differential host responses in peripheral macrophages and brain.**

* shared first authors

Contribution: Interpretation and visualization of microarray transcriptomic data, preparation of related text and figures.

4 Discussion

This dissertation presents the application of transcriptomic profiling with single-cell RNA sequencing in two projects focusing on two neurodegenerative diseases with distinct etiologies and model systems. The results of these studies have been summarized in two publications (**Publication I** and **Publication II**).

4.1 Minimal changes in cortical glia in SOD1(G93A) mouse model of ALS

In the ALS project (**Publication I**), we took advantage of the cell-level resolution of the scRNA-seq method to investigate the cortical pathology of SOD1(G93A) mouse model of ALS, particularly focusing on main glial cell types. This model is often used in ALS research and numerous studies have discussed molecular changes that precede and accompany the decline of motor function observed in these mice during several month-long time period (Gurney et al., 1994).

The SOD1 mutation has been reported to affect astrocytes, microglia, and oligodendrocytes in the spinal cord. We and others have shown that astrocytes and microglia adopt reactive phenotypes characterized by reduced branching and hypertrophy (Ohgomori et al., 2016; Özdinler et al., 2011; **Publication I**). At the gene expression level, astrocytes reduce metabolic support of neurons and become reactive and pro-inflammatory (Ferraiuolo et al., 2011; MacLean et al., 2022). Likewise, microglia upregulate pro-inflammatory, DAM-like signature genes (Keren-Shaul et al., 2017; MacLean et al., 2022). Oligodendrocytes exhibit aberrant maturation and myelination and decreased survival along the pathology progression in the spinal cord of the SOD1(G93A) mouse (Kang et al., 2013).

However, contradicting results can be found on the level of pathology in the cortex of this model (D'Arrigo et al., 2010; Gomes et al., 2019; Migliarini et al., 2021; Niessen et al., 2006; Özdinler et al., 2011). Considering that cortical changes such as hyperexcitability and degeneration of neurons (Nihei et al., 1993; Vucic et al., 2021), reactive gliosis (Dols-Icardo et al., 2020; Guttenplan et al., 2020), and demyelination in grey matter regions (Kang et al., 2013) have been observed in patients, the current literature lacked an in-depth transcriptomic study of the cortical glia populations in the SOD1(G93A) mouse model during the pathology progression, similar to the study by MacLean et al., 2022 in the spinal cord.

For our analysis, we selected four timepoints based on the progression of motor impairment, which was tested by the wire hanging test and the rotarod test. The timepoints covered presymptomatic (1 month of age), early symptomatic (2 months), symptomatic (3 months), and late (4 months) stages of the ALS-like pathology, in line with the known symptom progression in this model (Gurney et al., 1994).

Enriching for astrocytes (ACSA-2), microglia (CD11b), and oligodendrocytes (O4) with fluorescence activated cell sorting (FACS) of the cells isolated from cortices, we prepared sequencing libraries with the 10X Genomics technology. After quality control and filtering of

the sequencing data, we recovered the glia types of interest in balanced proportions: 27% astrocytes, 39% microglia, and 29% oligodendrocytes. The remaining cells classified as endothelial cells, pericytes, and others, were out of the scope of our study.

Focusing on pseudobulk differential gene expression in glia types, we found no substantial SOD1(G93A)-related gene expression changes at any timepoint. Moreover, based on the X and Y chromosome-linked transcripts, we distinguished between male and female mice and also addressed sex-specific gene expression. While behavioural tests suggested faster progression in males, which agrees with observations from some strains of SOD1(G93A) mice (Pfohl et al., 2015), it was not reflected in our transcriptomic data. However, mild sex-specific ALS-related gene expression changes were reported in SOD1(G93A) spinal cord (MacLean et al., 2022) and suggest that these differences may arise in the CNS areas affected by the pathology.

As multiple studies identified the disease-associated glia in neurodegenerative diseases, we performed a subpopulation analysis of each of the glial cell types and aligned the identified subpopulations with literature (**Fig. 4.1**). Disease-associated astrocytes and microglia have been described not only in AD but also other neurodegenerative diseases and aging CNS, increasing in numbers over time compared to healthy CNS (Habib et al., 2020; Keren-Shaul et al., 2017; Sala Frigerio et al., 2019). We found only a minimal increase in Gfap-high (Habib et al., 2020) astrocytes and ARM (Sala Frigerio et al., 2019) corresponding to previously defined populations of astrocytes and microglia. Immunohistochemical analysis of the cortical glia confirmed these observations at the level of protein and cellular morphology. We found only enlarged tips of microglial processes in the SOD1 cortex, a phenomenon previously associated with starting activation of microglia upon injury (Davalos et al., 2005).

The most notable change was found in oligodendrocytes. At 4 months in SOD1(G93A) mice, we identified a unique population characterized by upregulation of *Il33* and *ApoE*. Considering the recent studies reporting disease-associated oligodendrocytes with immune response-related gene expression signature (Kaya et al., 2022; Kenigsbuch et al., 2022), including the two genes in our dataset, and oligodendrocyte activation in the spinal cord of SOD1(G93A) mouse (MacLean et al., 2022), we can hypothesize about their early active role in ALS.

In our study, we encountered several difficulties that needed to be overcome. Initially, during suspension preparation we dealt with lower viability of cells, leading to reduced recovery in scRNA-seq compared to targeted numbers. The quality of the resulting dataset is, however, indicative of the robustness of the 10X Genomics library preparation procedure. Nevertheless, reflecting on the newly introduced library preparation strategies discussed in the Introduction chapter, for these branched and fragile cell types another approach such as fixed cell or nucleus profiling might be more convenient and facilitate higher cell recovery.

During our analysis, we noticed a clustering separation of 3-month-old control male astrocytes and oligodendrocytes driven by stress-associated genes, and a few mitochondrial and ribosomal transcripts among differential expression results that were not removed following quality control. After careful assessment, both were classified as technical artifacts. Importantly, this shows the high sensitivity of scRNA-seq and emphasizes the requirement of high-quality sus-

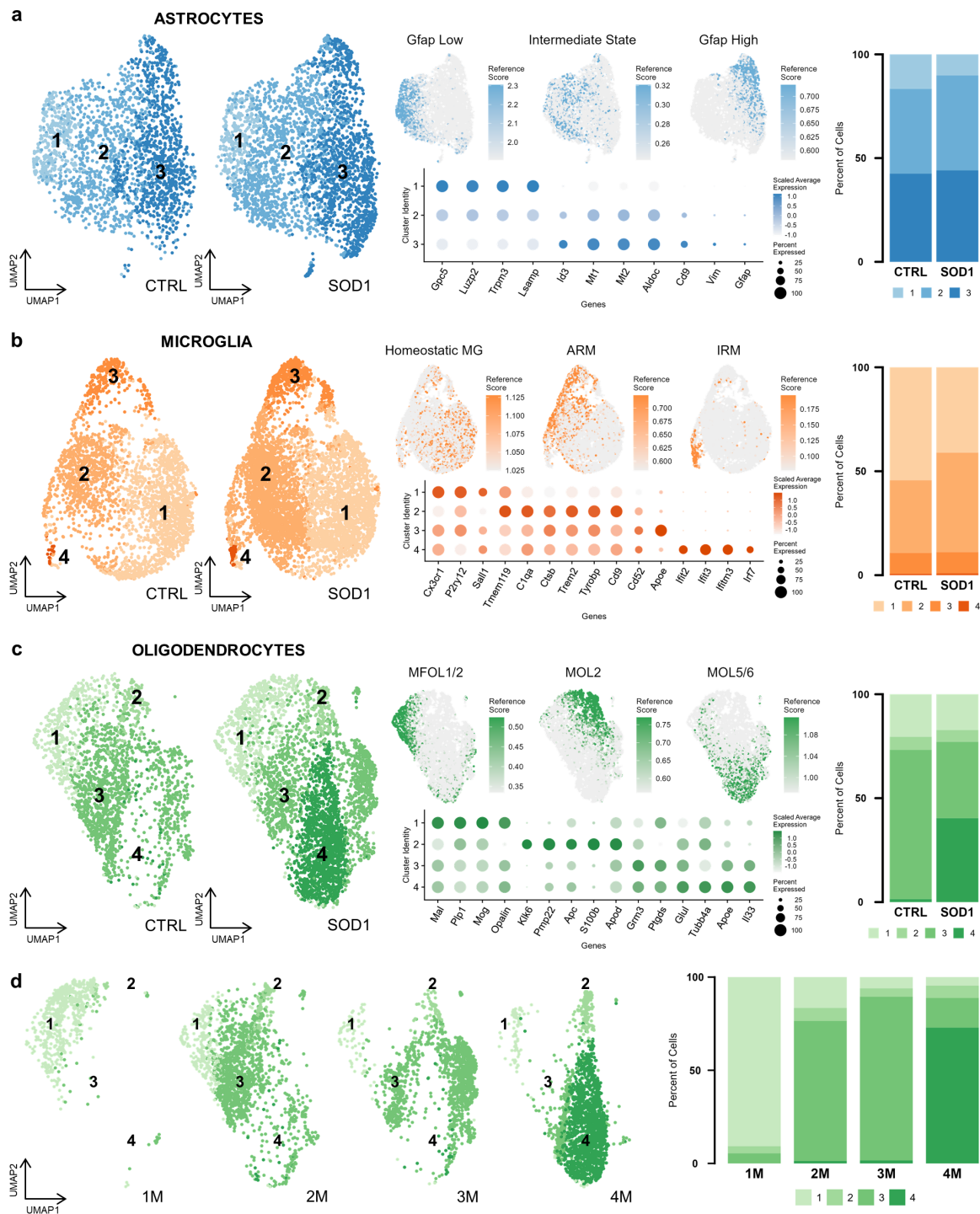


Figure 4.1: Analysis of astrocytes **a)**, microglia **b)**, and oligodendrocytes **c)** revealed subpopulations, whose transcriptional signature corresponded to literature (Habib et al., 2020; Marques et al., 2016; Sala Frigerio et al., 2019). **Left in a)–c):** clustering in UMAP plots split to CTRL and SOD1; **middle in a)–c):** overlap with reference populations and marker genes; **right in a)–c):** subpopulation proportions in barplots split to CTRL and SOD1. **d)** Subpopulations of oligodendrocytes evolving over time, with subpopulation 4 being unique to SOD1 at 4 months. **Abbreviations:** 1M–4M – months of age, ARM – activated response microglia, CTRL – control, IRM – interferon response microglia, MFOL – myelin-forming oligodendrocytes, MOL – mature oligodendrocytes, MG – microglia, SOD1 – SOD1(G93A) mouse. Figure from **Publication I**.

pension and reasonable quality control of the data in order to filter out the artifacts and interpret only the truly biological findings, which may sometimes be difficult to distinguish.

As opposed to extensive cortical pathology in ALS patients, we detected only mild pathological changes in the cortex of the SOD1(G93A) mouse model. However, the limited survival of the SOD1(G93A) model, progressing fast to severe pathology within 4 months and death following shortly afterward, does not enable studying the development of cortical changes at later timepoints. Therefore, based on our data, we suggest using different models for studying the cortical pathology in ALS.

4.2 Abnormal neurodevelopment in iPSC-derived models of AxD

AxD is a severe neurodegenerative disorder caused by mutations in the intermediate filament protein GFAP, which is expressed by astrocytes and radial glia in the CNS. Due to the rarity of AxD, patient samples are scarce, and the majority of available animal models recapitulate GFAP aggregation in astrocytes, but do not show white matter abnormalities typical for the pathology in patients (Hagemann et al., 2013; van der Knaap et al., 2001). Therefore, iPSC-derived astrocytes have proved to be indispensable for studying the disease on human genetic background (Battaglia et al., 2019; Jones et al., 2018; Kondo et al., 2016; Li et al., 2018). In our study (**Publication II**), we used a patient-derived iPSC line carrying the GFAP(R239C) mutation and an isogenic control cell line and generated two complex models that should mimic the interaction of GFAP-mutant astrocytes with other cell types in a co-culture with neurons and in 3D neural organoids.

Although we observed neither GFAP overexpression nor reactive astrogliosis characteristic for animal models and patients with symptomatic disease, our models showed altered neurogenesis and gliogenesis potentially preceding the GFAP overexpression and aggregation positive feedback loop (Messing et al., 2012). In fact, in the early mouse model of AxD, Hagemann et al., 2005 reported downregulation of genes related to neuronal development and function, reflecting either neuronal loss or faulty neurodevelopment in their mouse model of AxD. Later on, a follow-up study revealed aberrant adult neurogenesis in GFAP-mutant mice (Hagemann et al., 2013), manifested by proliferation deficits, radial glia with atypical morphology, and enrichment of an uncharacterized cell population representing abnormally dividing NSCs. The proposed mechanism involved dysregulation of pathways regulating NSC renewal and gliogenesis (Notch, WNT, Hedgehog, and TGF β), whose activity is normally controlled by the proteasome system (Baloghova et al., 2019; Hsia et al., 2015), which is, however, defective in AxD due to the presence of GFAP aggregates (Tang et al., 2010).

In our astrocyte-neuron co-culture model, we found a cluster of GFAP-mutant cells that did not fully differentiate into mature astrocytes (**Fig. 4.2**). This AxD-specific cluster was characterized by spherical morphology, expression of epithelial genes, and increased sensitivity to stress induced by mild oxygen-glucose deprivation (OGD) challenge. Notably, clusters of less differentiated, abnormal cells, were also identified within the populations of astrocytes and

neurons, suggesting a persisting effect of the mutation in cells that proceeded further in their differentiation trajectory. Additionally, mutant neurons dysregulated development, cytoskeleton, and neuropeptide signalling, indicating that the GFAP mutation in early GFAP-expressing progenitors of neurons interferes with their basic functions also in cell-autonomous manner. The analysis of cell-cell interactions with CellChat revealed dysregulation of signalling via FGF, $TGF\beta$, LIFR, non-canonical WNT, Notch, EGF, and reelin pathways, which are essential in neurodevelopment and astrogenesis (Dulabon et al., 2000; Suthon et al., 2021; Zarei-Kheirabadi et al., 2020; Zhang et al., 2023b).

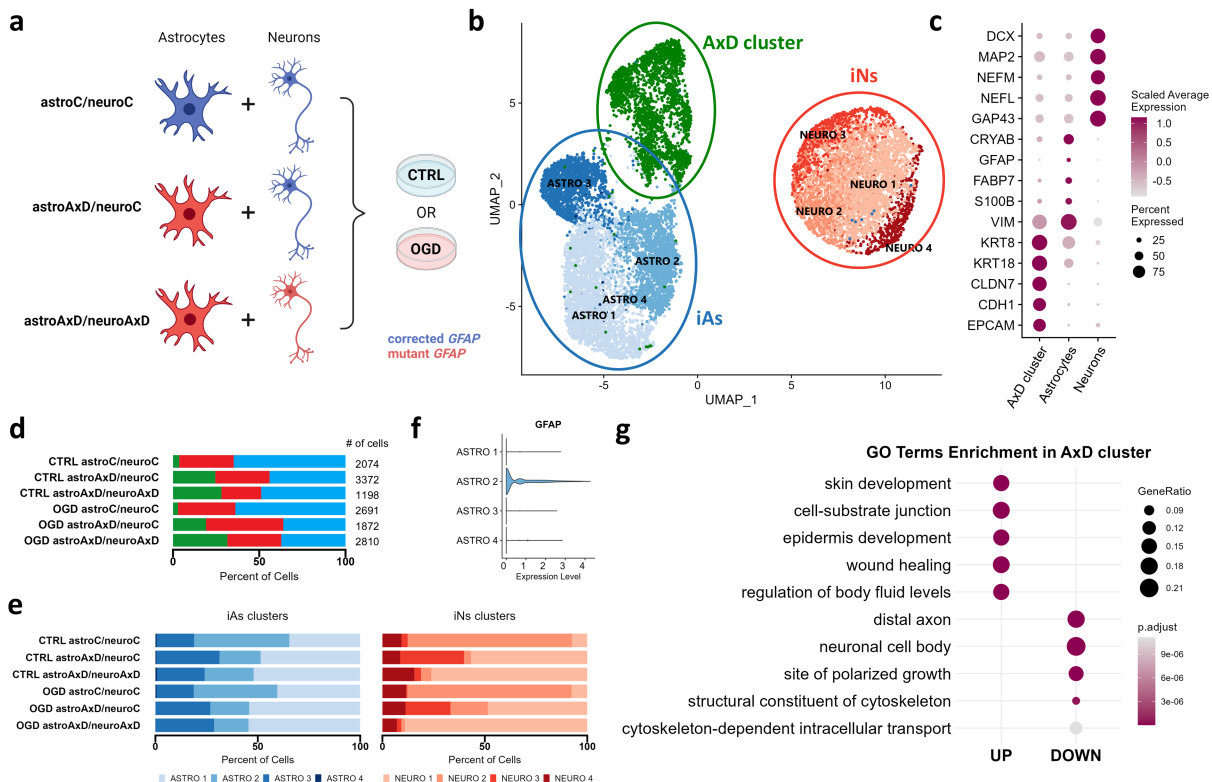


Figure 4.2: Co-cultures with GFAP-mutant astrocytes contained less mature cells compared to CTRL. **a)** Design of the scRNA-seq experiment showing combinations of cell types within co-cultures. **b)** The AxD cluster, iAs, and iNs were the main three cell populations in the dataset. **c)** Marker genes used for annotation of the populations. **d)** The AxD cluster was more abundant in co-cultures with GFAP mutation. **e)** Clusters of less mature iAs and iNs were more abundant within the iAs and iNs populations. **f)** Cluster of mature astrocytes ASTRO 2 contained GFAP-expressing cells. **g)** Enrichment analysis of the AxD cluster markers revealed enhanced epithelial signature genes and suppressed neural tissue signature genes. **Abbreviations:** AxD – Alexander disease, CTRL – control, GO – Gene Ontology, iA – induced astrocytes, iN – induced neurons, OGD – oxygen-glucose deprivation challenge. Figure from **Publication II**.

To investigate this differentiation deficit in a more complex model mimicking the *in vivo* environment, we generated unguided neural organoids, harvested them after 165 days in culture, and analyzed them with scRNA-seq. At this timepoint, we expected to find diverse neuronal populations and astrocytes as well (Kanton et al., 2019; Lancaster et al., 2013). Interestingly, in AxD organoids, we observed compromised and delayed neurogenesis and astrogenesis, resulting in a reduction of astrocyte population and a higher abundance of off-target cell pop-

ulations like epithelial, mesoderm-derived, and unexpectedly, pancreatic acinar cells. In fact, Notch, WNT, FGF, or EGF signalling pathways are also involved in development of the pancreas (Gonçalves et al., 2021; Li et al., 2015; Napolitano et al., 2023). Hence, the imbalance of these pathways in an unguided cell culture may have indeed resulted in overrepresentation of cell populations of a different than neuroectodermal origin.

Our scRNA-seq results also pointed to a dysregulation of mechanical properties of the AxD cells, including cytoskeleton, membrane, and ECM components, which has been observed before in a mouse model of AxD. While Hagemann et al., 2005 attributed this to tissue remodelling during ongoing gliosis, Wang et al., 2018 proposed that overexpression of GFAP followed by overstabilization of actin leads to increased mechanosensing and tissue stiffness. Although we did not directly measure the ECM stiffness, we noticed that GFAP-mutant cell cultures are more adherent than their control counterparts, supporting the idea that the mechanical properties of the AxD cells are distinct from the control cell line. Considering that environmental stress including tissue mechanics can modulate differentiation trajectories of pluripotent or multipotent stem cells (reviewed in Kaitsuka and Hakim, 2021), the altered mechanical properties of the AxD cells and the increased stress susceptibility might provide a link with their off-target differentiation in our organoids.

To reduce the differentiation potential of the AxD iPSCs, we inhibited two of the patterning pathways during the early days of cultivation – $TGF\beta$ and BMP, and we generated cortical organoids (Yoon et al., 2019). At Day 165, these organoids showed an enrichment of mesoderm-like populations and an impairment of cortical lineage specification and gliogenesis represented by the overrepresentation of radial glia and neurons without *FOXG1* and a lack of oligodendrocyte precursors and astrocytes (**Fig. 4.3**). Without time series analysis, we could not assess whether this was just a delay or a complete disruption of gliogenesis. However, considering that early cortical neurons are needed for the switch to gliogenesis, and the expression of related ligands and receptors is limited to a specific time window (Voss et al., 2023), we may speculate that the AxD cell line did not properly respond to the dual SMAD inhibition, and this developmental milestone failed in our model.

While GFAP is commonly associated with astrocytes and astrogliosis, its role in iPSCs and early neuronal precursors remains elusive. We can, therefore, hypothesize about the possible mode of action of mutant GFAP during early differentiation, which likely involves multiple mechanisms. Misfolded, dysfunctional, and aggregated GFAP increases stress and susceptibility to stress and destabilizes cytoskeleton. AxD astrocytes have shown increased oxidative stress and activation of stress response pathways (Hagemann et al., 2005; Heaven et al., 2022; Viedma-Poyatos et al., 2022; Wang et al., 2011), including the upregulation of metallothioneins (Hagemann et al., 2005), and have been more sensitive when exposed to additional stress (Cho and Messing, 2009; Viedma-Poyatos et al., 2022). Abnormal organization of the cytoskeleton can also interfere with normal mitochondrial function (reviewed in Gao et al., 2019; Solomon et al., 2022; Viedma-Poyatos et al., 2022). Furthermore, altered mechanical properties of the AxD cells and their surroundings can disrupt neurodevelopment within organoids.

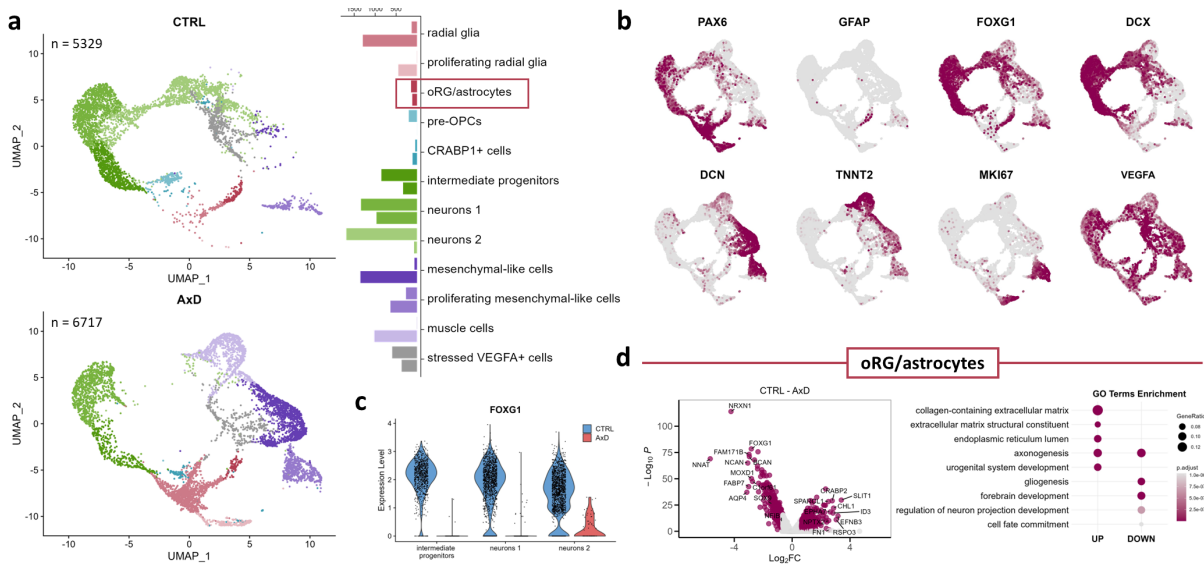


Figure 4.3: ScRNA-seq revealed lineage commitment impairment in AxD cortical organoids. **a)** Disproportional abundance of cell populations in CTRL and AxD. **b)** Marker genes of cell populations. **c)** Lower expression of *FOXG1* in AxD indicating failure of specification of cortical neuron identity. **d)** Differential expression analysis suggested downregulation of astrogenesis in the cluster of oRG/astrocytes. **Abbreviations:** AxD – Alexander disease, CTRL – control, GO – Gene Ontology, oRG – outer radial glia. Figure from **Publication II**.

Mechanosensing modulates cell differentiation in culture, with stiffer ECM suppressing neurogenesis and promoting mesoderm differentiation (Baek et al., 2022; Kaitsuka and Hakim, 2021; Keung et al., 2011; Rammensee et al., 2017). Given the interconnection of mechanosensing and crucial developmental pathways including WNT, TGF β , and Notch (Abuammah et al., 2018; Azzolin et al., 2014; Sen et al., 2021), it is plausible that their disbalance, together with altered mechanical properties, increased stress, and disruption of the essential timing can determine the differentiation outcome, leading to a shift from neuroectoderm to mesoderm, which interferes with neurogenesis and gliogenesis. However, experiments targeting the individual components of this proposed mechanism of GFAP action in iPSCs and early neurogenesis need to be performed to verify this hypothesis.

Interestingly, aberrant astrocyte differentiation was previously observed by Reyes-Ortiz et al., 2023 in iPSC-derived astrocytes modelling HD. The authors reported an impairment of glutamate signalling, maturation, and dysregulation of actin cytoskeleton-related signalling. In addition, impaired neurogenesis, namely an increased number of progenitors at the expense of mature neurons, were reported in iPSC-derived 2D and 3D cell culture models of fAD caused by PSEN1 mutations and was linked to dysregulation of Notch signalling (Arber et al., 2021; Hurley et al., 2023). It is, therefore, possible that the iPSC-derived models can reveal severe consequences of mutations that are otherwise mitigated in the *in vivo* environment and may represent an understudied developmental aspect of neurodegenerative diseases.

On the other hand, magnetic resonance imaging of AxD patients does not usually show abnormal cortical layering indicative of abnormal neurodevelopment (van der Knaap et al., 2001), no increase in prenatal death has been reported in the AxD rodent models, and despite the pres-

ence of GFAP aggregates, no alterations of differentiation were observed in iPSC-derived AxD astrocytes from different cell lines (Jones et al., 2018; Kondo et al., 2016). Therefore, more data from iPSC-derived models and especially patient tissue samples will be needed for extrapolation of our findings to AxD in general.

Finally, media contents, timing of introduction of regulatory factors, mechanical properties of the environment, and stress are all variables that shape iPSC fate decision (Kaitsuka and Hakim, 2021; Sanchís-Calleja et al., 2024). This makes the *in vitro* systems largely variable and requires consideration in experimental design and data interpretation. Nonetheless, organoids represent a highly promising model for studying complex biological processes in patient-derived cell lines and hold a great potential for future research and therapeutic applications.

Conclusion

RNA sequencing is a powerful approach to characterizing transcriptomic changes and cell populations in health and disease. It is also a fast-evolving field, with many analytical tools enabling extensive data mining. Due to the number of available methods and the uniqueness of each biological sample, RNA-seq lacks a standardized pipeline of sample and data processing. Therefore, every experiment requires careful planning and knowledge of the underlying biology that may aid in the decision-making process. While RNA-seq generates high-throughput and high-resolution data, offering a broad overview of gene expression, it is most effective when combined with targeted experiments and aligned with existing biological knowledge.

In this work, we performed an in-depth RNAseq analysis of two neurodegenerative disease models. While in the ALS project, we mapped glia populations and pathology-related gene expression changes in the cortex of the SOD1(G93A) mouse model throughout the pathology progression, in the AxD project, we studied previously unexplored neurodevelopmental changes caused by the GFAP(R239C) mutation in hiPSC-derived models of the disease.

The cell-level resolution of scRNA-seq allowed us to identify several populations of glia in the cortex of the SOD1(G93A) mouse and overlap them with populations described in other single-cell studies of neurodegenerative diseases. One outstanding observation was a population of oligodendrocytes exclusive to the late stage of the pathology, partially overlapping with other disease-associated oligodendrocytes with a potential active role in disease. However, overall we did not find significant gene expression differences, which supports the results of other studies reporting limited cortical pathology in the SOD1(G93A) mouse model.

In the AxD project, we used scRNA-seq to reveal an intriguing differentiation phenotype in astrocyte-neuron co-cultures and neural organoids derived from hiPSCs with the GFAP mutation. This phenotype was characterized by impaired neurogenesis, astrogenesis, and lineage specification, resulting in an increased abundance of cell types of other than neuroectodermal origin. We also showed that essential developmental pathways were perturbed in these models. Thus, the imbalance of these pathways along with elevated sensitivity of hiPSCs to stress caused by the GFAP mutation might have affected their ability to differentiate into neuroectoderm and form normal populations of neurons and glia, revealing a previously unknown effect of GFAP mutation on neurodevelopment.

In summary, we performed a thorough transcriptomic analysis of the cortex of a widely used ALS mouse model, adding another reference point to existing data on SOD1(G93A) mouse pathology. Given the minimal changes in the cortex, we recommend against using this model for studying cortical pathology in ALS. We also used transcriptomics to describe two novel hiPSC-derived models of AxD, observing their aberrant lineage commitment and increased susceptibility to stress during differentiation. Emerging studies presenting similar differentiation impairments in iPSC-derived models of neurodegenerative diseases suggest that focusing on this aspect may pave the way for early diagnosis and novel treatment strategies.

References

- Absinta, M., Maric, D., Gharagozloo, M., Garton, T., Smith, M. D., Jin, J., Fitzgerald, K. C., Song, A., Liu, P., Lin, J. P., Wu, T., Johnson, K. R., McGavern, D. B., Schafer, D. P., Calabresi, P. A., and Reich, D. S. A lymphocyte-microglia-astrocyte axis in chronic active multiple sclerosis. *Nature*, 597(7878):709–714, 2021. doi: 10.1038/s41586-021-03892-7.
- Abuammah, A., Maimari, N., Towhidi, L., Frueh, J., Chooi, K. Y., Warboys, C., and Krams, R. New developments in mechanotransduction: Cross talk of the Wnt, TGF- β and Notch signalling pathways in reaction to shear stress. *Current Opinion in Biomedical Engineering*, 5: 96–104, 2018. doi: 10.1016/j.cobme.2018.03.003.
- Agarwal, D., Sandor, C., Volpato, V., Caffrey, T. M., Monzón-Sandoval, J., Bowden, R., Alegre-Abarategui, J., Wade-Martins, R., and Webber, C. A single-cell atlas of the human substantia nigra reveals cell-specific pathways associated with neurological disorders. *Nature Communications*, 11(1):4183, 2020. doi: 10.1038/s41467-020-17876-0.
- Agrawal, A., Balci, H., Hanspers, K., Coort, S. L., Martens, M., Slenter, D. N., Ehrhart, F., Digles, D., Waagmeester, A., Wassink, I., Abbassi-Daloi, T., Lopes, E. N., Iyer, A., Acosta, J. M., Willighagen, L. G., Nishida, K., Riutta, A., Basaric, H., Evelo, C. T., Willighagen, E. L., Kutmon, M., and Pico, A. R. WikiPathways 2024: Next generation pathway database. *Nucleic Acids Research*, 52(D1):D679–D689, 2024. doi: 10.1093/nar/gkad960.
- Aibar, S., González-Blas, C. B., Moerman, T., Huynh-Thu, V. A., Imrichova, H., Hulselmans, G., Rambow, F., Marine, J. C., Geurts, P., Aerts, J., van den Oord, J., Atak, Z. K., Wouters, J., and Aerts, S. SCENIC: Single-cell regulatory network inference and clustering. *Nature Methods*, 14(11):1083–1086, 2017. doi: 10.1038/nmeth.4463.
- Ajami, B., Bennett, J. L., Krieger, C., Tetzlaff, W., and Rossi, F. M. Local self-renewal can sustain CNS microglia maintenance and function throughout adult life. *Nature Neuroscience*, 10(12):1538–1543, 2007. doi: 10.1038/nn2014.
- Al-Dalahmah, O., Sosunov, A. A., Shaik, A., Ofori, K., Liu, Y., Vonsattel, J. P., Adorjan, I., Menon, V., and Goldman, J. E. Single-nucleus RNA-seq identifies Huntington disease astrocyte states. *Acta Neuropathologica Communications*, 8(1):19, 2020. doi: 10.1186/s40478-020-0880-6.
- Allen, N. J. and Lyons, D. A. Glia as architects of central nervous system formation and function. *Science*, 362(6411):181–185, 2018. doi: 10.1126/science.aat0473.
- Alles, J., Karaiskos, N., Praktiknjo, S. D., Grosswendt, S., Wahle, P., Ruffault, P. L., Ayoub, S., Schreyer, L., Boltengagen, A., Birchmeier, C., Zinzen, R., Kocks, C., and Rajewsky, N. Cell fixation and preservation for droplet-based single-cell transcriptomics. *BMC Biology*, 15(1): 44, 2017. doi: 10.1186/s12915-017-0383-5.
- Anders, S. and Huber, W. Differential expression analysis for sequence count data. *Genome Biology*, 11(10):R106, 2010. doi: 10.1186/gb-2010-11-10-r106.
- Andronie-Cioara, F. L., Ardelean, A. I., Nistor-Cseppento, C. D., Jurcau, A., Jurcau, M. C., Pascalau, N., and Marcu, F. Molecular mechanisms of neuroinflammation in aging and Alzheimer’s disease progression. *International journal of Molecular Sciences*, 24(3):1869, 2023. doi: 10.3390/ijms24031869.
- Arber, C., Lovejoy, C., Harris, L., Willumsen, N., Alatza, A., Casey, J. M., Lines, G., Kerins, C., Mueller, A. K., Zetterberg, H., Hardy, J., Ryan, N. S., Fox, N. C., Lashley, T., and Wray, S. Familial Alzheimer’s disease mutations in PSEN1 lead to premature human stem cell neurogenesis. *Cell Reports*, 34(2):108615, 2021. doi: 10.1016/j.celrep.2020.108615.
- Azzolin, L., Panciera, T., Soligo, S., Enzo, E., Bicciato, S., Dupont, S., Bresolin, S., Frasson, C., Basso, G., Guzzardo, V., Fassina, A., Cordenonsi, M., and Piccolo, S. YAP/TAZ incorporation in the beta-catenin destruction complex orchestrates the Wnt response. *Cell*, 158(1):157–170, 2014. doi: 10.1016/j.cell.2014.06.013.
- Baalman, K., Marin, M. A., Ho, T. S., Godoy, M., Cherian, L., Robertson, C., and Rasband, M. N. Axon initial segment-associated microglia. *Journal of Neuroscience*, 35(5):2283–2292, 2015. doi: 10.1523/JNEUROSCI.3751-14.2015.
- Baburamani, A. A., Vontell, R. T., Uus, A., Pietsch, M., Patkee, P. A., Wyatt-Ashmead, J., Chin-Smith, E. C., Supramaniam, V. G., Donald Tournier, J., Deprez, M., and Rutherford, M. A. Assessment of radial glia in the frontal lobe of fetuses with Down syndrome. *Acta Neuropathologica Communications*, 8(1):141, 2020. doi: 10.1186/s40478-020-01015-3.
- Baek, J., Kumar, S., Schaffer, D. V., and Im, S. G. N-Cadherin adhesive ligation regulates mechanosensitive neural stem cell lineage commitment in 3D matrices. *Biomaterials Science*, 10(23):6768–6777, 2022. doi: 10.1039/d2bm01349e.
- Bakken, T. E., Hodge, R. D., Miller, J. A., Yao, Z., Nguyen, T. N., Aevermann, B., Barkan, E., Bertagnolli, D., Casper, T., Dee, N., Garren, E., Goldy, J., Graybuck, L. T., Kroll, M., Lasken, R. S., Lathia, K., Parry, S., Rimorin, C., Scheuermann, R. H., Schork, N. J., Shehata, S. I., Tieu, M., Phillips, J. W., Bernard, A., Smith, K. A., Zeng, H., Lein, E. S., and Tasic, B. Single-nucleus and single-cell transcriptomes compared in matched cortical cell types. *PLoS One*, 13(12):e0209648, 2018. doi: 10.1371/journal.pone.0209648.
- Baloghova, N., Lidak, T., and Cermak, L. Ubiquitin ligases involved in the regulation of Wnt, TGF-beta, and Notch signaling pathways and their roles in mouse development and homeostasis. *Genes (Basel)*, 10(10):815, 2019. doi: 10.3390/genes10100815.
- Barberio, J., Lally, C., Kupelian, V., Hardiman, O., and Flanders, W. D. Estimated familial Amyotrophic lateral sclerosis proportion: A literature review and meta-analysis. *Neurology Genetics*, 9(6):e200109, 2023. doi: 10.1212/NXG.0000000000200109.
- Barton, S. K., Lau, C. L., Chiam, M. D. F., Tomas, D., Muyderman, H., Beart, P. M., and Turner, B. J. Mutant TDP-43 expression triggers TDP-43 pathology and cell autonomous effects on primary astrocytes: Implications for non-cell autonomous pathology in ALS. *Neurochemical Research*, 45(6):1451–1459, 2020. doi: 10.1007/s11064-020-03048-5.

- Batiuk, M. Y., Martirosyan, A., Wahis, J., de Vin, F., Marneffe, C., Kusserow, C., Koeppen, J., Viana, J. F., Oliveira, J. F., Voet, T., Ponting, C. P., Belgard, T. G., and Holt, M. G. Identification of region-specific astrocyte subtypes at single cell resolution. *Nature Communications*, 11(1):1220, 2020. doi: 10.1038/s41467-019-14198-8.
- Battaglia, R. A., Beltran, A. S., Delic, S., Dumitru, R., Robinson, J. A., Kabiraj, P., Herring, L. E., Madden, V. J., Ravinder, N., Willems, E., Newman, R. A., Quinlan, R. A., Goldman, J. E., Perng, M. D., Inagaki, M., and Snider, N. T. Site-specific phosphorylation and caspase cleavage of GFAP are new markers of Alexander disease severity. *eLife*, 8:e47789, 2019. doi: 10.7554/eLife.47789.
- Bayraktar, O. A., Bartels, T., Holmqvist, S., Kleshchevnikov, V., Martirosyan, A., Polioudakis, D., Ben Haim, L., Young, A. M. H., Batiuk, M. Y., Prakash, K., Brown, A., Roberts, K., Paredes, M. F., Kawaguchi, R., Stockley, J. H., Sabeur, K., Chang, S. M., Huang, E., Hutchinson, P., Ullian, E. M., Hemberg, M., Coppola, G., Holt, M. G., Geschwind, D. H., and Rowitch, D. H. Astrocyte layers in the mammalian cerebral cortex revealed by a single-cell in situ transcriptomic map. *Nature Neuroscience*, 23(4):500–509, 2020. doi: 10.1038/s41593-020-0602-1.
- Bellamy, T. C. Interactions between Purkinje neurones and Bergmann glia. *Cerebellum*, 5(2):116–126, 2006. doi: 10.1080/14734220600724569.
- Benesova, S., Kubista, M., and Valihrach, L. Small RNA-sequencing: Approaches and considerations for miRNA analysis. *Diagnostics (Basel)*, 11(6):964, 2021. doi: 10.3390/diagnostics11060964.
- Bhaduri, A., Di Lullo, E., Jung, D., Müller, S., Crouch, E. E., Espinosa, C. S., Ozawa, T., Alvarado, B., Spatazza, J., Cadwell, C. R., Wilkins, G., Velmeshev, D., Liu, S. J., Malatesta, M., Andrews, M. G., Mostajo-Radji, M. A., Huang, E. J., Nowakowski, T. J., Lim, D. A., Diaz, A., Raleigh, D. R., and Kriegstein, A. R. Outer radial glia-like cancer stem cells contribute to heterogeneity of glioblastoma. *Cell Stem Cell*, 26(1):48–63 e6, 2020. doi: 10.1016/j.stem.2019.11.015.
- Birey, F., Andersen, J., Makinson, C. D., Islam, S., Wei, W., Huber, N., Fan, H. C., Metzler, K. R. C., Panagiotakos, G., Thom, N., O'Rourke, N. A., Steinmetz, L. M., Bernstein, J. A., Hallmayer, J., Huguenard, J. R., and Pasca, S. P. Assembly of functionally integrated human forebrain spheroids. *Nature*, 545(7652):54–59, 2017. doi: 10.1038/nature22330.
- Bisht, K., Sharma, K. P., Lecours, C., Sánchez, M. G., El Hajj, H., Milior, G., Olmos-Alonso, A., Gómez-Nicola, D., Luheshi, G., Vallières, L., Branchi, I., Maggi, L., Limatola, C., Butovsky, O., and Tremblay, M. E. Dark microglia: A new phenotype predominantly associated with pathological states. *Glia*, 64(5):826–839, 2016. doi: 10.1002/glia.22966.
- Bowles, K. R., Silva, M. C., Whitney, K., Bertucci, T., Berlind, J. E., Lai, J. D., Garza, J. C., Boles, N. C., Mahali, S., Strang, K. H., Marsh, J. A., Chen, C., Pugh, D. A., Liu, Y., Gordon, R. E., Goderie, S. K., Chowdhury, R., Lotz, S., Lane, K., Crary, J. F., Haggarty, S. J., Karch, C. M., Ichida, J. K., Goate, A. M., and Temple, S. ELAVL4, splicing, and glutamatergic dysfunction precede neuron loss in MAPT mutation cerebral organoids. *Cell*, 184(17):4547–4563 e17, 2021. doi: 10.1016/j.cell.2021.07.003.
- Browaeys, R., Saelens, W., and Saeys, Y. NicheNet: Modeling intercellular communication by linking ligands to target genes. *Nature Methods*, 17(2):159–162, 2020. doi: 10.1038/s41592-019-0667-5.
- Buenrostro, J. D., Wu, B., Chang, H. Y., and Greenleaf, W. J. ATAC-seq: A method for assaying chromatin accessibility genome-wide. *Current Protocols in Molecular Biology*, 109:21.29.1–21.29.9, 2015. doi: 10.1002/0471142727.mb2129s109.
- Bushong, E. A., Martone, M. E., Jones, Y. Z., and Ellisman, M. H. Protoplasmic astrocytes in CA1 stratum radiatum occupy separate anatomical domains. *Journal of Neuroscience*, 22(1):183–192, 2002. doi: 10.1523/JNEUROSCI.22-01-00183.2002.
- Butovsky, O. and Weiner, H. L. Microglial signatures and their role in health and disease. *Nature Reviews Neuroscience*, 19(10):622–635, 2018. doi: 10.1038/s41583-018-0057-5.
- Calafatti, M., Coccozza, G., Limatola, C., and Garofalo, S. Microglial crosstalk with astrocytes and immune cells in amyotrophic lateral sclerosis. *Frontiers in Immunology*, 14:1223096, 2023. doi: 10.3389/fimmu.2023.1223096.
- Camp, J. G., Badsha, F., Florio, M., Kanton, S., Gerber, T., Wilsch-Bräuninger, M., Lewitus, E., Sykes, A., Hevers, W., Lancaster, M., Knoblich, J. A., Lachmann, R., Pääbo, S., Huttner, W. B., and Treutlein, B. Human cerebral organoids recapitulate gene expression programs of fetal neocortex development. *PNAS USA*, 112(51):15672–15677, 2015. doi: 10.1073/pnas.1520760112.
- Canals, I., Ginisty, A., Quist, E., Timmerman, R., Fritze, J., Miskinyte, G., Monni, E., Hansen, M. G., Hidalgo, I., Bryder, D., Bengzon, J., and Ahlenius, H. Rapid and efficient induction of functional astrocytes from human pluripotent stem cells. *Nature Methods*, 15(9):693–696, 2018. doi: 10.1038/s41592-018-0103-2.
- Candiani, S., Carestati, S., Mack, A. F., Bani, D., Bozzo, M., Obino, V., Ori, M., Rosamilia, F., De Sarlo, M., Pestarino, M., Ceccherini, I., and Bachetti, T. Alexander disease modeling in zebrafish: An in vivo system suitable to perform drug screening. *Genes (Basel)*, 11(12):1490, 2020. doi: 10.3390/genes11121490.
- Cao, J., Packer, J. S., Ramani, V., Cusanovich, D. A., Huynh, C., Daza, R., Qiu, X., Lee, C., Furlan, S. N., Steemers, F. J., Adey, A., Waterston, R. H., Trapnell, C., and Shendure, J. Comprehensive single-cell transcriptional profiling of a multicellular organism. *Science*, 357(6352):661–667, 2017. doi: 10.1126/science.aam8940.
- Chamling, X., Kallman, A., Fang, W., Berlinicke, C. A., Mertz, J. L., Devkota, P., Pantoja, I. E. M., Smith, M. D., Ji, Z., Chang, C., Kaushik, A., Chen, L., Whartenby, K. A., Calabresi, P. A., Mao, H. Q., Ji, H., Wang, T. H., and Zack, D. J. Single-cell transcriptomic reveals molecular diversity and developmental heterogeneity of human stem cell-derived oligodendrocyte lineage cells. *Nature Communications*, 12(1):652, 2021. doi: 10.1038/s41467-021-20892-3.
- Chen, Z. Y. and Zhang, Y. Animal models of Alzheimer's disease: Applications, evaluation, and perspectives. *Zoological Research*, 43(6):1026–1040, 2022. doi: 10.24272/j.issn.2095-8137.2022.289.
- Cho, W. and Messing, A. Properties of astrocytes cultured from GFAP over-expressing and GFAP mutant mice. *Experimental Cell Research*, 315(7):1260–1272, 2009. doi: 10.1016/j.yexcr.2008.12.012.
- Chou, S. M. and Norris, F. H. Amyotrophic lateral sclerosis: Lower motor neuron disease spreading to upper motor neurons. *Muscle & Nerve*, 16(8):864–869, 1993. doi: 10.1002/mus.880160810.

- Clark, I. C., Fontanez, K. M., Meltzer, R. H., Xue, Y., Hayford, C., May-Zhang, A., D'Amato, C., Osman, A., Zhang, J. Q., Hettige, P., Ishibashi, J. S. A., Delley, C. L., Weisgerber, D. W., Replogle, J. M., Jost, M., Phong, K. T., Kennedy, V. E., Peretz, C. A. C., Kim, E. A., Song, S., Karlon, W., Weissman, J. S., Smith, C. C., Gartner, Z. J., and Abate, A. R. Microfluidics-free single-cell genomics with templated emulsification. *Nature Biotechnology*, 41(11):1557–1566, 2023. doi: 10.1038/s41587-023-01685-z.
- Dadwal, S. and Heneka, M. T. Microglia heterogeneity in health and disease. *FEBS Open Bio*, 14(2):217–229, 2024. doi: 10.1002/2211-5463.13735.
- D'Arrigo, A., Colavito, D., Peña-Altamira, E., Fabris, M., Dam, M., Contestabile, A., and Leon, A. Transcriptional profiling in the lumbar spinal cord of a mouse model of amyotrophic lateral sclerosis: A role for wild-type superoxide dismutase 1 in sporadic disease? *Journal of Molecular Neuroscience*, 41(3):404–415, 2010. doi: 10.1007/s12031-010-9332-2.
- Davalos, D., Grutzendler, J., Yang, G., Kim, J. V., Zuo, Y., Jung, S., Littman, D. R., Dustin, M. L., and Gan, W. B. ATP mediates rapid microglial response to local brain injury in vivo. *Nature Neuroscience*, 8(6):752–758, 2005. doi: 10.1038/nn1472.
- Dawson, T. M., Golde, T. E., and Lagier-Tourenne, C. Animal models of neurodegenerative diseases. *Nature Neuroscience*, 21(10):1370–1379, 2018. doi: 10.1038/s41593-018-0236-8.
- De Simone, M., Hoover, J., Lau, J., Bennet, H., Wu, B., Chen, C., Menon, H., Au-Yeung, A., Lear, S., Vaidya, S., Shi, M., Lund, J. M., Xavier-Magalhaes, A., Liang, Y., Kurdoglu, A., O'Gorman, W. E., Modrusan, Z., Le, D., and Darmanis, S. Comparative analysis of commercial single-cell RNA sequencing technologies. *bioRxiv*, 2024. doi: 10.1101/2024.06.18.599579.
- Dobson, R. and Giovannoni, G. Multiple sclerosis – A review. *European Journal of Neurology*, 26(1):27–40, 2019. doi: 10.1111/ene.13819.
- Dols-Icardo, O., Montal, V., Sirisi, S., López-Pernas, G., Cervera-Carles, L., Querol-Vilaseca, M., Muñoz, L., Belbin, O., Alcolea, D., Molina-Porcel, L., Pegueroles, J., Turón-Sans, J., Blesa, R., Lleó, A., Fortea, J., Rojas-García, R., and Clarimón, J. Motor cortex transcriptome reveals microglial key events in amyotrophic lateral sclerosis. *Neurology Neuroimmunology & Neuroinflammation*, 7(5):e829, 2020. doi: 10.1212/NXI.0000000000000829.
- Draghici, S., Khatri, P., Martins, R. P., Ostermeier, G. C., and Krawetz, S. A. Global functional profiling of gene expression. *Genomics*, 81(2):98–104, 2003. doi: 10.1016/s0888-7543(02)00021-6.
- Dulabon, L., Olson, E. C., Taglienti, M. G., Eisenhuth, S., McGrath, B., Walsh, C. A., Kreidberg, J. A., and Anton, E. S. Reelin binds alpha3beta1 integrin and inhibits neuronal migration. *Neuron*, 27(1):33–44, 2000. doi: 10.1016/s0896-6273(00)00007-6.
- Ehrlich, M., Mozafari, S., Glatza, M., Starost, L., Velychko, S., Hallmann, A. L., Cui, Q. L., Schambach, A., Kim, K. P., Bachelin, C., Marteyn, A., Hargus, G., Johnson, R. M., Antel, J., Sternecker, J., Zaehres, H., Schöler, H. R., Baron-Van Evercooren, A., and Kuhlmann, T. Rapid and efficient generation of oligodendrocytes from human induced pluripotent stem cells using transcription factors. *PNAS USA*, 114(11):E2243–E2252, 2017. doi: 10.1073/pnas.1614412114.
- Eisen, A., Kim, S., and Pant, B. Amyotrophic lateral sclerosis (ALS): A phylogenetic disease of the corticomotoneuron? *Muscle & Nerve*, 15(2):219–224, 1992. doi: 10.1002/mus.880150215.
- Ellwanger, D. C., Wang, S., Brioschi, S., Shao, Z., Green, L., Case, R., Yoo, D., Weishuhn, D., Rathanaswami, P., Bradley, J., Rao, S., Cha, D., Luan, P., Sambashivan, S., Gilfillan, S., Hasson, S. A., Foltz, I. N., van Lookeren Campagne, M., and Colonna, M. Prior activation state shapes the microglia response to antihuman TREM2 in a mouse model of Alzheimer's disease. *PNAS USA*, 118(3):e2017742118, 2021. doi: 10.1073/pnas.2017742118.
- Endo, F., Kasai, A., Soto, J. S., Yu, X., Qu, Z., Hashimoto, H., Gradinaru, V., Kawaguchi, R., and Khakh, B. S. Molecular basis of astrocyte diversity and morphology across the CNS in health and disease. *Science*, 378(6619):eadc9020, 2022. doi: 10.1126/science.adc9020.
- Erny, D., Hrabě de Angelis, A. L., Jaitin, D., Wieghofer, P., Staszewski, O., David, E., Keren-Shaul, H., Mhalkoiv, T., Jakobshagen, K., Buch, T., Schwierzeck, V., Utermöhlen, O., Chun, E., Garrett, W. S., McCoy, K. D., Diefenbach, A., Staeheli, P., Stecher, B., Amit, I., and Prinz, M. Host microbiota constantly control maturation and function of microglia in the CNS. *Nature Neuroscience*, 18(7):965–977, 2015. doi: 10.1038/nn.4030.
- Escartin, C., Galea, E., Lakatos, A., O'Callaghan, J. P., Petzold, G. C., Serrano-Pozo, A., Steinhäuser, C., Volterra, A., Carmignoto, G., Agarwal, A., Allen, N. J., Araque, A., Barbeito, L., Barzilai, A., Bergles, D. E., Bonvento, G., Butt, A. M., Chen, W. T., Cohen-Salmon, M., Cunningham, C., Deneen, B., De Strooper, B., Díaz-Castro, B., Farina, C., Freeman, M., Gallo, V., Goldman, J. E., Goldman, S. A., Götz, M., Gutiérrez, A., Haydon, P. G., Heiland, D. H., Hol, E. M., Holt, M. G., Iino, M., Kastanenka, K. V., Kettenmann, H., Khakh, B. S., Koizumi, S., Lee, C. J., Liddelow, S. A., MacVicar, B. A., Magistretti, P., Messing, A., Mishra, A., Molofsky, A. V., Murai, K. K., Norris, C. M., Okada, S., Oliet, S. H. R., Oliveira, J. F., Panatier, A., Parpura, V., Pekna, M., Pekny, M., Pellerin, L., Perea, G., Pérez-Nievas, B. G., Pfrieger, F. W., Poskanzer, K. E., Quintana, F. J., Ransohoff, R. M., Riquelme-Perez, M., Robel, S., Rose, C. R., Rothstein, J. D., Rouach, N., Rowitch, D. H., Semyanov, A., Sirko, S., Sontheimer, H., Swanson, R. A., Vitorica, J., Wanner, I. B., Wood, L. B., Wu, J., Zheng, B., Zimmer, E. R., Zorec, R., Sofroniew, M. V., and Verkhratsky, A. Reactive astrocyte nomenclature, definitions, and future directions. *Nature Neuroscience*, 24(3):312–325, 2021. doi: 10.1038/s41593-020-00783-4.
- Esumi, S., Wu, S. X., Yanagawa, Y., Obata, K., Sugimoto, Y., and Tamamaki, N. Method for single-cell microarray analysis and application to gene-expression profiling of GABAergic neuron progenitors. *Neuroscience Research*, 60(4):439–451, 2008. doi: 10.1016/j.neures.2007.12.011.
- Eze, U. C., Bhaduri, A., Haeussler, M., Nowakowski, T. J., and Kriegstein, A. R. Single-cell atlas of early human brain development highlights heterogeneity of human neuroepithelial cells and early radial glia. *Nature Neuroscience*, 24(4):584–594, 2021. doi: 10.1038/s41593-020-00794-1.
- Falcone, C., McBride, E. L., Hopkins, W. D., Hof, P. R., Manger, P. R., Sherwood, C. C., Noctor, S. C., and Martínez-Cerdeño, V. Redefining varicose projection astrocytes in primates. *Glia*, 70(1):145–154, 2022. doi: 10.1002/glia.24093.

- Falcão, A. M., van Bruggen, D., Marques, S., Meijer, M., Jäkel, S., Agirre, E., Samudyata, Floriddia, E. M., Vanichkina, D. P., French Constant, C., Williams, A., Guerreiro-Cacais, A. O., and Castelo-Branco, G. Disease-specific oligodendrocyte lineage cells arise in multiple sclerosis. *Nature Medicine*, 24(12):1837–1844, 2018. doi: 10.1038/s41591-018-0236-y.
- Farrawell, N. E. and Yerbury, J. J. Mutant Cu/Zn superoxide dismutase (A4V) turnover is altered in cells containing inclusions. *Frontiers in Molecular Neuroscience*, 14:771911, 2021. doi: 10.3389/fnmol.2021.771911.
- Ferraiuolo, L., Higginbottom, A., Heath, P. R., Barber, S., Greenald, D., Kirby, J., and Shaw, P. J. Dysregulation of astrocyte-motoneuron cross-talk in mutant superoxide dismutase 1-related amyotrophic lateral sclerosis. *Brain*, 134(Pt 9):2627–2641, 2011. doi: 10.1093/brain/awr193.
- Ferraiuolo, L., Meyer, K., Sherwood, T. W., Vick, J., Likhite, S., Frakes, A., Miranda, C. J., Braun, L., Heath, P. R., Pineda, R., Beattie, C. E., Shaw, P. J., Askwith, C. C., McTigue, D., and Kaspar, B. K. Oligodendrocytes contribute to motor neuron death in ALS via SOD1-dependent mechanism. *PNAS USA*, 113(42):E6496–E6505, 2016. doi: 10.1073/pnas.1607496113.
- Fiock, K. L., Smalley, M. E., Cray, J. F., Pasca, A. M., and Hefti, M. M. Increased Tau expression correlates with neuronal maturation in the developing human cerebral cortex. *eNeuro*, 7(3):ENEURO.0058–20.2020, 2020. doi: 10.1523/ENEURO.0058-20.2020.
- Floriddia, E. M., Lourenço, T., Zhang, S., van Bruggen, D., Hilscher, M. M., Kukanja, P., Gonçalves Dos Santos, J. P., Altunkök, M., Yokota, C., Llorens-Bobadilla, E., Mulinyawe, S. B., Grãos, M., Sun, L. O., Frisén, J., Nilsson, M., and Castelo-Branco, G. Distinct oligodendrocyte populations have spatial preference and different responses to spinal cord injury. *Nature Communications*, 11(1):5860, 2020. doi: 10.1038/s41467-020-19453-x.
- Franzén, O., Gan, L. M., and Björkegren, J. L. M. PanglaoDB: A web server for exploration of mouse and human single-cell RNA sequencing data. *Database (Oxford)*, 2019:baz046, 2019. doi: 10.1093/database/baz046.
- Fujimori, K., Ishikawa, M., Otomo, A., Atsuta, N., Nakamura, R., Akiyama, T., Hadano, S., Aoki, M., Saya, H., Sobue, G., and Okano, H. Modeling sporadic ALS in iPSC-derived motor neurons identifies a potential therapeutic agent. *Nature Medicine*, 24(10):1579–1589, 2018. doi: 10.1038/s41591-018-0140-5.
- Gao, C., Jiang, J., Tan, Y., and Chen, S. Microglia in neurodegenerative diseases: Mechanism and potential therapeutic targets. *Signal Transduction and Targeted Therapy*, 8(1):359, 2023. doi: 10.1038/s41392-023-01588-0.
- Gao, L., Zhang, Z., Lu, J., and Pei, G. Mitochondria are dynamically transferring between human neural cells and Alexander disease-associated GFAP mutations impair the astrocytic transfer. *Frontiers in Cellular Neuroscience*, 13:316, 2019. doi: 10.3389/fncel.2019.00316.
- Gene Ontology Consortium. The Gene Ontology resource: Enriching a Gold mine. *Nucleic Acids Research*, 49(D1):D325–D334, 2021. doi: 10.1093/nar/gkaa1113.
- Gerrits, E., Heng, Y., Boddeke, E. W. G. M., and Eggen, B. J. L. Transcriptional profiling of microglia; current state of the art and future perspectives. *Glia*, 68(4):740–755, 2020. doi: 10.1002/glia.23767.
- Ginhoux, F., Greter, M., Leboeuf, M., Nandi, S., See, P., Gokhan, S., Mehler, M. F., Conway, S. J., Ng, L. G., Stanley, E. R., Samokhvalov, I. M., and Merad, M. Fate mapping analysis reveals that adult microglia derive from primitive macrophages. *Science*, 330(6005):841–845, 2010. doi: 10.1126/science.1194637.
- Gleichman, A. J. and Carmichael, S. T. Glia in neurodegeneration: Drivers of disease or along for the ride? *Neurobiology of Disease*, 142:104957, 2020. doi: 10.1016/j.nbd.2020.104957.
- Gomes, C., Cunha, C., Nascimento, F., Ribeiro, J. A., Vaz, A. R., and Brites, D. Cortical neurotoxic astrocytes with early ALS pathology and miR-146a deficit replicate gliosis markers of symptomatic SOD1G93A mouse model. *Molecular Neurobiology*, 56(3):2137–2158, 2019. doi: 10.1007/s12035-018-1220-8.
- Gomez-Pinedo, U., Sierrol-Piquer, M. S., Durán-Moreno, M., Garcia-Verdugo, J. M., and Matías-Guiu, J. Alexander disease mutations produce cells with coexpression of glial fibrillary acidic protein and NG2 in neurosphere cultures and inhibit differentiation into mature oligodendrocytes. *Frontiers in Neurology*, 8:255, 2017. doi: 10.3389/fneur.2017.00255.
- Gonçalves, C. A., Larsen, M., Jung, S., Stratmann, J., Nakamura, A., Leuschner, M., Hersemann, L., Keshara, R., Perlman, S., Lundvall, L., Thuesen, L. L., Hare, K. J., Amit, I., Jørgensen, A., Kim, Y. H., del Sol, A., and Grapin-Botton, A. A 3D system to model human pancreas development and its reference single-cell transcriptome atlas identify signaling pathways required for progenitor expansion. *Nature Communications*, 12(1):3144, 2021. doi: 10.1038/s41467-021-23295-6.
- Grigor'eva, E. V., Malankhanova, T. B., Surumbayeva, A., Pavlova, S. V., Minina, J. M., Kizilova, E. A., Suldina, L. A., Morozova, K. N., Kiseleva, E., Sorokoumov, E. D., Lebedev, I. N., Zakian, S. M., and Malakhova, A. A. Generation of GABAergic striatal neurons by a novel iPSC differentiation protocol enabling scalability and cryopreservation of progenitor cells. *Cytotechnology*, 72(5):649–663, 2020. doi: 10.1007/s10616-020-00406-7.
- Grimm, H., Biller-Andorno, N., Buch, T., Dahlhoff, M., Davies, G., Cederroth, C. R., Maissen, O., Lukas, W., Passini, E., Törnqvist, E., Olsson, I. A. S., and Sandström, J. Advancing the 3Rs: Innovation, implementation, ethics and society. *Frontiers in Veterinary Science*, 10:1185706, 2023. doi: 10.3389/fvets.2023.1185706.
- Grubman, A., Chew, G., Ouyang, J. F., Sun, G., Choo, X. Y., McLean, C., Simmons, R. K., Buckberry, S., Vargas-Landin, D. B., Poppe, D., Pflueger, J., Lister, R., Rackham, O. J. L., Petretto, E., and Polo, J. M. A single-cell atlas of entorhinal cortex from individuals with Alzheimer's disease reveals cell-type-specific gene expression regulation. *Nature Neuroscience*, 22(12):2087–2097, 2019. doi: 10.1038/s41593-019-0539-4.
- Guarnieri, F. C., de Chevigny, A., Falace, A., and Cardoso, C. Disorders of neurogenesis and cortical development. *Dialogues in Clinical Neuroscience*, 20(4):255–266, 2018. doi: 10.31887/DCNS.2018.20.4/ccardoso.
- Gupta, D., Vagha, S., Dhingra, H., and Shirsath, H. Advances in understanding and treating amyotrophic lateral sclerosis (ALS): A comprehensive review. *Cureus*, 15(11):e48691, 2023. doi: 10.7759/cureus.48691.

- Gurney, M. E., Pu, H., Chiu, A. Y., Dal Canto, M. C., Polchow, C. Y., Alexander, D. D., Caliendo, J., Hentati, A., Kwon, Y. W., Deng, H. X., Chen, W., Zhai, P., Sufit, R. L., and Siddique, T. Motor neuron degeneration in mice that express a human Cu,Zn superoxide dismutase mutation. *Science*, 264(5166):1772–1775, 1994. doi: 10.1126/science.8209258.
- Guttenplan, K. A., Weigel, M. K., Adler, D. I., Couthouis, J., Liddelov, S. A., Gitler, A. D., and Barres, B. A. Knockout of reactive astrocyte activating factors slows disease progression in an ALS mouse model. *Nature Communications*, 11(1):3753, 2020. doi: 10.1038/s41467-020-17514-9.
- Habib, N., McCabe, C., Medina, S., Varshavsky, M., Kitsberg, D., Dvir-Szternfeld, R., Green, G., Dionne, D., Nguyen, L., Marshall, J. L., Chen, F., Zhang, F., Kaplan, T., Regev, A., and Schwartz, M. Disease-associated astrocytes in Alzheimer's disease and aging. *Nature Neuroscience*, 23(6):701–706, 2020. doi: 10.1038/s41593-020-0624-8.
- Hafemeister, C. and Satija, R. Normalization and variance stabilization of single-cell RNA-seq data using regularized negative binomial regression. *Genome Biology*, 20(1):296, 2019. doi: 10.1186/s13059-019-1874-1.
- Hagemann, T. L. Alexander disease: Models, mechanisms, and medicine. *Current Opinion in Neurobiology*, 72:140–147, 2022. doi: 10.1016/j.conb.2021.10.002.
- Hagemann, T. L., Gaeta, S. A., Smith, M. A., Johnson, D. A., Johnson, J. A., and Messing, A. Gene expression analysis in mice with elevated glial fibrillary acidic protein and Rosenthal fibers reveals a stress response followed by glial activation and neuronal dysfunction. *Human Molecular Genetics*, 14(16):2443–2458, 2005. doi: 10.1093/hmg/ddi248.
- Hagemann, T. L., Connor, J. X., and Messing, A. Alexander disease-associated glial fibrillary acidic protein mutations in mice induce Rosenthal fiber formation and a white matter stress response. *Journal of Neuroscience*, 26(43):11162–11173, 2006. doi: 10.1523/JNEUROSCI.3260-06.2006.
- Hagemann, T. L., Paylor, R., and Messing, A. Deficits in adult neurogenesis, contextual fear conditioning, and spatial learning in a Gfap mutant mouse model of Alexander disease. *Journal of Neuroscience*, 33(47):18698–18706, 2013. doi: 10.1523/JNEUROSCI.3693-13.2013.
- Hagemann, T. L., Powers, B., Lin, N. H., Mohamed, A. F., Dague, K. L., Hannah, S. C., Bachmann, G., Mazur, C., Rigo, F., Olsen, A. L., Feany, M. B., Perng, M. D., Berman, R. F., and Messing, A. Antisense therapy in a rat model of Alexander disease reverses GFAP pathology, white matter deficits, and motor impairment. *Science Translational Medicine*, 13(620):eabg4711, 2021. doi: 10.1126/scitranslmed.abg4711.
- Hagemann-Jensen, M., Ziegenhain, C., and Sandberg, R. Scalable single-cell RNA sequencing from full transcripts with Smart-seq3xpress. *Nature Biotechnology*, 40(10):1452–1457, 2022. doi: 10.1038/s41587-022-01311-4.
- Hammond, T. R., Dufort, C., Dissing-Olesen, L., Giera, S., Young, A., Wysoker, A., Walker, A. J., Gergits, F., Segel, M., Nemes, J., Marsh, S. E., Saunders, A., Macosko, E., Ginhoux, F., Chen, J., Franklin, R. J. M., Piao, X., McCarroll, S. A., and Stevens, B. Single-cell RNA sequencing of microglia throughout the mouse lifespan and in the injured brain reveals complex cell-state changes. *Immunity*, 50(1):253–271 e6, 2019. doi: 10.1016/j.immuni.2018.11.004.
- Hao, Y., Hao, S., Andersen-Nissen, E., Mauck, W. M., Jr., Zheng, S., Butler, A., Lee, M. J., Wilk, A. J., Darby, C., Zager, M., Hoffman, P., Stoeckius, M., Papalexi, E., Mimitou, E. P., Jain, J., Srivastava, A., Stuart, T., Fleming, L. M., Yeung, B., Rogers, A. J., McElrath, J. M., Blish, C. A., Gottardo, R., Smibert, P., and Satija, R. Integrated analysis of multimodal single-cell data. *Cell*, 184(13):3573–3587 e29, 2021. doi: 10.1016/j.cell.2021.04.048.
- Hao, Z. Z., Wei, J. R., Xiao, D., Liu, R., Xu, N., Tang, L., Huang, M., Shen, Y., Xing, C., Huang, W., Liu, X., Xiang, M., Liu, Y., Miao, Z., and Liu, S. Single-cell transcriptomics of adult macaque hippocampus reveals neural precursor cell populations. *Nature Neuroscience*, 25(6):805–817, 2022. doi: 10.1038/s41593-022-01073-x.
- Haque, A., Engel, J., Teichmann, S. A., and Lönnberg, T. A practical guide to single-cell RNA-sequencing for biomedical research and clinical applications. *Genome Medicine*, 9(1):75, 2017. doi: 10.1186/s13073-017-0467-4.
- Heaven, M. R., Flint, D., Randall, S. M., Sosunov, A. A., Wilson, L., Barnes, S., Goldman, J. E., Muddiman, D. C., and Brenner, M. Composition of Rosenthal fibers, the protein aggregate hallmark of Alexander disease. *Journal of Proteome Research*, 15(7):2265–2282, 2016. doi: 10.1021/acs.jproteome.6b00316.
- Heaven, M. R., Herren, A. W., Flint, D. L., Pacheco, N. L., Li, J., Tang, A., Khan, F., Goldman, J. E., Phinney, B. S., and Olsen, M. L. Metabolic enzyme alterations and astrocyte dysfunction in a murine model of Alexander disease with severe reactive gliosis. *Molecular & Cellular Proteomics*, 21(1):100180, 2022. doi: 10.1016/j.mcpro.2021.100180.
- Hendriks, D., Pagliaro, A., Andreatta, F., Ma, Z., van Giessen, J., Massalini, S., López-Iglesias, C., van Son, G. J. F., DeMartino, J., Damen, J. M. A., Zoutendijk, I., Staliarova, N., Bredenoord, A. L., Holstege, F. C. P., Peters, P. J., Margaritis, T., Chuva de Sousa Lopes, S., Wu, W., Clevers, H., and Artegiani, B. Human fetal brain self-organizes into long-term expanding organoids. *Cell*, 187(3):712–732 e38, 2024. doi: 10.1016/j.cell.2023.12.012.
- Hsia, E. Y., Gui, Y., and Zheng, X. Regulation of Hedgehog signaling by ubiquitination. *Frontiers in Biology*, 10(3):203–220, 2015. doi: 10.1007/s11515-015-1343-5.
- Huang, S. L., Wu, L. S., Lee, M., Chang, C. W., Cheng, W. C., Fang, Y. S., Chen, Y. R., Cheng, P. L., and Shen, C. J. A robust TDP-43 knock-in mouse model of ALS. *Acta Neuropathologica Communications*, 8(1):3, 2020. doi: 10.1186/s40478-020-0881-5.
- Huang, W. K., Wong, S. Z. H., Pather, S. R., Nguyen, P. T. T., Zhang, F., Zhang, D. Y., Zhang, Z., Lu, L., Fang, W., Chen, L., Fernandes, A., Su, Y., Song, H., and Ming, G. L. Generation of hypothalamic arcuate organoids from human induced pluripotent stem cells. *Cell Stem Cell*, 28(9):1657–1670 e10, 2021. doi: 10.1016/j.stem.2021.04.006.
- Humphrey, J., Birsa, N., Milioto, C., McLaughlin, M., Ule, A. M., Robaldo, D., Eberle, A. B., Kräuchi, R., Bentham, M., Brown, A. L., Jarvis, S., Bodo, C., Garone, M. G., Devoy, A., Soraru, G., Rosa, A., Bozzoni, I., Fisher, E. M. C., Mühlemann, O., Schiavo, G., Ruepp, M. D., Isaacs, A. M., Plagnol, V., and Fratta, P. FUS ALS-causative mutations impair FUS autoregulation and splicing factor networks through intron retention. *Nucleic Acids Research*, 48(12):6889–6905, 2020. doi: 10.1093/nar/gkaa410.

- Hurley, E. M., Mozolewski, P., Dobrowolski, R., and Hsieh, J. Familial Alzheimer's disease-associated PSEN1 mutations affect neurodevelopment through increased Notch signaling. *Stem Cell Reports*, 18(7):1516–1533, 2023. doi: 10.1016/j.stemcr.2023.05.018.
- Igreja, L., Menezes, C., Pinto, P. S., Freixo, J. P., and Chorão, R. Lissencephaly with cerebellar hypoplasia due to a new RELN mutation. *Pediatric Neurology*, 149:137–140, 2023. doi: 10.1016/j.pediatrneurol.2023.09.012.
- Ilicic, T., Kim, J. K., Kolodziejczyk, A. A., Bagger, F. O., McCarthy, D. J., Marioni, J. C., and Teichmann, S. A. Classification of low quality cells from single-cell RNA-seq data. *Genome Biology*, 17:29, 2016. doi: 10.1186/s13059-016-0888-1.
- Illumina, Inc. Illumina single-cell sequencing workflows: Critical steps and considerations. <https://www.illumina.com/content/dam/illumina-marketing/documents/gated/single-cell-sequencing-ebook-m-amr-00529.pdf>, 2024. Accessed: 2024-09-04.
- Illumina.com. Considerations for RNA seq read length and coverage. https://knowledge.illumina.com/library-preparation/rna-library-prep/library-preparation-rna-library-prep-reference_material-list/000001243, 2024. Accessed: 2024-05-03.
- Islam, S., Zeisel, A., Joost, S., La Manno, G., Zajac, P., Kasper, M., Lonnerberg, P., and Linnarsson, S. Quantitative single-cell RNA-seq with unique molecular identifiers. *Nature Methods*, 11(2):163–166, 2014. doi: 10.1038/nmeth.2772.
- Jensen, K. B. and Little, M. H. Organoids are not organs: Sources of variation and misinformation in organoid biology. *Stem Cell Reports*, 18(6):1255–1270, 2023. doi: 10.1016/j.stemcr.2023.05.009.
- Jerber, J., Seaton, D. D., Cuomo, A. S. E., Kumasaka, N., Haldane, J., Steer, J., Patel, M., Pearce, D., Andersson, M., Bonder, M. J., Mountjoy, E., Ghousaini, M., Lancaster, M. A., HipSci Consortium, Marioni, J. C., Merkle, F. T., Gaffney, D. J., and Stegle, O. Population-scale single-cell RNA-seq profiling across dopaminergic neuron differentiation. *Nature Genetics*, 53(3):304–312, 2021. doi: 10.1038/s41588-021-00801-6.
- Jin, S., Guerrero-Juarez, C. F., Zhang, L., Chang, I., Ramos, R., Kuan, C. H., Myung, P., Plikus, M. V., and Nie, Q. Inference and analysis of cell-cell communication using CellChat. *Nature Communications*, 12(1):1088, 2021. doi: 10.1038/s41467-021-21246-9.
- Jiwaji, Z. and Hardingham, G. E. Good, bad, and neglectful: Astrocyte changes in neurodegenerative disease. *Free Radical Biology & Medicine*, 182:93–99, 2022. doi: 10.1016/j.freeradbiomed.2022.02.020.
- Jones, J. R., Kong, L., Hanna, M. G. t., Hoffman, B., Krencik, R., Bradley, R., Hagemann, T., Choi, J., Doers, M., Dubovis, M., Sherafat, M. A., Bhattacharyya, A., Kendzioriski, C., Audhya, A., Messing, A., and Zhang, S. C. Mutations in GFAP disrupt the distribution and function of organelles in human astrocytes. *Cell Reports*, 25(4):947–958 e4, 2018. doi: 10.1016/j.celrep.2018.09.083.
- Jäkel, S., Agirre, E., Mendanha Falcão, A., van Bruggen, D., Lee, K. W., Knuesel, I., Malhotra, D., French Constant, C., Williams, A., and Castelo-Branco, G. Altered human oligodendrocyte heterogeneity in multiple sclerosis. *Nature*, 566(7745):543–547, 2019. doi: 10.1038/s41586-019-0903-2.
- Kaitsuka, T. and Hakim, F. Response of pluripotent stem cells to environmental stress and its application for directed differentiation. *Biology (Basel)*, 10(2):84, 2021. doi: 10.3390/biology10020084.
- Kanehisa, M. and Goto, S. KEGG: Kyoto encyclopedia of genes and genomes. *Nucleic Acids Research*, 28(1):27–30, 2000. doi: 10.1093/nar/28.1.27.
- Kang, S. H., Li, Y., Fukaya, M., Lorenzini, I., Cleveland, D. W., Ostrow, L. W., Rothstein, J. D., and Bergles, D. E. Degeneration and impaired regeneration of gray matter oligodendrocytes in amyotrophic lateral sclerosis. *Nature Neuroscience*, 16(5):571–579, 2013. doi: 10.1038/nn.3357.
- Kanton, S., Boyle, M. J., He, Z., Santel, M., Weigert, A., Sanchís-Calleja, F., Guijarro, P., Sidow, L., Fleck, J. S., Han, D., Qian, Z., Heide, M., Huttner, W. B., Khaitovich, P., Pääbo, S., Treutlein, B., and Camp, J. G. Organoid single-cell genomic atlas uncovers human-specific features of brain development. *Nature*, 574(7778):418–422, 2019. doi: 10.1038/s41586-019-1654-9.
- Kaya, T., Mattugini, N., Liu, L., Ji, H., Cantuti-Castelvetri, L., Wu, J., Schifferer, M., Groh, J., Martini, R., Besson-Girard, S., Kaji, S., Liesz, A., Gokce, O., and Simons, M. CD8(+) T cells induce interferon-responsive oligodendrocytes and microglia in white matter aging. *Nature Neuroscience*, 25(11):1446–1457, 2022. doi: 10.1038/s41593-022-01183-6.
- Kenigsbuch, M., Bost, P., Halevi, S., Chang, Y., Chen, S., Ma, Q., Hajbi, R., Schwikowski, B., Bodenmiller, B., Fu, H., Schwartz, M., and Amit, I. A shared disease-associated oligodendrocyte signature among multiple CNS pathologies. *Nature Neuroscience*, 25(7):876–886, 2022. doi: 10.1038/s41593-022-01104-7.
- Keren-Shaul, H., Spinrad, A., Weiner, A., Matcovitch-Natan, O., Dvir-Szternfeld, R., Ulland, T. K., David, E., Baruch, K., Lara-Astaiso, D., Toth, B., Itzkovitz, S., Colonna, M., Schwartz, M., and Amit, I. A unique microglia type associated with restricting development of Alzheimer's disease. *Cell*, 169(7):1276–1290 e17, 2017. doi: 10.1016/j.cell.2017.05.018.
- Kessarar, N., Fogarty, M., Iannarelli, P., Grist, M., Wegner, M., and Richardson, W. D. Competing waves of oligodendrocytes in the forebrain and postnatal elimination of an embryonic lineage. *Nature Neuroscience*, 9(2):173–179, 2006. doi: 10.1038/nn1620.
- Keung, A. J., de Juan-Pardo, E. M., Schaffer, D. V., and Kumar, S. Rho GTPases mediate the mechanosensitive lineage commitment of neural stem cells. *Stem Cells*, 29(11):1886–1897, 2011. doi: 10.1002/stem.746.
- Kirdajova, D., Valihrach, L., Valny, M., Kriska, J., Krocianova, D., Benesova, S., Abaffy, P., Zucha, D., Klassen, R., Kolenicova, D., Honsa, P., Kubista, M., and Anderova, M. Transient astrocyte-like NG2 glia subpopulation emerges solely following permanent brain ischemia. *Glia*, 69(11):2658–2681, 2021. doi: 10.1002/glia.24064.
- Koch, C. M., Chiu, S. F., Akbarpour, M., Bharat, A., Ridge, K. M., Bartom, E. T., and Winter, D. R. A beginner's guide to analysis of RNA sequencing data. *American Journal of Respiratory Cell and Molecular Biology*, 59(2):145–157, 2018. doi: 10.1165/rcmb.2017-0430TR.
- Kondo, T., Funayama, M., Miyake, M., Tsukita, K., Era, T., Osaka, H., Ayaki, T., Takahashi, R., and Inoue, H. Modeling Alexander disease with patient iPSCs reveals cellular and molecular pathology of astrocytes. *Acta Neuropathologica Communications*, 4(1):69, 2016. doi: 10.1186/s40478-016-0337-0.

- Krasemann, S., Madore, C., Cialic, R., Baufeld, C., Calcagno, N., El Fatimy, R., Beckers, L., O’Loughlin, E., Xu, Y., Fanek, Z., Greco, D. J., Smith, S. T., Tweet, G., Humulock, Z., Zrzavy, T., Conde-Sanroman, P., Gacias, M., Weng, Z., Chen, H., Tjon, E., Mazaheri, F., Hartmann, K., Madi, A., Ulrich, J. D., Glatzel, M., Worthmann, A., Heeren, J., Budnik, B., Lemere, C., Ikezu, T., Heppner, F. L., Litvak, V., Holtzman, D. M., Lassmann, H., Weiner, H. L., Ochando, J., Haass, C., and Butovsky, O. The TREM2-APOE pathway drives the transcriptional phenotype of dysfunctional microglia in neurodegenerative diseases. *Immunity*, 47(3):566–581 e9, 2017. doi: 10.1016/j.immuni.2017.08.008.
- Krawczyk, M. C., Haney, J. R., Pan, L., Caneda, C., Khankan, R. R., Reyes, S. D., Chang, J. W., Morselli, M., Vinters, H. V., Wang, A. C., Cobos, I., Gandal, M. J., Bergsneider, M., Kim, W., Liau, L. M., Yong, W., Jalali, A., Dencen, B., Grant, G. A., Mathern, G. W., Fallah, A., and Zhang, Y. Human astrocytes exhibit tumor microenvironment-, age-, and sex-related transcriptomic signatures. *Journal of Neuroscience*, 42(8):1587–1603, 2022. doi: 10.1523/JNEUROSCI.0407-21.2021.
- La Manno, G., Soldatov, R., Zeisel, A., Braun, E., Hochgerner, H., Petukhov, V., Lidschreiber, K., Kastrioti, M. E., Lönnerberg, P., Furlan, A., Fan, J., Borm, L. E., Liu, Z., van Bruggen, D., Guo, J., He, X., Barker, R., Sundström, E., Castelo-Branco, G., Cramer, P., Adameyko, I., Linnarsson, S., and Kharchenko, P. V. RNA velocity of single cells. *Nature*, 560(7719):494–498, 2018. doi: 10.1038/s41586-018-0414-6.
- Lafzi, A., Moutinho, C., Picelli, S., and Heyn, H. Tutorial: Guidelines for the experimental design of single-cell RNA sequencing studies. *Nature Protocols*, 13(12):2742–2757, 2018. doi: 10.1038/s41596-018-0073-y.
- Lancaster, M. A. and Knoblich, J. A. Organogenesis in a dish: Modeling development and disease using organoid technologies. *Science*, 345(6194):1247125, 2014. doi: 10.1126/science.1247125.
- Lancaster, M. A., Renner, M., Martin, C. A., Wenzel, D., Bicknell, L. S., Hurles, M. E., Homfray, T., Penninger, J. M., Jackson, A. P., and Knoblich, J. A. Cerebral organoids model human brain development and microcephaly. *Nature*, 501(7467):373–379, 2013. doi: 10.1038/nature12517.
- Lanfer, J., Kaindl, J., Krumm, L., Gonzalez Acera, M., Neurath, M., Regensburger, M., Krach, F., and Winner, B. Efficient and easy conversion of human iPSCs into functional induced microglia-like cells. *International Journal of Molecular Sciences*, 23(9):4526, 2022. doi: 10.3390/ijms23094526.
- Langfelder, P. and Horvath, S. WGCNA: An R package for weighted correlation network analysis. *BMC Bioinformatics*, 9:559, 2008. doi: 10.1186/1471-2105-9-559.
- Lau, S. F., Cao, H., Fu, A. K. Y., and Ip, N. Y. Single-nucleus transcriptome analysis reveals dysregulation of angiogenic endothelial cells and neuroprotective glia in Alzheimer’s disease. *PNAS USA*, 117(41):25800–25809, 2020. doi: 10.1073/pnas.2008762117.
- Lee, D. R., Rhodes, C., Mitra, A., Zhang, Y., Maric, D., Dale, R. K., and Petros, T. J. Transcriptional heterogeneity of ventricular zone cells in the ganglionic eminences of the mouse forebrain. *eLife*, 11:e71864, 2022a. doi: 10.7554/eLife.71864.
- Lee, H. G., Wheeler, M. A., and Quintana, F. J. Function and therapeutic value of astrocytes in neurological diseases. *Nature Reviews Drug Discovery*, 21(5):339–358, 2022b. doi: 10.1038/s41573-022-00390-x.
- Lee, S. H., Rezzonico, M. G., Friedman, B. A., Huntley, M. H., Meilandt, W. J., Pandey, S., Chen, Y. J., Easton, A., Modrusan, Z., Hansen, D. V., Sheng, M., and Bohlen, C. J. TREM2-independent oligodendrocyte, astrocyte, and T cell responses to tau and amyloid pathology in mouse models of Alzheimer disease. *Cell Reports*, 37(13):110158, 2021. doi: 10.1016/j.celrep.2021.110158.
- Leng, K., Li, E., Eser, R., Piergies, A., Sit, R., Tan, M., Neff, N., Li, S. H., Rodriguez, R. D., Suemoto, C. K., Leite, R. E. P., Ehrenberg, A. J., Pasqualucci, C. A., Seeley, W. W., Spina, S., Heinsen, H., Grinberg, L. T., and Kampmann, M. Molecular characterization of selectively vulnerable neurons in Alzheimer’s disease. *Nature Neuroscience*, 24(2):276–287, 2021. doi: 10.1038/s41593-020-00764-7.
- Leng, K., Rose, I. V. L., Kim, H., Xia, W., Romero-Fernandez, W., Rooney, B., Koontz, M., Li, E., Ao, Y., Wang, S., Krawczyk, M., TCW, J., Goate, A., Zhang, Y., Ullian, E. M., Sofroniew, M. V., Fancy, S. P. J., Schrag, M. S., Lippmann, E. S., and Kampmann, M. CRISPRi screens in human iPSC-derived astrocytes elucidate regulators of distinct inflammatory reactive states. *Nature Neuroscience*, 25(11):1528–1542, 2022. doi: 10.1038/s41593-022-01180-9.
- Li, C., Fleck, J. S., Martins-Costa, C., Burkard, T. R., Themann, J., Stuempflen, M., Peer, A. M., Vertesy, A., Littleboy, J. B., Esk, C., Elling, U., Kasprian, G., Corsini, N. S., Treutlein, B., and Knoblich, J. A. Single-cell brain organoid screening identifies developmental defects in autism. *Nature*, 621(7978):373–380, 2023. doi: 10.1038/s41586-023-06473-y.
- Li, L., Tian, E., Chen, X., Chao, J., Klein, J., Qu, Q., Sun, G., Sun, G., Huang, Y., Warden, C. D., Ye, P., Feng, L., Li, X., Cui, Q., Sultan, A., Douvaras, P., Fossati, V., Sanjana, N. E., Riggs, A. D., and Shi, Y. GFAP mutations in astrocytes impair oligodendrocyte progenitor proliferation and myelination in an hiPSC model of Alexander disease. *Cell Stem Cell*, 23(2):239–251 e6, 2018. doi: 10.1016/j.stem.2018.07.009.
- Li, Q., Cheng, Z., Zhou, L., Darmanis, S., Neff, N. F., Okamoto, J., Gulati, G., Bennett, M. L., Sun, L. O., Clarke, L. E., Marschallinger, J., Yu, G., Quake, S. R., Wyss-Coray, T., and Barres, B. A. Developmental heterogeneity of microglia and brain myeloid cells revealed by deep single-cell RNA sequencing. *Neuron*, 101(2):207–223 e10, 2019. doi: 10.1016/j.neuron.2018.12.006.
- Li, X. Y., Zhai, W. J., and Teng, C. B. Notch signaling in pancreatic development. *International Journal of Molecular Sciences*, 17(1):48, 2015. doi: 10.3390/ijms17010048.
- Li, Y., Li, Z., Yang, M., Wang, F., Zhang, Y., Li, R., Li, Q., Gong, Y., Wang, B., Fan, B., Wang, C., Chen, L., Li, H., Ong, J., Teng, Z., Jin, L., Wang, Y. L., Du, P., and Jiao, J. Decoding the temporal and regional specification of microglia in the developing human brain. *Cell Stem Cell*, 29(4):620–634 e6, 2022. doi: 10.1016/j.stem.2022.02.004.
- Liao, Y., Wang, J., Jaehnig, E. J., Shi, Z., and Zhang, B. WebGestalt 2019: Gene set analysis toolkit with revamped UIs and APIs. *Nucleic Acids Research*, 47(W1):W199–W205, 2019. doi: 10.1093/nar/gkz401.
- Liddelow, S. A. and Barres, B. A. Reactive astrocytes: Production, function, and therapeutic potential. *Immunity*, 46(6):957–967, 2017. doi: 10.1016/j.immuni.2017.06.006.

- Liddelow, S. A., Guttenplan, K. A., Clarke, L. E., Bennett, F. C., Bohlen, C. J., Schirmer, L., Bennett, M. L., Münch, A. E., Chung, W. S., Peterson, T. C., Wilton, D. K., Frouin, A., Napier, B. A., Panicker, N., Kumar, M., Buckwalter, M. S., Rowitch, D. H., Dawson, V. L., Dawson, T. M., Stevens, B., and Barres, B. A. Neurotoxic reactive astrocytes are induced by activated microglia. *Nature*, 541(7638): 481–487, 2017. doi: 10.1038/nature21029.
- Lin, H. C., He, Z., Ebert, S., Schörmig, M., Santel, M., Nikolova, M. T., Weigert, A., Hevers, W., Kasri, N. N., Taverna, E., Camp, J. G., and Treutlein, B. NGN2 induces diverse neuron types from human pluripotency. *Stem Cell Reports*, 16(9):2118–2127, 2021. doi: 10.1016/j.stemcr.2021.07.006.
- Ling, S. C., Polymenidou, M., and Cleveland, D. W. Converging mechanisms in ALS and FTD: Disrupted RNA and protein homeostasis. *Neuron*, 79(3):416–438, 2013. doi: 10.1016/j.neuron.2013.07.033.
- Liu, S., Thennavan, A., Garay, J. P., Marron, J. S., and Perou, C. M. MultiK: An automated tool to determine optimal cluster numbers in single-cell RNA sequencing data. *Genome Biology*, 22(1):232, 2021. doi: 10.1186/s13059-021-02445-5.
- Liu, W., Venugopal, S., Majid, S., Ahn, I. S., Diamante, G., Hong, J., Yang, X., and Chandler, S. H. Single-cell RNA-seq analysis of the brainstem of mutant SOD1 mice reveals perturbed cell types and pathways of amyotrophic lateral sclerosis. *Neurobiology of Disease*, 141: 104877, 2020. doi: 10.1016/j.nbd.2020.104877.
- Love, M. I., Huber, W., and Anders, S. Moderated estimation of fold change and dispersion for RNA-seq data with DESeq2. *Genome Biology*, 15(12):550, 2014. doi: 10.1186/s13059-014-0550-8.
- Lowe, R., Shirley, N., Bleackley, M., Dolan, S., and Shafee, T. Transcriptomics technologies. *PLoS Computational Biology*, 13(5):e1005457, 2017. doi: 10.1371/journal.pcbi.1005457.
- Luchena, C., Zuazo-Ibarra, J., Valero, J., Matute, C., Alberdi, E., and Capetillo-Zarate, E. A neuron, microglia, and astrocyte triple co-culture model to study Alzheimer's disease. *Frontiers in Aging Neuroscience*, 14:844534, 2022. doi: 10.3389/fnagi.2022.844534.
- Ma, F., Fuqua, B. K., Hasin, Y., Yukhtman, C., Vulpe, C. D., Lusic, A. J., and Pellegrini, M. A comparison between whole transcript and 3' RNA sequencing methods using Kapa and Lexogen library preparation methods. *BMC Genomics*, 20(1):9, 2019. doi: 10.1186/s12864-018-5393-3.
- Ma, H., Zhou, Y., Li, Z., Zhu, L., Li, H., Zhang, G., Wang, J., Gong, H., Xu, D., Hua, W., Liu, P., Zhang, X., Zhang, Y., Zhang, L., Hong, B., Zhou, W., Yang, P., and Liu, J. Single-cell RNA-sequencing analyses revealed heterogeneity and dynamic changes of metabolic pathways in astrocytes at the acute phase of ischemic stroke. *Oxidative Medicine and Cellular Longevity*, 2022:1817721, 2022. doi: 10.1155/2022/1817721.
- MacDougall, G., Brown, L. Y., Kantor, B., and Chiba-Falek, O. The path to progress preclinical studies of age-related neurodegenerative diseases: A perspective on rodent and hiPSC-derived models. *Molecular Therapy*, 29(3):949–972, 2021. doi: 10.1016/j.yjth.2021.01.001.
- MacLean, M., López-Diez, R., Vasquez, C., Gugger, P. F., and Schmidt, A. M. Neuronal-glia communication perturbations in murine SOD1(G93A) spinal cord. *Communications Biology*, 5(1):177, 2022. doi: 10.1038/s42003-022-03128-y.
- Maniatis, S., Äijö, T., Vickovic, S., Braine, C., Kang, K., Mollbrink, A., Fagegaltier, D., Andrusivová, Z., Saarenpää, S., Saiz-Castro, G., Cuevas, M., Watters, A., Lundeberg, J., Bonneau, R., and Phatnani, H. Spatiotemporal dynamics of molecular pathology in amyotrophic lateral sclerosis. *Science*, 364(6435):89–93, 2019. doi: 10.1126/science.aav9776.
- Marques, S., Zeisel, A., Codeluppi, S., van Bruggen, D., Mendanha Falcão, A., Xiao, L., Li, H., Häring, M., Hochgerner, H., Romanov, R. A., Gyllborg, D., Muñoz Manchado, A., La Manno, G., Lönnerberg, P., Floriddia, E. M., Rezayee, F., Ernfors, P., Arenas, E., Hjerling-Leffler, J., Harkany, T., Richardson, W. D., Linnarsson, S., and Castelo-Branco, G. Oligodendrocyte heterogeneity in the mouse juvenile and adult central nervous system. *Science*, 352(6291):1326–1329, 2016. doi: 10.1126/science.aaf6463.
- Marsh, S. E., Walker, A. J., Kamath, T., Dissing-Olesen, L., Hammond, T. R., de Soysa, T. Y., Young, A. M. H., Murphy, S., Abdulraouf, A., Nadaf, N., Dufort, C., Walker, A. C., Lucca, L. E., Kozareva, V., Vanderburg, C., Hong, S., Bulstrode, H., Hutchinson, P. J., Gaffney, D. J., Hafler, D. A., Franklin, R. J. M., Macosko, E. Z., and Stevens, B. Dissection of artifactual and confounding glial signatures by single-cell sequencing of mouse and human brain. *Nature Neuroscience*, 25(3):306–316, 2022. doi: 10.1038/s41593-022-01022-8.
- Marton, R. M., Miura, Y., Sloan, S. A., Li, Q., Revah, O., Levy, R. J., Huguenard, J. R., and Paşca, S. P. Differentiation and maturation of oligodendrocytes in human three-dimensional neural cultures. *Nature Neuroscience*, 22(3):484–491, 2019. doi: 10.1038/s41593-018-0316-9.
- Masuda, T., Sankowski, R., Staszewski, O., Böttcher, C., Amann, L., Sagar, Scheiwe, C., Nessler, S., Kunz, P., van Loo, G., Coenen, V. A., Reinacher, P. C., Michel, A., Sure, U., Gold, R., Grün, D., Priller, J., Stadelmann, C., and Prinz, M. Spatial and temporal heterogeneity of mouse and human microglia at single-cell resolution. *Nature*, 566(7744):388–392, 2019. doi: 10.1038/s41586-019-0924-x.
- Mathys, H., Adaikkan, C., Gao, F., Young, J. Z., Manet, E., Hemberg, M., De Jager, P. L., Ransohoff, R. M., Regev, A., and Tsai, L. H. Temporal tracking of microglia activation in neurodegeneration at single-cell resolution. *Cell Reports*, 21(2):366–380, 2017. doi: 10.1016/j.celrep.2017.09.039.
- Mathys, H., Davila-Velderrain, J., Peng, Z., Gao, F., Mohammadi, S., Young, J. Z., Menon, M., He, L., Abdurrob, F., Jiang, X., Martorell, A. J., Ransohoff, R. M., Hafler, B. P., Bennett, D. A., Kellis, M., and Tsai, L. H. Single-cell transcriptomic analysis of Alzheimer's disease. *Nature*, 570(7761):332–337, 2019. doi: 10.1038/s41586-019-1195-2.
- Matson, K. J. E., Russ, D. E., Kathe, C., Hua, I., Maric, D., Ding, Y., Krynskiy, J., Pursley, R., Sathyamurthy, A., Squair, J. W., Levi, B. P., Courtine, G., and Levine, A. J. Single cell atlas of spinal cord injury in mice reveals a pro-regenerative signature in spinocerebellar neurons. *Nature Communications*, 13(1):5628, 2022. doi: 10.1038/s41467-022-33184-1.
- McGinnis, C. S., Murrow, L. M., and Gartner, Z. J. DoubletFinder: Doublet detection in single-cell RNA sequencing data using artificial nearest neighbors. *Cell Systems*, 8(4):329–337 e4, 2019. doi: 10.1016/j.cels.2019.03.003.

- Mehta, S. R., Tom, C. M., Wang, Y., Bresee, C., Rushton, D., Mathkar, P. P., Tang, J., and Mattis, V. B. Human Huntington's disease iPSC-derived cortical neurons display altered transcriptomics, morphology, and maturation. *Cell Reports*, 25(4):1081–1096 e6, 2018. doi: 10.1016/j.celrep.2018.09.076.
- Meisingset, T. W., Risa, O., Brenner, M., Messing, A., and Sonnewald, U. Alteration of glial-neuronal metabolic interactions in a mouse model of Alexander disease. *Glia*, 58(10):1228–1234, 2010. doi: 10.1002/glia.21003.
- Mejzini, R., Flynn, L. L., Pitout, I. L., Fletcher, S., Wilton, S. D., and Akkari, P. A. ALS genetics, mechanisms, and therapeutics: Where are we now? *Frontiers in Neuroscience*, 13:1310, 2019. doi: 10.3389/fnins.2019.01310.
- Messing, A., Brenner, M., Feany, M. B., Nedergaard, M., and Goldman, J. E. Alexander disease. *Journal of Neuroscience*, 32(15):5017–5023, 2012. doi: 10.1523/JNEUROSCI.5384-11.2012.
- Middeldorp, J., Boer, K., Sluijs, J. A., De Filippis, L., Encha-Razavi, F., Vescovi, A. L., Swaab, D. F., Aronica, E., and Hol, E. M. GFAPdelta in radial glia and subventricular zone progenitors in the developing human cortex. *Development*, 137(2):313–321, 2010. doi: 10.1242/dev.041632.
- Migliarini, S., Scaricamazza, S., Valle, C., Ferri, A., Pasqualetti, M., and Ferraro, E. Microglia morphological changes in the motor cortex of hSOD1(G93A) transgenic ALS mice. *Brain Sciences*, 11(6):807, 2021. doi: 10.3390/brainsci11060807.
- Miller, S. J., Zhang, P. W., Glatzer, J., and Rothstein, J. D. Astroglial transcriptome dysregulation in early disease of an ALS mutant SOD1 mouse model. *Journal of Neurogenetics*, 31(1-2):37–48, 2017. doi: 10.1080/01677063.2016.1260128.
- Miller, S. J., Glatzer, J. C., Hsieh, Y. C., and Rothstein, J. D. Cortical astroglia undergo transcriptomic dysregulation in the G93A SOD1 ALS mouse model. *Journal of Neurogenetics*, 32(4):322–335, 2018. doi: 10.1080/01677063.2018.1513508.
- Miranda-Negrón, Y. and García-Arrarás, J. E. Radial glia and radial glia-like cells: Their role in neurogenesis and regeneration. *Frontiers in Neuroscience*, 16:1006037, 2022. doi: 10.3389/fnins.2022.1006037.
- Molina-Gonzalez, I., Holloway, R. K., Jiwaji, Z., Dando, O., Kent, S. A., Emelianova, K., Lloyd, A. F., Forbes, L. H., Mahmood, A., Skripuletz, T., Gudi, V., Febery, J. A., Johnson, J. A., Fowler, J. H., Kuhlmann, T., Williams, A., Chandran, S., Stangel, M., Howden, A. J. M., Hardingham, G. E., and Miron, V. E. Astrocyte-oligodendrocyte interaction regulates central nervous system regeneration. *Nature Communications*, 14(1):3372, 2023. doi: 10.1038/s41467-023-39046-8.
- Moll, P., Ante, M., Seitz, A., and Reda, T. QuantSeq 3' mRNA sequencing for RNA quantification. *Nature Methods*, 11:i–iii, 2014. doi: 10.1038/nmeth.f.376.
- Morabito, S., Miyoshi, E., Michael, N., Shahin, S., Martini, A. C., Head, E., Silva, J., Leavy, K., Perez-Rosendahl, M., and Swarup, V. Single-nucleus chromatin accessibility and transcriptomic characterization of Alzheimer's disease. *Nature Genetics*, 53(8):1143–1155, 2021. doi: 10.1038/s41588-021-00894-z.
- Moser, J. M., Bigini, P., and Schmitt-John, T. The wobbler mouse, an ALS animal model. *Molecular Genetics and Genomics*, 288(5-6):207–229, 2013. doi: 10.1007/s00438-013-0741-0.
- Månberg, A., Skene, N., Sanders, F., Trusohamn, M., Remnestål, J., Szczepińska, A., Aksoylu, I. S., Lönnnerberg, P., Ebarasi, L., Wouters, S., Lehmann, M., Olofsson, J., von Gohren Antequera, I., Domaniku, A., De Schaepdryver, M., De Vocht, J., Poesen, K., Uhlén, M., Anink, J., Mijnsbergen, C., Vergunst-Bosch, H., Hübers, A., Kläppe, U., Rodriguez-Vieitez, E., Gilthorpe, J. D., Hedlund, E., Harris, R. A., Aronica, E., Van Damme, P., Ludolph, A., Veldink, J., Ingre, C., Nilsson, P., and Lewandowski, S. A. Altered perivascular fibroblast activity precedes ALS disease onset. *Nature Medicine*, 27(4):640–646, 2021. doi: 10.1038/s41591-021-01295-9.
- Nagy, C., Maitra, M., Tanti, A., Suderman, M., Theroux, J. F., Davoli, M. A., Perlman, K., Yerko, V., Wang, Y. C., Tripathy, S. J., Pavlidis, P., Mechawar, N., Ragoussis, J., and Turecki, G. Single-nucleus transcriptomics of the prefrontal cortex in major depressive disorder implicates oligodendrocyte precursor cells and excitatory neurons. *Nature Neuroscience*, 23(6):771–781, 2020. doi: 10.1038/s41593-020-0621-y.
- Namboori, S. C., Thomas, P., Ames, R., Hawkins, S., Garrett, L. O., Willis, C. R. G., Rosa, A., Stanton, L. W., and Bhinge, A. Single-cell transcriptomics identifies master regulators of neurodegeneration in SOD1 ALS iPSC-derived motor neurons. *Stem Cell Reports*, 16(12):3020–3035, 2021. doi: 10.1016/j.stemcr.2021.10.010.
- Napolitano, T., Silvano, S., Ayachi, C., Plaisant, M., Sousa-Da-Veiga, A., Fofó, H., Charles, B., and Collombat, P. Wnt pathway in pancreatic development and pathophysiology. *Cells*, 12(4), 2023. doi: 10.3390/cells12040565.
- Nguyen, H. C. T., Baik, B., Yoon, S., Park, T., and Nam, D. Benchmarking integration of single-cell differential expression. *Nature Communications*, 14(1):1570, 2023. doi: 10.1038/s41467-023-37126-3.
- Niessen, H. G., Angenstein, F., Sander, K., Kunz, W. S., Teuchert, M., Ludolph, A. C., Heinze, H. J., Scheich, H., and Vielhaber, S. In vivo quantification of spinal and bulbar motor neuron degeneration in the G93A-SOD1 transgenic mouse model of ALS by T2 relaxation time and apparent diffusion coefficient. *Experimental Neurology*, 201(2):293–300, 2006. doi: 10.1016/j.expneurol.2006.04.007.
- Nihei, K., McKee, A. C., and Kowall, N. W. Patterns of neuronal degeneration in the motor cortex of amyotrophic lateral sclerosis patients. *Acta Neuropathologica*, 86(1):55–64, 1993. doi: 10.1007/BF00454899.
- Nowakowski, T. J., Pollen, A. A., Sandoval-Espinosa, C., and Kriegstein, A. R. Transformation of the radial glia scaffold demarcates two stages of human cerebral cortex development. *Neuron*, 91(6):1219–1227, 2016. doi: 10.1016/j.neuron.2016.09.005.
- Oakley, H., Cole, S. L., Logan, S., Maus, E., Shao, P., Craft, J., Guillozet-Bongaarts, A., Ohno, M., Disterhoft, J., Van Eldik, L., Berry, R., and Vassar, R. Intraneuronal beta-amyloid aggregates, neurodegeneration, and neuron loss in transgenic mice with five familial Alzheimer's disease mutations: Potential factors in amyloid plaque formation. *Journal of Neuroscience*, 26(40):10129–10140, 2006. doi: 10.1523/JNEUROSCI.1202-06.2006.
- Oberheim, N. A., Takano, T., Han, X., He, W., Lin, J. H., Wang, F., Xu, Q., Wyatt, J. D., Pilcher, W., Ojemann, J. G., Ransom, B. R., Goldman, S. A., and Nedergaard, M. Uniquely hominid features of adult human astrocytes. *Journal of Neuroscience*, 29(10):3276–3287, 2009. doi: 10.1523/JNEUROSCI.4707-08.2009.

- Oblak, A. L., Lin, P. B., Kotredes, K. P., Pandey, R. S., Garceau, D., Williams, H. M., Uyar, A., O'Rourke, R., O'Rourke, S., Ingraham, C., Bednarczyk, D., Belanger, M., Cope, Z. A., Little, G. J., Williams, S. G., Ash, C., Bleckert, A., Ragan, T., Logsdon, B. A., Mangravite, L. M., Sukoff Rizzo, S. J., Territo, P. R., Carter, G. W., Howell, G. R., Sasner, M., and Lamb, B. T. Comprehensive evaluation of the 5XFAD mouse model for preclinical testing applications: A MODEL-AD study. *Frontiers in Aging Neuroscience*, 13:713726, 2021. doi: 10.3389/fnagi.2021.713726.
- Ohgomori, T., Yamada, J., Takeuchi, H., Kadomatsu, K., and Jinno, S. Comparative morphometric analysis of microglia in the spinal cord of SOD1(G93A) transgenic mouse model of amyotrophic lateral sclerosis. *European Journal of Neuroscience*, 43(10):1340–1351, 2016. doi: 10.1111/ejn.13227.
- Ormel, P. R., Vieira de Sa, R., van Bodegraven, E. J., Karst, H., Harschnitz, O., Sneuboer, M. A. M., Johansen, L. E., van Dijk, R. E., Scheefhals, N., Berdenis van Berlekom, A., Ribes Martinez, E., Kling, S., MacGillavry, H. D., van den Berg, L. H., Kahn, R. S., Hol, E. M., de Witte, L. D., and Pasterkamp, R. J. Microglia innately develop within cerebral organoids. *Nature Communications*, 9(1):4167, 2018. doi: 10.1038/s41467-018-06684-2.
- O'Rourke, J. G., Bogdanik, L., Muhammad, A. K. M. G., Gendron, T. F., Kim, K. J., Austin, A., Cady, J., Liu, E. Y., Zarrow, J., Grant, S., Ho, R., Bell, S., Carmona, S., Simpkinson, M., Lall, D., Wu, K., Daugherty, L., Dickson, D. W., Harms, M. B., Petrucelli, L., Lee, E. B., Lutz, C. M., and Baloh, R. H. C9orf72 BAC transgenic mice display typical pathologic features of ALS/FTD. *Neuron*, 88(5):892–901, 2015. doi: 10.1016/j.neuron.2015.10.027.
- Özdinler, P. H., Benn, S., Yamamoto, T. H., Güzel, M., Brown, R. H., J., and Macklis, J. D. Corticospinal motor neurons and related subcerebral projection neurons undergo early and specific neurodegeneration in hSOD1(G93A) transgenic ALS mice. *Journal of Neuroscience*, 31(11):4166–4177, 2011. doi: 10.1523/JNEUROSCI.4184-10.2011.
- Pandey, S., Shen, K., Lee, S. H., Shen, Y. A., Wang, Y., Otero-Garcia, M., Kotova, N., Vito, S. T., Laufer, B. I., Newton, D. F., Rezzonico, M. G., Hanson, J. E., Kaminker, J. S., Bohlen, C. J., Yuen, T. J., and Friedman, B. A. Disease-associated oligodendrocyte responses across neurodegenerative diseases. *Cell Reports*, 40(8):111189, 2022. doi: 10.1016/j.celrep.2022.111189.
- Park, B., Nicaise, A. M., Tsitsipatis, D., Pirvan, L., Prasad, P., De Novalles, M. L. L., Whitten, J., Culig, L., Llewellyn, J., Ionescu, R.-B., Willis, C. M., Krzak, G., Fan, J., De, S., Suarez Cubero, M., Spathopoulou, A., Peruzzotti-Jametti, L., Leonardi, T., Edenhofer, F., Gorospe, M., Mohorianu, I., Pluchino, S., and Beerman, I. Integrative single-cell analysis of neural stem/progenitor cells reveals epigenetically dysregulated interferon response in progressive multiple sclerosis. *bioRxiv*, 2024. doi: 10.1101/2024.02.09.579648.
- Pasko, V. I., Churkina, A. S., Shakhov, A. S., Kotlobay, A. A., and Alieva, I. B. Modeling of neurodegenerative diseases: 'Step by step' and 'network' organization of the complexes of model systems. *International Journal of Molecular Sciences*, 24(1):604, 2022. doi: 10.3390/ijms24010604.
- Pasquini, G., Rojo Arias, J. E., Schafer, P., and Busskamp, V. Automated methods for cell type annotation on scRNA-seq data. *Computational and Structural Biotechnology Journal*, 19:961–969, 2021. doi: 10.1016/j.csbj.2021.01.015.
- Pekny, M. and Pekna, M. Astrocyte reactivity and reactive astrogliosis: Costs and benefits. *Physiological Reviews*, 94(4):1077–1098, 2014. doi: 10.1152/physrev.00041.2013.
- Pereira, J. D., DuBreuil, D. M., Devlin, A. C., Held, A., Sapir, Y., Berezovski, E., Hawrot, J., Dorfman, K., Chander, V., and Wainger, B. J. Human sensorimotor organoids derived from healthy and amyotrophic lateral sclerosis stem cells form neuromuscular junctions. *Nature Communications*, 12(1):4744, 2021. doi: 10.1038/s41467-021-24776-4.
- Pfohl, S. R., Halicek, M. T., and Mitchell, C. S. Characterization of the contribution of genetic background and gender to disease progression in the SOD1 G93A mouse model of amyotrophic lateral sclerosis: A meta-analysis. *Journal of Neuromuscular Diseases*, 2(2):137–150, 2015. doi: 10.3233/JND-140068.
- Picelli, S., Björklund, A. K., Faridani, O. R., Sagasser, S., Winberg, G., and Sandberg, R. Smart-seq2 for sensitive full-length transcriptome profiling in single cells. *Nature Methods*, 10:1096–1098, 2013. doi: 10.1038/nmeth.2639.
- Picelli, S., Faridani, O. R., Björklund, A. K., Winberg, G., Sagasser, S., and Sandberg, R. Full-length RNA-seq from single cells using Smart-seq2. *Nature Protocols*, 9(1):171–181, 2014. doi: 10.1038/nprot.2014.006.
- Polazzi, E. and Contestabile, A. Neuron-conditioned media differentially affect the survival of activated or unstimulated microglia: Evidence for neuronal control on apoptotic elimination of activated microglia. *Journal of Neuropathology and Experimental Neurology*, 62(4):351–362, 2003. doi: 10.1093/jnen/62.4.351.
- Pollen, A. A., Nowakowski, T. J., Chen, J., Retallack, H., Sandoval-Espinosa, C., Nicholas, C. R., Shuga, J., Liu, S. J., Oldham, M. C., Diaz, A., Lim, D. A., Leyrat, A. A., West, J. A., and Kriegstein, A. R. Molecular identity of human outer radial glia during cortical development. *Cell*, 163(1):55–67, 2015. doi: 10.1016/j.cell.2015.09.004.
- Prust, M., Wang, J., Morizono, H., Messing, A., Brenner, M., Gordon, E., Hartka, T., Sokohl, A., Schiffmann, R., Gordish-Dressman, H., Albin, R., Amartino, H., Brockman, K., Dinopoulos, A., Dotti, M. T., Fain, D., Fernandez, R., Ferreira, J., Fleming, J., Gill, D., Griebel, M., Heilstedt, H., Kaplan, P., Lewis, D., Nakagawa, M., Pedersen, R., Reddy, A., Sawaishi, Y., Schneider, M., Sherr, E., Takiyama, Y., Wakabayashi, K., Gorospe, J. R., and Vanderver, A. GFAP mutations, age at onset, and clinical subtypes in Alexander disease. *Neurology*, 77(13):1287–1294, 2011. doi: 10.1212/WNL.0b013e3182309f72.
- Pullin, J. M. and McCarthy, D. J. A comparison of marker gene selection methods for single-cell RNA sequencing data. *Genome Biology*, 25(1):56, 2024. doi: 10.1186/s13059-024-03183-0.
- Qiu, H., Lee, S., Shang, Y., Wang, W. Y., Au, K. F., Kamiya, S., Barmada, S. J., Finkbeiner, S., Lui, H., Carlton, C. E., Tang, A. A., Oldham, M. C., Wang, H., Shorter, J., Filiano, A. J., Roberson, E. D., Tourtellotte, W. G., Chen, B., Tsai, L. H., and Huang, E. J. ALS-associated mutation FUS-R521C causes DNA damage and RNA splicing defects. *The Journal of Clinical Investigation*, 124(3):981–999, 2014. doi: 10.1172/JCI72723.

- Quadrato, G., Nguyen, T., Macosko, E. Z., Sherwood, J. L., Min Yang, S., Berger, D. R., Maria, N., Scholvin, J., Goldman, M., Kinney, J. P., Boyden, E. S., Lichtman, J. W., Williams, Z. M., McCarroll, S. A., and Arlotta, P. Cell diversity and network dynamics in photosensitive human brain organoids. *Nature*, 545(7652):48–53, 2017. doi: 10.1038/nature22047.
- R Core Team. R: A language and environment for statistical computing. <https://www.R-project.org>, 2022.
- Rahman, M. M., Islam, M. R., Yamin, M., Islam, M. M., Sarker, M. T., Meem, A. F. K., Akter, A., Emran, T. B., Cavalu, S., and Sharma, R. Emerging role of neuron-glia in neurological disorders: At a glance. *Oxidative Medicine and Cellular Longevity*, 2022:3201644, 2022. doi: 10.1155/2022/3201644.
- Rammensee, S., Kang, M. S., Georgiou, K., Kumar, S., and Schaffer, D. V. Dynamics of mechanosensitive neural stem cell differentiation. *Stem Cells*, 35(2):497–506, 2017. doi: 10.1002/stem.2489.
- Ramos, S. I., Mussa, Z. M., Falk, E. N., Pai, B., Giotti, B., Allette, K., Cai, P., Dekio, F., Sebra, R., Beaumont, K. G., Tsankov, A. M., and Tsankova, N. M. An atlas of late prenatal human neurodevelopment resolved by single-nucleus transcriptomics. *Nature Communications*, 13(1):7671, 2022. doi: 10.1038/s41467-022-34975-2.
- Rasband, M. N. Glial contributions to neural function and disease. *Molecular and Cellular Proteomics*, 15(2):355–361, 2016. doi: 10.1074/mcp.R115.053744.
- Reyes-Ortiz, A. M., Abud, E. M., Burns, M. S., Wu, J., Hernandez, S. J., McClure, N., Wang, K. Q., Schulz, C. J., Miramontes, R., Lau, A., Michael, N., Miyoshi, E., Van Vactor, D., Reidling, J. C., Blurton-Jones, M., Swarup, V., Poon, W. W., Lim, R. G., and Thompson, L. M. Single-nuclei transcriptome analysis of huntington disease iPSC and mouse astrocytes implicates maturation and functional deficits. *iScience*, 26(1):105732, 2023. doi: 10.1016/j.isci.2022.105732.
- Rosenberg, A. B., Roco, C. M., Muscat, R. A., Kuchina, A., Sample, P., Yao, Z., Graybuck, L. T., Peeler, D. J., Mukherjee, S., Chen, W., Pun, S. H., Sellers, D. L., Tasic, B., and Seelig, G. Single-cell profiling of the developing mouse brain and spinal cord with split-pool barcoding. *Science*, 360(6385):176–182, 2018. doi: 10.1126/science.aam8999.
- Sadick, J. S., O’Dea, M. R., Hasel, P., Dykstra, T., Faustin, A., and Liddelow, S. A. Astrocytes and oligodendrocytes undergo subtype-specific transcriptional changes in Alzheimer’s disease. *Neuron*, 110(11):1788–1805 e10, 2022. doi: 10.1016/j.neuron.2022.03.008.
- Saez-Atienzar, S., Bandres-Ciga, S., Langston, R. G., Kim, J. J., Choi, S. W., Reynolds, R. H., International ALS Genomics Consortium, Italsgen, Abramzon, Y., Dewan, R., Ahmed, S., Landers, J. E., Chia, R., Ryten, M., Cookson, M. R., Nalls, M. A., Chiò, A., and Traynor, B. J. Genetic analysis of amyotrophic lateral sclerosis identifies contributing pathways and cell types. *Science Advances*, 7(3):eabd9036, 2021. doi: 10.1126/sciadv.abd9036.
- Safaiyan, S., Besson-Girard, S., Kaya, T., Cantuti-Castelvetri, L., Liu, L., Ji, H., Schifferer, M., Gouna, G., Usifo, F., Kannaiyan, N., Fitzner, D., Xiang, X., Rossner, M. J., Brendel, M., Gokce, O., and Simons, M. White matter aging drives microglial diversity. *Neuron*, 109(7):1100–1117 e10, 2021. doi: 10.1016/j.neuron.2021.01.027.
- Saito, K., Shigetomi, E., Shinozaki, Y., Kobayashi, K., Parajuli, B., Kubota, Y., Sakai, K., Miyakawa, M., Horiuchi, H., Nabekura, J., and Koizumi, S. Microglia sense astrocyte dysfunction and prevent disease progression in an Alexander disease model. *Brain*, 147(2):698–716, 2024. doi: 10.1093/brain/awad358.
- Sala Frigerio, C., Wolfs, L., Fattorelli, N., Thrupp, N., Voytyuk, I., Schmidt, I., Mancuso, R., Chen, W. T., Woodbury, M. E., Srivastava, G., Möller, T., Hudry, E., Das, S., Saido, T., Karran, E., Hyman, B., Perry, V. H., Fiers, M., and De Strooper, B. The major risk factors for Alzheimer’s disease: Age, sex, and genes modulate the microglia response to Abeta plaques. *Cell Reports*, 27(4):1293–1306 e6, 2019. doi: 10.1016/j.celrep.2019.03.099.
- Salmon, I., Grebenyuk, S., Abdel Fattah, A. R., Rustandi, G., Pilkington, T., Verfaillie, C., and Ranga, A. Engineering neurovascular organoids with 3D printed microfluidic chips. *Lab on a Chip*, 22(8):1615–1629, 2022. doi: 10.1039/d1lc00535a.
- Sanchís-Calleja, F., Jain, A., He, Z., Okamoto, R., Rusimbi, C., Rifés, P., Rathore, G. S., Santel, M., Janssens, J., Seimiya, M., Fleck, J. S., Kirkeby, A., Gray Camp, J., and Treutlein, B. Decoding morphogen patterning of human neural organoids with a multiplexed single-cell transcriptomic screen. *bioRxiv*, 2024. doi: 10.1101/2024.02.08.579413.
- Scholes, A. N. and Lewis, J. A. Comparison of RNA isolation methods on RNA-Seq: Implications for differential expression and meta-analyses. *BMC Genomics*, 21(1):249, 2020. doi: 10.1186/s12864-020-6673-2.
- Schroeder, A., Mueller, O., Stocker, S., Salowsky, R., Leiber, M., Gassmann, M., Lightfoot, S., Menzel, W., Granzow, M., and Ragg, T. The RIN: An RNA integrity number for assigning integrity values to RNA measurements. *BMC Molecular Biology*, 7:3, 2006. doi: 10.1186/1471-2199-7-3.
- Seeker, L. A. and Williams, A. Oligodendroglia heterogeneity in the human central nervous system. *Acta Neuropathologica*, 143(2):143–157, 2022. doi: 10.1007/s00401-021-02390-4.
- Sen, D., Voulgaropoulos, A., and Keung, A. J. Effects of early geometric confinement on the transcriptomic profile of human cerebral organoids. *BMC Biotechnology*, 21(1):59, 2021. doi: 10.1186/s12896-021-00718-2.
- Shen, K., Reichelt, M., Kyauk, R. V., Ngu, H., Shen, Y. A., Foreman, O., Modrusan, Z., Friedman, B. A., Sheng, M., and Yuen, T. J. Multiple sclerosis risk gene *Mertk* is required for microglial activation and subsequent remyelination. *Cell Reports*, 34(10):108835, 2021. doi: 10.1016/j.celrep.2021.108835.
- Shi, X., Luo, L., Wang, J., Shen, H., Li, Y., Mamtilahun, M., Liu, C., Shi, R., Lee, J. H., Tian, H., Zhang, Z., Wang, Y., Chung, W. S., Tang, Y., and Yang, G. Y. Stroke subtype-dependent synapse elimination by reactive gliosis in mice. *Nature Communications*, 12(1):6943, 2021. doi: 10.1038/s41467-021-27248-x.
- Shiau, C. K., Lu, L., Kieser, R., Fukumura, K., Pan, T., Lin, H. Y., Yang, J., Tong, E. L., Lee, G., Yan, Y., Huse, J. T., and Gao, R. High throughput single cell long-read sequencing analyses of same-cell genotypes and phenotypes in human tumors. *Nature Communications*, 14(1):4124, 2023. doi: 10.1038/s41467-023-39813-7.

- Shigemoto-Mogami, Y., Hoshikawa, K., Goldman, J. E., Sekino, Y., and Sato, K. Microglia enhance neurogenesis and oligodendrogenesis in the early postnatal subventricular zone. *Journal of Neuroscience*, 34(6):2231–2243, 2014. doi: 10.1523/JNEUROSCI.1619-13.2014.
- Simons, M. and Nave, K. A. Oligodendrocytes: Myelination and axonal support. *Cold Spring Harbor Perspectives in Biology*, 8(1):a020479, 2015. doi: 10.1101/cshperspect.a020479.
- Skinnder, M. A., Squair, J. W., Kathe, C., Anderson, M. A., Gautier, M., Matson, K. J. E., Milano, M., Hutson, T. H., Barraud, Q., Phillips, A. A., Foster, L. J., La Manno, G., Levine, A. J., and Courtine, G. Cell type prioritization in single-cell data. *Nature Biotechnology*, 39(1): 30–34, 2021. doi: 10.1038/s41587-020-0605-1.
- Sloan, S. A., Darmanis, S., Huber, N., Khan, T. A., Birey, F., Caneda, C., Reimer, R., Quake, S. R., Barres, B. A., and Paşca, S. P. Human astrocyte maturation captured in 3D cerebral cortical spheroids derived from pluripotent stem cells. *Neuron*, 95(4):779–790 e6, 2017. doi: 10.1016/j.neuron.2017.07.035.
- Smajić, S., Prada-Medina, C. A., Landoulsi, Z., Ghelfi, J., Delcambre, S., Dietrich, C., Jarazo, J., Henck, J., Balachandran, S., Pachcek, S., Morris, C. M., Antony, P., Timmermann, B., Sauer, S., Pereira, S. L., Schwamborn, J. C., May, P., Grünewald, A., and Spielmann, M. Single-cell sequencing of human midbrain reveals glial activation and a Parkinson-specific neuronal state. *Brain*, 145(3):964–978, 2022. doi: 10.1093/brain/awab446.
- Smits, L. M., Reinhardt, L., Reinhardt, P., Glatza, M., Monzel, A. S., Stanslowsky, N., Rosato-Siri, M. D., Zanon, A., Antony, P. M., Bellmann, J., Nicklas, S. M., Hemmer, K., Qing, X., Berger, E., Kalmbach, N., Ehrlich, M., Bolognin, S., Hicks, A. A., Wegner, F., Sternecker, J. L., and Schwamborn, J. C. Modeling Parkinson's disease in midbrain-like organoids. *NPJ Parkinson's Disease*, 5:5, 2019. doi: 10.1038/s41531-019-0078-4.
- Solomon, T., Rajendran, M., Rostovtseva, T., and Hool, L. How cytoskeletal proteins regulate mitochondrial energetics in cell physiology and diseases. *Philosophical Transactions of the Royal Society of London, Series B, Biological Sciences*, 377(1864):20210324, 2022. doi: 10.1098/rstb.2021.0324.
- Song, L., Yuan, X., Jones, Z., Griffin, K., Zhou, Y., Ma, T., and Li, Y. Assembly of human stem cell-derived cortical spheroids and vascular spheroids to model 3-D brain-like tissues. *Scientific Reports*, 9(1):5977, 2019. doi: 10.1038/s41598-019-42439-9.
- Sosunov, A. A., McKhann, G. M. n., and Goldman, J. E. The origin of Rosenthal fibers and their contributions to astrocyte pathology in Alexander disease. *Acta Neuropathologica Communications*, 5(1):27, 2017. doi: 10.1186/s40478-017-0425-9.
- Stogsdill, J. A., Harwell, C. C., and Goldman, S. A. Astrocytes as master modulators of neural networks: Synaptic functions and disease-associated dysfunction of astrocytes. *Annals of the New York Academy of Sciences*, 1525(1):41–60, 2023. doi: 10.1111/nyas.15004.
- Ståhl, P. L., Salmén, F., Vickovic, S., Lundmark, A., Navarro, J. F., Magnusson, J., Giacomello, S., Asp, M., Westholm, J. O., Huss, M., Mollbrink, A., Linnarsson, S., Codeluppi, S., Borg, A., Pontén, F., Costea, P. I., Sahlén, P., Mulder, J., Bergmann, O., Lundeberg, J., and Frisén, J. Visualization and analysis of gene expression in tissue sections by spatial transcriptomics. *Science*, 353(6294):78–82, 2016. doi: 10.1126/science.aaf2403.
- Subramanian, A., Tamayo, P., Mootha, V. K., Mukherjee, S., Ebert, B. L., Gillette, M. A., Paulovich, A., Pomeroy, S. L., Golub, T. R., Lander, E. S., and Mesirov, J. P. Gene set enrichment analysis: A knowledge-based approach for interpreting genome-wide expression profiles. *PNAS USA*, 102(43):15545–15550, 2005. doi: 10.1073/pnas.0506580102.
- Sun, X. Y., Ju, X. C., Li, Y., Zeng, P. M., Wu, J., Zhou, Y. Y., Shen, L. B., Dong, J., Chen, Y. J., and Luo, Z. G. Generation of vascularized brain organoids to study neurovascular interactions. *eLife*, 11:e76707, 2022. doi: 10.7554/eLife.76707.
- Suthon, S., Perkins, R. S., Bryja, V., Miranda-Carboni, G. A., and Krum, S. A. WNT5B in physiology and disease. *Frontiers in Cell and Developmental Biology*, 9:667581, 2021. doi: 10.3389/fcell.2021.667581.
- Szebenyi, K., Wenger, L. M. D., Sun, Y., Dunn, A. W. E., Limegrover, C. A., Gibbons, G. M., Conci, E., Paulsen, O., Mierau, S. B., Balmus, G., and Lakatos, A. Human ALS/FTD brain organoid slice cultures display distinct early astrocyte and targetable neuronal pathology. *Nature Neuroscience*, 24(11):1542–1554, 2021. doi: 10.1038/s41593-021-00923-4.
- Tanaka, K. F., Takebayashi, H., Yamazaki, Y., Ono, K., Naruse, M., Iwasato, T., Itohara, S., Kato, H., and Ikenaka, K. Murine model of Alexander disease: Analysis of GFAP aggregate formation and its pathological significance. *Glia*, 55(6):617–631, 2007. doi: 10.1002/glia.20486.
- Tang, G., Perng, M. D., Wilk, S., Quinlan, R., and Goldman, J. E. Oligomers of mutant glial fibrillary acidic protein (GFAP) inhibit the proteasome system in alexander disease astrocytes, and the small heat shock protein alphaB-crystallin reverses the inhibition. *Journal of Biological Chemistry*, 285(14):10527–10537, 2010. doi: 10.1074/jbc.M109.067975.
- Tasca, C. I., Dal-Cim, T., and Cimarosti, H. In vitro oxygen-glucose deprivation to study ischemic cell death. *Methods in Molecular Biology*, 1254:197–210, 2015. doi: 10.1007/978-1-4939-2152-2_15.
- Tay, T. L., Mai, D., Dautzenberg, J., Fernández-Klett, F., Lin, G., Sagar, Datta, M., Drougard, A., Stempf, T., Ardura-Fabregat, A., Staszewski, O., Margineanu, A., Sporb, A., Steinmetz, L. M., Pospisilik, J. A., Jung, S., Priller, J., Grün, D., Ronneberger, O., and Prinz, M. A new fate mapping system reveals context-dependent random or clonal expansion of microglia. *Nature Neuroscience*, 20(6):793–803, 2017. doi: 10.1038/nn.4547.
- Traiffort, E., Kassoussi, A., Zahaf, A., and Laouarem, Y. Astrocytes and microglia as major players of myelin production in normal and pathological conditions. *Frontiers in Cellular Neuroscience*, 14:79, 2020. doi: 10.3389/fncel.2020.00079.
- Trapnell, C., Cacchiarelli, D., Grimsby, J., Pokharel, P., Li, S., Morse, M., Lennon, N. J., Livak, K. J., Mikkelsen, T. S., and Rinn, J. L. The dynamics and regulators of cell fate decisions are revealed by pseudotemporal ordering of single cells. *Nature Biotechnology*, 32(4): 381–386, 2014. doi: 10.1038/nbt.2859.
- Uzquiano, A., Kedaigle, A. J., Pigoni, M., Paulsen, B., Adiconis, X., Kim, K., Faits, T., Nagaraja, S., Anton-Bolaños, N., Gerhardinger, C., Tucewicz, A., Murray, E., Jin, X., Buenrostro, J., Chen, F., Velasco, S., Regev, A., Levin, J. Z., and Arlotta, P. Proper acquisition of cell

- class identity in organoids allows definition of fate specification programs of the human cerebral cortex. *Cell*, 185(20):3770–3788 e27, 2022. doi: 10.1016/j.cell.2022.09.010.
- Valihrach, L. and Benešová, Z. An international scientific consortium is working to elucidate the mechanism of ultra-rare Alexander’s disease. <https://www.biocev.eu/en/services/gene-core-quantitative-and-digital-pcr.7/an-international-scientific-consortium-is-working-to-elucidate-the-mechanism-of-ultra-rare-alexander-s-disease.305?t=p>, 2022. Accessed: 2024-09-05.
- Valny, M., Honsa, P., Waloschkova, E., Matuskova, H., Kriska, J., Kirdajova, D., Androvic, P., Valihrach, L., Kubista, M., and Anderova, M. A single-cell analysis reveals multiple roles of oligodendroglial lineage cells during post-ischemic regeneration. *Glia*, 66(5):1068–1081, 2018. doi: 10.1002/glia.23301.
- van der Knaap, M. S., Naidu, S., Breiter, S. N., Blaser, S., Stroink, H., Springer, S., Begeer, J. C., van Coster, R., Barth, P. G., Thomas, N. H., Valk, J., and Powers, J. M. Alexander disease: Diagnosis with MR imaging. *AJNR American Journal of Neuroradiology*, 22(3):541–552, 2001.
- Van Harten, A. C. M., Phatnani, H., and Przedborski, S. Non-cell-autonomous pathogenic mechanisms in amyotrophic lateral sclerosis. *Trends in Neurosciences*, 44(8):658–668, 2021. doi: 10.1016/j.tins.2021.04.008.
- Velasco, S., Kedaigle, A. J., Simmons, S. K., Nash, A., Rocha, M., Quadrato, G., Paulsen, B., Nguyen, L., Adiconis, X., Regev, A., Levin, J. Z., and Arlotta, P. Individual brain organoids reproducibly form cell diversity of the human cerebral cortex. *Nature*, 570(7762):523–527, 2019. doi: 10.1038/s41586-019-1289-x.
- Verkerke, M., Berdenis van Berlekom, A., Donega, V., Vonk, D., Sluijs, J. A., Butt, N. F., Kistemaker, L., de Witte, L. D., Pasterkamp, R. J., Middeldorp, J., and Hol, E. M. Transcriptomic and morphological maturation of human astrocytes in cerebral organoids. *Glia*, 72(2):362–374, 2024. doi: 10.1002/glia.24479.
- Viedma-Poyatos, A., González-Jiménez, P., Pajares, M. A., and Pérez-Sala, D. Alexander disease GFAP R239C mutant shows increased susceptibility to lipoxidation and elicits mitochondrial dysfunction and oxidative stress. *Redox Biology*, 55:102415, 2022. doi: 10.1016/j.redox.2022.102415.
- von Bartheld, C. S., Bahney, J., anderculano-Houzel, S. The search for true numbers of neurons and glial cells in the human brain: A review of 150 years of cell counting. *Journal of Comparative Neurology*, 524(18):3865–3895, 2016. doi: 10.1002/cne.24040.
- Voss, A. J., Lanjewar, S. N., Sampson, M. M., King, A., Hill, E. J., Sing, A., Sojka, C., Bhatia, T. N., Spangle, J. M., and Sloan, S. A. Identification of ligand-receptor pairs that drive human astrocyte development. *Nature Neuroscience*, 26(8):1339–1351, 2023. doi: 10.1038/s41593-023-01375-8.
- Vucic, S., Ziemann, U., Eisen, A., Hallett, M., and Kiernan, M. C. Transcranial magnetic stimulation and amyotrophic lateral sclerosis: pathophysiological insights. *Journal of Neurology, Neurosurgery, and Psychiatry*, 84(10):1161–1170, 2013. doi: 10.1136/jnnp-2012-304019.
- Vucic, S., Pavey, N., Haidar, M., Turner, B. J., and Kiernan, M. C. Cortical hyperexcitability: Diagnostic and pathogenic biomarker of ALS. *Neuroscience Letters*, 759:136039, 2021. doi: 10.1016/j.neulet.2021.136039.
- Wallis, N., Lau, C. L., Farg, M. A., Atkin, J. D., Beart, P. M., and O’Shea, R. D. SOD1 mutations causing familial amyotrophic lateral sclerosis induce toxicity in astrocytes: Evidence for bystander effects in a continuum of astrogliosis. *Neurochemical Research*, 43(1):166–179, 2018. doi: 10.1007/s11064-017-2385-7.
- Wang, L., Colodner, K. J., and Feany, M. B. Protein misfolding and oxidative stress promote glial-mediated neurodegeneration in an Alexander disease model. *Journal of Neuroscience*, 31(8):2868–2877, 2011. doi: 10.1523/JNEUROSCI.3410-10.2011.
- Wang, L., Xia, J., Li, J., Hagemann, T. L., Jones, J. R., Fraenkel, E., Weitz, D. A., Zhang, S. C., Messing, A., and Feany, M. B. Tissue and cellular rigidity and mechanosensitive signaling activation in Alexander disease. *Nature Communications*, 9(1):1899, 2018. doi: 10.1038/s41467-018-04269-7.
- Wang, M., Zhang, L., Novak, S. W., Yu, J., Gallina, I. S., Xu, L. L., Lim, C. K., Fernandes, S., Shokhirev, M. N., Williams, A. E., Saxena, M. D., Coorapati, S., Parylak, S. L., Quintero, C., Molina, E., Andrade, L. R., Manor, U., and Gage, F. H. Morphological diversification and functional maturation of human astrocytes in glia-enriched cortical organoid transplanted in mouse brain. *Nature Biotechnology*, 2024. doi: 10.1038/s41587-024-02157-8.
- Wang, Q., Boenigk, S., Boehm, V., Gehring, N. H., Altmueller, J., and Dieterich, C. Single cell transcriptome sequencing on the Nanopore platform with SeNapBar. *RNA*, 27(7):763–770, 2021a. doi: 10.1261/rna.078154.120.
- Wang, S., Zheng, H., Choi, J. S., Lee, J. K., Li, X., and Hu, H. A systematic evaluation of the computational tools for ligand-receptor-based cell-cell interaction inference. *Briefings in Functional Genomics*, 21(5):339–356, 2022. doi: 10.1093/bfpg/elac019.
- Wang, X., He, Y., Zhang, Q., Ren, X., and Zhang, Z. Direct comparative analyses of 10X Genomics Chromium and Smart-seq2. *Genomics, Proteomics, and Bioinformatics*, 19(2):253–266, 2021b. doi: 10.1016/j.gpb.2020.02.005.
- Wheeler, M. A., Clark, I. C., Tjon, E. C., Li, Z., Zandee, S. E. J., Couturier, C. P., Watson, B. R., Scalisi, G., Alkwai, S., Rothhammer, V., Rotem, A., Heyman, J. A., Thaploo, S., Sanmarco, L. M., Ragoussis, J., Weitz, D. A., Petrecca, K., Moffitt, J. R., Becher, B., Antel, J. P., Prat, A., and Quintana, F. J. MAFG-driven astrocytes promote CNS inflammation. *Nature*, 578(7796):593–599, 2020. doi: 10.1038/s41586-020-1999-0.
- Wu, T., Hu, E., Xu, S., Chen, M., Guo, P., Dai, Z., Feng, T., Zhou, L., Tang, W., Zhan, L., Fu, X., Liu, S., Bo, X., and Yu, G. clusterProfiler 4.0: A universal enrichment tool for interpreting omics data. *Innovation (Cambridge)*, 2(3):100141, 2021. doi: 10.1016/j.xinn.2021.100141.
- Xiang, R., Wang, W., Yang, L., Wang, S., Xu, C., and Chen, X. A comparison for dimensionality reduction methods of single-cell RNA-seq data. *Frontiers in Genetics*, 12:646936, 2021. doi: 10.3389/fgene.2021.646936.

- Xu, R., Boreland, A. J., Li, X., Erickson, C., Jin, M., Atkins, C., Pang, Z. P., Daniels, B. P., and Jiang, P. Developing human pluripotent stem cell-based cerebral organoids with a controllable microglia ratio for modeling brain development and pathology. *Stem Cell Reports*, 16(8): 1923–1937, 2021. doi: 10.1016/j.stemcr.2021.06.011.
- Yang, A. W., Lin, N. H., Yeh, T. H., Snider, N., and Perng, M. D. Effects of Alexander disease-associated mutations on the assembly and organization of GFAP intermediate filaments. *Molecular Biology of the Cell*, 33(8):ar69, 2022. doi: 10.1091/mbc.E22-01-0013.
- Yang, T., Dai, Y., Chen, G., and Cui, S. Dissecting the dual role of the glial scar and scar-forming astrocytes in spinal cord injury. *Frontiers in Cellular Neuroscience*, 14:78, 2020. doi: 10.3389/fncel.2020.00078.
- Yao, Z., van Velthoven, C. T. J., Kunst, M., Zhang, M., McMillen, D., Lee, C., Jung, W., Goldy, J., Abdelhak, A., Aitken, M., Baker, K., Baker, P., Barkan, E., Bertagnolli, D., Bhandiwad, A., Bielstein, C., Bishwakarma, P., Campos, J., Carey, D., Casper, T., Chakka, A. B., Chakrabarty, R., Chavan, S., Chen, M., Clark, M., Close, J., Crichton, K., Daniel, S., DiValentin, P., Dolbeare, T., Ellingwood, L., Fiabane, E., Fliss, T., Gee, J., Gerstenberger, J., Glandon, A., Gloe, J., Gould, J., Gray, J., Guilford, N., Guzman, J., Hirschstein, D., Ho, W., Hooper, M., Huang, M., Hupp, M., Jin, K., Kroll, M., Lathia, K., Leon, A., Li, S., Long, B., Madigan, Z., Malloy, J., Malone, J., Maltzer, Z., Martin, N., McCue, R., McGinty, R., Mei, N., Melchor, J., Meyerdieks, E., Mollenkopf, T., Moonsman, S., Nguyen, T. N., Otto, S., Pham, T., Rimorin, C., Ruiz, A., Sanchez, R., Sawyer, L., Shapovalova, N., Shepard, N., Slaughterbeck, C., Sulc, J., Tieu, M., Torkelson, A., Tung, H., Valera Cuevas, N., Vance, S., Wadhvani, K., Ward, K., Levi, B., Farrell, C., Young, R., Staats, B., Wang, M. M., Thompson, C. L., Mufti, S., Pagan, C. M., Kruse, L., Dee, N., Sunkin, S. M., Esposito, L., Hawrylycz, M. J., Waters, J., Ng, L., Smith, K., Tasic, B., Zhuang, X., et al. A high-resolution transcriptomic and spatial atlas of cell types in the whole mouse brain. *Nature*, 624(7991):317–332, 2023. doi: 10.1038/s41586-023-06812-z.
- Yoon, S. J., Elahi, L. S., Paşca, A. M., Marton, R. M., Gordon, A., Revah, O., Miura, Y., Walczak, E. M., Holdgate, G. M., Fan, H. C., Huguenard, J. R., Geschwind, D. H., and Paşca, S. P. Reliability of human cortical organoid generation. *Nature Methods*, 16(1):75–78, 2019. doi: 10.1038/s41592-018-0255-0.
- Yoshida, T., Sasaki, M., Yoshida, M., Namekawa, M., Okamoto, Y., Tsujino, S., Sasayama, H., Mizuta, I., Nakagawa, M., and Alexander Disease Study Group in Japan. Nationwide survey of Alexander disease in Japan and proposed new guidelines for diagnosis. *Journal of Neurology*, 258(11):1998–2008, 2011. doi: 10.1007/s00415-011-6056-3.
- Zamanian, J. L., Xu, L., Foo, L. C., Nouri, N., Zhou, L., Giffard, R. G., and Barres, B. A. Genomic analysis of reactive astrogliosis. *Journal of Neuroscience*, 32(18):6391–6410, 2012. doi: 10.1523/JNEUROSCI.6221-11.2012.
- Zamboni, M., Llorens-Bobadilla, E., Magnusson, J. P., and Frisen, J. A widespread neurogenic potential of neocortical astrocytes is induced by injury. *Cell Stem Cell*, 27(4):605–617 e5, 2020. doi: 10.1016/j.stem.2020.07.006.
- Zappia, L., Phipson, B., and Oshlack, A. Exploring the single-cell RNA-seq analysis landscape with the scRNA-tools database. *PLoS Computational Biology*, 14(6):e1006245, 2018. doi: 10.1371/journal.pcbi.1006245.
- Zare, I., Paul, D., and Moody, S. Doublecortin mutation in an adolescent male. *Child Neurology Open*, 6:2329048X19836589, 2019. doi: 10.1177/2329048X19836589.
- Zarei-Kheirabadi, M., Vaccaro, A. R., Rahimi-Movaghar, V., Kiani, S., and Baharvand, H. An overview of extrinsic and intrinsic mechanisms involved in astrocyte development in the central nervous system. *Stem Cells and Development*, 29(5):266–280, 2020. doi: 10.1089/scd.2019.0189.
- Zeisel, A., Muñoz-Manchado, A. B., Codeluppi, S., Lönnerberg, P., La Manno, G., Juréus, A., Marques, S., Munguba, H., He, L., Betsholtz, C., Rolny, C., Castelo-Branco, G., Hjerling-Leffler, J., and Linnarsson, S. Brain structure. cell types in the mouse cortex and hippocampus revealed by single-cell RNA-seq. *Science*, 347(6226):1138–1142, 2015. doi: 10.1126/science.aaa1934.
- Zhang, R., Quan, H., Wang, Y., and Luo, F. Neurogenesis in primates versus rodents and the value of non-human primate models. *National Science Review*, 10(11):nwad248, 2023a. doi: 10.1093/nsr/nwad248.
- Zhang, S., Cooper-Knock, J., Weimer, A. K., Shi, M., Moll, T., Marshall, J. N. G., Harvey, C., Nezhad, H. G., Franklin, J., Souza, C. D. S., Ning, K., Wang, C., Li, J., Dilliot, A. A., Farhan, S., Elhaik, E., Pasniceanu, I., Livesey, M. R., Eitan, C., Hornstein, E., Kenna, K. P., Project MinE ALS Sequencing Consortium, Veldink, J. H., Ferraiuolo, L., Shaw, P. J., and Snyder, M. P. Genome-wide identification of the genetic basis of amyotrophic lateral sclerosis. *Neuron*, 110(6):992–1008 e11, 2022. doi: 10.1016/j.neuron.2021.12.019.
- Zhang, X., Xiao, G., Johnson, C., Cai, Y., Horowitz, Z. K., Mennicke, C., Coffey, R., Haider, M., Threadgill, D., Eliscu, R., Oldham, M. C., Greenbaum, A., and Ghashghaei, H. T. Bulk and mosaic deletions of Egfr reveal regionally defined gliogenesis in the developing mouse forebrain. *iScience*, 26(3):106242, 2023b. doi: 10.1016/j.isci.2023.106242.
- Zhang, Y., Sloan, S. A., Clarke, L. E., Caneda, C., Plaza, C. A., Blumenthal, P. D., Vogel, H., Steinberg, G. K., Edwards, M. S., Li, G., Duncan, J. A., r., Cheshier, S. H., Shuer, L. M., Chang, E. F., Grant, G. A., Gephart, M. G., and Barres, B. A. Purification and characterization of progenitor and mature human astrocytes reveals transcriptional and functional differences with mouse. *Neuron*, 89(1):37–53, 2016. doi: 10.1016/j.neuron.2015.11.013.
- Zhao, J., Jaffe, A., Li, H., Lindenbaum, O., Sefik, E., Jackson, R., Cheng, X., Flavell, R. A., and Kluger, Y. Detection of differentially abundant cell subpopulations in scRNA-seq data. *PNAS USA*, 118(22):e2100293118, 2021. doi: 10.1073/pnas.2100293118.
- Zheng, G. X., Terry, J. M., Belgrader, P., Ryvkin, P., Bent, Z. W., Wilson, R., Ziraldo, S. B., Wheeler, T. D., McDermott, G. P., Zhu, J., Gregory, M. T., Shuga, J., Montesclaros, L., Underwood, J. G., Masquelier, D. A., Nishimura, S. Y., Schnall-Levin, M., Wyatt, P. W., Hindson, C. M., Bharadwaj, R., Wong, A., Ness, K. D., Beppu, L. W., Deeg, H. J., McFarland, C., Loeb, K. R., Valente, W. J., Ericson, N. G., Stevens, E. A., Radich, J. P., Mikkelsen, T. S., Hindson, B. J., and Bielas, J. H. Massively parallel digital transcriptional profiling of single cells. *Nature Communications*, 8:14049, 2017. doi: 10.1038/ncomms14049.
- Zhou, W. and Xu, R. Current insights in the molecular genetic pathogenesis of amyotrophic lateral sclerosis. *Frontiers in Neuroscience*, 17: 1189470, 2023. doi: 10.3389/fnins.2023.1189470.

- Zhou, Y., Song, W. M., Andhey, P. S., Swain, A., Levy, T., Miller, K. R., Poliani, P. L., Cominelli, M., Grover, S., Gilfillan, S., Cella, M., Ulland, T. K., Zaitsev, K., Miyashita, A., Ikeuchi, T., Sainouchi, M., Kakita, A., Bennett, D. A., Schneider, J. A., Nichols, M. R., Beausoleil, S. A., Ulrich, J. D., Holtzman, D. M., Artyomov, M. N., and Colonna, M. Human and mouse single-nucleus transcriptomics reveal TREM2-dependent and TREM2-independent cellular responses in Alzheimer's disease. *Nature Medicine*, 26(1):131–142, 2020. doi: 10.1038/s41591-019-0695-9.
- Zhou, Y., Song, H., and Ming, G. L. Genetics of human brain development. *Nature Reviews Genetics*, 25(1):26–45, 2024. doi: 10.1038/s41576-023-00626-5.
- Ziff, O. J., Clarke, B. E., Taha, D. M., Crerar, H., Luscombe, N. M., and Patani, R. Meta-analysis of human and mouse ALS astrocytes reveals multi-omic signatures of inflammatory reactive states. *Genome Research*, 32(1):71–84, 2022. doi: 10.1101/gr.275939.121.
- Zou, Z. Y., Zhou, Z. R., Che, C. H., Liu, C. Y., He, R. L., and Huang, H. P. Genetic epidemiology of amyotrophic lateral sclerosis: a systematic review and meta-analysis. *Journal of Neurology, Neurosurgery, and Psychiatry*, 88(7):540–549, 2017. doi: 10.1136/jnnp-2016-315018.
- Zuo, X., Zhou, J., Li, Y., Wu, K., Chen, Z., Luo, Z., Zhang, X., Liang, Y., Esteban, M. A., Zhou, Y., and Fu, X. D. TDP-43 aggregation induced by oxidative stress causes global mitochondrial imbalance in ALS. *Nature Structural & Molecular Biology*, 28(2):132–142, 2021. doi: 10.1038/s41594-020-00537-7.

